

From the: *Institute of Lung Biology and Disease, Helmholtz Zentrum München*



Dissertation

zum Erwerb des Doctor of Philosophy (Ph.D.) an der
Medizinischen Fakultät der
Ludwig-Maximilians-Universität zu München

***Next generation bioreactor with cyclic mechanical stretch on
biomimetic lung tissue***

vorgelegt von

Ali Doryab

aus Tehran, Iran

2021

Mit Genehmigung der Medizinischen Fakultät der
Ludwig-Maximilians-Universität zu München

First Supervisor: PD Dr. med. Anne Hilgendorff

Second Supervisor: Dr. Otmar Schmid

Third Supervisor: Prof. Markus Rehberg

Dean: Prof. Dr. med. dent. Reinhard HICKEL

Datum der Verteidigung:

27.05.2021

Affidavit



Affidavit

Doryab, Ali

Surname, first name

Ingolstädter Landstr. 1

Street

85764 Munich, Germany

Zip code, town, country

I hereby declare, that the submitted thesis entitled:

Next generation bioreactor with cyclic mechanical stretch on biomimetic lung tissue

is my own work. I have only used the sources indicated and have not made unauthorized use of services of a third party. Where the work of others has been quoted or reproduced, the source is always given.

I further declare that the submitted thesis or parts thereof have not been presented as part of an examination degree to any other university.

Munich, 29.05.2021

place, date

Ali Doryab

Signature doctoral candidate

Confirmation of congruency



LUDWIG-
MAXIMILIANS-
UNIVERSITÄT
MÜNCHEN

Promotionsbüro
Medizinische Fakultät



**Confirmation of congruency between printed and electronic version of
the doctoral thesis**

Doryab, Ali

Surname, first name

Ingolstädter Landstr. 1

Street

85764 Munich, Germany

Zip code, town, country

I hereby declare, that the submitted thesis entitled:

Next generation bioreactor with cyclic mechanical stretch on biomimetic lung tissue

is congruent with the printed version both in content and format.

Munich, 29.05.2021

place, date

Ali Doryab

Signature doctoral candidate

*To my wonderful wife **Motaharehsadat***

Table of content

Affidavit	3
Confirmation of congruency.....	4
Table of content	6
List of abbreviations	7
List of publications	10
1. Contribution to the publications.....	13
1.1 Contribution to Paper I.....	13
1.2 Contribution to Paper II.....	16
1.3 Contribution to Paper III.....	19
1.4 Contribution to Paper IV (Appendix).....	21
1.5 Contribution to other publications.....	22
2. Introductory summary.....	23
2.1 Definition of problem and aim of the study	24
2.2 Previous studies.....	27
2.3 Overview of our approach.....	32
2.4 Concluding remarks.....	38
2.5 Chapter 1: Design and manufacturing of a biomimetic membrane for pulmonary epithelial cells.....	43
2.6 Chapter 2: Particokinetic study under cyclic stretch and air-liquid interface conditions.....	44
2.7 Chapter 3: An <i>in vitro</i> lung model with aerosol delivery	45
3. Paper I.....	46
4. Paper II.....	72
5. Paper III.....	92
References	113
Appendix A: Paper IV.....	118
Acknowledgements.....	138

List of abbreviations

Abbreviation	Description
3D	Three-dimensional
A549	Immortalized human alveolar epithelial cell line
ADSCs	Human adipose-derived stem cells
AFM	Atomic force microscopy
ALI	Air-liquid interface
ARDS	Acute respiratory distress syndrome
ASMs	Airway smooth muscle cells
ATs	Alveolar epithelial cells
ATIs	Type I alveolar epithelial cells
ATIIs	Type II alveolar epithelial cells
BASMCs	Bovine aortic smooth muscle cell
BETA (membrane)	Membrane for biphasic elastic thin for air-liquid culture conditions
cAMP	Cyclic adenosine 3',5'-monophosphate
CCD	Central composite design
COPD	Chronic obstructive pulmonary disease
CIVIC	Cyclic in vitro cell-stretch
CLSM	Confocal laser scanning microscopy
DCs	Dendritic cells
dECM	Decellularized extracellular matrix
DMSO	Dimethylsulfoxide
DoE	Design of experiment
ECM	Extracellular matrix
EDS/SEM	Energy dispersive x-ray spectroscopy/ scanning electron microscopy
EGF	Epidermal growth factor
EGFR	Epidermal growth factor receptor
EMT	Mesenchymal transition
ERK	Extracellular-regulated protein kinase
ES	Electrospinning
EVs	Extracellular vesicles
FAK	Focal adhesion kinase
FEK4	Human skin primary fibroblast cells

FIB/SEM	Focused ion beam/ scanning electron microscopy
FT-IR	Fourier transform infrared spectroscopy
GAPDH	Glyceraldehyde 3-phosphate dehydrogenase
HA	Hyaluronan
HBSMCs	Human bronchial smooth muscle cells
HFIP	1,1,1,3,3,3-Fluoro-2-propanol
HFP	Hexafluoro-2-propanol
HIF-1 α	Hypoxia-inducible factor 1 α
HLEC	Human limbal epithelial cell
HPAEC	Primary human pulmonary alveolar epithelial cells
HPMEC	Primary human pulmonary microvascular endothelial cell
HSAEC	Primary human small airway epithelial cells
HUSMCs	Human umbilical arterial smooth muscle cells
HUVECs	Human umbilical vein endothelial cells
iCVD	Initiated chemical vapor deposition
IKVAV	Isoleucine-lysine-valine-alanine-valine
IL-8	Interleukin-8
IPF	Pulmonary fibrosis
LSFM	Light sheet fluorescence microscopy
MALI	Moving air liquid interface
MAPK	Mitogen-activated protein kinases
mATII	Mouse alveolar epithelial type II cells
MLE-12	Mouse lung epithelial cells
NCI-H441	Human pulmonary epithelial cell line
NCO-sP(EO-stat-PO)	Star-shaped poly(ethylene oxide-stat-propylene oxide) with isocyanate end groups
NOF	Normal oral fibroblasts
NOK	Normal oral keratinocytes
OSA	Obstructive sleep apnea
P(LLA-CL)	Poly(l-lactide-co-caprolactone)
PCL	Poly(ϵ -)caprolactone
PCLS	Precision-cut lung slices
PCU	Polycarbonate polyurethane
PDMS	Polydimethylsiloxane

PDS	Polydioxanone
PEECs	Porcine esophageal epithelial cells
PEGdma	Poly(ethylene glycol) dimethacrylate
PET	Polyethylene terephthalate
PGA	Polyglutamic acid
PGS	Poly(glycerol sebacate)
pHPAEC	Primary human pulmonary alveolar epithelial cells
PKA	Protein kinase A
PLA	Poly(lactic acid)
PLGA	Poly(lactic-co-glycolic acid)
PLLA	Poly-L-lactic acid
PTFE	Poly(tetrafluoroethylene)
PVA	Poly(vinyl alcohol)
rATII	Rat alveolar epithelial type II cells
RGD	Arginylglycylaspartic acid
RSM	Response surface methodology
rhTE	Recombinant human tropoelastin
rMSCs	Rat mesenchymal stem cells
SEM	scanning electron microscopy
SMCs	Smooth muscle cells
SP-B	Surfactant protein B
SP-C	Surfactant protein C
TACE	Tumor necrosis factor-alpha-converting enzyme
TAZ	Transcriptional co-activator with PDZ-binding motif
TEER	Transepithelial electrical resistance
TFE	Trifluoroethanol
VECs	Valvular endothelial cells
VICs	Valvular interstitial cells
VILI	Ventilator-induced lung injury
WCA	Water contact angle
WST1	cell proliferation reagent
YAP	Yes-associated protein
ZO-1	Zonula occludens-1

List of publications

Peer-reviewed Research Journal

(1*, 2*, 3*, and 4* are part of this cumulative dissertation)

- 1.* **Doryab A.**, Taskin M., Stahlhut P., Groll J., Wagner D.E., Schmid O. **2020**. “A Biomimetic, Copolymeric Membrane for Cell-Stretch Experiments with Pulmonary Epithelial Cells at the Air-Liquid Interface”. *Advanced Functional Materials*: 2004707. <https://onlinelibrary.wiley.com/doi/10.1002/adfm.202004707>
- 2.* **Doryab A.**, Taskin M., Stahlhut P., Orak S. Voss C., Hilgendorff A., Rehberg M., Stöger T., Groll J., Schmid O. **2021**. “A Bioinspired In Vitro Lung Model to Study Particokinetics of Nano-/Microparticles under Cyclic Stretch and Air-Liquid Interface Conditions.” *Frontiers in Bioengineering and Biotechnology* 9: 42. <https://doi.org/10.3389/fbioe.2021.616830>
- 3.* Cei D[#], **Doryab A[#]**, Lenz AG., Schröppel A., Mayer P., Burgstaller G., Nossa R., Ahluwalia A., Schmid O. **2021**. “Development of a dynamic *in vitro* stretch model of the alveolar interface with aerosol delivery.” *Biotechnology and Bioengineering*. 118 (2): 690–702. <https://onlinelibrary.wiley.com/doi/10.1002/bit.27600>
([#]share first authorship)
- 4.* **Doryab A.**, Tas S., Taskin M. B., Yang L., Hilgendorff A., Groll J., Wagner D. E., Schmid O. **2019**. “Evolution of bioengineered lung models: Recent advances and challenges in tissue mimicry for studying the role of mechanical forces in cell biology.” *Advanced Functional Materials* 29 (39): 1903114. <https://onlinelibrary.wiley.com/doi/abs/10.1002/adfm.201903114>
5. Bölükbas D., Datz S., Meyer-Schwickerath C., Morrone C, **Doryab A.**, Gössl D., Vreka, M., Yang L., Argyo C., van Rijt S., Linder M., Eickelberg O., Stöger T., Schmid O. **2020**. Lindstedt S., Stathopoulos G., Bein T., Wagner D., Meiners, S., “Organ-restricted vascular delivery of nanoparticles for lung cancer therapy.” *Advanced Therapeutics* 3 (7): 2000017. <https://doi.org/10.1002/adtp.202000017>
6. Costa R., Wagner D. E., **Doryab A.**, De Santis M. M., Schorpp K., Rothenaiger I., Lehmann M., Baarsma H. A., Schmid O., Campillos M., Yildirim A. Ö., Hadian K., Königshoff M. (*In Press*) “A drug screen with approved compounds identifies amlexanox as a novel Wnt/ β -catenin activator inducing lung epithelial organoid formation”, *British Journal of Pharmacology*.
7. **Doryab, A.**, Amoabediny, G. & Salehi-Najafabadi. **2016**. “Advances in Pulmonary Therapy and Drug Development: Lung Tissue Engineering to Lung-on-a-Chip.” *Biotechnology Advances* 34 (5): 588–96. <https://doi.org/10.1016/j.biotechadv.2016.02.006>

8. Mahfouzi S.H., Amoabediny, G., **Doryab, A.**, Safiabadi-Tali S.H., Ghanei M. **2018**. “Noninvasive Real-Time Assessment of Cell Viability in a Three-Dimensional Tissue.” *Tissue Engineering Part C: Methods* 24 (4): 197–204. <https://doi.org/10.1089/ten.tec.2017.0371>
9. **Doryab, A.**, Heydarian M., Amoabediny, G., Sadroddiny, E., Mahfouzi S. **2017**. “Recellularization on Acellular Lung Tissue Scaffold Using Perfusion-Based Bioreactor: An Online Monitoring Strategy.” *Journal of Medical and Biological Engineering* 37 (1): 53–62. <https://doi.org/10.1007/s40846-016-0205-1>

Chapter Book

1. Bölükbas, D.A., De Santis, M.M., Alsafadi, H.N., **Doryab, A.**, Wagner, D.E. 2019. “The preparation of decellularized mouse lung matrix scaffolds for analysis of lung regenerative cell potential.” In: *Mouse Cell Culture*. 275-295 (Methods Mol. Biol.; 1940). DOI:10.1007/978-1-4939-9086-3_20.

Patent

1. **Doryab A.**, Schröppel A., Taskin M. B., Groll J., Schmid O. “Biocompatible composite membrane, method for fabricating the membrane, bioreactor and method for investigating cells attached to the biocompatible composite membrane” (European patent application was filed by INNO, HMGU on 24.11.2020).

Selected Conference Abstract

1. **Doryab A.**, Wagner D.E., M. Taskin M., Voss C., Schröppel A., Hilgendorff A., Groll J., Schmid O., Biomimetic Thin Polycarbonate/Gelatin Membrane for Alveolar-capillary Barrier Application, Annual Meeting of the International Society for Biofabrication, October 28-31, 2018, Würzburg, Germany
2. **Doryab A.**, Wagner D.E., Voss C., Schröppel A., Hilgendorff A., Schmid O., A stretchable porous PCL/gelatin hybrid membrane to support growth of pulmonary epithelial cells at the air-liquid interface under cyclic stretch conditions, 12th Biobarriers, August 27-29, 2018, Germany
3. De Santis, M, Alsafadi H, Tas S., Prithiviraj S, Bölükbas1 D., Da Silva I., Mitterdorfer M., Ota C., **Doryab A.**, Königshoff M., Tassieri M., Bourguine P., Lindstedt S., Mohlin S., Wagner D.E., 3D bioprinting small airways with a hybrid alginate-ECM hydrogel, 11th Symposium for Biologic Scaffolds for Regenerative Medicine, April 30 – May 2, 2020, California, USA

4. Bölükbas D. A., Morrone C, **Doryab A.**, Datz S., Gössl D., van Rijt S., Stöger T., Bein T., Meiners, Wagner D., Fine-tuning Lung Cancer Nanotherapy Using Closed Cardiopulmonary Circulation, Annual conference of Society For Biomaterials (SFB), April 3–6, 2019, SEATTLE, WA, USA
5. De Santis M., Taş S., Ota C, **Doryab A.**, Alsafadi H.N, Bölükbas D., Königshoff M., Mohlin S., Wagner D.E., Development of a Hybrid Alginate-ECM Hydrogel as a Potential Bioink for 3D Bioprinting Pulmonary Tissue, Annual Meeting of the International Society for Biofabrication, October 28-31, 2018, Würzburg, Germany
6. Costa R., Wagner D. E., De Santis M, Bailey K., **Doryab A.**, Schorpp K., Rothenaiger I., Ota C., Baarsma H., Campillos M., Hadian K., Königshoff M., Drug repurposing for WNT/ β -catenin induced lung repair in chronic obstructive pulmonary disease, *Am J Respir Crit Care Med* 2018;197: A7653
7. Bölükbas D. A., Datz S., **Doryab A.**, Meyer-Schwickckerath C., Morone C., Meiners S., Wagner D.E., An ex vivo lung model for screening of nanoparticle targeting, 16th ERS lung Science Conference, March 08 - 11, 2018, Portugal

1. Contribution to the publications

1.1 Contribution to Paper I

A Biomimetic, Copolymeric Membrane for Cell-Stretch Experiments with Pulmonary Epithelial Cells at the Air-Liquid Interface

Ali Doryab, Mehmet Berat Taskin, Philipp Stahlhut, Andreas Schröppel, Darcy E. Wagner, Jürgen Groll, Otmar Schmid. 2020. *Advanced Functional Materials*. 2004707. <https://onlinelibrary.wiley.com/doi/10.1002/adfm.202004707>.

SUMMARY

In this paper, we presented a novel membrane technology for culturing lung epithelial cells under air-liquid interface (ALI) and dynamic (cyclic stretch) conditions. The fundamental concept and the manufacturing method of the **BETA** (Biphasic Elastic Thin for Air-liquid culture conditions) membrane are described. The copolymeric biphasic membrane consisting of poly(ϵ -)caprolactone (PCL) and gelatin with tunable physicochemical and biological properties guided by the characteristics of the alveolar basement membrane of the lung. As validation of the membrane, we used the newly developed **CIVIC** (Cyclic *In Vitro* Cell-stretch) cell-stretch bioreactor to study the cellular responses due to cyclic stretch with respect to the formation of F-actin cytoskeleton and tight junction, cell apoptosis, inflammatory response (IL-8) activity, and apparent permeability of an alveolar epithelial cell-layer. We also investigated the cellular uptake of particles (nano- and microparticles) by alveolar epithelial cells cultured at the ALI under more physiologically relevant conditions (cyclic mechanical stretch and medium flow) as compared to static conditions.

CONTRIBUTION

The fundamental biphasic membrane concept was developed by my supervisor (Otmar Schmid) and me. The two materials (PCL and gelatin) were selected by my supervisor (Otmar Schmid) and me based on a thorough review of currently available porous, elastic

membranes used for *in vitro* cell-stretch models of the alveolar barrier, which we recently published (see paper IV in the Appendix (Doryab et al., 2019)). My supervisor and I designed the experiments. I conducted all of the experiments, recorded the data and provided an initial analysis. I designed and manufactured the BETA membrane involving an extensive optimization process. I implemented a design of experiment (DoE) approach using the response surface methodology (RSM)– central composite design (CCD), to co-optimize physicochemical properties of the membrane. I characterized the physical (thickness, wettability, and porosity), mechanical (elastic modulus, modulus of resilience, and stretchability) properties, and lung epithelial cells (A549 and 16HBE14o–) cytocompatibility (cell viability and attachment) of the membrane. For the membrane characterization, I performed scanning electron microscopy (SEM), energy dispersive x-ray spectroscopy (EDS)/SEM, focused ion beam (FIB)/SEM, and Fourier transform infrared spectroscopy (FT-IR). I did a uniaxial tensile test to measure the mechanical properties of the membranes. I also measured the water contact angle (WCA) of the membranes to study their surface wettability. Moreover, I quantified the porosity (and the pore size) of the membranes using both the liquid displacement method and quantification of the SEM images (in phase II).

In addition to the membrane fabrication, I technically optimized the MALI (Moving Air-Liquid Interface) bioreactor system that now it is referred to as **CIVIC** (**Cyclic In Vitro Cell-stretch**) mainly with respect to the real-time monitoring of the stiffness (elastic modulus) of the membrane during the cell-stretch experiment. More details of the optimization of the CIVIC and MALI bioreactor systems were published in paper II and III, respectively. I also performed all the cell experiments under both static and cell-stretch conditions, including seeding and growing lung epithelial cells (A549 and 16HBE14o–) on the BETA membrane and Transwell[®] insert, following by cell proliferation and cell viability assay (WST1). Furthermore, I analyzed biological endpoints using different methods, including immunofluorescence, confocal laser scanning microscopy (CLSM; both qualitative and quantitative via processing and quantification of images), SEM, qualitative elemental and

chemical microanalysis using EDS/SEM, FIB/SEM tomography for site-specific analysis, *in vitro* functional analysis (Trans-epithelial electrical resistance (TEER) measurement and apparent permeability), and measurement of pro-inflammatory IL-8 release. Moreover, I conducted particle (nanoparticle and microparticle) studies and investigated cell uptake of particles. I performed all the Immunofluorescence staining (F-actin, ZO-1, collagen I, cell nuclei, and particles), and CLSM image acquisition. I also processed and quantified all the CLSM, SEM and SEM/FIB images using FIJI (NIH) and IMARIS software.

Together with my supervisor, the analysis was refined and the data were interpreted. I also carried out all the statistical analysis using GraphPad Prism and Minitab software. My supervisor and I designed all of the figures. I generated all of the figures and prepared a complete first draft of the manuscript, which was then revised by my supervisor. His requested modifications were implemented by me and I then uploaded the manuscript to the journal webpage. I assisted my supervisor with the writing of the point-by-point rebuttal letter and the revision of the manuscript.

1.2 Contribution to Paper II

A Bioinspired *In Vitro* Lung Model to Study Particokinetics of Nano-/Micro-particles under Cyclic Stretch and Air-Liquid Interface Conditions

Ali Doryab, Mehmet Berat Taskin, Philipp Stahlhut, Andreas Schröppel, Sezer Orak, Carola Voss, Arti Ahluwalia, Markus Rehberg, Anne Hilgendorff, Tobias Stöger, Jürgen Groll, Otmar Schmid. 2021. *Frontiers in Bioengineering and Biotechnology* 9: 42. <https://doi.org/10.3389/fbioe.2021.616830>

SUMMARY

In this paper, we described more precisely the optimization of the **CIVIC** (Cyclic *In Vitro* Cell-stretch) lung bioreactor system as compared to the original so-called MALI bioreactor (see paper III (Appendix)), which is able to mimic culture conditions for pulmonary epithelial cells at the air-liquid interface (ALI) experiencing cyclic stretch with aerosol delivery. The modifications are mainly related to improved geometry, material stability (silicone-free), (BETA) membrane fixation, and pressure sealing, and the real-time monitor the stretch-related parameters (amplitude, frequency, and elastic modulus of the membrane). Moreover, we presented further BETA membrane characterizations. We also tried but failed to improve the biomimetic features of the BETA membrane by changing the mixing ratio of copolymer (PCL/gelatin) composition. We also investigated the role of physiologic cyclic mechanical stretch on uptake of nano- (100 nm) and microparticles (1000 nm) by A549 epithelial cells cultured at ALI and trans-epithelial transport of particles across the epithelial cell barrier.

CONTRIBUTION

My supervisor and I designed the experiments. I conducted all of the experiments, recorded the data, and provided an initial analysis. Together with my supervisor, the analysis was refined and the data were interpreted. I carried out all the statistical analysis using GraphPad Prism. My supervisor and I designed all of the figures. I made all of the

figures and prepared a complete first draft of the manuscript, which was then revised by my supervisor. His requested modifications were implemented by me and I then uploaded the manuscript to the journal webpage. I assisted my supervisor with the writing of the point-by-point rebuttal letter and the revision of the manuscript.

More specifically, I modified the BETA membrane in terms of its chemical composition, permeability, elasticity (elastic modulus and stretchability), and bioactivity. In paper I, we determined the optimum concentration of the membrane compound (poly(ϵ -)caprolactone and gelatin). In this paper, we explored a higher range for component concentration to further optimize the membrane. I performed atomic force microscopy (AFM), scanning electron microscopy (SEM), energy dispersive x-ray spectroscopy (EDS)/SEM, focused ion beam (FIB)/SEM, uniaxial tensile test, water contact angle measurement, and liquid displacement test (porosity) to analyze the physicochemical properties of the membrane.

I developed the MALI (Moving Air-Liquid Interface) bioreactor system that now it is referred to as CIVIC. Since the working volume of the CIVIC bioreactor is in the range of “milliliter”, we can then refer to this bioreactor as a “*millifluidic*” system (as compared to smaller-scale, microfluidic systems). In this version, the millifluidic system was modified to improve its efficiency and handling. The modifications include designing and manufacturing the new membrane holder and the vacuum sealing, changing the material of the bioreactor (silicone-free), and the new membrane for culturing cells at ALI. I also performed all of the cell experiments including seeding and growing cells (A549 and 16HBE14o-) on the BETA membrane and Transwell[®] insert, following by cell proliferation and cell viability assays (WST1 and LDH assays), Immunofluorescence, confocal laser scanning microscopy (CLSM), and SEM. I also measured the TEER of the established epithelial cell layer as a functional analysis. I also processed and quantified all the CLSM, SEM and SEM/FIB images using FIJI (NIH) and IMARIS software. Moreover, I conducted particle and particokinetic studies. I investigated the role of physiologic cyclic mechanical stretch on cellular uptake and transepithelial transport of nanoparticles (100

nm) and microparticles (1000 nm). I exerted qualitative and quantitative CLSM to study the cellular uptake and transepithelial transport of particles. I performed all the Immunofluorescence staining (F-actin, E-cadherin, ZO-1, cell nuclei, and particles), CLSM image acquisition, processing, and quantification.

1.3 Contribution to Paper III

Development of a Dynamic *In Vitro* Stretch Model of the Alveolar Interface with Aerosol Delivery

Daniele Cei[#], **Ali Doryab[#]**, Anke-Gabriele Lenz, Andreas Schröppel, Paula Mayer, Gerald Burgstaller, Roberta Nossa, Arti Ahluwalia, Otmar Schmid. 2021. *Biotechnology and Bioengineering*. 118 (2): 690–702.

<https://onlinelibrary.wiley.com/doi/10.1002/bit.27600>

([#] share first authorship)

SUMMARY

In this paper, we described the engineering and computer-aided methods of design and performance characterization of a Moving Air-Liquid Interface (MALI) bioreactor for the study of aerosol deposition on a cyclically stretched, “breathing” *in vitro* model of the lung. As a proof of concept, we showed that lung epithelial cells (A549) can be mechanically stimulated under air-liquid interface and physiologic stretch conditions without loss of cell viability.

CONTRIBUTION

As the *shared co-first author* of this research paper, I performed aerosol delivery measurements in the MALI system for different nebulizer duty cycles. I also analyzed aerosol dosimetry and aerosol deposition (delivery) efficiency data and depicted the results in Figure 4. I also cultured A549 and 16HBE14o– on the commercial Bionate[®] electrospun membrane, which was the only membrane used in this paper. For evaluation of the cell viability, I performed all of the Immunofluorescence staining (F-actin and cell nuclei) and CLSM analysis (image acquisition and processing) of the A549 cells on the Bionate[®] membrane (Figure 7). I also evaluated the attachment of 16HBE14o– cells to the electrospun membrane using SEM analysis (Supplementary Figure S9). Moreover, I prepared Figure 5 and Supplementary Figure 8 (image processing).

I assisted my supervisor in writing the manuscript and analyzing data both for the initial submission and implementation of the reviewer-requested revision, which included the revised and supplementary information. Moreover, I assisted with writing the point-by-point rebuttal letter.

1.4 Contribution to Paper IV (Appendix)

Evolution of Bioengineered Lung Models: Recent Advances and Challenges in Tissue Mimicry for Studying the Role of Mechanical Forces in Cell Biology

Ali Doryab, Sinem Tas, Mehmet Berat Taskin, Lin Yang, Anne Hilgendorff, Jürgen Groll Darcy E. Wagner, Otmar Schmid. 2019. *Advanced Functional Materials*. 29 (39):1903114. <https://onlinelibrary.wiley.com/doi/abs/10.1002/adfm.201903114>

SUMMARY

In this review paper, we summarized the role of mechanical stretch in lung biology, disease, and regeneration. Then, the key technical aspects of currently available *in vitro* cell-stretching devices with a focus on lung models (including lung-on-a-chip) were presented, which identifies the lack of suitable membranes for cell growth at the air-liquid interface as key aspect hampering progress in this field. Subsequently, the main physiologic parameters of the native basal membrane of the alveolar-capillary tissue were defined as guidance for future membrane design. This paper offers a glimpse on future perspectives for evolving the cell-stretching membrane technology as a determinative factor of more advanced, biomimetic *in vitro* models of the lung and other stretch-related tissue models.

CONTRIBUTION

Together with my supervisor, we determined the main direction of the manuscript. I prepared a complete first draft of the manuscript, which was then revised by my supervisor. My supervisor and I designed all of the figures and I generated all of the figures/schematics and his requested modifications were implemented by me and I then uploaded the manuscript to the journal webpage. I assisted my supervisor with the writing of the point-by-point rebuttal letter and the revision of the manuscript.

1.5 Contribution to other publications

During my PhD project, I contributed to two side projects.

In *Bölükbas et al. (Advanced Therapeutics 2020)*, we showed the organ-restricted vascular delivery (ORVD) enhances tumor cell-specific uptake of nanoparticles at cellular resolution. I assisted the lead authors with the organ-restricted vascular delivery (ORVD) by designing and manufacturing an *ex vivo* lung perfusion and ventilation system. We described the detail of the *ex vivo* lung perfusion system in (Bölükbas et al., 2019).

In *Costa et al. (British Journal of Pharmacology; under revision)*, we studied the regenerative potential of FDA-approved compounds for Wnt/ β -catenin signaling in murine adult epithelial cell-derived lung organoids and *in vivo* model of chronic obstructive pulmonary disease (COPD). We found that amlexanox, an approved drug with potential for COPD treatment, can rapidly translate into the clinics. I assisted the lead author with the lung organoids quantification.

2. Introductory summary

Chronic respiratory diseases are one of the leading causes of death with almost no effective cure. The failure rate of successfully preclinically tested drug in clinical studies which is high probably, at least partially due to the lack of effectiveness of preclinical models. The failure of missing therapies might in part be owed to the inefficiency of the current *in vivo* and *in vitro* lung models to develop therapies since the mechanisms underlying chronic lung diseases and their pathogenesis are poorly understood. Thus, over the last decades, numerous *in vitro* models for the lung –as an alternative for animal models– have been developed from simple monoculture to complex microfluidic co-culture models of the lung, often referred to as airway- or even lung-on-a-chip models; however, none of them could completely emulate the intricacy of the lung microenvironment and architecture, hampering the progress in finding the cures for lung diseases. We, therefore, intended to contribute to the development of more physiologically relevant and robust *in vitro* lung models for improving the translation of preclinical research into a more reliable prediction of clinical outcome in human studies.

Here, we present a next generation of the cell-stretch bioreactor system for pulmonary/alveolar epithelial cells cultured at the air-liquid interface (ALI) –with potential applicability to multi-coculture models– equipped with an aerosolized drug delivery unit and a biomimetic copolymeric membrane, resembling the main physico-mechanical characteristics of the alveolar basement membrane. The main emphasis of this dissertation lies on (i) technical improvements of the bioreactor with particular focus on real-time monitoring of stretch-related characteristic parameters (amplitude, frequency, and membrane stiffness), (ii) introduction of the concept, design and manufacturing of a novel biphasic, elastic, and porous membrane for more biomimetic cell culture, and (iii) develop a bioinspired *in vitro* model for particokinetic study (nano-/microparticles) on pulmonary lung epithelial barrier under cyclic mechanical stretch and ALI culture conditions. With these technologies, we confirmed the well-known pivotal role of cyclic mechanical stretch on alveolar epithelial cell physiology for both physiologic and non-physiologic (over-) stretch

conditions, including the formation of F-actin cytoskeleton and tight junction integrity, activation of the inflammatory response (IL-8), and permeability. Moreover, particokinetic studies demonstrated that cyclic physiologic stretch can significantly affect cellular uptake and transepithelial transport of nanoparticles. We believe this study presents a valuable step towards the improvement of the predictive value of advanced lung cell models.

2.1 Definition of problem and aim of the study

The lung is a vital organ in the human body with the main function of oxygen-carbon dioxide exchange between inhaled air and blood. The organ characteristics of the human lungs emphasize its critical function. The lung is the largest organ in the body, comprising only half of a liter of tissue, which is built to have a huge gas exchange surface area (100 m^2) –ca. half of the size of a tennis court. This superior design i.e. limited space for locating the lung in the chest cavity with large epithelial tissue surface area, requires an extremely intricate structure (Weibel, 2009) (Figure 1A). The lung has a complex architecture partitioned into 23 generations of branching, encompassing from trachea (generation $z = 0$), bronchioles ($z = 4$), terminal bronchioles ($z = 15$) to alveolar ducts and sacs ($z = 20-23$) (Figure 1B) (Weibel, 1963). The respiratory bronchioles are further divided into acinar airways ($z = 16-23$), which is included of respiratory bronchioles ($z = 16-18$), alveolar ducts ($z = 19-22$), and alveolar sacs ($z = 23$). The alveoli have a complex 3D structure where the gas exchange occurs via the large air-liquid interface (ALI) presented by the huge surface area of the alveolar tissue (Gil et al., 1979; Weibel, 1963). The tissue barrier separating air and blood consists of two cell layers, the alveolar epithelium and the capillary endothelium (Figure 1A), attached to the alveolar basement membrane. This tissue layer is an ultrathin (alveolar-capillary barrier thickness is $\approx 1.1 \mu\text{m} \pm 0.1$; harmonic mean), which also includes the basement membrane (ca. $0.1 \mu\text{m}$) consisting of small fibrils of collagen and elastin and occasionally occurring fibroblasts (Weibel, 1970, 2009). The alveolar epithelium consists of the squamous type I cell,

covering 97% of the alveolar surface and providing the area for gas exchange, and the cuboidal type II cell (only $\approx 5\%$), a progenitor of type I cells, which are responsible for synthesis and secretion of surfactant and homeostasis (Castranova et al., 1988; Crapo et al., 1982).

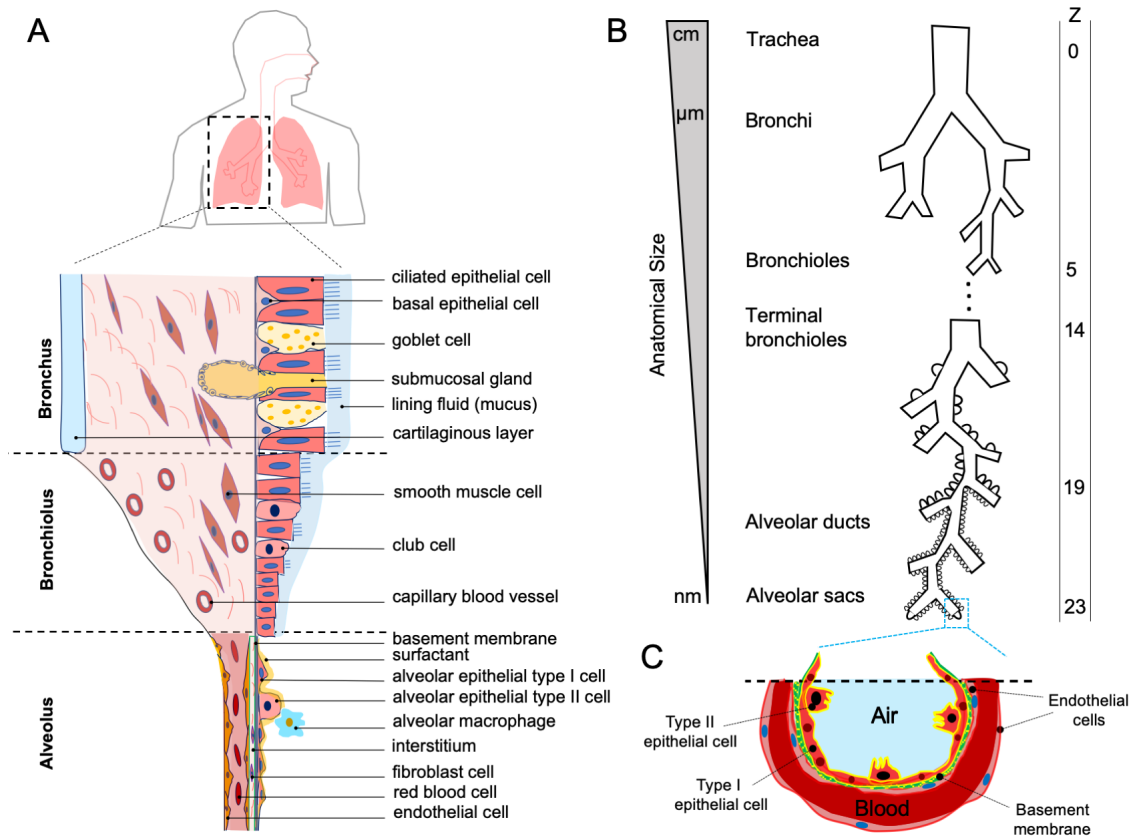


Figure 1. Lung morphology, cellular structure, and architecture (A) Schematic of the cellular composition of the human airway tree from bronchus to alveolus. In the alveoli, a thin layer (membrane) of small fibrils of collagen and elastin (and rare fibroblasts) separates the epithelial and endothelial cell layers. (B) Schematic of airway branching in human lung, starting from the trachea (generation $z=0$), over bronchi and terminal bronchioles (Conducting airway; $z=1-14$), to alveolar ducts and sacs (Acinar airways; $z=20-23$). The anatomical size (diameter) decreases from cm (trachea) to nm (alveolar sacs). (C) The lung alveolar region consists of alveolar epithelial type I and II (airside) and epithelial side (in the blood side) with an ultrathin basement membrane (thickness of gas exchange region is ca. $0.1 \mu\text{m}$), which separates epithelial and endothelial cell layers. A thin layer of surfactant ($<0.1 \mu\text{m}$) covers the epithelial cells to lessen surface tension and hence prevent the collapse of the alveoli. A and C were reproduced with permission from (Doryab et al., 2021b). Panel B was inspired by Weibel et al. (Weibel, 1963), reproduced with permission).

What makes the lung an extremely complicated organ to be modelled *in vitro*? In the gas exchange region of the lung (alveolar-capillary barrier, 1 μm thick), a micro-scale membrane (thickness of ca. 0.1 μm) separates alveolar epithelial cells (airside) from capillary endothelial cells (blood side) (Figure 1C). This membrane has extraordinary physico-mechanical properties including significant high stretchability and permeability while maintaining structural integrity, providing the delicate alveolar sac structure.

This membrane/scaffold mostly consists of extracellular matrix (ECM) proteins. ECM is a fiber-like network of proteins and polysaccharides, which surrounds the cells. The important roles of ECM are structural support for cells and the transport of nutrients and biomolecules. Furthermore, ECM provides a unique microenvironment for cells, which can be highly variable depending on cell type and location. However, a simplified version of the ECM is typically employed in even the most advanced *in vitro* lung models, which acts as a passive cell-substrate only without reflecting special characteristics of the ECM (Doryab et al., 2019). In addition to the exceptional architecture of the lung tissue, which is difficult to recapitulate *in vitro*, pulmonary cells are exposed to a cyclic mechanical stretch-induced by breathing. The microenvironment of epithelial cells along with a physiologic cyclic mechanical stretch at ALI provides a more realistic model of the lung than most currently available *in vitro* models of the lung.

The complexity of imitating the main features of culture conditions for the lung cells has prevented researchers from bioengineering a more physiological *in vitro* model of the lung for studying respiratory disease under biomimetic conditions. As a result of the lack of proper *in vitro* lung models, there are currently no cures for chronic lung diseases – only symptomatic therapies and lung transplantation for end-stage disease patients (Beasley et al., 2015; May and Li, 2015). The absence of therapeutic approaches is also contributing to the exponentially increasing expenditure involved in respiratory disease. For instance, *in Germany only*, the mean annual direct and indirect costs for chronic obstructive pulmonary disease (COPD) grades 1-4 was estimated as 115,581 € per patient in 2012 with an increase factor of 2.5-5.7 in annual healthcare costs (based on the

cohort of COSYCONET, 2,139 COPD patients) while the total cost for healthy people (for participants aged < 65 years only) was 7,983 € (Wacker et al., 2016).

With the current project, we aimed to improve the predictive value of advanced lung cell models through improved membrane technology with more biomimetic features. In this project, an ultra-thin membrane ($\leq 5 \mu\text{m}$) has been developed, mimicking the main characteristics of the cell-substrate in the alveolar epithelial cells. We characterized the physical and mechanical properties as well as bioactivity of the manufactured membrane. The findings showed that the membrane is permeable and stretchable enough to emulate the properties of the ECM of the lung. The membrane provides a biomimetic environment for cellular attachment and proliferation of lung epithelial cells by granting cell-responsive motifs such as arginine-glycine-aspartic (RGD) and stimulating the physiologic secretion of ECM proteins by the resident cells themselves. The developed membrane provides the basis for an advanced *in vitro* lung model for studying the implications of cyclic mechanical stretch (physiologic and non-physiologic) on cell physiology.

Nanoparticles can serve as drug carriers for the targeted therapeutics in cancer therapy and delivery of proteins, protein-based materials, and antibiotics (Bölükbas et al., 2020; Pontes and Grenha, 2020). It has been shown that the mechanical forces such as cyclic stretch and shear stress induced by medium flow affect the cellular uptake and transport of nanoparticles across the biological barriers (Freese et al., 2014; Huh et al., 2010; Schmitz et al., 2019). The advanced biomimetic *in vitro* lung model enables us to study the effect of cyclic mechanical stretch on cell-nanoparticle interactions i.e. cellular uptake and transbarrier transport (particokinetics) of aerosolized nanoparticles on a pulmonary tissue barrier, which were cultured at ALI.

2.2 Previous studies

Animal models are playing a pivotal role in pre-clinical drug discovery and development since they allow us to study the biologically complicated responses of drugs in complex organisms under *in vivo* conditions by providing physiologic tissue-tissue and organ-

organ interaction. Nevertheless, it has been estimated that up to 96% of the drug testing in preclinical animal models fails in clinical settings (patients) because of the lack of effectiveness and safety problems (Akhtar, 2015; Matthews, 2008). Unreliable extrapolation from animals to humans is mainly due to the species differences in biological mechanisms (Pound and Ritskes-Hoitinga, 2018).

Over the last decades, many efforts have been made to improve the biomimicry level of the *in vitro* models of the lung –as an alternative to animal models. Conventional *in vitro* lung cell models rely on static submerged culture conditions, where cells are completely covered with cell culture medium, preventing them from polarization and secretion of a protective lining fluid such as mucus or surfactant (Doryab et al., 2019). Lately, ALI cell culture systems mainly based on Transwell® technology have been introduced, where epithelial cells are cultured on a porous membrane (such as PET (polyethylene terephthalate) and PC (polycarbonates)), with air on the apical side and cell culture medium on the basal side, offering more physiologic conditions. Under ALI conditions, epithelial cells can polarize and secrete the protective liquid layer such as surfactant (Birkness et al., 1999; Gueven et al., 1996; Heise et al., 2011; Liu et al., 1995; Trepap, 2006; Trepap et al., 2004). Nevertheless, these membranes are rigid and are not able to mimic the structural integrity and high elasticity of the ECM (or cell-substrate) of the lung.

The lung as a dynamic organ experiences cyclic mechanical stretch due to breathing activity, which is under both physiological and non-physiological conditions, playing a key role in the physiology of alveolar epithelial cells (Doryab et al., 2019). Numerous investigations have suggested that several stretch-induced biological endpoints can be activated/mediated during cell-stretch such as secretion of surfactant proteins, cell proliferation, apoptosis, activation of pro/inflammatory responses, and permeability (Figure 2). Among them, secretion of surfactant proteins by alveolar epithelial cells is one of the main stretch-activated endpoints via triggering of the transcription factor-dependent protein kinase (cAMP-PKA-dependent) signaling pathway and Ca²⁺–regulated mechanisms (Arold et al., 2009; Nakamura et al., 2000; Sanchez-Esteban et al., 1998; Scott et al.,

1993; Wang et al., 2006; Wirtz and Dobbs, 1990). Mechanical stretch under physiologic and non-physiologic strain can stimulate extracellular signal-regulated protein kinases 1 and 2 (ERK1/2), which are members of the mitogen-activated protein kinase (MAPK) family, mediating cell proliferation and apoptosis (Chaturvedi et al., 2007; Chess et al., 2000; Edwards et al., 1999; Felder et al., 2019; Hammerschmidt et al., 2004; Kuhn et al., 2017; McAdams et al., 2006; Savla and Waters, 1998; Stucki et al., 2015; Tschumperlin and Margulies, 1998).

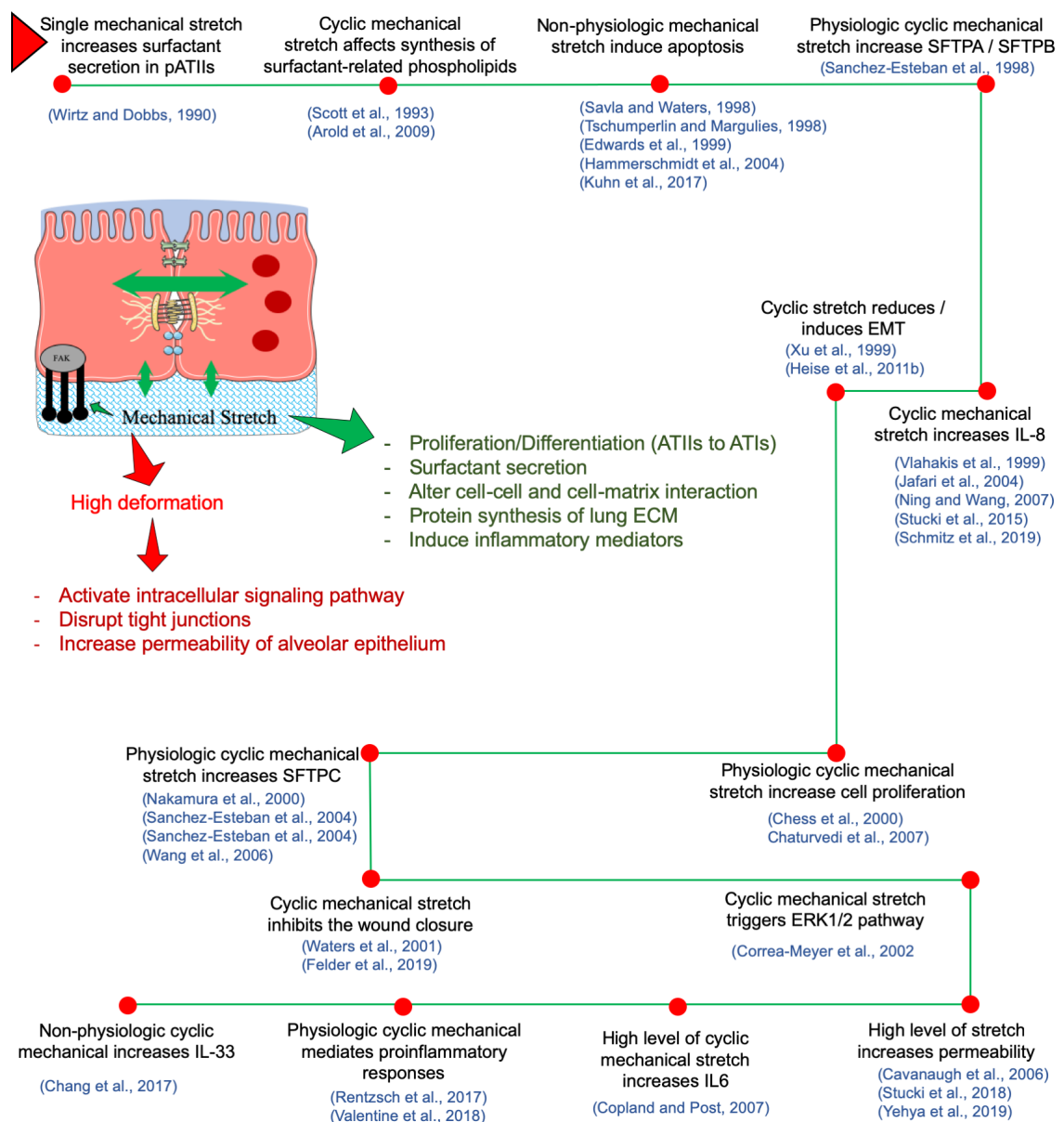


Figure 2. Effects of (cyclic) mechanical stretch on lung epithelial cell physiology observed under *in vitro* conditions. The cell schematic has been reproduced with permission from (Doryab et al., 2019).

It has been also shown that the cyclic mechanical stretch can provoke pro-inflammatory (Rentzsch et al., 2017; Valentine et al., 2018) and inflammatory responses (Chang et al., 2017; Copland and Post, 2007; Jafari et al., 2004; Ning and Wang, 2007; Schmitz et al., 2019; Stucki et al., 2015; Vlahakis et al., 1999) in both physiologic or non-physiologic range in the lung alveolar epithelial cell.

Furthermore, paracellular and transcellular transport of small molecules across the epithelial cell barrier are increased under short term cell-stretch conditions at 37% $\Delta SA/SA$ (relative change in surface area, 10-60 min (Cavanaugh et al., 2006; Yehya et al., 2019)) or long-term cell-stretch (21-72h) at a physiologic amplitude and rate ($\approx 8-10\%$ linear or 16-21% $\Delta SA/SA$, at 0.2 Hz) (Stucki et al., 2015, 2018). The majority of these *in vitro* investigations used available commercial cell-stretch technologies (e.g. Flexcell® FX-6000™ Tension System; Flexcell Intl. Corp., USA) (Figure 3), which are suitable for submerged culture conditions only.

More recently, several lung-on-a-chip technologies have been proposed most notably the ground-breaking work by the WYSS Institute of Harvard University, USA, which is able to coculture lung cells not only under cyclic stretch but also at ALI culture (Huh et al., 2010; Jain et al., 2018; Li et al., 2019; Si et al., 2020) (Figure 3). Typically, these microchip devices are comprised of polydimethylsiloxane (PDMS) apical and basal cell culture chambers that are separated by a thin porous membrane, on which cells are cultured (Doryab et al., 2016; Huh et al., 2010). Some of these platforms can also provide a relevant medium/blood flow to mimic both blood movement and breathing-induced mechanical stretch. These microfluidics systems or similar airway-on-chip are evidence of a great technological advancement as compared to the conventional 2D ALI culture models on static, rigid porous membrane to the extent that they recently are being considered as an alternative for animal models for the repurposing of FDA-approved drugs as possible therapeutics for *Coronavirus disease 2019* (COVID-19) (Gard et al., 2020; Ingber, 2020; Si et al., 2020).

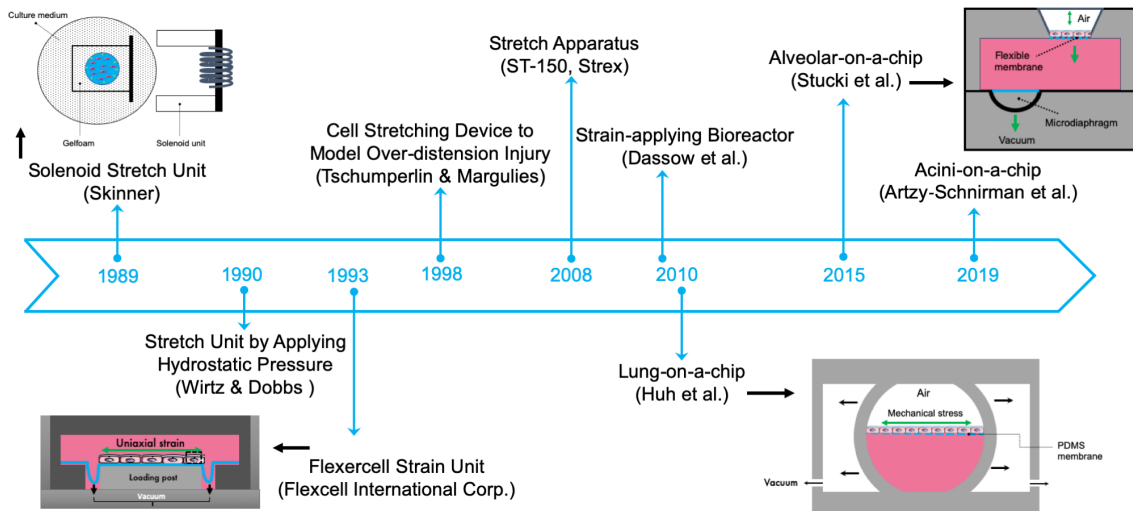


Figure 3. Advancement of cell stretch devices employed in studies on cell and tissue models of the lung (*in vitro*). Schematics have been reproduced with permission from (Doryab et al., 2019).

Despite these recent innovations, more investigations are required to address several critical drawbacks of these microfluidic devices. In these platforms, a porous/permeable PDMS-based membrane is employed as a cell-substrate (or ECM). PDMS is considered chemically inert and provides suitable mechanoelastic properties. However, PDMS is not cell-friendly since it has hydrophobic nature, which requires surface treatment prior to cell seeding such as chemical and physical modification or coating with ECM proteins (e.g. collagen) to allow for cell attachment and growth. This may be seen as an obvious flaw of ECM-coated PDMS membranes since the aggregation and/or dislodgment of cells from PDMS membranes frequently happens, especially for long-term culture and/or stretch conditions (Chuah et al., 2016). PDMS also absorbs lipophilic drugs (passive drug absorption) and adsorbs some natural biomolecules and pharmaceutical agents in the culture medium as a thin layer on the surface of the PDMS membrane, which can interfere with drug studies, mitigate cell viability and impair the predictive capacity of *in vitro* testing concerning clinical relevance. It has been shown that the level of passive drug absorption by the PDMS is comparable with fat absorption in some cases e.g. nicotine and cisplatin in human gut-liver-kidney chips modeling (Herland et al., 2020).

Hence, the performance of PDMS-based systems has to be tested for different drugs. Furthermore, PDMS can release cell-toxic substances (Carter et al., 2020; Regehr et al., 2009), which may affect the cell physiology probably cell apoptosis.

Lately, alternative synthetic/natural scaffolds have been fabricated with a thickness range of ≈ 20 -200 μm and proper properties for lung cells mainly using electrospinning. These hybrid electrospun scaffolds showed promising results for adherence and proliferation of lung cells. For instance, poly-L-lactic acid (PLLA)/ decellularized pig lung ECM (PLECM) (Young et al., 2017), poly(ϵ -caprolactone) (PCL)/ star-shaped polyethylene glycols (sPEG) functionalized with biomolecules (Nishiguchi et al., 2017), and PCL/ gelatin (Higuera-Castro et al., 2017) have presented the advantage of employing natural polymers in combination with synthetic polymers to obtain a membrane with superior physico-mechanical properties. The stretchability of these scaffolds/membranes, however, has not been tested yet since these scaffolds were used only under static (unstretched) cell culture conditions. Besides, these alternative membranes are mainly rigid, which cannot mimic the stiffness of ECM and connective tissues in the alveolar region. This aspect is particularly important especially for mimicry of specific lung disease in the lab such as pulmonary fibrosis. Although enormous efforts have been invested in the development of a tunable membrane/scaffold for the lung epithelial cells, several key biomimetic features are still missing, including thickness, stretchability, permeability, and stiffness. As mentioned above, each of these parameters directly or indirectly impacts on cell micro-environment, causing adverse effects on cell functions.

2.3 Overview of our approach

The current Ph.D. project aimed to (i) manufacture and validate a biomimetic stretchable porous membrane highly conducive to the growth of pulmonary cells, (ii) optimize cell growth and viability under both static and dynamic conditions, (iii) study the effects of dynamic conditions on cell physiology, and (iv) investigate the effect of cyclic mechanical

stretch on cellular uptake and transbarrier transport (particokinetics) of aerosolized nano- and microparticle on a pulmonary tissue barrier.

During this project, we have modified the cell-stretch Moving Air-Liquid Interface (MALI) bioreactor –which was originally developed as part of the Ph.D. thesis by Daniele Cei under the supervision of Otmar Schmid and Arti Ahluwalia (University of Pisa, Italy) (Cei, 2015; Cei et al., 2021)– that is now referred to as **CIVIC** (**C**yclic **I**n **V**itro **C**ell-stretch) bioreactor. This millifluidic bioreactor system or “breathing” *in vitro* model of the lung was designed to mimic the culture conditions of the alveolar tissue barrier in the lung, for the study of the role of cyclic mechanical stretch on cell physiology under physiologic and pathophysiologic stretch conditions (Figure 5A). The CIVIC system also allows for aerosolized delivery of liquid drugs (here: nano- and microparticle suspensions) and encompasses a medium flow/ perfusion to recapitulate blood movement associated with shear stress applied to the basal side of the cells. A recently added feature of the CIVIC system is the implementation of two pressure sensors to monitor the stretch profile (amplitude and frequency) and the elastic modulus of the membrane in real-time, which is a unique feature of this cell-stretch lung bioreactor.

We equipped the CIVIC bioreactor system with a biphasic ultrathin BETA membrane (BETA: **B**iphasic **E**lastic **T**hin for **A**ir-liquid culture conditions) for models of the alveolar air-blood barrier (*European patent application was filed by INNO, HMGU on 24.11.2020*) to overcome the limitations of PDMS (polydimethylsiloxane) or PET (polyethylene terephthalate) membranes, which are commonly used in ALI culture and/or cell-stretch system (Figure 5A).

The conceptual idea of the biphasic membrane was inspired by the two distinctly different membrane characteristics required during the two phases of *in vitro* cell-stretch experiments with epithelial cells of the lung, namely (i) the initial phase of cell seeding and proliferation (under static and submerged conditions) and (ii) the culture of cells at ALI and cyclic mechanical stretch conditions (Figure 5B). During *phase I*, the membrane should be wettable and conducive to cell growth (surface hydrophilicity) to support initial

adhesion and cell growth. After the formation of a cell monolayer, the cells are air-lifted in *phase II* of cell culture, which requires a permeable membrane (low thickness with suitable porosity), allowing for contact with air from the apical side and transporting nutrient/growth factors supply to the cells through the pores of the membrane (from basal to apical side) (Figure 1C). After polarization of cells at ALI conditions, the cells are exposed to a cyclic cell-stretch, demanding not only a porous but also a flexible/stretchable membrane to endure cyclic stretch.

In addition to this bifunctional characteristic, a suitable membrane for culturing pulmonary epithelial cells undergoing cell-stretch should meet a broad range of requirements including cytocompatibility, wettability, switchable permeability, and durability. We screened various polymers as candidate materials for stretchable and porous membranes (See *Table 4* of paper IV). Natural-derived polymers such as gelatin and collagen are greatly used for remodeling *in vitro* tissue models due to their high bioactivity and cytocompatibility. Nevertheless, the application of natural-derived polymers in scaffold fabrication is limited due to (mainly) their low mechanical properties. The blends of natural and synthetic-derived polymers, however, have been shown tunable mechanical (elastic modulus and reversible strain) and physical (porosity, thickness, and wettability) properties (more detail can be found in section 4.3. *Material Selection* of paper IV). After evaluating various natural and synthetic-based polymers, we concluded that a hybrid copolymer (natural-synthetic) consisting of poly(ϵ -)caprolactone (PCL) and gelatin is the superior candidate for a biomimetic membrane used in pulmonary cell-stretching models with a combination of physicommechanical and cytocompatibility properties (Figure 4). Gelatin is a water-soluble and bioresorbable polymer, which is widely employed in the field of tissue engineering and regenerative medicine due to its high cytocompatibility, tunable biophysical properties, abundance of cell-responsive motifs, easy to access, and reproducibility. PCL is an FDA-approved biodegradable, biocompatible, and bioresorbable polymer. By using gelatin as sacrificial material which initially fills the pores of the PCL membrane but is gradually dissolved during contact with cell culture medium, the

initial non-porous, stiff membrane gradually transitions into a porous elastic membrane, which matches the requirements during phase I and phase II of cell-stretch experiments as described above. In sum, a biomimetic membrane (BETA) was tailored to mimic the main physicochemical characteristics similar to the ECM of the lung alveolar region (Figure 4) and to improve the cell adherence and proliferation of the lung epithelial cells.

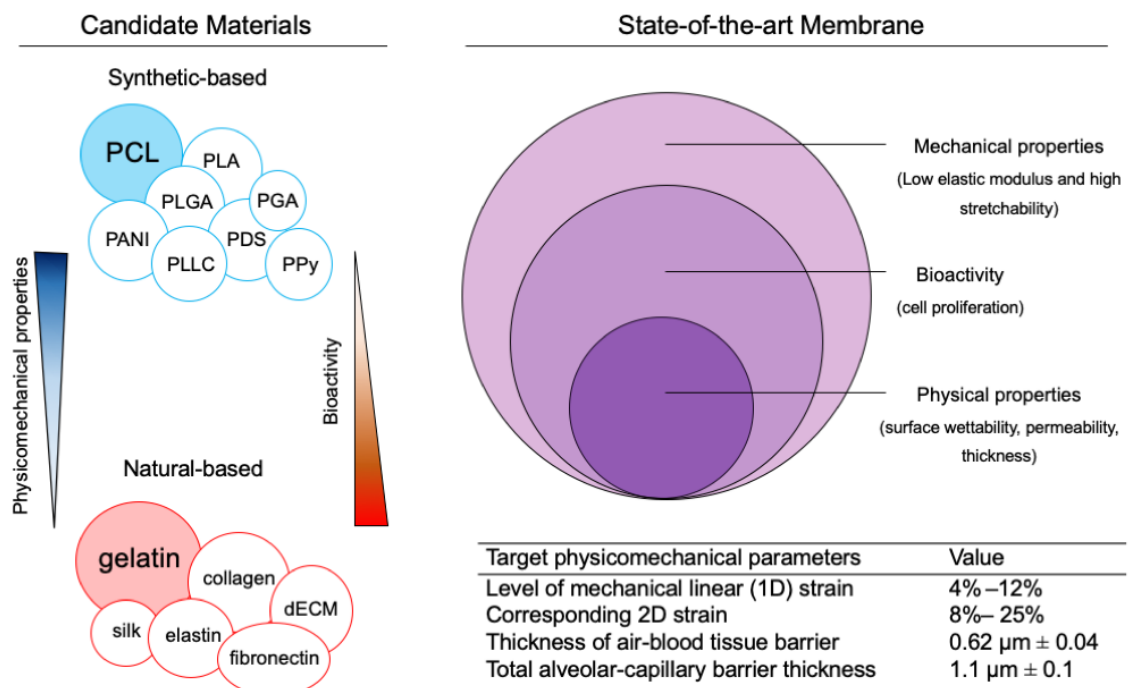


Figure 4. The state-of-the-art membrane for alveolar tissue. The candidate materials (both synthetic and natural-based) were screened based on their physical, mechanical, and bioactivity characteristics. The natural-synthetic copolymers are favorable candidates for suitable stretchable membranes, mimicking human alveolar tissue. A suitable membrane should have both biomimetic physicochemical and bioactivity properties. These properties include stretch- and permeability-related physiologic parameters as listed in the table, which was reproduced with permission from (Doryab et al., 2019).

As an application of the BETA membrane and the CIVIC bioreactor system, we investigated the role of cyclic mechanical stretch (both physiologic and non-physiologic) on the cell physiology such as F-actin and tight junction formation, cell layer permeability, and

inflammatory responses (IL-8) (Figure 5B). This revealed that tight junctions (ZO-1) are formed and oriented along the stretch direction under a physiologic stretch while non-physiologic (over-)stretch may disrupt the tight junction formation. We also showed that the cyclic cell-stretch can increase the permeability of the cell layer as well as the release of IL-8.

Exploiting more physiologically relevant cell models could affect cell–nanoparticle interactions, altering the fate of nanoparticles after administration to the body i.e transbarrier transportation through biological barriers such as air-blood. In addition, the pharmacokinetics profiles of particles (e.g. time-resolved drug concentration in the blood after drug inhalation) are a mandatory part of clinical trials for regulatory approval of drugs. We, therefore, performed particle transport studies (nanoparticles (100 nm) and microparticles (1000 nm)) under unstretched and physiologically stretched conditions. The data suggest that a physiologic stretch can increase cellular uptake and internalization/trafficking of nanoparticles (100 nm), resulted in higher transcytosis.

A summary of the advantages of the CIVIC and BETA technology as well as an overview of the main properties of the optimized BETA membrane and the effect of cyclic stretch on nanoparticle transport across an alveolar barrier model is presented in Figure 5. To the best of our knowledge, this is the first investigation of the effect of cyclic stretch on transbarrier transport of aerosolized particles deposited on an *in vitro* alveolar barrier model at ALI culture, closely resembling the conditions during inhalation of nanoparticles in the lung. Moreover, real-time monitoring of the stretch characteristics and the membrane stiffness (elastic modulus) is an important measure of quality control during cell-stretch experiments.

The technological progress introduced by the CIVIC bioreactor system and the BETA membrane presents a significant advancement with respect to biomimicry of *in vitro* models of the lung, providing a more biomimetic model for more reliable translation of *in vitro* response studies into clinical outcome. Nevertheless, several challenges involved in the newly developed CIVIC bioreactor system equipped with the BETA membrane (see

Table 1), which demand further studies to develop the membrane and the bioreactor technology together with more thorough cellular and particokinetic analysis, improving the competence of the advanced *in vitro* lung cell models.

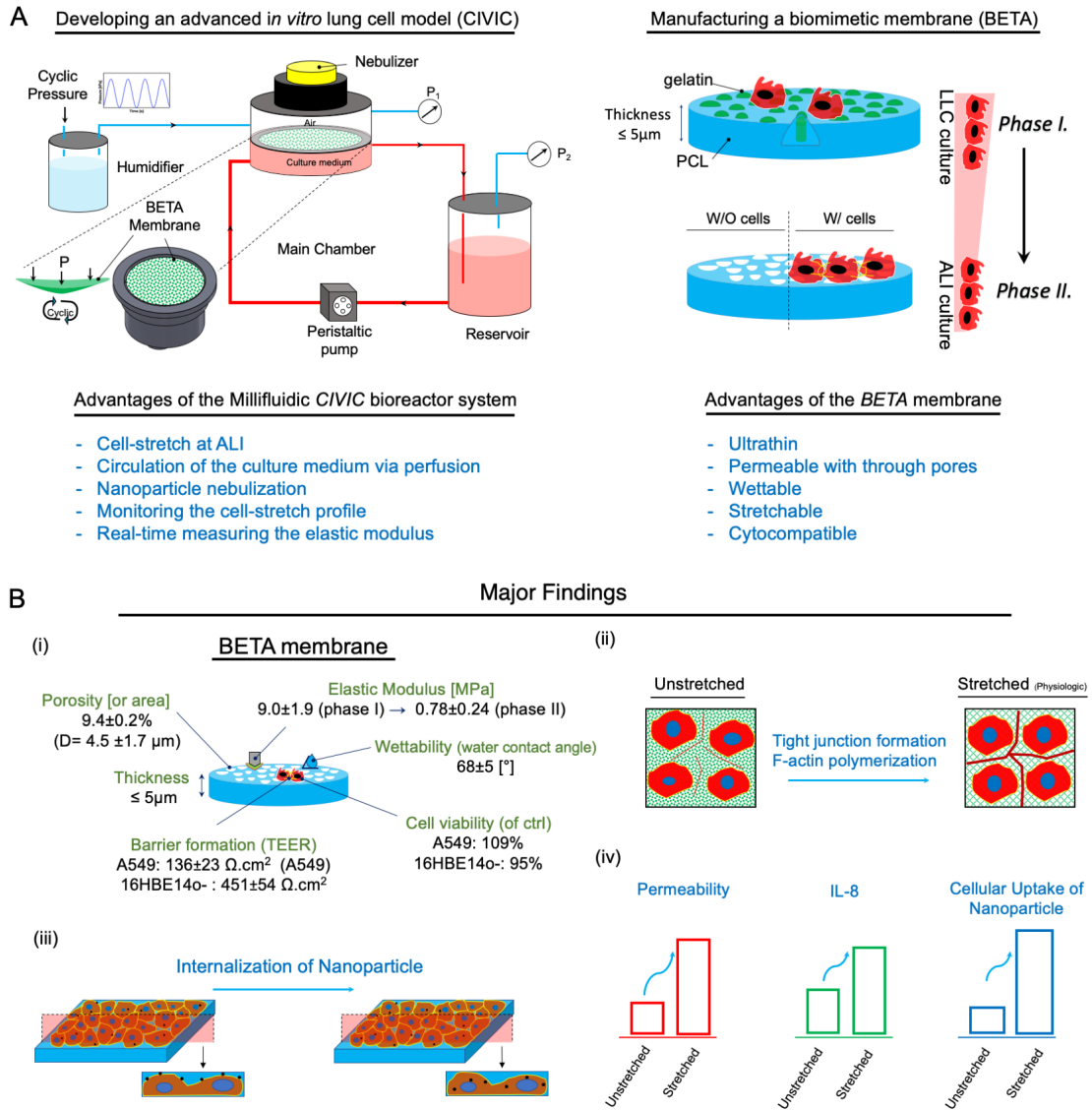


Figure 5. The overview of the main results of this Ph.D. study. (A) (Left panel) Schematic depiction of the *in vitro* cell stretching bioreactor system (CIVIC), which was modified in this study. This bioreactor system mimics the culture conditions for pulmonary epithelial cells, including cyclic mechanical stretch and medium flow (in the basal chamber using perfusion). The platform incorporates pressure sensors to monitor stretch profile and measure the elastic modulus (stiffness) of the membrane in real-time (further details in Figure 1 of paper II). (Right panel) A biomimetic membrane (BETA) with relevant physicommechanical properties was designed and manufactured, which then integrated into the CIVIC system for studying the role of cyclic mechanical stretch

(both physiologic and non-physiologic) on the physiology of pulmonary epithelial cells and cell-particle interactions. Reproduced with permission from (Doryab et al., 2021b). (B) Schematic depiction of a summary of the outcomes of the current study. (i) Selection of a PCL/gelatin mixing ratio providing optimum (biomimetic) properties of the BETA membrane (further details in Figures 1-5 of paper I). (ii) Stretch-induced formation of ZO-1 tight junctions and polymerization of F-actin, and (iii) the enhanced internalization of nanoparticles (100 nm). (iv) The role of physiologic cell-stretch on cell layer permeability, inflammatory responses (IL-8) (further details in Figure 6 of paper I), and the cellular uptake of nanoparticles (further details in Figure 7 of paper I and Figure 4 of paper II).

2.4 Concluding remarks

In the present study, we developed a biomimetic *in vitro* model for the lung application consisting of a stretch-activated lung bioreactor system (CIVIC) and a bioinspired membrane (BETA). Proliferation of two lung epithelial cells (A549 and 16HBE14o-) on the BETA membrane exhibited its excellent cytocompatibility at ALI culture. We showed the CIVIC bioreactor system can mimic the cell-stretch induced by breathing motions and shear stress stimulated by blood flow. For proof-of-concept experiments, we integrated the BETA membrane into the CIVIC system and investigated the effect of cyclic mechanical stretch (physiologic and non-physiologic) on cell physiology at ALI, including cell proliferation/apoptosis, polymerization of the F-actin cytoskeleton, formation/disruption of ZO-1 tight junctions, the permeability of cell monolayer, and inflammatory response (IL-8). Moreover, the CIVIC bioreactor system enables us to study particle-cell interactions at ALI conditions. We then studied the role of cell-stretch on cellular uptake and transport of particles (100 nm and 1000 nm) across an alveolar barrier model at ALI culture. The results demonstrated the advantages of the novel *in vitro* cell-stretch model for investigation of the role of mechanical stretch on the pulmonary epithelial cell model, which could pave the way for more biomimetic *in vitro* models of the lung, providing more robust translation into clinical outcome. Nevertheless, more studies are required to understand the role of cyclic mechanical stretch on key pathways mediated by stretch such

as Yes-associated protein (YAP)/Transcriptional co-activator with PDZ-binding motif (TAZ). The membrane, however, could be further modified to support the proliferation of primary cells and to improve physicochemical properties (such as thickness and stiffness) in the range of physiologic level.

Table 1. Advantages and challenges of the next generation of the *in vitro* model based on the BETA membrane and CIVIC bioreactor system.

Advantages	Challenges/ Future Studies
BETA Membrane	
<p>The <i>stiffness/ elastic</i> modulus of the BETA membrane is 0.78 ± 0.24 MPa (phase II, day 6) (Doryab et al., 2021b), which is lower than the commonly used PDMS membranes with Young's modulus of $\approx 1\text{--}3$ MPa (Wang et al., 2014).</p>	<p>It is still ≈ 100-fold larger than that of alveolar tissue with 3 – 6 kPa (Bou Jawde et al., 2020; Polio et al., 2018).</p>
<p>The BETA membrane could withstand <i>cyclic mechanical stretch up to 25% (linear) up to 48 h</i> (the maximum time tested in paper I), which embraces the physiologic mechanical strain (linear (1D) strain 4%–12% (normal breathing-deep inspiration and heavy exercise) and pathological conditions (20 % linear) in the lung (Forrest, 1970; Fredberg and Kamm, 2006; ICRP, 1994; Roan and Waters, 2011; Waters et al., 2012).</p>	<p>The role of cyclic stretch (24 h for cell physiology/response; 2 h for particokinetics) on cellular physiology and particle transportation/uptake were studied. A longer period of cell-stretch (more than 24 h) is required.</p>
<p>The BETA membrane is <i>thin</i> ($\leq 5 \mu\text{m}$) compared to the available membranes for lung application at ALI ($\approx 10 \mu\text{m}$).</p>	<p>It is still ≈ 100-fold larger in thickness; therefore, a thinner membrane is required to cover the thickness of the total alveolar-capillary barrier: $1.1 \mu\text{m} \pm 0.1$ (Weibel, 1970, 2009).</p>
<p>The BETA membrane is <i>permeable</i> ($9.9 \times 10^{-6} \text{ cm s}^{-1}$ for FITC-dextran 4 kDa and 15.3% 3D porosity) with through pores (an equivalent area diameter of $4.5 \pm 1.7 \mu\text{m}$).</p>	<p>A thinner membrane is required to circumvent the artifact effect of the membrane during the permeability experiments.</p>

Two types of lung epithelial cell lines (A549 and 16HBE14o-) were grown successfully on the BETA membrane.

- It is necessary to use primary lung cells (or at least immortalized primary cells) to investigate the bioactivity of the BETA membrane.
- loss of barrier integrity for A549 cells (2 h physiologic stretch) indicates a better cell model is required for transport studies.

The copolymer (PCL/gelatin) represents a great combination of *biophysicomechanical properties suitable for culturing lung epithelial cells at ALI culture*

It does not represent the fiber-like structure and molecular composition of the innate basement membrane.

The Millifluidic CIVIC Bioreactor

The millifluidic CIVIC bioreactor utilizes positive pressure to mechanically stretch a cell-covered elastic membrane, allowing for *precise selection of stretch amplitude* during the cell-stretch experiment.

The maximum positive pressure (2.5 kPa) is similar to mechanical ventilation at the intensive care unit of a hospital (normal: 1.5 – 2.0 kPa, 2.5 kPa acceptable peak value) (Hall, 2016) but higher than exerted onto the lung tissue during normal exhalation (0.1 – 0.5 kPa).

The CIVIC bioreactor system could *cover the entire clinically relevant amplitude range* (5% linear (Cei et al., 2021), 10-17% linear (Doryab et al., 2021a, 2021b)) compared to human breathing patterns.

Further studies are required to decipher the role of non-physiologic cell stretch on cellular physiology in complex lung cell models (coculture and triple coculture).

The *medium perfusion* rate used in the CIVIC system mimics a blood perfusion rate of $400 \mu\text{L min}^{-1}$ with the ratio of area and perfusion rate of $1.25 \text{ m}^2/(\text{L min}^{-1})^{-1}$.

- The ratio of area and perfusion rate of the CIVIC is considerably lower than that of the lung ($20 \text{ m}^2/(\text{L min}^{-1})^{-1} = 100 \text{ m}^2/(\text{L min}^{-1})^{-1}$).
- The flow rate of the lung (6.4 L min^{-1}) can be established in the CIVIC system, which requires tubing with a much larger diameter.

The CIVIC bioreactor system is able to *apply simultaneously cell stretch* (mimicking breathing motions) *and perfusion* (mimicking blood flow).

More studies are required to understand the role of blood perfusion on cell-stretched experiments.

Particokinetic Studies

The efficiency of aerosolized substance delivery is ca. 50% (only liquids; no dry powder) with the delivered dose of $0.5 \mu\text{L cm}^{-2} \text{min}^{-1}$, which is corresponding to typical drug inhalation times of ca. 3 min –delivery rate (0.1 min (metered-dose inhalers) to 15 min (nebulizer) in clinics) and efficiency (10 – 30%) similar to clinical conditions.

- Enhanced cellular uptake of nanoparticles, but not of microparticles (2 h physiologic stretch) –strong inverse size dependence of transport is consistent with *in vivo* data (Kreyling et al., 2013).

- More in-depth investigations on cellular uptake of particles based on particle physicochemical characteristics such as material, size, shape, and surface charge are required.

2.5 Chapter 1: Design and manufacturing of a biomimetic membrane for pulmonary epithelial cells

In this chapter, we report the design and manufacturing of a bioinspired BETA (**B**iphasic **E**lastic **T**hin for **A**ir-liquid culture conditions) membrane, mimicking key features of the alveolar-capillary barrier of the human lung. The BETA is a biphasic copolymeric thin membrane consisting of poly(ϵ -)caprolactone and gelatin with appropriate surface wettability, porosity and stretchability (up to 25% linear strain) for culturing lung epithelial cells under cell-stretch conditions at ALI. Moreover, we investigated the role of physiologic and non-physiologic cyclic mechanical stretch (at ALI culture) on cell viability, formation of F-actin cytoskeleton and tight junction, apparent permeability (barrier integrity), and activity of inflammatory response (IL-8). We also showed that cyclic physiologic stretch can enhance the cellular uptake of nanoparticles.

The method for fabricating BETA membrane has been filed for European patent application. This study was published in *Advanced Functional Materials* (Doryab et al., 2021b) and reprinted with permission from the corresponding publishers. *Copyright © 2020. The Authors. Advanced Functional Materials published by Wiley-VCH GmbH.*

2.6 Chapter 2: Particokinetic study under cyclic stretch and air-liquid interface conditions

In this chapter, we describe the technical details of the CIVIC (Cyclic In Vitro Cell-stretch) bioreactor system with particular emphasis on the new or refined aspects as compared to the MALI system. The CIVIC incorporates in-line two pressure sensors for real-time monitoring of the stretch profile (amplitude) and the elastic modulus of the (cell-covered) membrane during cell-stretch experiments. The latter has the potential of real-time monitoring of the stiffness of the cells grown on the membrane, which could be used for real-time sensing of fibrotic modifications of the cell layer. The CIVIC system is PDMS-free to prevent any unwanted leaching/release of silicone into the culture medium. We studied the role of physiologic cyclic mechanical stretch on cellular uptake and transepithelial transport of nanoparticles (100 nm) and microparticles (1000 nm), which demonstrated that the cyclic physiologic mechanical stretch can enhance the cellular uptake and transepithelial translocation of only nanoparticles.

The method for investigating cells attached to the biocompatible composite membrane (BETA) have been filed for European patent application. This study was published in *Frontiers in Bioengineering and Biotechnology* (Doryab et al., 2021a) and reprinted with permission from the corresponding publishers. *Copyright © 2021. The Authors. Under the terms of the Creative Commons Attribution License (CC BY).*

2.7 Chapter 3: An *in vitro* lung model with aerosol delivery

In this chapter, we explain the engineering design, computational modeling, and empirical performance of a Moving Air-Liquid Interface (MALI) bioreactor system for the study of aerosol deposition on lung epithelial cells (A549) cultured at Air-Liquid Interface (ALI) under cyclic mechanical stretch. The main chamber was designed to recapitulate the ALI conditions using apical (air) and basal (cell culture media) compartments separated by an elastic porous membrane for cell growth. The membrane can be stretched by oscillating airflow in the apical chamber to apply a cyclic mechanical strain to cells. Furthermore, highly efficient liquid aerosol deposition (ca. 51.5%) can be accurately modeled using finite element methods. As a proof of concept, we showed that A549 cells can be mechanically stimulated under ALI and physiologic stretch conditions without loss of cell viability.

This study was published in *Biotechnology and Bioengineering* (Cei et al., 2021) and reprinted with permission from the corresponding publishers. *This publication reprinted with permission from the corresponding publishers. © 2021 Wiley Periodicals LLC.*

3. Paper I

FULL PAPER



A Biomimetic, Copolymeric Membrane for Cell-Stretch Experiments with Pulmonary Epithelial Cells at the Air-Liquid Interface

Ali Doryab, Mehmet Berat Taskin, Philipp Stahlhut, Andreas Schröppel, Darcy E. Wagner, Jürgen Groll, and Otmar Schmid*

Chronic respiratory diseases are among the leading causes of death worldwide, but only symptomatic therapies are available for terminal illness. This in part reflects a lack of biomimetic *in vitro* models that can imitate the complex environment and physiology of the lung. Here, a copolymeric membrane consisting of poly(ϵ -caprolactone and gelatin with tunable properties, resembling the main characteristics of the alveolar basement membrane is introduced. The thin bioinspired membrane ($\leq 5 \mu\text{m}$) is stretchable (up to 25% linear strain) with appropriate surface wettability and porosity for culturing lung epithelial cells under air–liquid interface conditions. The unique biphasic concept of this membrane provides optimum characteristics for initial cell growth (phase I) and then switch to biomimetic properties for cyclic cell-stretch experiments (phase II). It is shown that physiologic cyclic mechanical stretch improves formation of F-actin cytoskeleton filaments and tight junctions while non-physiologic over-stretch induces cell apoptosis, activates inflammatory response (IL-8), and impairs epithelial barrier integrity. It is also demonstrated that cyclic physiologic stretch can enhance the cellular uptake of nanoparticles. Since this membrane offers considerable advantages over currently used membranes, it may lead the way to more biomimetic *in vitro* models of the lung for translation of *in vitro* response studies into clinical outcome.

1. Introduction

The lung is one of the vital organs in the body that is responsible for gas exchange between air and blood during breathing. Although the prevalence of lung diseases such as chronic obstructive pulmonary disease (COPD) is rising, few causal therapies are available for respiratory diseases due to the complex internal structure and functions of the lung tissue, which cannot easily be recreated in the lab.^[1] The availability of preclinical models of lung disease for reliable prediction of clinical outcome is recognized as an important bottleneck for the development of new drugs against lung diseases.^[2] Consequently, significant efforts are undertaken to enhance the biomimetic level of currently available *in vitro* models of lung diseases.^[3,4]

The main purpose of the lung is to allow for an efficient supply of oxygen to and removal of carbon dioxide from the red blood cells (erythrocyte). From the trachea, the gas is directed through a complex branching network of conducting

A. Doryab, A. Schröppel, Dr. O. Schmid
Comprehensive Pneumology Center Munich (CPC-M)
Member of the German Center for Lung Research (DZL)
Munich 81377, Germany
E-mail: otmar.schmid@helmholtz-muenchen.de

A. Doryab, A. Schröppel, Dr. O. Schmid
Institute of Lung Biology and Disease (iLBD)
Helmholtz Zentrum München—German Research Center for
Environmental Health
Neuherberg 85764, Germany

The ORCID identification number(s) for the author(s) of this article can be found under <https://doi.org/10.1002/adfm.202004707>.

© 2020 The Authors. Advanced Functional Materials published by Wiley-VCH GmbH. This is an open access article under the terms of the Creative Commons Attribution-NonCommercial License, which permits use, distribution and reproduction in any medium, provided the original work is properly cited and is not used for commercial purposes.

DOI: 10.1002/adfm.202004707

Dr. M. B. Taskin, P. Stahlhut, Prof. J. Groll
Department of Functional Materials in Medicine and
Dentistry and Bavarian Polymer Institute (BPI)
University of Würzburg
Würzburg 97070, Germany

Prof. D. E. Wagner
Department of Experimental Medical Sciences
Lung Bioengineering and Regeneration
Lund University
Lund 22100, Sweden

Prof. D. E. Wagner
Stem Cell Centre
Lund University
Lund 22184, Sweden

Prof. D. E. Wagner
Wallenberg Center for Molecular Medicine
Lund University
Lund 22100, Sweden

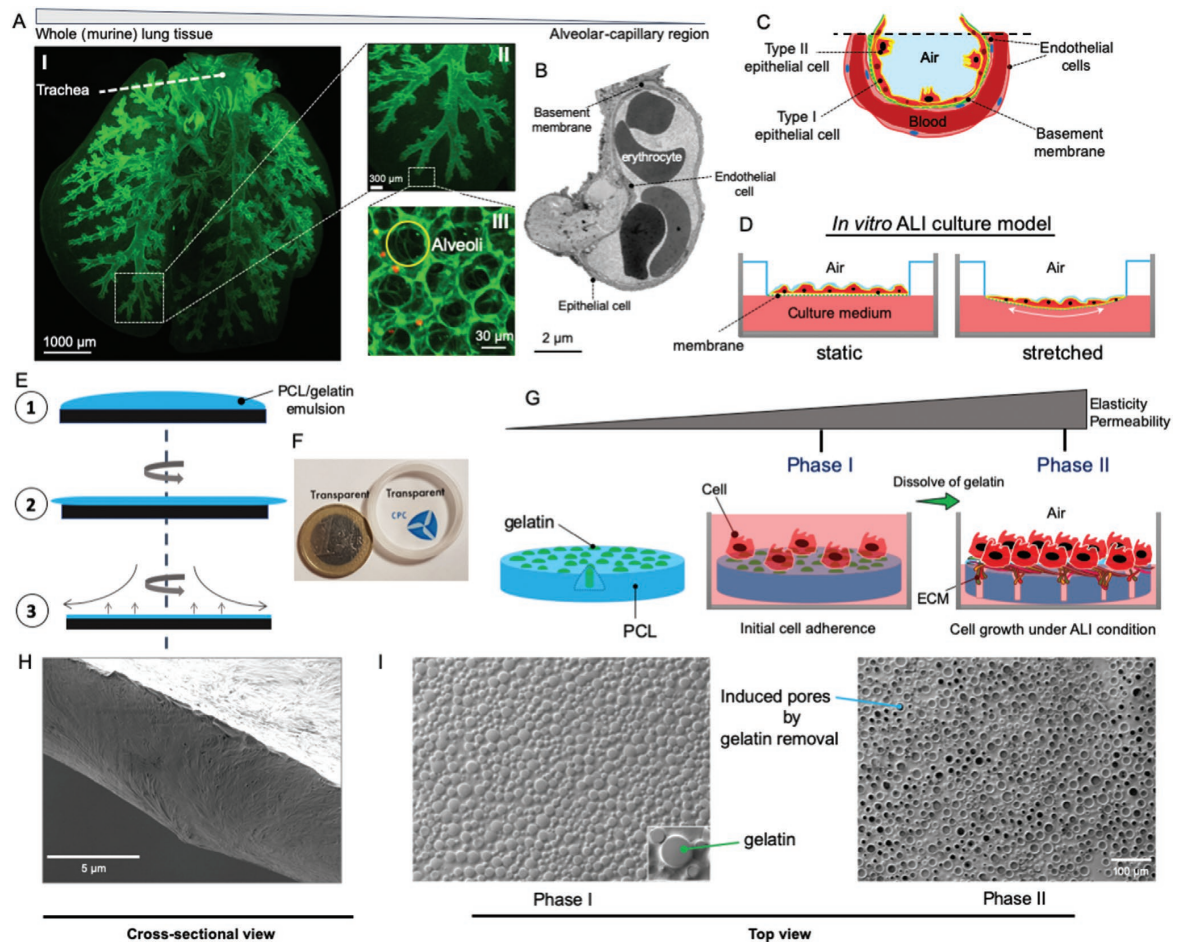


Figure 1. Manufacturing of the BETA membrane. A) A 3D reconstruction of the whole murine lung tissue obtained with light sheet fluorescence microscopy (LSFM) depicting trachea, bronchi, small (terminal) bronchioles (I), distal bronchial tree (II) and 3D honeycomb structure of the alveolar region as observed with confocal microscopy on precision cut lung slices (III). B) Transmission Electron Microscopy (TEM) image of alveolar-capillary region, depicting the alveolar epithelium, capillary endothelium, basement membrane as part of the air–blood barrier, and erythrocyte. Panels of (A,B) reproduced with permission.^[6] Copyright 2019, John Wiley and Sons. C) Schematic of lung alveolar region, showing the air–liquid (blood) interface (ALI) in vivo. An ultrathin basement membrane ($\leq 1 \mu\text{m}$), which separates epithelial and endothelial cell layers (liquid side). A thin layer of surfactant, which is secreted by type II alveolar epithelial cells, is sitting on the top of epithelial cells to reduce surface tension at ALI in the alveolar region. D) Schematic of in vitro ALI culture models under static and stretch conditions. Cells are seeded on a porous/flexible membrane and air-lifted after forming a confluent cell layer. E) Schematic of the membrane fabrication consisting of poly(ϵ -caprolactone (PCL) and gelatin using spin-coating. F) Photograph of the fabricated membrane and a 1-euro coin, showing that it is transparent enough for cell imaging technologies such as live cell imaging and confocal microscopy. G) Depiction of the two phases of the membrane. Phase I: After the spin-coating of a PCL–gelatin mixture, a uniform, non-porous PCL–gelatin membrane is produced, which consists of PCL with embedded “islands” of gelatin serving as adhesion point for cells facilitating subsequent cell proliferation. Spin-coating of a gelatin–PCL mixture results in an initially non-porous PCL–gelatin membrane, where the “islands” of gelatin allow the epithelial cells to grow into a confluent cell monolayer. Phase II: Gradually gelatin is dissolved away by cell culture medium. This opens pores for the nourishment of the cells under ALI conditions, which enhances not only membrane permeability but also elasticity. H) A cross-sectional view of the manufactured membrane. Scale bar is $5 \mu\text{m}$. I) SEM image (top view) of the membrane during phase I and phase II. The scale bar is $100 \mu\text{m}$.

airways into the alveolar region, where gas exchange takes place (Figure 1A). For efficient gas exchange, a micro-scale alveolar-capillary tissue barrier (minimum thickness of $\approx 1 \mu\text{m}$) is required, which essentially consists of an ultrathin basement membrane ($\approx 0.1 \mu\text{m}$) covered with a confluent layer of alveolar type-I and type-II (ATI and ATII, respectively) epithelial

cells on the apical (air-facing) side and a confluent layer of endothelial cells on the blood side (Figure 1B,C).^[5,6] The main functions of this basement membrane include structural support for resident cells as well as transport of nutrients and biomolecules between blood and lung tissue.^[6] Thus, the basement membrane of the alveolar region needs to be stiff enough

for supporting the delicate honeycomb structure of the alveolar sacs and yet provide sufficient elasticity to allow for a breathing-induced cyclic stretch at low energy consumption.

Current membrane technologies employed in *in vitro* lung models focus on structural support for the cells, but are too thick and lack elasticity as compared to basement membranes of the lung.^[5,6] Standard cell culture models are grown in multi-well polycarbonate plates under submerged culture conditions, i.e., the cells are completely covered with cell culture media. More advanced, complex, multi-cell, physiologically structured cell cultures of the lung epithelium for studying normal homeostasis and regeneration or co-cultured with disease-specific effector cells (e.g., fibroblasts for pulmonary fibrosis) are commercially available from both healthy donors and patients.^[7] These advanced *in vitro* models are cultured in Transwell inserts under air-liquid interface (ALI) conditions and exposed to aerosolized drugs under dose-controlled conditions.^[8–10] On the other hand, these inserts culture the cells on perforated, stiff polyethylene terephthalate (PET) membranes (more rarely polycarbonate or polytetrafluoroethylene (PTFE) membranes are used), which do not mimic the elastic ECM and cyclic stretch conditions in a “breathing” lung, which has been shown to play a key role in the development of chronic lung diseases such as pulmonary fibrosis.^[11]

Several cell-stretch devices have been described in the literature, but only a few devices are commercially available and all of them utilize submerged cell cultures.^[6] On the other hand, newly designed microfluidic systems for stretch-activated ALI culture conditions have been described 10 years ago but—in spite of significant efforts—are just reaching the marketplace and are not widely used, yet.^[12] Most of these cell-stretch devices rely on membranes made out of poly(dimethylsiloxane) (PDMS) since they are considered chemically inert and provide suitable mechano-elastic properties.^[12,13] However, they do have disadvantages, which hamper the progress of cell-stretch technologies. PDMS membranes are hydrophobic requiring pre-conditioning of the membrane (e.g., coating with ECM proteins) to enhance wettability and cell adhesion. Achieving a confluent monolayer of epithelial cells on a coated-PDMS membrane is a major challenge since the aggregation and/or dislodgment of cells from the PDMS surface due to protein dissociation often occurs especially for long-term culture conditions and under stretch conditions.^[14] Moreover, PDMS adsorbs some drugs and proteins/growth factors contained in the cell culture media and leaching of uncured PDMS oligomers into the culture media can influence cell physiology.^[15] Thus, an appropriate membrane providing both optimum cell culture conditions and physico-mechanical properties inspired by the microenvironment of alveolar epithelium is still missing, which presents a major obstacle for the development of biomimetic *in vitro* cell-stretch models of the lung.

Polymeric systems (natural and synthetic-based) are widely used to manufacture suitable scaffolds with biomimetic features for soft tissue applications including lung due to their diversity in chemical groups, allowing for remarkable physical and mechanical properties.^[6,16,17]

In this study, we introduce a biphasic copolymeric membrane consisting of gelatin and poly(ϵ -caprolactone (PCL) chosen for their cell-conductive and mechano-elastic properties

to mimic the microenvironment of alveolar epithelial (AT) cells with respect to important functional features such as mechanical, biophysical, and bioactive properties. This Biphasic Elastic Thin for Air-liquid culture conditions (BETA) membrane facilitates cell adhesion and proliferation without pre-treatment of the membrane and it provides sufficient porosity and biomimetic elasticity as required for *in vitro* cell-stretch applications under ALI culture conditions. The hybrid membrane is integrated into a stretch-activated lung bioreactor, which allows us to investigate the effect of cyclic mechanical stretch on cell physiology and the transport of nanoparticles across an alveolar barrier model. We also present novel methods for real-time monitoring of cyclic stretch and measuring the elastic modulus of membrane during cell-stretch experiments.

2. Results and Discussion

2.1. The Biphasic Membrane Concept

Mimicking the lung *in vitro* models of the alveolar barrier often culture a confluent monolayer of epithelial cells under static ALI conditions, where air-exposed epithelial cells are growing on a rigid perforated membrane, which is in contact with cell culture medium on the basal side for the nourishment of the cells (Figure 1D). Only recently, static ALI culture models have been adapted to allow for cyclic stretch conditions, mimicking the mechano-elastic strain exerted during the breathing activity of the lung (Figure 1D).

During the growth of these static or dynamic ALI cell culture models, two main phases can be distinguished; i) an initial phase of cell adhesion, proliferation, and growth of alveolar epithelial cells into a 2D and confluent cell monolayer. Since this is done under submerged cell culture conditions (with cell culture medium in the apical compartment), the membrane does not have to be perforated, yet (phase I). ii) Once a confluent cell layer is formed the cell culture is air-lifted (i.e., cell culture medium is withdrawn from the apical compartment) and left for acclimatization allowing the cells to polarize and secrete protective lining fluid^[18] prior to performing the actual cell culture experiments under physiologic ALI conditions (phase II), i.e., a perforated membrane is required for this phase.

Consequently, the “ideal” membrane is tailored toward sequentially meeting the two different sets of specifications corresponding to those two phases of cell culture conditions. For phase I (initial cell growth), the “ideal” membrane is bioactive (i.e., conducive to cell adhesion and growth), wettable and non-porous (prevents cells to migrate into/through the membrane) to facilitate the formation of a planar, confluent epithelial (and endothelial) cell layer under submerged culture conditions. On the other hand, after air-lifting of the cells (phase II), the membrane should be porous/permeable enough to allow for sufficient exchange of nutrients, growth factors, and cell signaling molecules between cells and basal cell culture medium,^[19] mimic elasticity/stiffness of the ECM of the lung^[20,21] and be resilient to cyclic stretch while being in contact with cell culture medium (Figure 1D). Moreover, the membrane should be as thin as possible ($\approx 0.1 \mu\text{m}$ in the lung) minimum interference of the membrane with cell

experiments and analytical tools such as microscopy requires the membrane to be as thin as possible (basement membrane of lung: 0.1 μm), optically transparent, chemically inert (no leaching of membrane materials into cell culture medium) and non-adsorptive toward drugs, proteins, and growth factors contained in the cell culture medium. The most widely used current membrane technology tries to accomplish this by using an elastic but hydrophobic material (e.g., PDMS), which requires pre-treatment prior to cell seeding such as chemical and physical modification or coating with ECM proteins (i.e., collagen (or gelatin), fibronectin, and laminin). Moreover, the membrane is always porous as required for phase II, but the pore size is limited to 1–3 μm to prevent epithelial (or endothelial) cells from migrating into or through the membrane during phase I.

Here we pursue a different, biphasic membrane approach, which sequentially adapts the membrane properties to meet the different requirements of the two phases of cell culture conditions during cell-stretch experiments under ALI conditions. We fabricated this biphasic stretchable membrane (BETA) by spin-coating of a copolymer emulsion consisting of PCL and gelatin into a thin ($\leq 5 \mu\text{m}$) membrane (Figure 1E–I). Since PCL and gelatin are immiscible in the solvent used here, the spin-coated membrane initially consists of poorly wettable PCL with “islands” of wettable gelatin due to phase separation (Figure 1I). The amide groups of gelatin form hydrogen bonds with water molecules in phase I, improving surface wettability of the initially smooth and nonporous membrane. Moreover, gelatin contains the tripeptide Arg-Gly-Asp (RGD) cell adhesion motif that ligates several integrins and mediates cell attachment.^[22] As cells proliferate, they secrete their own ECM allowing them to gradually migrate into the poorly wettable PCL regions and eventually forming a confluent cell layer. Moreover, water-soluble gelatin serves as a sacrificial polymer which is gradually dissolved in cell culture medium, inducing porosity in the originally nonporous membrane as required for phase II (Figures 1I, 2A, B and Figure S1, Supporting Information). In addition, selective removal of the relatively stiff gelatin (as compared to the elastic PCL) increases the elasticity of the membrane to a value typically observed for lung tissue (see Section 2.2). Hence, the biphasic membrane concept introduced here leverages the specific properties of a hybrid membrane for the controlled transformation of an initially relatively stiff, nonporous, wettable membrane, which is ideal for the formation of a planar confluent epithelial barrier under submerged culture conditions (phase I), into a porous, elastic and stretchable membrane as required for the cell-stretch experiments under ALI culture conditions (phase II).

2.2. Selection and Characterization of Optimum Membrane

The ideal mixing ratio of the copolymer emulsion (PCL, gelatin) for spin-coating of the membrane was experimentally determined with a design of experiment (DoE) approach using the response surface methodology (RSM) which examines up to 2nd order effects of PCL and gelatin concentration on multiple biophysical and mechanical properties of the membrane.

Based on our recently published review paper on physiologic properties of basement membranes of the lung^[6] and the membrane requirements listed above, we selected target values of elastic modulus (Young's modulus; 5–10 MPa with $\leq 10\%$ linear strain), surface wettability (water contact angle WCA $\leq 70^\circ$) and porosity/permeability (sufficient for nutrient exchange; good cell viability in phase II) as well as cytocompatibility (good cell proliferation) as most relevant parameters for optimization of the copolymer mixing ratio.

To this end, we fabricated nine spin-coated PCL/gelatin thin ($\leq 5 \mu\text{m}$) membranes in different PCL and gelatin mixing ratios (Table 1). All of them formed a uniformly distributed, complex, 3D interconnected gelatin network within a PCL matrix as evidenced by the distribution of gelatin islands (disc-shaped structures) on SEM images of the membrane (Figure 2A and Figure S2A, Supporting Information) and the observed cell viability under ALI conditions. However, PCL/gelatin mixing ratio affects pore size and pore-covered area fraction, which influences cell adhesion, growth, and viability.

The membranes have WCA and porosity in a range of $62.1 \pm 5.2 \leq \text{WCA} \leq 80.6 \pm 2.9 [^\circ]$ and $8.80 \pm 1.03 \leq P \leq 28.71 \pm 1.21 [\%$ of area], respectively (Table 1 and Figure 2C, D). During $\approx 24 \text{ h}$ of contact with cell culture medium, 20–45% of the gelatin is dissolved and the membranes have an elastic (Young's) modulus in a range of $6.25 \pm 0.41 \leq E \leq 14.19 \pm 0.30 [\text{MPa}]$ depending on PCL/gelatin mixing ratio (Figure 2E) where a membrane with higher PCL concentration is stiffer (lower Young's modulus) and capable to absorb more energy without plastic deformation ($U_r \leq 32 \text{ kPa}$ for $\leq 7.5\%$ PCL; 65–154 kPa for 10% PCL) (Figure 2F). For the assessment of cytocompatibility, we seeded an alveolar type II-like epithelial cell line (A549) on the membrane. Real-time WST-1 metabolic activity showed that there is no general cytotoxicity for any of the membranes (metabolic activity increases with time; Figure 2G). On the other hand, cells formed a confluent monolayer only on membranes with pores smaller than the size of an individual cell ($\approx 8 \mu\text{m}$), i.e., especially for low gelatin concentration (6%), but also for higher gelatin concentration, if the PCL concentration was low (5%) (Figure S3, Supporting Information).

WCA and porosity depend linearly on both PCL and gelatin concentrations (Figure 3A, B), while the elastic modulus of the membrane is affected by both one-way mixing ratio and two-way interaction of PCL and gelatin concentrations (Figure 3C). Applying the DoE approach to the experimental data listed in Figure 2 (and Table 1) revealed that the polymer blend consisting of 9.35% PCL and 6.34% gelatin [w/v solvent] provides the optimal membrane properties with respect to co-optimization of elastic modulus, wettability, and porosity (Figure 3D, E).

To validate the fitted model, five membranes with an “optimum” PCL/gelatin mixing ratio (9.35% PCL and 6.34% gelatin) were fabricated and experimentally examined with respect to these parameters. The WCA was found to be $68.8 \pm 5.3^\circ$ which is in-between the limiting values of $119.2 \pm 4.2^\circ$ and $46.8 \pm 8.1^\circ$ measured for PCL and gelatin, respectively (Figure 4A). The 2D fractional porosity of the membrane area (in phase II) was determined as $9.4 \pm 0.2\%$ with an area-weighted diameter distribution of $4.5 \pm 1.7 \mu\text{m}$ (mean \pm SD) (Figure 4B). The elastic modulus of the membrane in phase I and II was 9.01 ± 1.95 and $1.84 \pm 0.66 \text{ MPa}$, respectively with an extended reversible

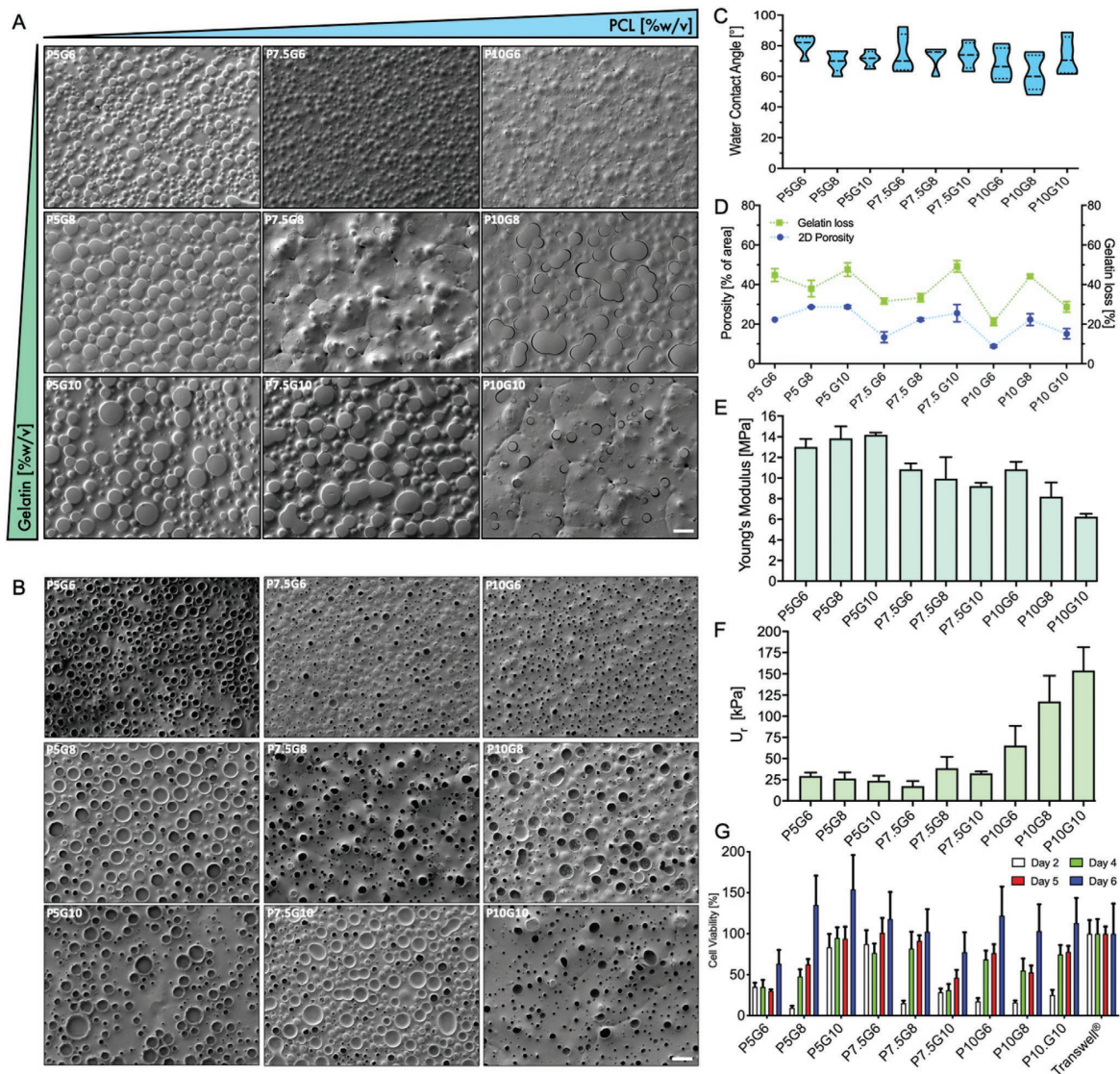


Figure 2. Structural, biophysical and mechanical characterization of the fabricated membranes following a co-optimization strategy. SEM analysis of the fabricated membranes in A) phase I and B) phase II by various combination of PCL (P) and gelatin (G) mixing ratio (Table 1), indicating that higher PCL and lower gelatin concentration result in a narrow-distributed porosity with smaller pore size, which is in favor of ALI culture application. Scale bar is 20 μm . C) Surface wettability of the membrane quantified by WCA. D) Generated porosity after removal of gelatin in phase II quantified by SEM images is a function of the mixing ratio of PCL (p -value ≤ 0.2) and gelatin (p -value ≤ 0.03). E) Elastic modulus of the membranes measured by the 1D tensile stress test (phase I). F) The modulus of resilience (U_r) calculated by the area underneath the stress–strain curve up to yield (elastic region). G) WST-1 metabolic activity at days 2, 4, 5, and 6 of cell culturing. Data were baseline-corrected by the OD value of the Corning Costar Transwell cell culture inserts (PET, 12-well, 1.1 cm^2 ; 0.4 μm pore). Three replicate samples were used for each analysis ($n = 3$, mean \pm SEM).

deformation region up to 25% (linear) (Figure 4C). These results showed no statistically significant differences between model-predicted and experimentally determined parameters (WCA_{exp} vs WCA_{pred} , p -value = 0.834; $\text{Porosity}_{\text{exp}}$ vs $\text{Porosity}_{\text{pred}}$, p -value = 0.171; E_{exp} vs E_{pred} , p -value = 0.587).

These five “optimum” membranes (9.35% PCL and 6.34% gelatin) were experimentally examined in more in-depth. A 1D fatigue test was conducted to measure the behavior of the

membrane under continued cyclic stretch with an amplitude of 12% linear strain (sinusoidal cyclic stretch) and a frequency of 0.33 Hz (20 cpm). No hysteresis or creep was observed for the maximum test period (4 h), indicating that the BETA membrane can endure cyclic mechanical stretch without any plastic deformation or rupture (Figure 4D). Moreover, 3D Young's modulus of the membrane was measured in the bioreactor during cell culturing after day 1 (1.33 ± 0.14 MPa), day 3 (1.19 ± 0.21 MPa), and

Table 1. Range of PCL/Gelatin mixing ratios and experimental responses entering the design of experiment (DoE) approach to obtain the most biomimetic membrane properties by response surface methodology (RSM) based on Central Composite Design (CCD) arrangement.

Parameters	PCL [%w/v]			GGG Gelatin [%w/v]			WCA [°]	Po Porosity [%]	E [MPa]
Levels	-1	0	1	-1	0	1			
[65,66]	5	7.5	10	6	8	10			
Run									
1		5			6		80.6 ± 6.6	22.28 ± 1.82	13.02 ± 1.09
2		10			6		68.0 ± 10.3	8.80 ± 1.03	10.84 ± 1.03
3		5			10		71.5 ± 5.2	28.71 ± 1.21	14.20 ± 0.30
4		10			10		72.9 ± 12.6	15.14 ± 4.53	6.25 ± 0.41
5		5			8		69.9 ± 6.8	28.70 ± 0.53	13.85 ± 1.65
6		10			8		62.1 ± 11.6	22.34 ± 5.12	8.21 ± 1.94
7		7.5			6		74.8 ± 12.5	13.40 ± 4.77	10.85 ± 0.82
8		7.5			10		72.4 ± 8.4	22.29 ± 1.15	9.95 ± 1.94
9		7.5			8		73.8 ± 8.5	25.53 ± 7.57	9.22 ± 0.46

day 6 (0.78 ± 0.24 MPa), revealing that 3D Young's modulus continues to moderately decrease by about a factor of 2 between day 1 and day 6. It is noteworthy that at day 6, 3D Young's modulus (0.78 ± 0.24 MPa) is more than 2-fold lower than the corresponding 1D value (1.84 ± 0.66 MPa), i.e. the BETA membrane is somewhat more elastic under actual cell culture conditions (with cells in place) than determined by standard 1D elastic modulus testing without cells (Figure 4E). The BETA membrane at day 6, which will be used for cell-stretch experiments, remained elastic for 48 h of 3D cyclic stretch (under submerged conditions) with no deformation, rupture, and creep. Thus, this membrane is suitable for cell-stretch experiments for at least up to 48 h, which covers the typically used experimental periods for in vitro cell-stretch experiments.

FTIR analysis of the chemical composition of the BETA membrane in the transition between phase I and phase II showed clear evidence for the removal of gelatin from the membrane (Figure 4F). The characteristic peaks of PCL were approximately observed at 2917 cm^{-1} (asymmetric CH_2), 2850 cm^{-1} (symmetric CH_2), 1722 cm^{-1} ($\text{C}=\text{O}$), 1293 cm^{-1} ($\text{C}-\text{O}$ and $\text{C}-\text{C}$), 1239 cm^{-1} (asymmetric $\text{C}-\text{O}-\text{C}$), and 1162 cm^{-1} (symmetric $\text{C}-\text{O}-\text{C}$). The FTIR spectrum of the pure gelatin film shows absorption peaks at 3290 cm^{-1} (N-H stretching of amide A), 1629 cm^{-1} (amide I), and 1539 cm^{-1} (amide II).^[23,24] All of the characteristic bands of PCL and gelatin were detectable on the membrane before immersion in culture media. Some shifting of bands is observed due to interaction between the ester group of PCL and an amine group of gelatin.^[23] After incubation in cell culture medium (phase II), the FT-IR spectrum of porous PCL/gelatin membrane shows only characteristic bands of PCL, indicating that gelatin has been largely washed away (Figure S2B, Supporting Information). The optimum membrane also performed well with respect to cell adherence and growth. A549 epithelial cells formed a confluent monolayer on the membrane (Figure 5A,B) with a transepithelial electrical resistance (TEER) of $136 \pm 23\ \Omega\text{ cm}^2$ (under static culture). This relatively low barrier integrity is typical for A549 cells (Figure 4H). Hence, we also tested a bronchial epithelial cell line (16HBE14o-) known to be capable of forming

a tighter barrier. Similar to the A549 cells, 16HBE14o- cells also form a uniform confluent monolayer on the membrane (Figure 5C and Figure S4A, Supporting Information), reaching the full barrier integrity as evidenced by the (maximum) TEER value of $452 \pm 55\ \Omega\text{ cm}^2$ after 6 days (Figure 4H), which is in agreement with data reported in the literature.^[25] The observed gradual build-up of a confluent 16HBE14o- cell layer is also consistent with the proliferation assay reaching its maximum value on day 7 (Figure 4G). A summary of the characteristics of the optimum membrane is given in Figure 4I. All of these values are in agreement with the target values specified above.

2.3. Improvements over Conventional Membranes

The properties of the (optimum) BETA membrane reported above provide a significant advancement over currently used membranes for ALI cell culture models of the lung, namely PET and PDMS for static and stretch-activated ALI cell culture models, respectively. PET membranes are stiff (Young's modulus of $\approx 2\text{--}3$ GPa) but relatively conducive to cell adherence. On the other hand, PDMS is elastic and allows for cyclic cell-stretch, but it is not conducive to cell growth due to its hydrophobic nature ($\text{WCA} \geq 105^\circ$). The BETA membrane presented here combines conduciveness to cell growth with biomimetic elasticity and resilience to cyclic stretch for at least 48 h (longest time period investigated here). The currently used PET and PDMS membranes are typically at least $10\ \mu\text{m}$ thick and use fixed-sized $1\text{--}3\ \mu\text{m}$ pores to provide sufficient permeability for nourishment of cells under ALI culture conditions and to prevent inadvertent migration of epithelial cells from the apical to the basal side (or vice versa for endothelial cells) during phase I.^[6] However, $1\text{--}3\ \mu\text{m}$ pores are too small to allow for innate cell migration such as infiltration of neutrophils from the blood to the luminal side of the lung epithelium during inflammatory events. The BETA membrane introduced here is not only thinner ($<5\ \mu\text{m}$) but also allows for larger pores during the cell culture experiments (no pores initially; during phase II: $4.5 \pm 1.7\ \mu\text{m}$ (mean \pm SD) corresponds to a range of $1.1\text{--}7.9\ \mu\text{m}$),

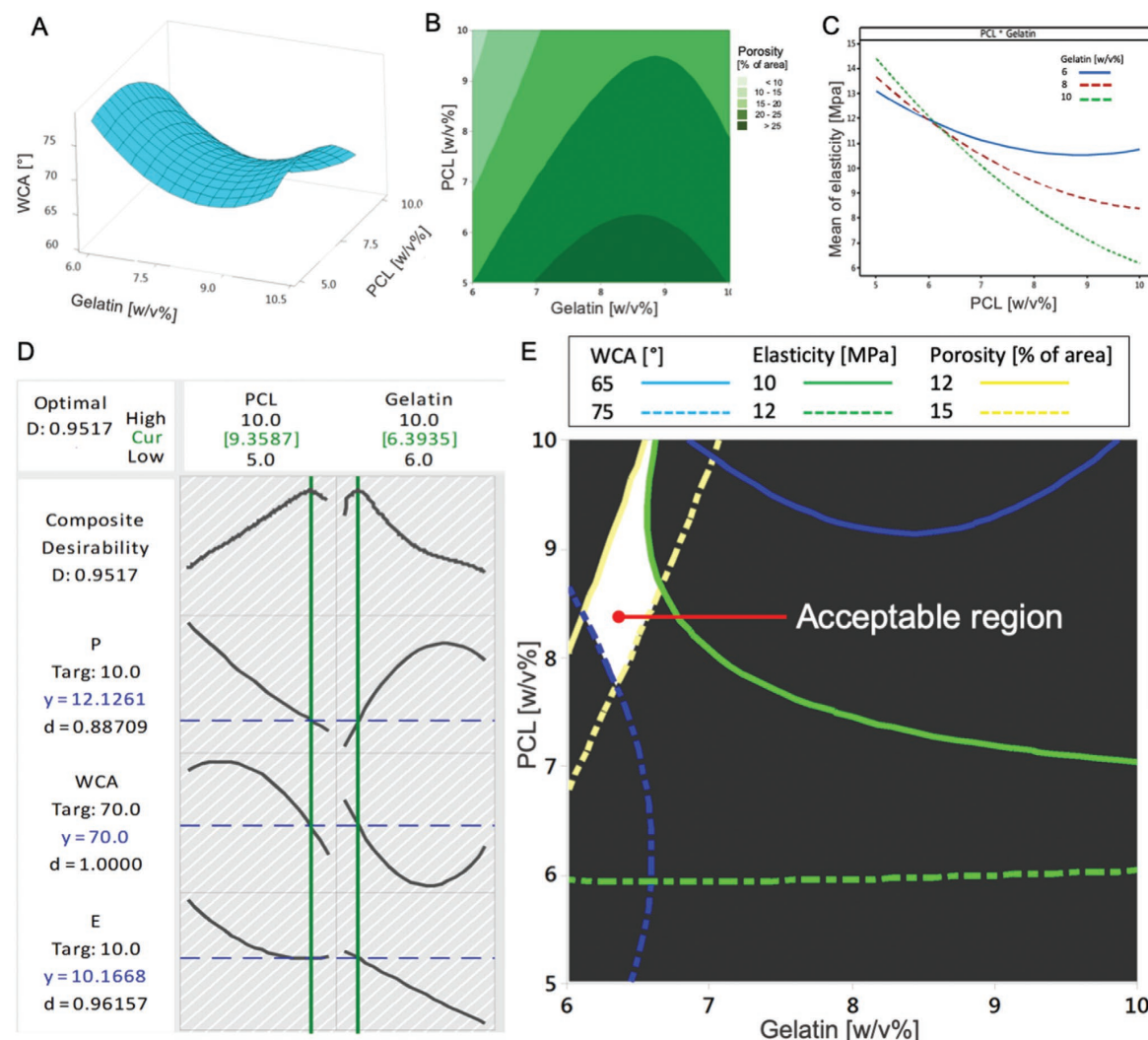


Figure 3. Multi-parameter optimization of PCL-gelatin mixing ratio of the BETA membrane (based on data presented in Figure 2). A) Surface plot of membrane wettability (WCA) for the technically feasible range of PCL and gelatin mixing ratios explored in Figure 2. Both gelatin (p -value ≤ 0.033) and PCL (p -value ≤ 0.017) concentrations affect WCA and thus cell attachment. Second-order polynomial regression analysis revealed $WCA = 156.6 + 6.7P - 25.5G - 0.6P^2 + 1.4G^2 + 0.1P^*G$; $R^2 = 0.96$. B) Contour plot of porosity (P) versus PCL and gelatin mixing ratio, indicating a linear dependence of porosity on both PCL and gelatin concentration (Porosity = $-42.6 - 5.8P + 21.6G + 0.1P^*P - 1.3G^*G + 0.2P^*G$; one-way PCL (p -value < 0.05) and gelatin (p -value < 0.05); $R^2 = 0.94$). C) Interaction plot of PCL and gelatin mixing ratio on the elastic modulus ($E = 14.5 - 1.3P + 1.5G + 0.2P^*P + 0.02G^*G - 0.3P^*G$; $R^2 = 0.99$), showing that both one-way PCL (p -value ≤ 0.0001 ; gelatin p -value ≤ 0.001) and two-way interaction of PCL and gelatin concentration alter the membrane elasticity. D) The optimization plot, which was provided by the response optimizer demonstrating the composite desirability. E) Weights for WCA, porosity, and elastic modulus were considered as 1, representing equal importance. Overlaid contour plot of membrane response parameters namely elastic modulus (E), water contact angle (WCA), and porosity (P) to select an optimum region of mixing ratios by co-optimization of all relevant variables and responses, reaching the target values (see Section 2.2). The design of experiment (DoE) was applied using Minitab 18 software (Minitab Inc., State College, PA, US). The variables were optimized and the significance of the coefficients was evaluated through the coefficient of determination of the R-squared (R^2) (ability to explain variance) by ANOVA at a 95% confidence level. The experiments were performed with three replicate membranes for each mixing ratio, which were analyzed in a randomized order, to avoid systematic bias.

which reduces inadvertent artifacts of the membrane itself and is likely to allow for trans-membrane migration of migratory cells such as neutrophils (was not investigated here). In addition to these micron-sized pores, the phase II membrane has also numerous much smaller secondary pores (< 400 nm) as evidenced by focused ion beam-scanning electron microscopy

(FIB-SEM) tomography (Figure 5E). It is also evident from Figure 5E, that the voids left by the sacrificial gelatin provide a connected 3D network of pores suitable for nutrient supply under ALI cell culture conditions. The primary pores are often occupied with cells since this is where the sacrificial gelatin provided the most suitable substrate for cell attachment

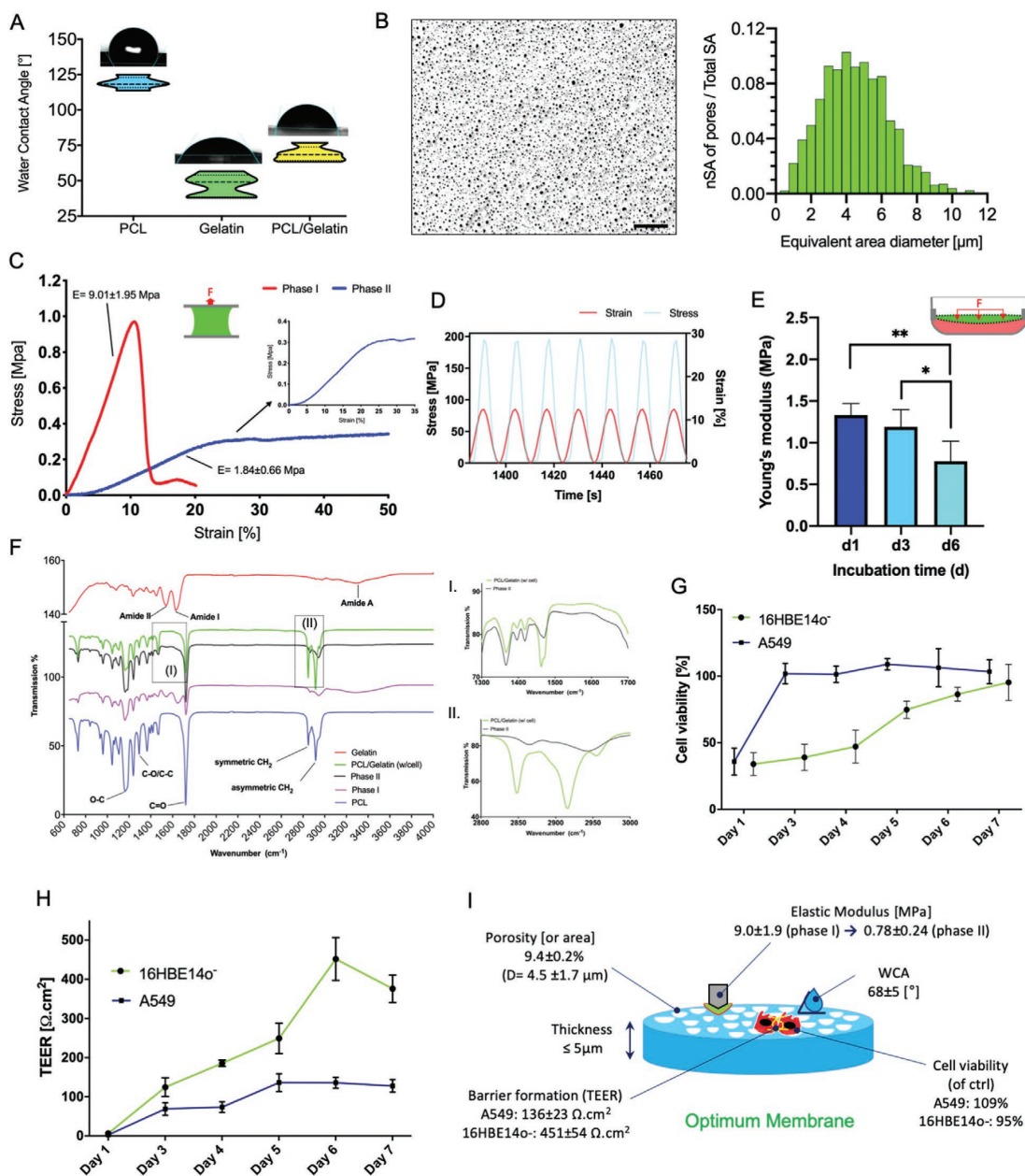


Figure 4. Characterization of the optimized membrane. A) Violin plot of WCA of the membrane compared to the pristine PCL and pristine gelatin films. B) Quantification of porosity of the membrane after day 6 of incubation in cell culture medium (phase II). The pores account for $9.4 \pm 0.2\%$ of the membrane surface area and equivalent area diameter of 4.5 ± 1.7 μm. Scale bar is 100 μm. C) 1D stress-strain curves of the membrane before (phase I) and after inducing porosity (phase II; 6d in cell culture medium) showing a 4.9-fold increase in elastic modulus after washing out gelatin. D) Segmented fatigue test using sinusoidal cyclic 1D stretch at 12% linear strain at 0.33 Hz for 4 h. E) Time-dependence of 3D Young's modulus of the membrane incubated with cell culture medium in the bioreactor, showing that the elastic modulus of the membrane increases between day 1 and day 6 by $\approx 30\%$ (phase II). F) FT-IR spectra of pristine gelatin and PCL, PCL/gelatin blend (phase I), porous PCL/gelatin (phase II) and PCL/gelatin membrane after cell culture (6 d incubation). The FT-IR spectrum of the membrane with cells (green curve) and without cells (black curve) in wavenumber of i) 1300–1700 cm⁻¹ ii) and 2800–3000 cm⁻¹. G) Time series of cell viability measured by WST-1 assay of A549 and 16HBE14o- cells on the membrane. Maximum barrier tightness (confluency) is reached after 6 to 7 days of LLC. K) Schematic of the optimum membrane (9.35% PCL, 6.34% gelatine) showing its unique bio-physicomechanical properties. Data are reported as the mean \pm SD. $n \geq 5$; * $P < 0.05$, ** $P < 0.001$ by one-way ANOVA with Tukey test.

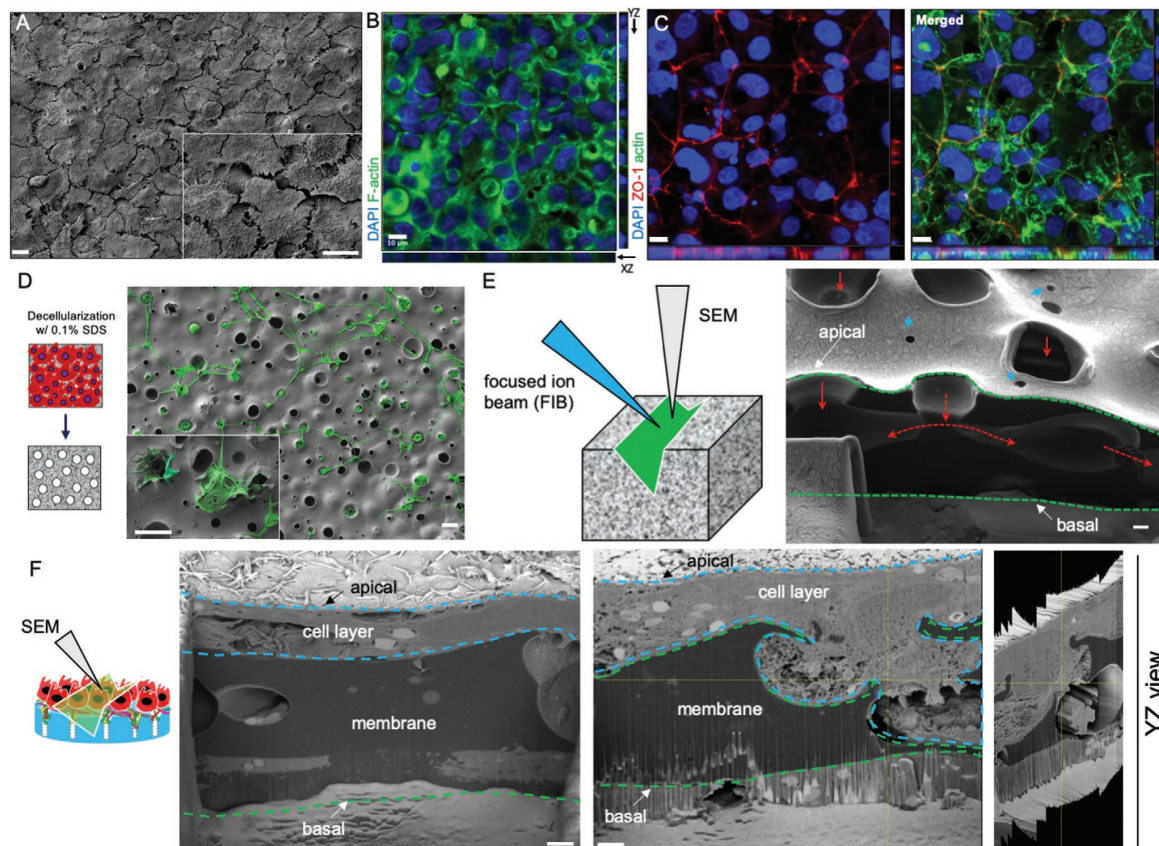


Figure 5. Ultrastructural, morphological and tomographic analysis of cell-membrane interactions. A) SEM image of A549 cells adhering to the surface of the membrane during proliferation on the (optimum) membrane. Scale bar is 10 μm . B) CLSM orthogonal (XY) view and side views of YZ (right) and XZ (bottom), depicting a confluent monolayer of A549 cells (cell seeding density: 1.5×10^5 cells cm^{-2} , 6 days LLC culture) and C) 16HBE14o– cells (cell seeding density: 2×10^5 cells cm^{-2} ; incubation: 6 days under LLC and 1 day under ALI conditions) on the membrane. 16HBE14o– cells form tight junctions between cells. Cell nucleus (blue, DAPI), cytoskeleton (green, F-actin), and ZO-1 tight junction (red). Scale bar is 10 μm . D) SEM analysis of the membrane after removal of A549 cells (0.1% SDS) reveals that cells deposit their own ECM (pseudocolored in green) on the BETA membrane. Scale bar is 10 μm . E) Schematic depiction of the focused ion beam (FIB)-SEM tomography for site-specific analysis. FIB-SEM image of the membrane in phase II (without cells). The green dotted lines show the cross-section of the membrane. Red and blue arrows illustrate the primary and secondary pores, respectively. Dashed red arrows show the interconnectivity of the pores in the structure. The scale bar is 1 μm . F) FIB-SEM z-stack image of the cross-section of the membrane populated with A549 cells, showing the cells (blue dotted line) located on the membrane (green dotted line) as a monolayer (left panel) and situated in the micron-sized primary pores (middle and right panel) occasionally even contacting adjacent cells via the 3D pore network. Scale bar is 1 μm .

(Figure 5F). Considering that the innate basement membrane of the alveolar region is ultra-thin (≈ 0.05 μm), has a substantial fraction of nanopores (< 2.5 nm in diameter) and few larger pores (< 400 nm), but is fibrous in nature allowing super-micron sized cells to “squeeze” through under certain conditions (e.g., neutrophil influx into the lung during inflammation).^[26] The BETA membrane is more biomimetic than conventional engineered membranes, but is still not perfectly representing the basement membrane of the alveolar tissue.

It is also noteworthy that both A549 and 16HBE14o– lung cells secrete their own ECM on the BETA membrane, which contributes to the biomimetic nature of the microenvironment of the cells (Figure 5D) and even more pronounced for 16HBE14o– cells (Figure S4B, Supporting Information). ECM secretion is further

evidenced by FT-IR analysis of the decellularized membrane, which reveals new bonds and shifted FT-IR peaks at wavenumbers of 1469, 1461, 2848, 2915, and 2955 cm^{-1} when compared to pristine membranes (Figure 4F-i,ii). Since ECM is a mixture of proteins, lipids, and glycosaminoglycans (GAGs), it is difficult to unambiguously assign a specific functional group to each characteristic peak. However, it has been shown that these peaks can correspond to nucleic acid, ECM proteins, and lipids.^[27] We also found some fibrillar structures of ECM on A549 decellularized membranes (Figure 5D). These results, as well as the immunohistochemical identification of ECM proteins such as type I collagen (Figure 6B), indicate that epithelial cells do not only proliferate well on the BETA membranes, they also shape their microenvironment by secreting their own ECM components.

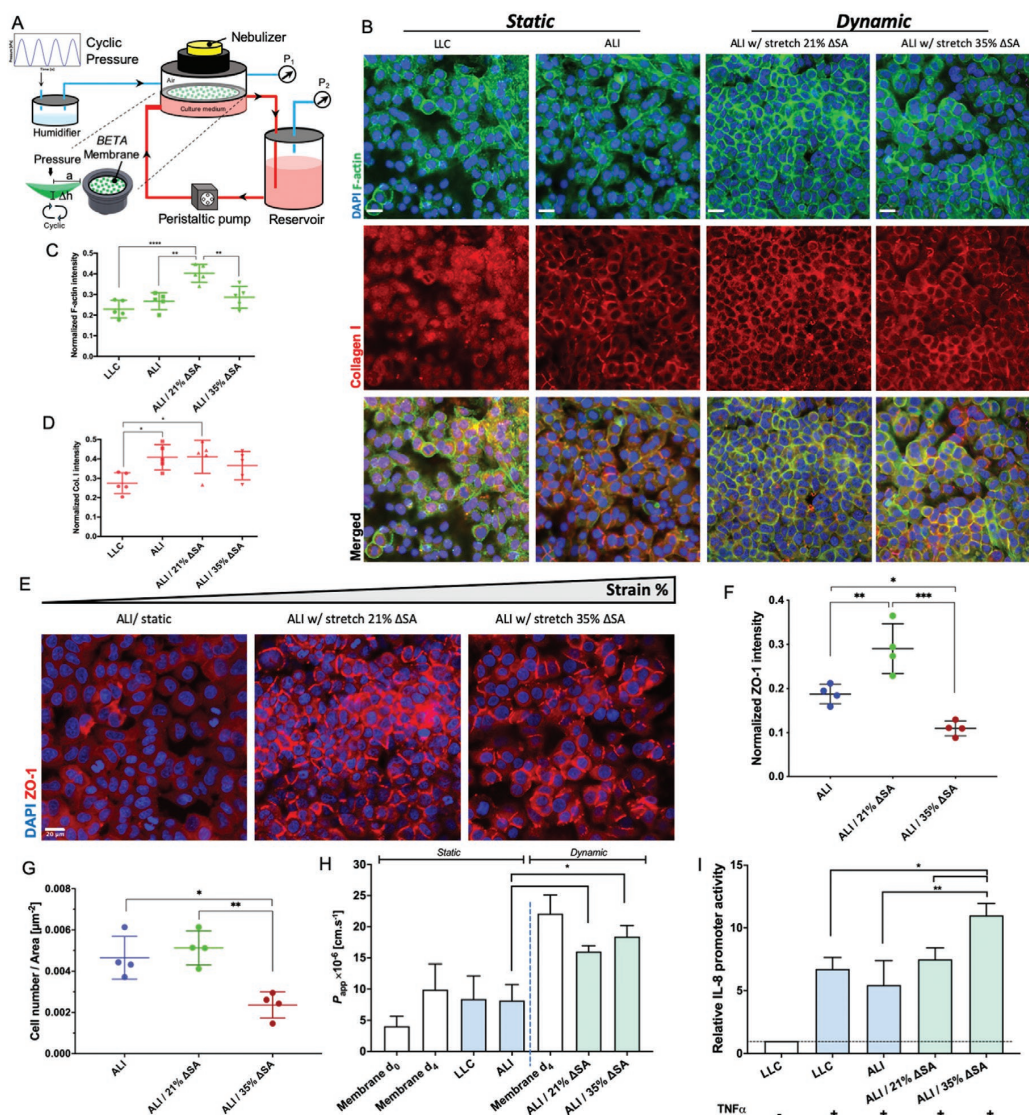


Figure 6. The effect of cyclic mechanical stretch on the cytoskeleton, deposited-ECM, tight junction formation, and barrier integrity. A) Schematic of the in vitro cyclic cell-stretch bioreactor system used in this study. A small positive pressure (maximal 4% above ambient pressure) is applied to the apical side of the membrane, resulting in membrane deformation, which is associated to the volume displacement of cell culture medium into the media reservoir can be monitored via the pressure sensor (P_2) in the medium reservoir. B) Fluorescent CLSM images (obtained for optimum gain/pinhole settings of CLSM) of A549 cells grown on the (optimum) BETA membrane under static (6d LLC and 6d LLC plus 24 h ALI) and dynamic/ALI (21% and 35% Δ SA for 24 h) culture conditions ($n = 5$). Cells under cyclic strain (21% Δ SA) formed more F-actin (green) and collagen I (red). Non-physiologic high levels of strain (35% Δ SA) disrupted the cytoskeleton (no increase in F-actin). On the other hand, deposited collagen I is polymerized under both static and dynamic ALI culture as compared to LLC conditions. Cell nuclei stained with DAPI (blue). Scale bar is 20 μ m. These trends are confirmed by quantitative fluorescence analysis (total fluorescence intensity of z-stack—obtained for a given reference gain/pinhole CLSM setting—normalized to the number of cell nuclei) of C) F-actin and D) collagen I in panel B under dynamic ALI and static (LLC and ALI) culture conditions. E) Qualitative (optimum CLSM settings) and F) quantitative CLSM analysis of ZO-1 tight junction formation of A549 cells (reference CLSM settings normalized to the number of cells/nuclei) under physiologic and non-physiologic cyclic mechanical stretch (ALI) conditions ($n = 4$). For each experimental setting, five representative images (z-stacks) were recorded at independent fields of view (region of view: 212.55 μ m \times 212.55 μ m) for each sample. Nuclei (DAPI, blue) and ZO-1 (red). G) The number of cells (nuclei) per area were quantified to investigate the dependence of cell viability under static and stretch conditions. H) Apparent permeability (P_{app}) of a confluent A549 cell monolayer under static (LLC and ALI) and cyclic cell-stretch (21% Δ SA and 35% Δ SA) conditions with respect to FITC-Dextran (4 kDa). Pristine membranes (without cells; white bars) at day 0 and 4 under static and stretch conditions were used as control ($n \geq 4$). I) IL-8 release of pIL8-Luc-A549 cells after stimulating with TNF- α (15 ng mL⁻¹). LLC without TNF- α stimulation was used as a control ($n \geq 4$). Data are reported as the mean \pm SD; * $P < 0.05$, ** $P < 0.001$ and **** $P < 0.00001$ by one-way ANOVA with Tukey test.

This is important for cell culture studies since it is likely that the secretion of ECM modulates the interaction between the cell cytoskeleton and the membrane/ECM, which are linked by transmembrane receptors so-called integrins that regulate AT cell migration and proliferation.^[28] Z-stack FIB-SEM analysis shows the spreading of A549 cells on the membrane, formation of ECM inside pores, and cell-cell interaction via interconnected pores (Figure 5F and Movie S1, Supporting Information). Transmission electron microscopy (TEM) study of the human alveolar wall has shown that alveolar epithelial cells (both type I and II) and human alveolar fibroblasts make contact through gaps in the epithelial basement membrane. In addition, fibroblasts may directly connect the endothelium to the epithelium via apertures in the basement membrane.^[29] Mimicry of these aspects may be possible with the BETA membrane presented here.

Furthermore, alveolar epithelial cells such as primary rat alveolar epithelial type II (rATIIIs) and human alveolar epithelial type-II like cells (A549) are responsive to membrane stiffness and surface architecture, where softer membranes enhance actin cytoskeletal distribution and diminish tight junction formation^[20,21,30] and stiffer membranes increase the formation of F-actin cytoskeleton (Figure S5, Supporting Information), which is consistent with other studies.^[31,32] These studies signify the importance of the membrane mimicking the stiffness of the basement membrane of the lung. The membrane under wet conditions has Young's modulus of 0.78 ± 0.24 MPa, which complies with the average of Young's modulus of a single alveolar wall (≈ 0.30 MPa).^[33] As the lungs are under continuous expansion and contraction, and the membrane stretch should remain reversible for at least a few hours, which has been shown to be required for adaptation of cells to cyclic stretch, to the entire lifetime of the cell culture model (here several days). We have shown that the biphasic membrane remains elastic under physiologic cyclic mechanical stretch up to 10% linear strain for 2 days (largest investigated time period).^[6]

2.4. Cyclic Mechanical Stretch Regulates Pulmonary Cell Physiology

Cyclic mechanical stretch induces several biological endpoints and activates several pathways involved in the physiology of lung epithelial cells.^[6] Here, we implement our (optimum) BETA membrane in the cyclic in vitro cell-stretch (CIVIC) bio-reactor, which was designed for culturing of in vitro lung cell models under cyclic mechanical stretch with the possibility of delivering aerosolized substances to the cells, to investigate cellular responses to cyclic stretch under ALI conditions (Figure 6A). It is noteworthy that during physiologic cell stretch experiments cells ALI conditions remain intact remain, i.e., cells do not detach from the membrane and no medium is seeping onto the apical surface. Its unique feature of monitoring the pressure in the apical chamber (P_1) and the pressure in the medium reservoir (P_2) allows for not only for real-time monitoring of amplitude and frequency of cyclic cell stretch during the entire cell-stretch experiment but also of Young's modulus of the membrane. A549 epithelial cells were grown on the membrane to reach confluency and then cyclically stretched (tri-axial (3D), 20 cpm (0.33 Hz)) for 24 h under physiologic

(21% Δ SA (surface area); 10% linear) and non-physiologic (35% Δ SA; 16.5% linear) conditions using the CIVIC cell-stretch bio-reactor system.

While quantitative confocal laser scanning microscopy (CLSM) analysis showed that the culture condition itself (ALI versus submerged) does not affect F-actin expression, cell-stretch stimulated actin accumulation under physiologic stretch conditions (21% Δ SA strain), but not under overdistension conditions (35% Δ SA strain) (Figure 6B,C). In contrast, secretion of the ECM protein collagen I was stimulated for ALI conditions, but not affected by cyclic mechanical stretch regardless of amplitude (Figure 6B,D). We also found that physiologic stretch induces ZO-1 tight junction formation, while non-physiologic stretch (35% Δ SA) causes a loss of cells (Figure 6G) and a disruption of the integrity of the cell monolayer (Figure 6E,F and Figure S6, Supporting Information). ZO-1 tight junctions were intensified especially at cell-cell junctions, revealing that cyclic physiologic stretch enhances tight junction formation/arrangement (Figure 6E). Moreover, pathologic stretch (35% Δ SA) damaged the cell layer as evidenced by the reduced number of cells possibly due to apoptosis (Figure 6G).

We then studied the paracellular transport of small molecules to evaluate the role of mechanical stretch on barrier integrity. Figure 6H shows the apparent permeability (P_{app}) of FITC-dextran (4 kDa) under stretch conditions compared to static conditions. The permeability of FITC-dextran under submerged (static), ALI (static), ALI 21% Δ SA (dynamic) and ALI 35% Δ SA (dynamic) conditions was measured as $8.48 \pm 3.69 \times 10^{-6}$, $8.18 \pm 2.54 \times 10^{-6}$, $16.03 \pm 0.92 \times 10^{-6}$ and $18.44 \pm 1.74 \times 10^{-6}$ cm s⁻¹, respectively. Apparent permeability analysis indicated that the translocation of (4 kDa) molecules across the cell barrier under ALI conditions is significantly increased under stretch for 24 h compared to static conditions (21% Δ SA vs ALI, $p < 0.03$; 35% Δ SA vs ALI, $p < 0.01$). It is also important to note that the membrane itself has larger permeability under physiologic stretch ($16.01 \pm 0.65 \times 10^{-6}$ cm s⁻¹) than under static conditions ($8.18 \pm 2.54 \times 10^{-6}$ cm s⁻¹), which is likely due to expanding pores (≈ 1.10 -fold larger for 21% Δ SA) and convective dextran transport during the cyclic stretch. Assuming that the transport resistance ($\approx 1/P_{app}$) of the membrane and the cell barrier are additive, the membrane-corrected permeability of the stretched layer of A549 cells can be determined as 59.5×10^{-6} and 109.9×10^{-6} cm s⁻¹ for 21% Δ SA and 35% Δ SA stretch, respectively (Equation (1))

$$P_{app,cell} = (P_{app,total} \times P_{app,membrane}) / (P_{app,total} - P_{app,membrane}) \quad (1)$$

This indicates that for non-physiologic stretch (35% Δ SA), the A549 barrier integrity is impaired. It is also instructive to consider P_{app} values (for 4 kDa dextran) for A549 cells cultured on standard Transwell inserts under static conditions. Typical literature values range between 2.5×10^{-6} and 10×10^{-6} cm s⁻¹.^[34,35] but only very few studies also report P_{app} of the membrane without cells. From Frost et al 2019 (Figure 5 of^[34]), one can calculate P_{app} for the membrane (1.70×10^{-5} cm s⁻¹ for 12-well Transwell insert; pore size 0.4 μ m) and the membrane with cells (758×10^{-6} cm s⁻¹) yielding $P_{app} = 1.36 \times 10^{-5}$ cm s⁻¹ for A549 cells. This is about 6-fold lower than the value we found for A549

on BETA membrane under physiologic stretch. Thus, cyclic stretch apparently enhances the permeability of A549 cells, but we cannot rule out that the large difference in membrane elastic modulus (≈ 1000 -fold higher as compared to PET) also has an effect on A549 permeability. This effect cannot be assessed from our data since there is no significant difference between P_{app} of the membrane with and without cells (Figure 6H). However, for a PDMS membrane under static conditions in a lung-on-a-chip device, P_{app} of A549 cells was found to be $5.6 \times 10^{-6} \text{ cm s}^{-1}$ (as derived from P_{app} of the membrane with ($2.5 \times 10^{-6} \text{ cm s}^{-1}$) and without A549 cells ($4.5 \times 10^{-6} \text{ cm s}^{-1}$).^[34]

We conclude that our results are in general agreement with previously reported results, which validates our BETA membrane for cell-stretch experiments. Formation of actin as one of the main components of the anchored cytoskeleton that is necessary for the maintenance of epithelial barriers can be stimulated by stretch due to an increase in intracellular calcium ion levels that influences epithelial permeability.^[36–38] Tight junctions are cell-cell adhesion complexes in epithelial cells that carry out important functions, including controlling paracellular and transcellular transport, maintaining cellular polarity, and regulating a variety of intracellular signals.^[39,40] Crucial tight junction proteins in the alveolar epithelium are occludin, ZO-1, and claudin-4.^[38] Among them, ZO-1 influences the structure and function of the alveolar epithelial barrier and acts as a connection between transmembrane tight junction proteins and the actin cytoskeleton.^[38] It has been shown that a physiological stretch of 8% linear did not affect the integrity of a cell monolayer and ZO-1 formation.^[12] On the other hand, a cyclic non-physiologic stretch during mechanical ventilation is playing a pivotal role in disease development (e.g., acute respiratory distress syndrome (ARDS)) via increasing protein permeability, inhibiting tight junction proteins, and disarrangement of actin filaments.^[38,41] Cavanaugh et al. showed that the overall expression of ZO-1 is negatively affected by a high level of stretch (37% Δ SA) in rat AT-type II cells.^[41] Song et al. also showed that the mechanical overdistension (37% Δ SA strain) causes a disconnection of claudin 4 and 7 from ZO-1 in precision-cut lung slices (PCLS).^[42]

Changes in the arrangement of actin cytoskeleton and interaction between F-actin and the tight junction complexes modulate the paracellular permeability.^[38–40] Similar to our finding for 4 kDa dextran, it has been reported that cyclic mechanical stretch increases the transport of FITC-sodium (0.4 kDa) in the 16HBE14o- cell line and primary AT cells.^[12,43] The apparent permeability for FITC-dextran (70 kDa) is also increased under a physiological stretch of 8% linear strain.^[12] High amplitude strain increases the translocation of micro-molecules across the alveolar epithelium, which can partly happen through calcium- and actin-dependent mechanisms^[37] or by paracellular signaling pathways such as stretch-associated superoxide release.^[44]

Albeit stretch-induced enhanced barrier permeability is an important factor for in vitro pharmacokinetic studies, the majority of the research in this field has been carried out under non-physiologic submerged or static ALI conditions.^[2,45] There is very little data on the effect of cyclic stretch on the permeability of in vitro barrier models of the lung.

2.5. Inflammatory Response Can Be Activated by Stretch

Interleukin-8 (IL-8) plays a key role in the pathogenesis of inflammatory lung diseases such as ARDS.^[46] It has been shown that cyclic stretch promotes IL-8 gene expression and protein release in A549 cells.^[47] We used IL-8 release as a marker of deformation-induced inflammatory signaling induced by cyclic stretch. Here, we seeded the IL8-Luc-A549 reporter cell line on the membrane^[48] and IL-8 promoter activity was measured using the luciferase assay. IL-8 release of the cells cultured under cyclic stretch of 35% Δ SA for 24 h was significantly higher than under physiologic stretch (21% Δ SA; p -value < 0.04), static conditions under both ALI (p -value < 0.003) and liquid-liquid culture (LLC) conditions (p -value < 0.01), indicating that non-physiologically high stretch (35% Δ SA) activates inflammatory responses (Figure 6I). Again these results agree with previous studies that reported no significant increase in IL-8 secretion by A549 and primary human alveolar epithelial cells under physiologic mechanical strain (10–15% Δ SA strain)^[43,49] and intense mechanical stretch (30% Δ SA strain) induced inflammatory mediators such as IL-8 in A549 cells.^[47]

2.6. Cellular Uptake of Nano- and Microparticles under Stretch

The effect of cell-stretch on the mechanisms of cellular uptake and paracellular transport of nanoparticles (NPs) is very difficult to study under in vivo conditions. While in vitro studies under static ALI conditions have been performed, to the best of our knowledge, this has not been investigated for cell-stretch conditions, yet. The effect of cyclic stretch on particle uptake was only performed under physiologic conditions (21% Δ SA) since non-physiologically high deformation of the cell layer (35% Δ SA) not only disrupts the tight junctions but also reduces cell viability and loss of cells. While the loss of cells and disruption of tight junctions is expected to substantially enhance transepithelial translocation of particles (Figure 6E,F), reduced cell viability (Figure 6G) inhibits all cellular processes including cellular uptake. Since such a severely injured alveolar cell barrier does not exist in patients, cellular uptake and transepithelial transport of particles were not measured for 35% Δ SA stretch conditions.

Ultrafine ambient NPs (less than 100–300 nm in diameter) are often implicated as particularly hazardous due to their enhanced surface area per mass which has been associated with both acute and chronic lung disease.^[50,51] Moreover, NPs smaller than ≈ 100 nm have a relatively high probability of translocation from the lung to blood circulation (transbarrier transport)^[52] which may induce adverse health effects in the secondary target organ (e.g., liver, heart),^[53] but it also makes inhaled nanosized particles attractive as drug carriers for both pulmonary and systemic drug delivery.^[54]

We chose two sizes (NP: 100 nm diameter; microparticle (MP): 1000 nm) of amine-modified polystyrene (PS-NH₂) particles to investigate the size-dependent effect of physiologic cyclic stretch on cellular uptake dynamics of particles under ALI culture conditions (Figure 7A). An aqueous suspension of monodisperse particles (PS-NH₂; 100 and 1000 nm) was

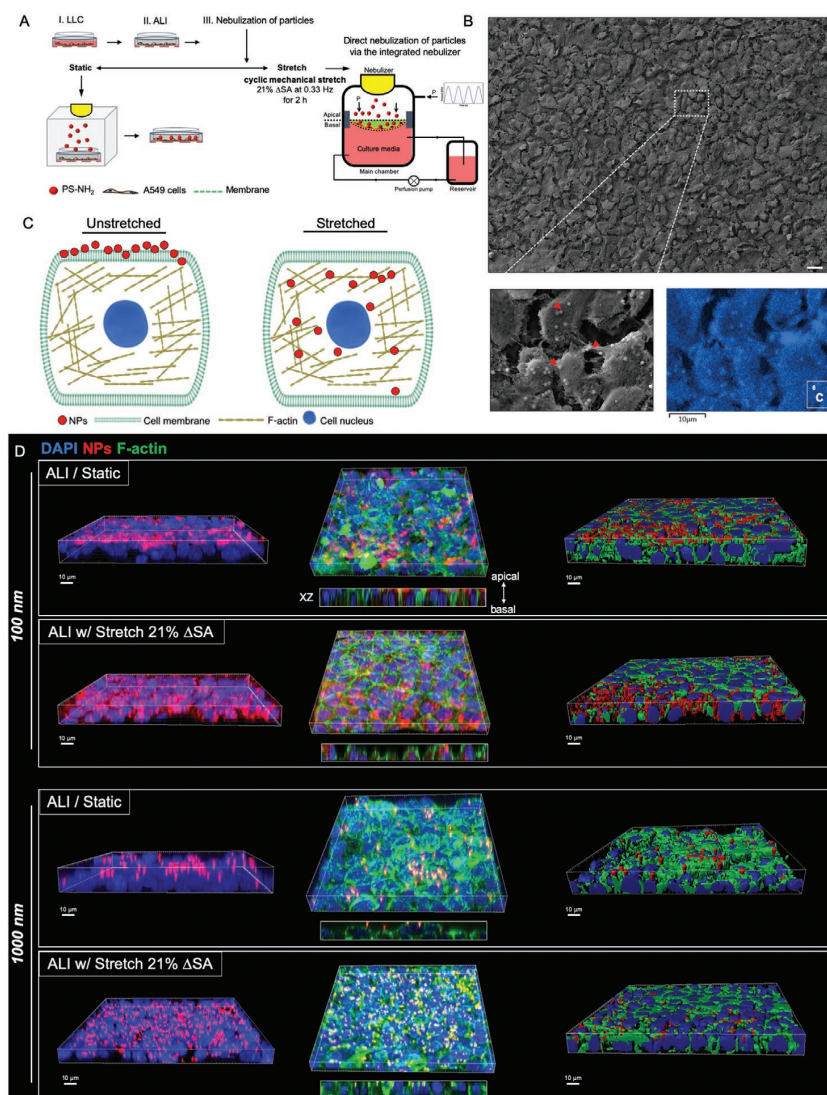


Figure 7. Cell uptake of nano- and microparticles under static and stretch conditions. A) Workflow for particle study. A549 cells (cell density: 2×10^5 cells cm^{-2}) were seeded on the membrane. The cells were cultured under LLC for 4 days and after obtaining a confluent cell monolayer, cells were air-lifted and maintained as ALI culture for 1 day. Amine-modified polystyrene (PS-NH₂) nano- and microparticles (100 and 1000 nm diameter, respectively) are then nebulized onto the cells (within a few minutes) either with the nebulizer of the bioreactor (for cell-stretch conditions) and the VITROCELL CLOUD 6 system (static conditions). After 2 h, the cells were fixed and prepared for CLSM analysis. B) (top) SEM analysis of microparticle (MP) distribution (Red arrow, 1000 nm) on A549 lung cells. Scale bar is 20 μm . (bottom) Detection of MPs (by carbon) using SEM/EDS analysis. Scale bar is 10 μm . C) Schematic depiction of internalization nanoparticles into a cell under static and stretched conditions based on results from panel D. D) 3D reconstruction CLSM images of nano- and microparticles after 2 h under static and physiologic stretch (21% ΔSA) conditions. (left) The perspective (by IMARIS) and XZ (by Fiji) view of CLSM images based on the results of the z-stack and cross-section. (middle) XZ view of CLSM image shows only the NPs (red) and cell nucleus (blue). (right) Surface rendering of CLSM images by IMARIS. These images reveal retention of the MPs near the apical (top) side of the cells for both static and dynamic conditions. Nanoparticles also reside near the apical side of the cell layer under static conditions, but get internalized deeply across the cell membrane and reside in close proximity with actin filaments. Nuclei (DAPI, blue), PS-NH₂ (red), and F-actin (green).

nebulized within a few minutes onto the cells under static/ALI and physiologic cell-stretch/ALI conditions. The exposure process itself does not substantially change the nominal particle diameter. Albeit nebulization increased the nominal

particle diameter by about 20% likely due to agglomeration (see Figure S7, Supporting Information), this does not significantly affect our comparison of cellular uptake of nano- versus micron-sized particles. Moreover, the cell-delivered particle

dose of $2.1 \mu\text{g cm}^{-2}$ was chosen to avoid multi-layered stacking of the particles (agglomeration) by low fractional area coverage of the cells (here: 30% and 3% for 100 and 1000 nm particles, respectively). After 2 h of particle exposure (deposited dose: $2.1 \mu\text{g cm}^{-2}$), no cytotoxicity (WST-1 assay) was detected (data not shown) under these conditions. SEM analysis also presented no cell detachment after the nebulization of particles (Figure 7B). Hence, cells were viable enough for reliable cellular uptake measurements.

Localization of particles on the A549 cell layer showed that after 2 h under static conditions, the particles of both sizes (100 and 1000 nm) are located on top of the cell layer often attached to F-actin (Figure 7D and Movies S2–S3, Supporting Information), which is in line with previous studies.^[55,56] Under physiological cell-stretch conditions (21% ΔSA strain), the same situation was observed for 1000 nm particles. However, 100 nm NPs were found to efficiently penetrate the cell layer reaching the subcellular compartments in the vicinity of the nucleus and again attaching to the actin filament structure (Figure 7D and Movie S4, Supporting Information).

The knowledge of the effect of stretch on NP internalization in the lung is controversial. In support of our results, Hu et al. showed that physiological mechanical stretch (10% linear strain) enhanced cellular uptake (A549) and internalization of 100 nm PS-NH₂ NPs under ALI conditions.^[13] On the other hand, Schmitz et al. reported that physiologic cyclic stretch (15% ΔSA strain) did not increase cellular uptake (A549) of 25 nm SiO₂ NPs under LLC conditions.^[49]

For pulmonary epithelial cells, particle uptake primarily occurs via endocytosis, which is limited to particle sizes smaller than ≈ 500 nm.^[57,58] This explains the lack of uptake of 1000 nm particles under both static and cyclic stretch conditions (Figure 7D). Passive para- or transcellular diffusion into and across the cell barrier was ruled out as relevant uptake mechanism by demonstrating that transcellular transport of 100 nm particles was inhibited almost completely at low temperature (4 °C) conditions (data not shown), which implies that an energy-consuming, active cellular mechanism like endocytosis governs cellular uptake. In contrast to previous studies, 100 nm NPs were also found to be attached to the cell surface without penetrating deeper into the cells.^[58] Only after cyclic stretch, NPs were abundantly taken up and internalized by A549 cells (Figure 7C). As all previous studies were performed on extremely stiff plastic multi-well plates, this surprising lack of NP uptake under static conditions may be evidence for the impact of membrane elasticity on cellular function and response.

2.7. Advantages of BETA Membrane

Most in vitro cell culture experiments with alveolar epithelial cells cultured under physiologic ALI conditions are performed either on standard PET Transwell inserts (no stretch) or on stretchable PDMS membranes. Alternatively, natural polymers such as collagen and decellularized ECM (derived from pig lung) in combination with synthetic polymers such as poly-L-lactic acid^[17] showed an improvement in the physical characteristics of hybrid scaffolds used for lung applications.

Here we presented a biphasic copolymeric membrane concept (PCL/gelatin) which provides optimized conditions for the two different phases of toxicological or pharmacological studies with alveolar barrier models, namely the cell growth (phase I) and cyclic stretch (phase II). The spin-coated PCL/gelatin membrane (9.35% PCL and 6.34% gelatin [w/v solvent]) demonstrated various improved biomimetic features as compared to conventional porous membranes (stiff: PET; elastic: PDMS) such as low interference with transbarrier transport processes, biomimetic elasticity, while maintaining the structural integrity of the membrane even under cyclic stretch, and ease-of-handling.

The bio-inspired membrane manufactured here is ultrathin (thickness $\leq 5 \mu\text{m}$), mimicking the total alveolar-capillary barrier thickness ($1.1 \mu\text{m} \pm 0.1$, harmonic mean). The prerequisite for low interference with transbarrier transport processes is i) low membrane thickness ($\leq 5 \mu\text{m}$ is similar to $1.1 \mu\text{m}$ of alveolar-capillary tissue (harmonic mean) while PET and PDMS membranes are typically $>10 \mu\text{m}$), ii) large pore size of up to $8 \mu\text{m}$ ($4.5 \pm 1.7 \mu\text{m}$ (mean \pm SD) as compared to $< 3 \mu\text{m}$), and iii) large porosity ($9.4 \pm 0.2\%$, instead of 3.5 % or 0.5% for PET membranes with 3 and $0.4 \mu\text{m}$ pores, respectively (e.g., Corning specification sheet). This results in an apparent permeability (for 4 kDa FITC-dextran) of $8.18 \pm 2.54 \times 10^{-6}$ and $16.03 \pm 0.92 \times 10^{-6} \text{ cm s}^{-1}$ under static and dynamic (stretch) conditions, respectively, as compared to $4.0 \pm 5.5 \times 10^{-6} \text{ cm s}^{-1}$ typically reported for PET and PDMS membranes.^[34] In addition to the reduced interference of our membrane with transbarrier molecule/particle transport, it is conceivable that up to $8 \mu\text{m}$ pores (instead of typically $3 \mu\text{m}$ pores for epithelial cells on PET or PDMS membranes) will facilitate the important features of migration of neutrophils from the basal/blood into the luminal compartment (airside), which is a hallmark of pulmonary inflammation.

Another important aspect of cell functionality is the elastic modulus of the membrane. The BETA membrane has Young's modulus of $0.78 \pm 0.24 \text{ MPa}$, which is very similar to alveolar tissue of the lung (0.30 MPa) and much smaller than typical Young's modulus of PDMS membranes (2.61 ± 0.02 – $3.59 \pm 0.11 \text{ MPa}$ for 10:1–5:1 base: agent mass ratio).^[59] In addition to the high elasticity, the membrane is resilient to fatigue under cyclic stretch for at least up to 48 h, which covers the typically used experimental periods for in vitro cell-stretch experiments and maintains structural integrity not only for small microfluidic lung chips ($< \text{mm}^2$), but also for millifluidic ($> \text{cm}^2$) membranes similar to 6-, 12-, and 24-well Transwell inserts. The translucent nature of the manufactured membrane makes it suitable for all optical imaging modalities. Its conduciveness to cell growth does not require physical or chemical functionalization or protein coating of the membrane to stimulate cell adherence and growth.

3. Outlook

The development of even more biomimetic in vitro models of biological organs and barriers is essential for their prediction capacity for human/clinical outcomes with respect to protection and restoration of health. The biphasic copolymer membrane

designed here is capable of closely mimicking several key features of the alveolar-capillary barrier of the human lung.

In this proof-of-concept study with an alveolar type-II like (A549) and bronchial (16HBE14o-) epithelial cell line, we were able to confirm stretch-induced functional changes of these cells reported in the literature. These features include remodeling of the actin cytoskeleton and enhanced barrier function associated with higher levels of tight junction proteins (ZO-1) and permeability (P_{app}) under physiologic stretch conditions (21% Δ SA strain, 0.33 Hz), while non-physiologic stretch (35% Δ SA strain, 0.33 Hz) induced apoptosis, provoked inflammatory responses (IL-8) and disrupted actin cytoskeleton, and barrier integrity. Application of this cell stretch model to aerosolized particles showed that 2 h of physiologic cyclic stretch enhances cellular uptake of NPs (100 nm), but not of MPs (1000 nm). The latter indicates that cyclic stretch does not extend the size limit of 500 nm for endocytic uptake by epithelial cells to 1000 nm.

The BETA membrane introduced here should be tested with advanced cell culture models such as immortalized primary alveolar epithelial cells (hAELVi) and it could be integrated with microfluidic lung-on-a-chip devices to extend their biomimetic features with respect to membrane elasticity, ease of cell growth and reduced membrane thickness. All of these features combined could pave the way for significantly improved in vitro toxicity, drug and pharmacokinetics testing of inhaled substances.

4. Experimental Section

Membrane Fabrication: Poly(ϵ -caprolactone) (PCL; Sigma-Aldrich, Mn 80 000), and gelatin (Type A from porcine skin, Sigma) were dissolved in TFE ((2,2,2-trifluoroethanol) with $\geq 99\%$ purity, Roth) and stirred until the emulsion was homogenous. The copolymer emulsion of PCL/gelatin was then added to a homemade spin-coater (2000 rpm) to produce a dense skin layer (Figure 1E–G). The fabricated film was subsequently dried under vacuum (300 mbar) to obtain a uniform layer. The film was then fixed between two polycarbonate holders to create apical and basal chambers. Membranes were sterilized before cell culture experiments with phosphate buffered saline (PBS), ethanol 80% and UV exposure. The film thickness depends on spinning speed, initial viscosity, and evaporation rate.¹⁶⁰ The manufacturing process was optimized to obtain an ultrathin membrane ($\leq 5 \mu\text{m}$) (Figure 1H). Design of experiment (DoE) approach using the response surface methodology (RSM)—the central composite design (CCD)—was applied (Minitab 18 software, Minitab Inc., State College, PA, US) to find the optimal mixing ratio of PCL and gelatin (Table 1). The significance and the effect size of variables (concentration of PCL and gelatin) and the corresponding linear and quadratic interactions on the response variables (WCA, porosity, and elastic modulus) were evaluated based on the coefficient of determination (R-squared). Analysis of variance (ANOVA) was used to evaluate whether the model is statistically significant at 95% confidence level.

Membrane Characterization: The morphology of the membranes was observed by scanning electron microscopy (SEM, Zeiss Crossbeam 340, Carl Zeiss AG, Oberkochen, Germany) at an operating voltage of 2 kV. To evaluate cell attachment, the samples were fixed in 6% v/v glutaraldehyde (Sigma-Aldrich) and subsequently post-fixed with 1% OsO₄ ((Plano, Wetzlar, Germany)) and 1.5% K₄Fe(CN)₆ (Sigma) in 0.1 M CAC buffer for 1 h (4 °C). The samples were then dehydrated in gradient ethanol solutions followed by HDMS (hexamethyldisilazane, Sigma-Aldrich) for 15 min and subsequently mounted onto aluminum stubs, sputter-coated with platinum, and imaged by SEM. ECM materials were pseudocolored in SEM images using the GNU Image Manipulation Program (GIMP 2.10.8) (<http://www.gimp.org/>).

Focused ion beam (FIB)-SEM tomography (Zeiss Crossbeam 340, Carl Zeiss AG, Oberkochen, Germany) in sectional series (24.5 nm interval) was used to study the internal structures of samples at high resolution (30 kV; 100 and 300 pA). The images were aligned using NIH Fiji (Registration tool) and then reconstructed by IMARIS software (version 9.0; Bitplane, Zurich, Switzerland) and NIH Fiji.

Energy dispersive X-ray spectroscopy (EDS, X-max^N, Oxford instruments) analysis with acceleration voltage of 8 kV was also used to provide qualitative elemental and chemical microanalysis.

To calculate the porosity and the pore diameter size of the membranes, 12 independent fields per sample of SEM images quantified by NIH Fiji macro (Threshold, make binary, watershed and analyze particles).

The water contact angle (WCA) of the membranes was determined with the sessile drop method using an automated contact angle system OCA20 with an image processing system. Deionized water droplets of 1 μL were deposited via a syringe at a velocity of 1 $\mu\text{L s}^{-1}$. The drop shape was recorded with a high-speed framing camera and measurements were performed 5 s after droplet addition. Five measurements per sample type were performed.

Fourier transform infrared spectroscopy (FT-IR; Nicolet iS 10 FTIR Spectrometer (Thermo Fisher Scientific, Waltham/Massachusetts, USA) was used to analyze the structural properties and chemical changes of the membranes. All spectra were recorded with 32 scans per sample in the attenuated total reflection (ATR) mode in the wavelength range of 400–4000 cm^{-1} .

The mechanical properties of the membranes were characterized using a dynamical mechanical testing instrument (BOSE 5500 system, ElectroForce, Eden Prairie, MN, USA) with a load capacity of 22 N. Film strips membrane (10 \times 10 mm) were stretched at a rate of 0.01 mm s^{-1} until rupture. Sample thickness was measured using the cross-section area of the membranes using SEM. Tensile strength and maximum elongation at the elastic region were calculated. Young's modulus was calculated as the slope of the most linear region of the stress–strain curves in the elastic region. The modulus of resilience (U_r , kPa) which is the area under the strain–stress curve in the elastic region was calculated using the Area Below Curves macro, Sigma Plot 12.0.

Static Cell Culture: Immortalized human alveolar epithelial type-II like A549 cell line was cultured and maintained in Dulbecco's Modified Eagle Medium: Nutrient Mixture F-12 (DMEM/F12, 1:1 v/v, Gibco) supplemented with 10% FCS (Gibco), 1% v/v Pen/Strep (100 U mL^{-1} , Gibco), 1% L-glutamine (2×10^{-3} M, Gibco), and 2-phospho-L-ascorbic acid (0.1×10^{-3} M, Sigma). For cell proliferation study, cell suspension with a cell density of 1×10^5 cells cm^{-2} was seeded on a pre-wetted and sterilized membrane (effective growth area: 1.3 cm^2). Cells first were cultured under liquid–liquid conditions (LLC, 6 days) and then were air-lifted for ALI conditions (24 h).

Bronchial epithelial 16HBE14o- cells were also used for cell model barrier studies such as cell monolayer integrity and TEER measurements. 16HBE14o- cells (cell seeding density: 2×10^5 cells cm^{-2}) were cultured on the membranes (6 days under LLC and 1 day under ALI conditions) in MEM medium (Gibco) supplemented with 10% FCS (Gibco), 1% v/v Pen/Strep (100 U mL^{-1} , Gibco).

Cell viability was measured by WST1-assay. Each membrane was incubated with 1 mL diluted WST1 reagent (Roche, Mannheim, Germany) (1:15) at 37 °C. After 15 min, 150 μL supernatant was transferred to 96-well plate (4 times for each membrane) and was measured in a plate reader (Magellan Tecan) at 450 nm. All the results were normalized to the mean value of blank.

Dynamic Cell Culturing: The CIVIC system was used to apply cyclic stretch to cells grown on the BETA membrane under ALI culture conditions. The CIVIC system is a modified version of the previously described MALI system,^{161,162} which has been improved for technical performance mainly related to material stability, membrane fixation, and pressure sealing. While the geometry of the bioreactor system was not changed over the previously described version, some parts were modified to improve the airtightness of the bioreactor chamber and ease of handling. All of the elements, which are in contact with the culture

medium, were manufactured with polycarbonate (PDMS-free materials) to prevent leaching of PDMS to the culture medium. The upgraded polycarbonate holder enables to prevent the membrane sliding and leakage of the culture medium during the cell-stretching experiment. Briefly, the main chamber of the bioreactor consists of an apical (air) and a basal (cell culture media) compartment separated by a membrane for cell growth (Figure 6A). Cell culture medium circulates through the basolateral surface of the membrane using a peristaltic pump to mimic the blood flow ($400 \mu\text{L min}^{-1}$) while cyclic pressure pulses induced by oscillating airflow in and out of the apical chamber subjects the membrane (and the cells) to a uniform cyclic triaxial strain in surface area (ΔSA). The CIVIC is equipped with a clinically relevant vibrating mesh nebulizer (Aeroneb Pro/Lab, Aerogen Inc, Galway Ireland) for aerosolized substance delivery to the cells. Typically, $10 \mu\text{L}$ of liquid is nebulized and deposited with a deposition efficiency of 52% onto the ALI cultured cells within ≈ 1 min. This patented ALICE Cloud technology has become commercially available as VITROCELL Cloud MAX (VITROCELL Systems, Waldkirch, Germany).^[61,62]

The elastic modulus of the membrane was measured using the bioreactor system during cell culturing. Two pressure sensors (MPX5050, Freescale Semiconductor, Munich, Germany) were devised in the apical compartment of the bioreactor (P_1) and the headspace of the reservoir chamber (P_2) as depicted in Figure 6A. During cell-stretch, the membrane expands and pushes the culture medium of the basal chamber into the medium reservoir. This compresses the air in the reservoir chamber (ΔV , mL), which can be measured by increased pressure in the reservoir ($\Delta P = P_2 - P_0$), where P_0 is the pressure in both air volumes (ambient air pressure, typically $P_0 = 98$ kPa) when the membrane is relaxed and V_0 is the corresponding volume of air in the medium reservoir (30 mL). Assuming the membrane motion can be approximated by a spherical cap geometry, the corresponding membrane displacement (ΔV , mL) is associated with the radius (a : 12.6 mm) and axial deflection of the membrane (Δh , cm) (Equations (2) and (3)). The elastic modulus (E , kPa) of the membrane (Young's modulus) can then be calculated from Equation (4).^[63]

To study the role of mechanical stretch on cell physiology, A549 cells were seeded on the membrane under dynamic/LLC culture conditions. After 80% of cell confluence, the cells were air-lifted (ALI conditions) and a cyclic mechanical stretch of 21% ΔSA (or 10% radius) and 35% ΔSA (16.5% linear) strain at the 0.33 Hz was subsequently applied to cells to mimic physiologic and non-physiologic conditions, respectively (Equation (5))

$$\Delta V = \Delta P \left(\frac{V_0}{P_0} \right), \text{ where } \Delta P = P_2 - P_0 \quad (2)$$

$$\Delta V = \pi \Delta h \left(\frac{a^2}{2} + \frac{\Delta h^2}{6} \right) \quad (3)$$

$$\Delta P' = (P_1 - P_2) = \frac{4E \left(\frac{\Delta h}{a} \right) t}{3a \left(\left(\frac{\Delta h}{a} \right)^2 + 1 \right)} \left(1 - \frac{1}{\left(1 + \left(\frac{\Delta h}{a} \right)^2 \right)^{3/2}} \right) \quad (4)$$

$$\Delta S = S \left(\frac{\Delta h}{a} \right); 0 \leq \Delta h \leq 0.11 \text{ cm (stretch}_{\text{max}}: \text{ here 35\% SA)} \quad (5)$$

For physiologic stretch (21% ΔSA); $P_1 = 100.5$ kPa and $P_2 = 99.5$ kPa

For non-physiologic stretch (35% ΔSA); $P_1 = 102$ kPa and $P_2 = 100.5$ kPa

Immunofluorescence: Cells were fixed in 4% paraformaldehyde (Sigma-Aldrich) for 20 min at room temperature (RT). After washing two times with PBS, cells were permeabilized by 0.3% Triton X-100 (Sigma-Aldrich) in PBS, 10 min at RT. To prevent any unspecific antibody binding, a blocking buffer (5% BSA and 0.1% TritonX-100) was added for 10 min. The cells were then incubated overnight at 4 °C with anti-ZO-1 monoclonal (mouse, 1:100; Invitrogen), anti-collagen type 1 polyclonal (rabbit, 1:100; Rockland) antibodies. After washing with PBS, cells

incubated for 1 h in RT with secondary antibody Alexa Fluor 555 goat anti-mouse IgG (1:500; Invitrogen) and Alexa Fluor 488 donkey anti-rabbit IgG (1:500; Invitrogen). The F-actin cytoskeleton and cell nuclei were stained with Phalloidin 594 (1:40) and 4',6-diamidin-2-phenylindol (DAPI) at $1 \mu\text{g mL}^{-1}$ in 5% BSA, 0.1% TritonX-100 in PBS, respectively. After rinsing three times with blocking solution, the membranes were embedded in Glycergel (DAKO Schweiz AG, Baar, Switzerland). All cell images were acquired using the confocal laser scanning microscope (LSM710, Carl Zeiss; Oberkochen, Germany), coupled to the Zen2009 software. Images were further processed using the 3D reconstruction IMARIS software (version 9.0; Bitplane, Zurich, Switzerland). For qualitative image analysis (all CLSM figures shown in the manuscript), CLSM images recorded under optimum CLSM settings were presented as selected by the CLSM system (pinhole and gain setting). For quantification, representative 40x images (z-stacks) were recorded under reference gain and pinhole settings of the CLSM (not under sample-specific optimum settings to account for setting-specific CLSM sensitivity) at 5 independent fields of view for each sample (biological replicate). The rectangular tool in Fiji was used to measure the total fluorescence intensity for F-actin, collagen type I, and ZO-1 for each view. Subsequently, the total fluorescence intensity was normalized to the number of cells in each view as determined from the number of nuclei (DAPI staining), which accounts for artefacts due to differences in cell packing.

In Vitro Functional Analysis: Trans-epithelial electrical resistance (TEER) measurements of epithelial cells grown on the optimized membrane were measured periodically using the Millicell-ERS system (Millicell ERS-2, Millipore, USA). The cell-specific resistance can be obtained by subtracting the total resistance across the cell culture membrane with cells from the resistance reading across the acellular membrane. TEER is calculated by multiplying the cell-specific resistance (Ohm, Ω) and the effective surface area of the membrane (cm^2). The experiments were repeated three times and a mean value was determined. For ALI culture, 200 μL of cell culture media was added to the apical part and resistance measured.

To measure the permeability in the apical-to-basolateral direction, first, the culture medium was removed from the basolateral compartment and the cells were washed with PBS. Then, 1 mL of culture media (phenol red-free) and 0.5 mL FITC-Dextran (4 kDa, Sigma-Aldrich) were added to the basolateral and the apical compartment of the epithelial barrier, respectively. Cells were then incubated at 37 °C to equilibrate. Samples from the basolateral were taken at 0, 30, 60, 90, and 120 min (culture media replaced with an equal volume) in a black 96-well plate and were analyzed by the plate reader (Safire 2, Tecan) with excitation and emission wavelengths of 490 and 525 nm, respectively. The apparent permeability coefficient (P_{app} , cm s^{-1}) is calculated using the Equation 6, where dQ/dt is the steady-state flux or the transport rate, A is the surface area of the membrane (cm^2) and C_0 is the initial concentration of FITC-Dextran added to the apical compartment (mg mL^{-1}).^[64] Before and after the experiment, TEER was measured to monitor the integrity of the cell monolayer.

$$P_{\text{app}} = \frac{dQ}{dt} * \frac{1}{(A * C_0)} \quad (6)$$

IL-8 Release: The pro-inflammatory IL-8 protein released by the interleukin-8 promoter (pIL8)-reporter A549 cell line was quantified using the luciferase reporter assay ONE-GloTM (Promega, Cat.No. E6120, Mannheim, Germany) according to the manufacturer's instruction. After stimulating cells for 24 h by adding TNF-alpha (15 ng mL^{-1}) to the cell culture medium^[8,48] and subsequent stretching (24 h), a mixture of cell lysate and reagent (1:1) measured by the luminometer (96-well format, GLOMAX, Promega, Germany). IL-8 challenge did not impair cell viability (WST-1) or barrier integrity (TEER) (data not shown).

Cell Uptake of Nanoparticle: A549 cells were grown on the BETA membrane (growth area: 4.9 cm^2) until cells reached confluence. Culture media (Phenol red-free DMEM (Gibco) supplemented with 10% FCS (Gibco) and 1% v/v Pen/Strep (100 U mL^{-1} , Gibco)) was aspirated from

the apical part and allowed cells to culture under ALI conditions for 1 day. Afterward, two scenarios were followed I) unstretched and II) stretched conditions (Figure 7A). For static conditions, the membranes were placed in the VITROCELL CLOUD 6 (Vitrocell, Waldkirch, Germany) for nebulization of 100 and 1000 nm amine-modified polystyrene (PS-NH₂) particles (Sigma-Aldrich, St. Louis, USA), diluted by a factor of 10 in 0.3% NaCl. The light intensity-weighted hydrodynamic size distribution (z-diameter) of the PS particles in suspension was measured by dynamic light scattering (DLS) using a Malvern Zetasizer Nano ZS Plus (Model Nr. ZEN3600, Malvern Instruments, UK) both prior and after nebulization (nebulized droplets were collected in a 50 mL Falcon tube). This revealed a ≈20% increase of the (z-average) diameters from 100.4 to 118.8 nm and from 1026 to 1193 nm due to nebulization (see Figure S7, Supporting Information). For the cell-stretch model, particles were nebulized directly onto the cells via the integrated nebulizer in the apical chamber (Figure 7A). The cell-deposited particle dose of 2.1 μg cm⁻² was determined from the previously determined aerosol deposition efficiency of 52% of the CIVIC system.^[61] For this dose, the fractional area coverage was determined to be 30% and 3% for NPs and MPs, respectively (density of PS-NH₂: 1.05 g cm⁻³). After the nebulization of particles, a cyclic physiologic mechanical stretch (21% ΔSA strain) was applied to the cells. The output rate of the nebulizer and the sedimentation time for both scenarios were 0.5 mL min⁻¹ and 3 min, respectively. After 2 h, the cells (under static and stretched conditions) were fixed and prepared for the CLSM analysis.

Statistical Analysis: All data except those designed by Minitab were analyzed using GraphPad Prism 8 (GraphPad Software, La Jolla, CA, USA). Outliers were identified using the Grubbs' method. Student's *t*-test (unpaired, two-tailed) and one-way ANOVA followed by post hoc Tukey's multiple comparison test were used to compare the means of two groups and the means of multiple groups, respectively. Results with a *p* < 0.05 or smaller were considered as a significant level. DoE were designed and the variables were optimized using Minitab 18 software (Minitab Inc., State College, PA, US). ANOVA was applied to evaluate whether the model is statistically significant at a 95% confidence level.

Supporting Information

Supporting Information is available from the Wiley Online Library or from the author.

Acknowledgements

Open access funding enabled and organized by Projekt DEAL.

Conflict of Interest

The authors declare no conflict of interest.

Keywords

alveolar-capillary barrier, cyclic mechanical stretch, hybrid polymers, in vitro cell-stretch model, tunable ultra-thin biphasic membrane

Received: June 2, 2020

Revised: September 10, 2020

Published online:

[1] F. M. E. Franssen, P. Alter, N. Bar, B. J. Benedikter, S. Iurato, D. Maier, M. Maxheim, F. K. Roessler, M. A. Spruit, C. F. Vogelmeier,

- E. F. M. Wouters, B. Schmeck, *Int. J. Chronic Obstruct. Pulm. Dis.* **2019**, *14*, 1465.
- [2] C. Darquenne, J. S. Fleming, I. Katz, A. R. Martin, J. Schroeter, O. S. Usmani, J. Venegas, O. Schmid, *J. Aerosol Med. Pulm. Drug Delivery* **2016**, *29*, 107.
- [3] A. Artzy-Schnirman, C. M. Lehr, J. Sznitman, *Expert Opin. Drug Delivery* **2020**, *17*, 621.
- [4] S. Ehrmann, O. Schmid, C. Darquenne, B. Rothen-Rutishauser, J. Sznitman, L. Yang, H. Barosova, L. Vecellio, J. Mitchell, N. Heuze-Vourc'h, *Expert Opin. Drug Delivery* **2020**, *17*, 463.
- [5] E. R. Weibel, *Respir. Physiol.* **1970**, *11*, 54.
- [6] A. Doryab, S. Tas, M. B. Taskin, L. Yang, A. Hilgendorff, J. Groll, D. E. Wagner, O. Schmid, *Adv. Funct. Mater.* **2019**, *29*, 1903114.
- [7] A. Doryab, G. Amoabediny, A. Salehi-Najafabadi, *Biotechnol. Adv.* **2016**, *34*, 588.
- [8] A.-G. Lenz, T. Stoeger, D. Cei, M. Schmidmeir, N. Semren, G. Burgstaller, B. Lentner, O. Eickelberg, S. Meiners, O. Schmid, *Am. J. Respir. Cell Mol. Biol.* **2014**, *51*, 526.
- [9] M. Röhm, S. Carle, F. Maigler, J. Flamm, V. Kramer, C. Mavougou, O. Schmid, K. Schindowski, *Int. J. Pharm.* **2017**, *532*, 537.
- [10] A. Artzy-Schnirman, N. Hobi, N. Schneider-Daum, O. T. Guenat, C.-M. Lehr, J. Sznitman, *Eur. J. Pharm. Biopharm.* **2019**, *144*, 11.
- [11] H. Wu, Y. Yu, H. Huang, Y. Hu, S. Fu, Z. Wang, M. Shi, X. Zhao, J. Yuan, J. Li, X. Yang, E. Bin, D. Wei, H. Zhang, J. Zhang, C. Yang, T. Cai, H. Dai, J. Chen, N. Tang, *Cell* **2020**, *180*, 107.
- [12] J. D. Stucki, N. Hobi, A. Galimov, A. O. Stucki, N. Schneider-Daum, C.-M. Lehr, H. Huwer, M. Frick, M. Funke-Chambour, T. Geiser, O. T. Guenat, *Sci. Rep.* **2018**, *8*, 14359.
- [13] D. Huh, B. D. Matthews, A. Mammoto, M. Montoya-Zavala, H. Y. Hsin, D. E. Ingber, *Science* **2010**, *328*, 1662.
- [14] Y. J. Chuah, Y. T. Koh, K. Lim, N. V. Menon, Y. Wu, Y. Kang, *Sci. Rep.* **2016**, *5*, 18162.
- [15] K. J. Regehr, M. Domenech, J. T. Koepsel, K. C. Carver, S. J. Ellison-Zelski, W. L. Murphy, L. A. Schuler, E. T. Alarid, D. J. Beebe, *Lab Chip* **2009**, *9*, 2132.
- [16] C. P. Laurent, C. Vaquette, X. Liu, J.-F. Schmitt, R. Rahouadj, *J. Biomater. Appl.* **2018**, *32*, 1276.
- [17] B. M. Young, K. Shankar, B. P. Allen, R. A. Pouliot, M. B. Schneck, N. S. Mikhael, R. L. Heise, *ACS Biomater. Sci. Eng.* **2017**, *3*, 3480.
- [18] H.-R. Paur, F. R. Cassee, J. Teeguarden, H. Fissan, S. Diabate, M. Aufderheide, W. G. Kreyling, O. Hänninen, G. Kasper, M. Riediker, B. Rothen-Rutishauser, O. Schmid, *J. Aerosol Sci.* **2011**, *42*, 668.
- [19] A. Khademhosseini, R. Langer, *Biomaterials* **2007**, *28*, 5087.
- [20] N. Higuaita-Castro, M. T. Nelson, V. Shukla, P. A. Agudelo-Garcia, W. Zhang, S. M. Duarte-Sanmiguel, J. A. Englert, J. J. Lannutti, D. J. Hansford, S. N. Ghadiali, *Sci. Rep.* **2017**, *7*, 11623.
- [21] M. Koval, C. Ward, M. K. Findley, S. Roser-Page, M. N. Helms, J. Roman, *Am. J. Respir. Cell Mol. Biol.* **2010**, *42*, 172.
- [22] N. Davidenko, C. F. Schuster, D. V. Bax, R. W. Farndale, S. Hamaia, S. M. Best, R. E. Cameron, *J. Mater. Sci. Mater. Med.* **2016**, *27*, 148.
- [23] S. Gautam, A. K. Dinda, N. C. Mishra, *Mater. Sci. Eng. C* **2013**, *33*, 1228.
- [24] S. Yuan, G. Xiong, A. Roguin, C. Choong, *Biointerphases* **2012**, *7*, 30.
- [25] K. Luyts, D. Napierska, D. Dinsdale, S. G. Klein, T. Serchi, P. H. M. Hoet, *Toxicol. In Vitro* **2015**, *29*, 234.
- [26] C. Hermans, A. Bernard, *Eur. Respir. J.* **1998**, *11*, 801.
- [27] M. J. Baker, J. Trevisan, P. Bassan, R. Bhargava, H. J. Butler, K. M. Dorling, P. R. Fielden, S. W. Fogarty, N. J. Fullwood, K. A. Heys, C. Hughes, P. Lasch, P. L. Martin-Hirsch, B. Obinaju, G. D. Sockalingum, J. Sulé-Suso, R. J. Strong, M. J. Walsh, B. R. Wood, P. Gardner, F. L. Martin, *Nat. Protoc.* **2014**, *9*, 1771.
- [28] A. Girault, J. Chebli, A. Privé, N. T. N. Trinh, E. Maillé, R. Grygorczyk, E. Brochiero, *Respir. Res.* **2015**, *16*, 100.
- [29] F. E. Sirianni, F. S. F. Chu, D. C. Walker, *Am. J. Respir. Crit. Care Med.* **2003**, *168*, 1532.

- [30] A. Mammoto, T. Mammoto, M. Kanapathipillai, C. W. Yung, E. Jiang, A. Jiang, K. Lofgren, E. P. S. Gee, D. E. Ingber, *Nat. Commun.* **2013**, *4*, 1759.
- [31] B. M. Baker, B. Trappmann, W. Y. Wang, M. S. Sakar, I. L. Kim, V. B. Shenoy, J. A. Burdick, C. S. Chen, *Nat. Mater.* **2015**, *14*, 1262.
- [32] A. J. Engler, S. Sen, H. L. Sweeney, D. E. Discher, *Cell* **2006**, *126*, 677.
- [33] F. S. A. Cavalcante, S. Ito, K. Brewer, H. Sakai, A. M. Alencar, M. P. Almeida, J. S. Andrade, A. Majumdar, E. P. Ingenito, B. Suki, *J. Appl. Physiol.* **2005**, *98*, 672.
- [34] T. S. Frost, L. Jiang, R. M. Lynch, Y. Zohar, *Micromachines* **2019**, *10*, 533.
- [35] K. J. Elbert, U. F. Schäfer, H. J. Schäfers, K. J. Kim, V. H. L. Lee, C. M. Lehr, *Pharm. Res.* **1999**, *16*, 601.
- [36] H. R. Wirtz, L. G. Dobbs, *Science* **1990**, *250*, 1266.
- [37] K. J. Cavanaugh, T. S. Cohen, S. S. Margulies, *Am. J. Physiol.* **2006**, *290*, C1179.
- [38] R. Herrero, G. Sanchez, J. A. Lorente, *Ann. Transl. Med.* **2018**, *6*, 32.
- [39] E. E. Schneeberger, R. D. Lynch, *Am. J. Physiol.* **2004**, *286*, C1213.
- [40] L. González-Mariscal, A. Betanzos, P. Nava, B. E. Jaramillo, *Prog. Biophys. Mol. Biol.* **2003**, *81*, 1.
- [41] K. J. Cavanaugh, J. Oswari, S. S. Margulies, *Am. J. Respir. Cell Mol. Biol.* **2001**, *25*, 584.
- [42] M. J. Song, N. Davidovich, G. G. Lawrence, S. S. Margulies, *J. Biomech.* **2016**, *49*, 1330.
- [43] A. O. Stucki, J. D. Stucki, S. R. R. Hall, M. Felder, Y. Mermoud, R. A. Schmid, T. Geiser, O. T. Guenat, *Lab Chip* **2015**, *15*, 1302.
- [44] B. C. DiPaolo, N. Davidovich, M. G. Kazanietz, S. S. Margulies, *Am. J. Physiol.* **2013**, *305*, L141.
- [45] O. Schmid, C. Jud, Y. Umehara, D. Mueller, A. Bucholski, F. Gruber, O. Denk, R. Egle, A. Petri-Fink, B. Rothen-Rutishauser, *J. Aerosol Med. Pulm. Drug Delivery* **2017**, *30*, 411.
- [46] S. Chollet-Martin, P. Montravers, C. Gibert, C. Elbim, J. M. Desmonts, J. Y. Fagon, M. A. Gougerot-Pocidallo, *Infect. Immun.* **1993**, *61*, 4553.
- [47] N. E. Vlahakis, M. A. Schroeder, A. H. Limper, R. D. Hubmayr, *Am. J. Physiol.* **1999**, *277*, L167.
- [48] G. J. Oostingh, M. Schmittner, A. K. Ehart, U. Tischler, A. Duschl, *Toxicol. In Vitro* **2008**, *22*, 1301.
- [49] C. Schmitz, J. Welck, I. Tavernaro, M. Grinberg, J. Rahnenführer, A. K. Kierner, C. van Thriel, J. G. Hengstler, A. Kraegeloh, *Nanotoxicology* **2019**, *13*, 1227.
- [50] A. Peters, H. E. Wichmann, T. Tuch, J. Heinrich, J. Heyder, *Am. J. Respir. Crit. Care Med.* **1997**, *155*, 1376.
- [51] O. Schmid, T. Stoeger, *J. Aerosol Sci.* **2016**, *99*, 133.
- [52] W. G. Kreyling, M. Semmler-Behnke, S. Takenaka, W. Möller, *Acc. Chem. Res.* **2013**, *46*, 714.
- [53] K. Ganguly, D. Ettehadi, S. Upadhyay, S. Takenaka, T. Adler, E. Karg, F. Krombach, W. G. Kreyling, H. Schulz, O. Schmid, T. Stoeger, *Part. Fibre Toxicol.* **2017**, *14*, 19.
- [54] S. H. van Rijt, D. A. Bölükbas, C. Argyo, K. Wipplinger, M. Naureen, S. Datz, O. Eickelberg, S. Meiners, T. Bein, O. Schmid, T. Stoeger, *Nanoscale* **2016**, *8*, 8058.
- [55] S. G. Klein, T. Serchi, L. Hoffmann, B. Blömeke, A. C. Gutleb, *Part. Fibre Toxicol.* **2013**, *10*, 31.
- [56] R. Firdessa, T. A. Oelschlaeger, H. Moll, *Eur. J. Cell Biol.* **2014**, *93*, 323.
- [57] F. M. Winnik, D. Maysinger, *Acc. Chem. Res.* **2013**, *46*, 672.
- [58] I.-L. H. Annika Mareike Gramatke, *J. Nanomed. Nanotechnology* **2014**, *5*, <https://doi.org/10.4172/2157-7439.1000248>.
- [59] Z. Wang, A. A. Volinsky, N. D. Gallant, *J. Appl. Polym. Sci.* **2014**, *131*, 41050.
- [60] D. Meyerhofer, *J. Appl. Phys.* **1978**, *49*, 3993.
- [61] D. Cei, A. Doryab, A.-G. Lenz, A. Schröppel, P. Mayer, G. Burgstaller, R. Nossa, A. Ahluwalia, O. Schmid, *Biotechnol. Bioeng.* **2020**, 27600, <https://doi.org/10.1002/bit.27600>.
- [62] D. Cei, Ph.D. Thesis, University of Pisa **2015**.
- [63] A. L. Flory, D. A. Brass, K. R. Shull, *J. Polym. Sci., Part B: Polym. Phys.* **2007**, *45*, 3361.
- [64] I. Hubatsch, E. G. E. Ragnarsson, P. Artursson, *Nat. Protoc.* **2007**, *2*, 2111.
- [65] S. Sharma, S. Mohanty, D. Gupta, M. Jassal, A. K. Agrawal, R. Tandon, *Mol. Vision* **2011**, *17*, 2898.
- [66] Y. Zhang, H. Ouyang, C. T. Lim, S. Ramakrishna, Z.-M. Huang, *J. Biomed. Mater. Res.* **2005**, *72B*, 156.

© 2020 Wiley-VCH GmbH

**ADVANCED
FUNCTIONAL
MATERIALS**

Supporting Information

for *Adv. Funct. Mater.*, DOI: 10.1002/adfm.202004707

A Biomimetic, Copolymeric Membrane for Cell-Stretch Experiments with Pulmonary Epithelial Cells at the Air-Liquid Interface

*Ali Doryab, Mehmet Berat Taskin, Philipp Stahlhut, Andreas Schröppel, Darcy E. Wagner, Jürgen Groll, and Otmar Schmid**

Supporting Information

Figure S1. FIB-SEM micrograph of the membrane at phase I (non-porous), showing some superficial hollows on the apical side (marked by *). The green and red dotted lines indicate the cross-section of the membrane (basal to apical) and the “gelatin islands” in the structure, respectively. Scale bar is 2 μm .

Figure S2. EDX-SEM analysis of the fabricated membrane in phases I and II. (A) in phase I, the disc-shapes in the membrane structure are full of nitrogen, which is representative of gelatins that have been distributed on the PCL bulk. (B) Removal of gelatin from the membrane in phase II after incubation in culture media for 6 days, showing no nitrogen in the structure.

Figure S3. SEM images of A549 cells grown on the nine different membrane types with varying PCL/gelatin mixing ratio, evidencing the morphology and adhesion of the cells (seeding cell density: 1×10^5 cells cm^{-2} , LLC culture for 6d). For cell culture, the membranes were placed between two polycarbonate holders and kept under static, submerged culture conditions (LLC) for 6 days. Scale bar is 20 μm .

Figure S4. (A) SEM micrograph of bronchial epithelial 16HBE14o– cells were fully grown on the membrane (cell density: 2×10^5 cells cm^{-2}). (B) Semi-decellularized membrane by 0.1% SDS, which shows ECM materials and protein strands deposited on the membrane. Scale bar is 10 μm .

Figure S5. Role of the initial stiffness of the membrane on the formation/arrangement of F-actin. The stiffness of the membranes in phase I alters the arrangement and formation of F-actin in A549 cells while no significant changes were detected in the cell numbers (seeding cell density: 1×10^5 cells cm^{-2} , LLC culture for 6d). Images were further quantified using the surface rendering of IMARIS (version 9.0; Bitplane, Zurich, Switzerland). The representative images (z- stacks) were quantified at 5 independent fields of view (regions-of-interest: $134.95 \mu\text{m} \times 134.95 \mu\text{m}$) for each sample. The cell nucleus (blue, DAPI), cytoskeleton (green, F-actin). The scale bare is $10 \mu\text{m}$. Data are reported as the mean \pm SD; *P < 0.05 by one-way ANOVA with Tukey test.

Figure S6. The effect of cyclic mechanical stretch on ZO-1 tight junction formation, and barrier integrity. Fluorescent CLSM images of ZO-1 tight junction formation of A549 cells under static (ALI culture), physiologic (21% Δ SA), and non-physiologic (35% Δ SA) cyclic mechanical stretch (ALI) conditions. A549 cells grown on the (optimum) BETA membrane under static (6d LLC and 6d LLC plus 24 h ALI) and dynamic/ALI (21% and 35% Δ SA for 24 h) culture conditions. Nuclei (DAPI, blue) and ZO-1 (red). The scale bar is $20 \mu\text{m}$.

Figure S7. Hydrodynamic, light-intensity weighted size (Z-diameter) distribution of nominal 100 nm and 1000 nm particles before (red line) and after (green line) nebulization measured by dynamic light scattering (DLS, Zetasizer). This reveals an approximate 20% increase in average particle size due to nebulization.

Movie 1. Z-stack FIB-SEM tomography of an already populated membrane with A549 cells (24.5 nm interval). The images were aligned using NIH Fiji and then reconstructed by IMARIS software and NIH Fiji.

Movie 2. Surface rendering (by IMARIS) of 3D reconstruction CLSM images of 100 nm NPs after 2 h under static (ALI) conditions. DAPI (blue), PS-NH₂ (red), and F-actin (green).

Movie 3. Surface rendering (by IMARIS) of 3D reconstruction CLSM images of 1000 nm microparticles after 2 h under static (ALI) conditions. DAPI (blue), PS-NH₂ (red), and F-actin (green).

Movie 4. Surface rendering (by IMARIS) of 3D reconstruction CLSM images of 100 nm NPs under physiologic cyclic mechanical stretch conditions (ALI culture, 21% Δ SA, 2 h). DAPI (blue), PS-NH₂ (red), and F-actin (green).

Figure S1.

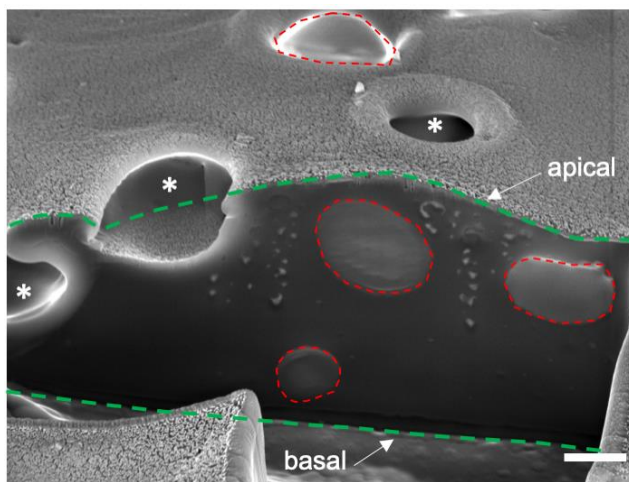


Figure S2.

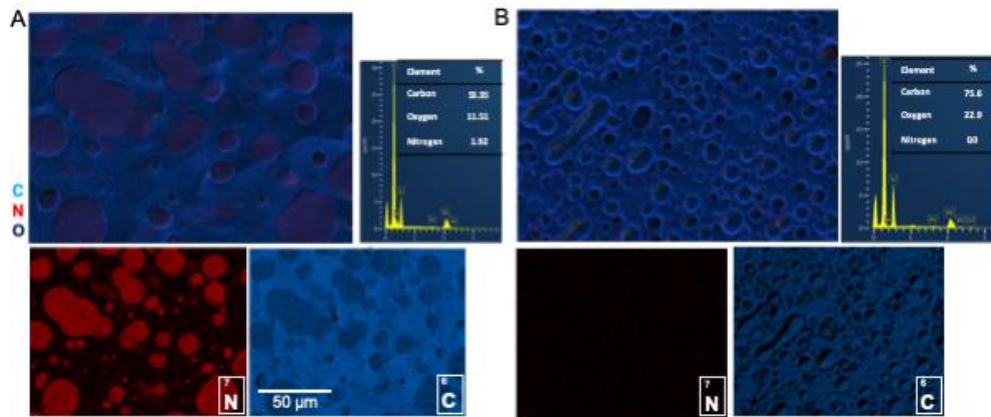


Figure S3.

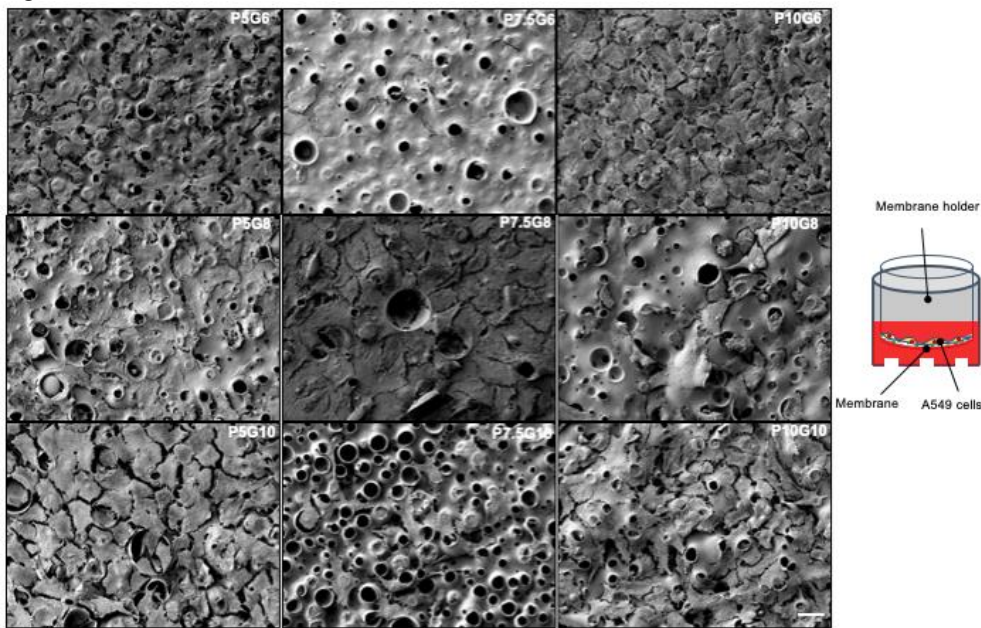


Figure S4.

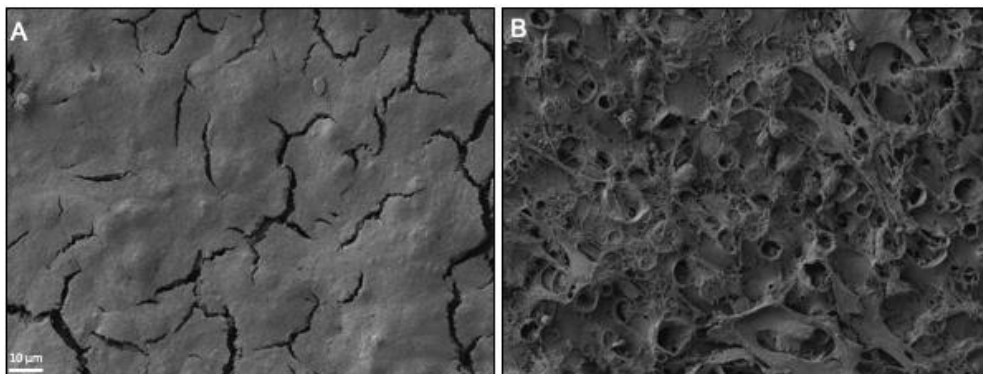
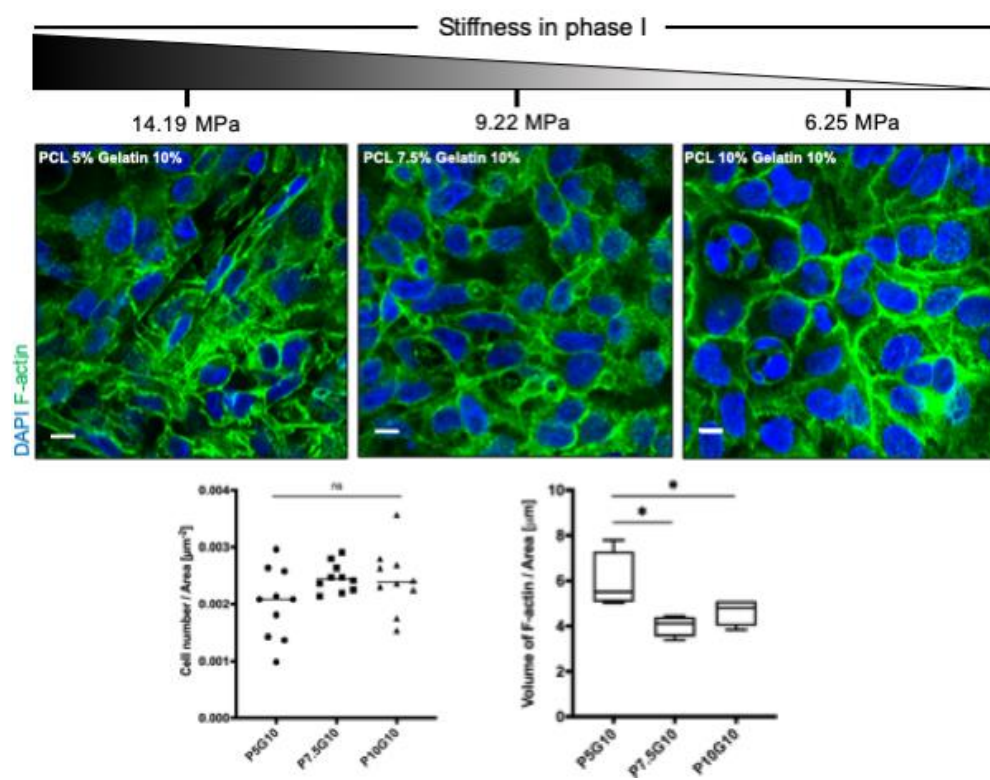


Figure S5.



5

Figure S6.

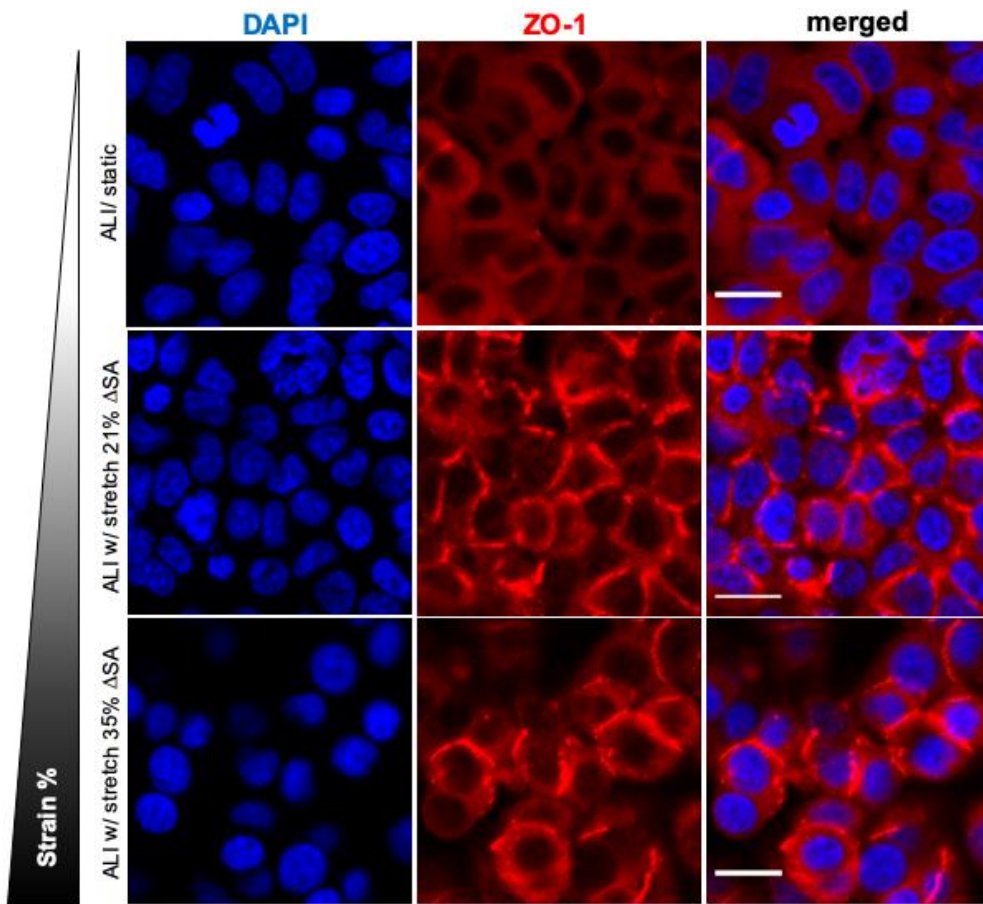
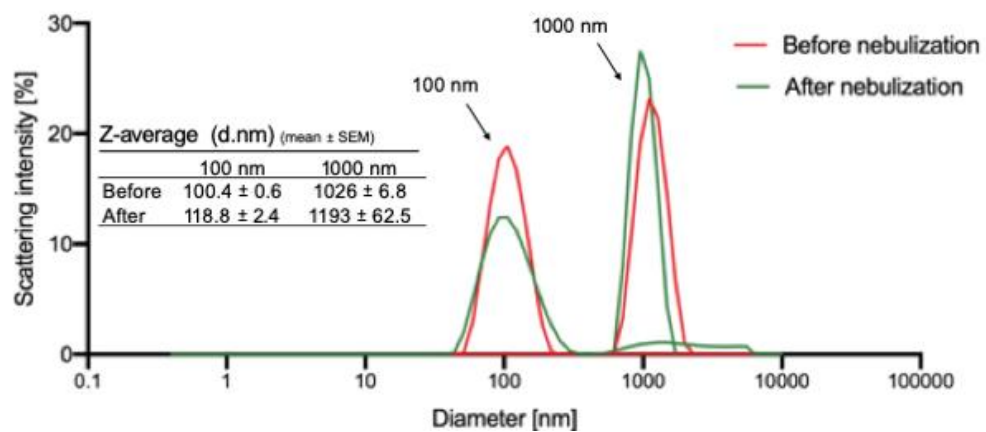


Figure S7.



4. Paper II



A Bioinspired *in vitro* Lung Model to Study Particokinetics of Nano-/Microparticles Under Cyclic Stretch and Air-Liquid Interface Conditions

Ali Doryab^{1,2}, Mehmet Berat Taskin³, Philipp Stahlhut³, Andreas Schröppel^{1,2}, Sezer Orak^{1,2}, Carola Voss^{1,2}, Arti Ahluwalia^{4,5}, Markus Rehberg^{1,2}, Anne Hilgendorff^{1,2,6}, Tobias Stöger^{1,2}, Jürgen Groll³ and Otmar Schmid^{1,2*}

OPEN ACCESS

Edited by:

Josue Snitman,
Technion Israel Institute of
Technology, Israel

Reviewed by:

Jorge Otero,
Centro de Investigación Biomédica en
Red Enfermedades Respiratorias
(CIBERES), Spain
Anja Lena Thiebes,
RWTH Aachen University, Germany

***Correspondence:**

Otmar Schmid
otmar.schmid
@helmholtz-muenchen.de

Specialty section:

This article was submitted to
Biomaterials,
a section of the journal
Frontiers in Bioengineering and
Biotechnology

Received: 13 October 2020

Accepted: 13 January 2021

Published: 29 January 2021

Citation:

Doryab A, Taskin MB, Stahlhut P,
Schröppel A, Orak S, Voss C,
Ahluwalia A, Rehberg M,
Hilgendorff A, Stöger T, Groll J and
Schmid O (2021) A Bioinspired *in vitro*
Lung Model to Study Particokinetics
of Nano-/Microparticles Under Cyclic
Stretch and Air-Liquid Interface
Conditions.
Front. Bioeng. Biotechnol. 9:616830.
doi: 10.3389/fbioe.2021.616830

¹ Comprehensive Pneumology Center Munich, Member of the German Center for Lung Research, Munich, Germany,

² Helmholtz Zentrum München—German Research Center for Environmental Health, Institute of Lung Biology and Disease,

Munich, Germany, ³ Department of Functional Materials in Medicine and Dentistry, Bavarian Polymer Institute, University of

Würzburg, Würzburg, Germany, ⁴ Research Center “E. Piaggio”, University of Pisa, Pisa, Italy, ⁵ Department of Information

Engineering, University of Pisa, Pisa, Italy, ⁶ Center for Comprehensive Developmental Care (CDeC^{LMU}), Dr. von Haunersches

Children’s Hospital University, Hospital of the Ludwig-Maximilians University, Munich, Germany

Evolution has endowed the lung with exceptional design providing a large surface area for gas exchange area (ca. 100 m²) in a relatively small tissue volume (ca. 6 L). This is possible due to a complex tissue architecture that has resulted in one of the most challenging organs to be recreated in the lab. The need for realistic and robust *in vitro* lung models becomes even more evident as causal therapies, especially for chronic respiratory diseases, are lacking. Here, we describe the **Cyclic *In Vitro* Cell-stretch (CIVIC)** “breathing” lung bioreactor for pulmonary epithelial cells at the air-liquid interface (ALI) experiencing cyclic stretch while monitoring stretch-related parameters (amplitude, frequency, and membrane elastic modulus) under real-time conditions. The previously described biomimetic copolymeric BETA membrane (5 μm thick, bioactive, porous, and elastic) was attempted to be improved for even more biomimetic permeability, elasticity (elastic modulus and stretchability), and bioactivity by changing its chemical composition. This biphasic membrane supports both the initial formation of a tight monolayer of pulmonary epithelial cells (A549 and 16HBE14o⁻) under submerged conditions and the subsequent cell-stretch experiments at the ALI without preconditioning of the membrane. The newly manufactured versions of the BETA membrane did not improve the characteristics of the previously determined optimum BETA membrane (9.35% PCL and 6.34% gelatin [w/v solvent]). Hence, the optimum BETA membrane was used to investigate quantitatively the role of physiologic cyclic mechanical stretch (10% linear stretch; 0.33 Hz: light exercise conditions) on size-dependent cellular uptake and transepithelial transport of nanoparticles (100 nm) and microparticles (1,000 nm) for alveolar epithelial cells (A549) under ALI conditions. Our results show that physiologic

stretch enhances cellular uptake of 100 nm nanoparticles across the epithelial cell barrier, but the barrier becomes permeable for both nano- and micron-sized particles (100 and 1,000 nm). This suggests that currently used static *in vitro* assays may underestimate cellular uptake and transbarrier transport of nanoparticles in the lung.

Keywords: lung cell model, cyclic stretch, ALI culture, bioinspired membrane, particle study

INTRODUCTION

The lung is the largest organ of the human body built to accommodate the extraordinary size of required gas (oxygen-carbon dioxide) exchange surface area (ca. 100 m²) corresponding to about half the size of a tennis court (Weibel, 1970, 2009) within a relatively small volume (ca. 6 l; <10% of body volume). Direct exposure to airborne particles, such as cigarette smoke particles, urban dust and particles from indoor sources (e.g., cooking and laser printer) jeopardizes the fragile architecture of this organ, causing pulmonary lung diseases, such as asthma and chronic obstructive pulmonary disease (Pope et al., 2009; Hänninen et al., 2010; Schaumann et al., 2014). Out of the wide size range of inhalable particles (up to 10 μm diameter), nanoparticles (NPs) with a diameter between 100 and 300 nm have been shown to undergo epithelial-endothelial translocation, i.e., they can cross the alveolar tissue barrier into the blood circulation and from there to other organs (Kreyling et al., 2013). Moreover, ultrafine NPs (<100 nm in diameter) have received increasing attention due to their enhanced surface area per mass of particles, which has been associated with both acute and chronic lung disease (Peters et al., 1997; Schmid and Stoeger, 2016).

Improvement of the predictive power of pre-clinical *in vitro* models as an alternative to animal experiments according to the 3R principles (replacement, refinement, and reduction) relies on enhancing their biomimetic features. Over the past decades *in vitro* cell culture models of the lung epithelial cells have evolved significantly from technologically simple, non-physiologic, submerged cell culture systems to an advanced level of *in vitro* cell culture models at the air-liquid interface (ALI) (Doryab et al., 2016). In these advanced lung models, epithelial lung cells are seeded on the apical (air) side of a porous/perforated membrane, which is in contact with the cell culture medium located on the basal side. This setup mimics *in vivo* conditions, initiating polarization of cells, and secretion of protective lining fluids (surfactant), which do not occur under submerged conditions where cells are completely covered with cell culture medium (Doryab et al., 2019). Hence, ALI cell cultures provide more physiologic conditions and potentially clinically more relevant results when testing drug/toxin effects on the lung as compared to submerged cultures (Paur et al., 2011).

Moreover, *in vitro* lung models have been developed to exert cyclic mechanical stretch to cells mimicking the breathing-induced cyclic stretch conditions in the alveolar lung tissue in order to include this important stimulus for cell physiology and

morphology in the cell culture models (Doryab et al., 2019). Hence, addition of this type of stimulus may prove useful for preclinical drug testing and assessment of toxin- and/or particle-induced toxicity. Most of the studies reported in the literature used commercially available cell-stretch technologies (e.g., Flexcell strain unit; Flexcell International Corp., USA) that are only suitable for submerged culture conditions (Edwards et al., 1999; Vlahakis et al., 1999; Hammerschmidt et al., 2004; Guenat and Berthiaume, 2018; Doryab et al., 2019).

Nevertheless, a variety of *in vitro* models has been developed to combine cyclic cell-stretch and ALI culture conditions for more biomimetic models of the alveolar air-blood barrier. Ideally, these advanced models enable (I) cyclic mechanical activation of the (multi-)cell cultures at the ALI, (II) basal perfusion of the culture medium, mimicking blood circulation, and (III) dose-controlled, aerosolized substance delivery. While the former two items have been implemented in various models, the latter is often missing (Doryab et al., 2019; Artzy-Schnirman et al., 2020). In 2010, the seminal work performed by Ingber et al. at the WYSS Institute of Harvard University introduced a microfluidic lung bioreactor often referred to as “lung-on-a-chip” (Huh et al., 2010). The concept of these systems is comparable to standard (multi-)cell culture models of the lung cultured at the ALI on an elastic, perforated membrane, which can be mechanically activated (stretched) combined with basal medium perfusion on a miniature-scale (shift from milli- to microfluidic system). Nowadays, these microfluidic systems have been evolved from a simple bi-channel structure (Huh et al., 2010; Stucki et al., 2015) to a complex airway network (acini-on-chips) (Artzy-Schnirman et al., 2019). However, wide-spread use of these systems is still hampered by the high degree of complexity associated with operating these systems (Ehrmann et al., 2020). These types of biomimetic alveolar barrier models not only have the potential to predict clinical outcome during early preclinical drug or toxin testing and accurate but also for mimicking drug/particle transport from the lung into the blood. In fact, the latter is part of the clinical testing (phase I of clinical trial) required for regulatory licensing of safety and efficacy of novel drugs.

All of these models and recent developments suffer from a lack of a suitable biomimetic membrane, acting as a cell-substrate. An appropriate membrane should emulate the main characteristics of the supporting extracellular matrix (ECM) of the cells, such as thickness, stiffness, permeability, and bioactivity. Commercially available polycarbonate (PC) and polyethylene terephthalate (PET) membranes are widely used in (static) ALI culture systems that do not mimic the stiffness

(or rather “softness”) of the ECM in the lung. Silicone-based materials, such as poly(dimethylsiloxane) (PDMS, Sylgard 184) are generally cast for cell-stretch applications due to their suitable mechanoelastic properties (Doryab et al., 2019). Nonetheless, adsorption of proteins/growth factors to and leaching of uncured oligomers from PDMS membranes has been recognized as potential cause of adverse effects on cell physiology (Regehr et al., 2009). Recently, synthetic/natural electrospun scaffolds with a thickness range of $\approx 20\text{--}200\ \mu\text{m}$ have been fabricated with suitable properties for lung cells using co-polymers consisting of poly(ϵ -caprolactone) (PCL)/star-shaped polyethylene glycols (sPEG) functionalized with biomolecules (Nishiguchi et al., 2017), poly-L-lactic acid (PLLA)/decellularized pig lung ECM (PLECM) (Young et al., 2017), and PCL/gelatin (Higuita-Castro et al., 2017). The stretchability of these scaffolds/membranes has not been determined as they were employed only under static cell culture conditions.

We have recently introduced a novel porous and elastic membrane for *in vitro* cell-stretch models of the lung cultured under ALI conditions (Doryab et al., 2020). This innovative hybrid biphasic membrane, henceforth referred to as **Biphasic Elastic Thin for Air-liquid culture conditions (BETA)** membrane, was developed to optimize membrane characteristics for the two phases of cell-stretch experiments under ALI conditions, namely the initial cell seeding, attachment and growth phase under submerged cell culture conditions (phase I) followed by an ALI acclimatization and cell-stretch phase at the ALI (phase II). As these phases require distinctly different membrane properties, the BETA membrane has been designed to be biphasic. As the pores are initially filled with a wettable, water-soluble and hence sacrificial material (gelatin), the BETA membrane provides initially a non-porous and wettable enough ($\text{WCA} \leq 70^\circ$) substrate for initial cell adhesion and growth into a confluent epithelial monolayer on the apical side of the membrane (closed pores avoid inadvertent transmembrane migration of cells) (phase I). Subsequently, dissolution of the sacrificial material results in sufficient porosity, permeability and stretchability for up to 25% reversible linear strain (without plastic deformation), granting suitable ALI cell culture conditions under cyclic mechanical stretch (phase II). In contrast to typically used stretchable poly(dimethylsiloxane) (PDMS) membranes, the BETA membrane is bioactive enough to support the proliferation and formation of a confluent layer of alveolar (A549) and bronchial (16HBE14o⁻) epithelial cells without pre-coating with ECM proteins (e.g., Matrigel) (Doryab et al., 2020).

Right now, the main limitations of the BETA membrane are the relatively larger thickness (ca. $5\ \mu\text{m}$) compared to the alveolar-capillary tissue barrier (ca. $1\ \mu\text{m}$) and higher stiffness [uniaxial Young's modulus: $1.8 \pm 0.7\ \text{MPa}$ (1D stretch); $0.78 \pm 0.24\ \text{MPa}$ (3D stretch)], which is similar to or better than other typically used porous membranes for lung cell-stretch cultures (e.g., PDMS), but still about 100-fold larger than the elastic modulus (3–6 kPa) reported for alveolar walls/tissue (Doryab et al., 2020). Moreover, the ideal membrane is as bioactive as possible to provide optimum

growth conditions for (primary) cell cultures and perfectly permeable to minimize membrane effects on transbarrier transport measurements.

In the present study, we attempted to improve the previously described limitations of the “optimum” BETA membrane with respect to thickness, permeability, elasticity (elastic modulus and stretchability), and bioactivity by changing its chemical composition. This is supported by newly applied analytical parameters (e.g., 3D porosity and mapping of surface topology of the membrane). Moreover, we provide a detailed technical description of the recently introduced **Cyclic *In Vitro* Cell-stretch (CIVIC)** bioreactor for cell-stretch experiments under ALI conditions (Doryab et al., 2020) with particular attention to refinements over its earlier version (MALI, Moving Air-Liquid Interface bioreactor) (Cei et al., 2020). Subsequently, the effect of cyclic stretch on the particokinetics of aerosol-delivered nano- (100 nm) and microparticles (1,000 nm) in an alveolar tissue barrier model (A549) cultured under ALI conditions was investigated quantitatively with respect to size-dependent cellular uptake and transepithelial transport of particles.

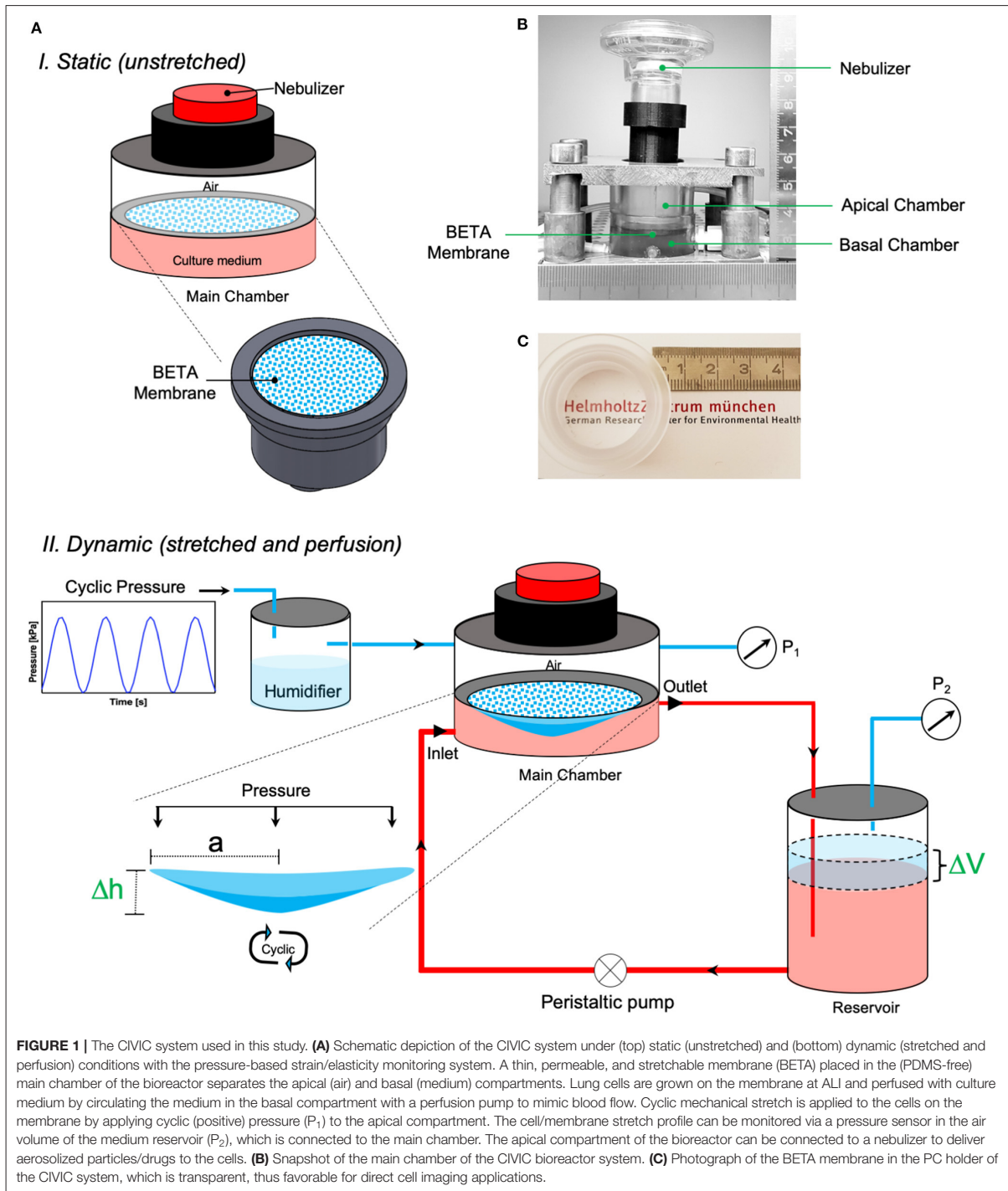
RESULTS

Advanced *in vitro* Cell-Stretch System (CIVIC)

The **Cyclic *In Vitro* Cell-stretch (CIVIC)** system, which was employed for cell-stretch experiments with the BETA membrane, is a modified version of our previously described MALI system (Cei et al., 2020) mainly with respect to material stability, (BETA) membrane fixation, pressure sealing, and quality control including real-time monitoring of the amplitude and frequency of the cyclically stretched cell-covered membrane. The CIVIC system allows for culturing of lung epithelial cells under ALI, cyclic mechanical stretch, and medium (blood) perfusion conditions in combination with dose-controlled delivery of aerosolized substances to the cells. This *in vitro* scenario resembles closely aerosol deposition onto the air-blood barrier of the lung as encountered during inhalation therapy or breathing of ambient aerosol. The details of the technical aspects of the CIVIC system are presented in **Figures 1A,B** and the Methods and Materials section. A movie of the cyclically stretched membrane in the “breathing” CIVIC system can be found in the **Supplementary Video 1**.

Characterization and Optimization Bioinspired Stretchable Membrane (BETA)

As mentioned above, we recently described an optimized biphasic copolymeric membrane for cell growth inspired by the ECM in the alveolar region of the lung (Doryab et al., 2020). The initially non-porous membrane consists of two polymeric components namely poly(ϵ -caprolactone) (PCL) and gelatin, tailored to facilitate initial cell adhesion and growth under submerged condition (phase I) (**Figures 1C, 2A**). Upon contact with cell culture medium, the gelatin at the surface of the membrane turns into a hydrogel, which is conducive to cell growth (lowers water contact angle; provides favorable conditions for cell adhesion



and proliferation). Gelatin also serves as “sacrificial” material, i.e., it is gradually dissolved by the medium turning the initially non-porous, stiff membrane into a porous/permeable and more

elastic membrane as required for nurturing ALI cell cultures via basolateral medium and during cell-stretch experiments (phase II) (Figure 2B). We previously determined the optimum

concentrations of PCL and gelatin (9.35% PCL and 6.34% gelatin [w/v solvent]) for membrane fabrication by spin coating with respect to matching the properties of the BETA membrane to the basement membrane of the alveolar tissue using a widely used optimization approach [design of experiment (DoE)].

Due to remaining limitations of the “optimum” BETA membrane with respect to thickness and stiffness (ca. 100-fold reduction needed to match alveolar basement membrane) (Polio et al., 2018; Doryab et al., 2019; Bou Jawde et al., 2020), we attempted to improve the performance characteristics of the membrane by expanding the previously tested range of PCL/gelatin mixing ratios. For this, new membranes were manufactured with PCL concentration larger than the previously explored upper limit of 10% [w/v solvent], namely 15% PCL mixed with 6, 8, and 10% [w/v] (Figure 2A). The characteristics of these three newly generated BETA membranes were compared with previously characterized membranes consisting of 10% PCL mixed with 6, 8, and 10% [w/v] and the optimum BETA membrane (9.35% PCL and 6.34% gelatin [w/v]).

Surface analysis of the optimum BETA membrane (9.35% PCL and 6.34% gelatin [w/v solvent]) using Atomic Force Microscopy (AFM) showed an average roughness height of 1.31 μm (Figure 2C). The cross-sectional structure of the membrane was studied using Focused Ion Beam-Scanning Electron Microscopy (FIB-SEM). The data show that gelatin forms spherical “islands” in the PCL membrane (Figure 2D, left panel). These gelatin islands also extend deep into the PCL membrane, leaving a favorable interconnected 3D network of pores after dissolution of the gelatin in phase II, as confirmed by Energy Dispersive X-ray Spectroscopy (EDS)-FIB-SEM (Figure 2D, right panel).

Analysis of the water contact angle (WCA)—one of the key properties of cell attachment and growth of the three new membranes reveals a range of 70–76° indicating that all of these membranes are wettable (Figure 2E). The uniaxial tensile test of the membranes prior to cell seeding (in phase I) revealed that Young’s modulus (elastic modulus) varies between 5.33 \pm 1.90 and 21.41 \pm 4.65 MPa (Figure 2F). Moreover, all of the membranes can endure at least 8% linear reversible strain, which is required for physiologic cell stretch conditions in the lung (Doryab et al., 2019), except for PCL 10% gelatin 6% [w/v], which can withstand only 4% linear strain. Another important parameter for culturing of cells under ALI conditions is the porosity of the membrane at the end of phase II (ALI culture), which varies between 1.8 \pm 2.5 and 49.7 \pm 1.4%, where the highest and lowest porosity corresponds to the membrane consisting of PCL 10% gelatin 10% and PCL 15% gelatin 8% [w/v], respectively (Figure 2G). It is noteworthy, that there is excellent agreement between empirically determined porosity and theoretically derived (upper limit of) porosity (volume fraction of gelatin), if the composition-derived theoretical porosity exceeds 40% (here: PCL 10% gelatin 8% and PCL 10% gelatin 10%).

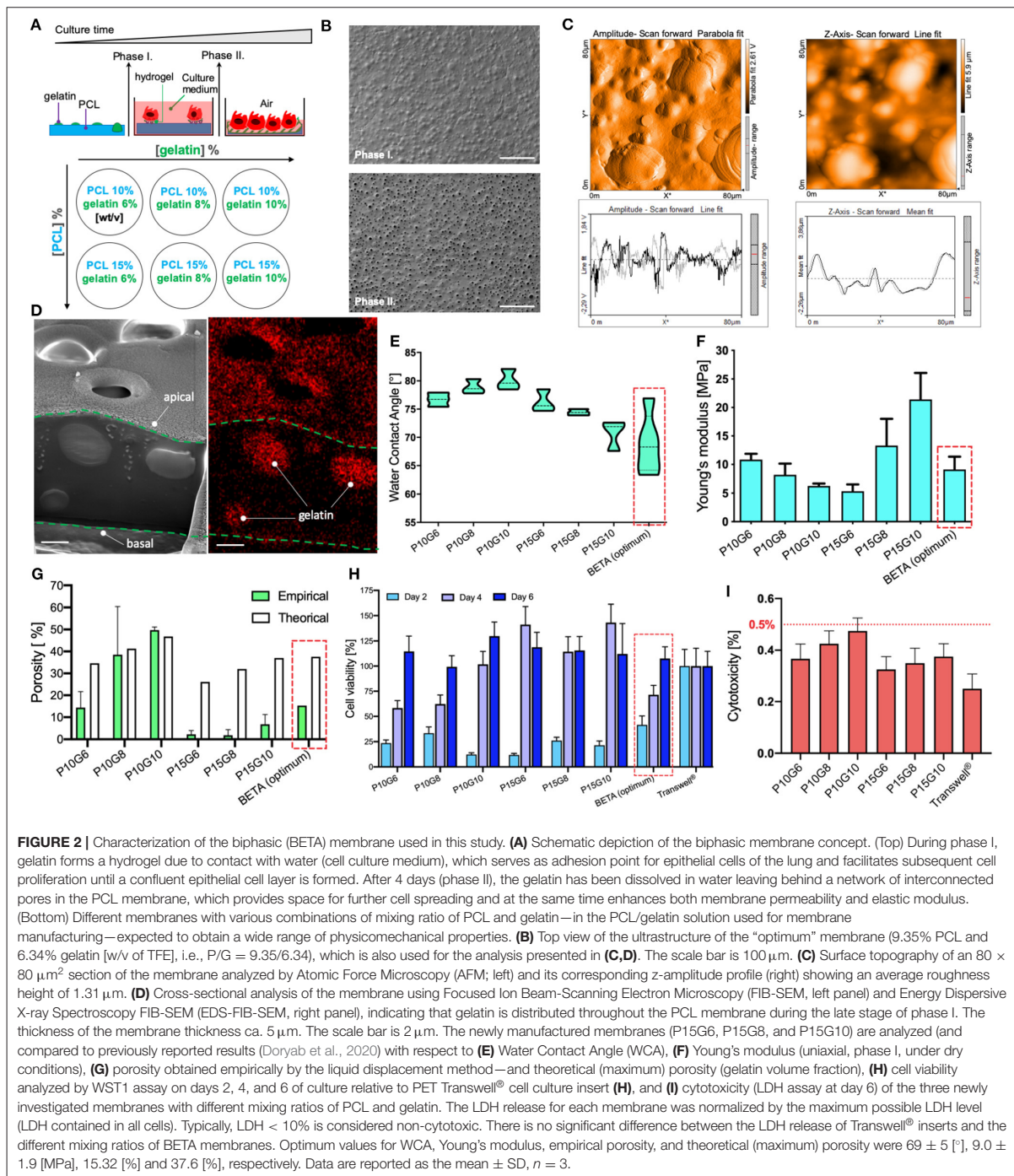
In addition, repeatedly performed WST1 assays showed that the metabolic activity (cell viability) of A549 cells increases with incubation time on the membranes (Figure 2H). This indicates that the relatively few initial seeded cells are proliferating and gradually covering the entire membrane as indicated by WST1

values near 100%, representing the WST1 signal obtained for standard Transwell PET inserts. After a 4–6 days growth period (depending on membrane composition), all of the membranes are covered with a confluent monolayer layer of epithelial cells (Figure 3A). As an additional measure of cytocompatibility, the release of intracellular lactate dehydrogenase (LDH) from the cytosol due to uncontrolled cell death was measured. The small release of LDH (<0.5% of totally available LDH) indicates that these membranes display low cytotoxicity (Figure 2I), which implies that the membranes do not release or leach significant amounts of toxic materials when incubated with the cell culture medium.

In summary, the three new membranes consisting of 15% [w/v] (with 6–10% [w/v] of gelatin) did not improve the key characteristics of a membrane for cell-stretch experiments at the ALI. While their wettability as quantified by WCA was not statistically different from that of the optimum BETA membrane (Figure 2D), the membrane with the lowest Young’s modulus and hence highest elasticity (prior to removal of gelation) displayed an extremely low porosity of 2% as compared to the 15.32% of the optimum BETA membrane (Figure 2F). Such a low porosity value is a knock-out criterion for the membrane since it prevents efficient trans-membrane transport of nutrients (or drugs or nanoparticles) and hence nourishment of cells cultured at the ALI. Hence, the previously determined optimum BETA membrane (9.35% PCL and 6.34% gelatin [w/v solvent]) is superior to all of the 15% PCL membranes and therefore remains the composition of the optimum BETA membrane, which is used for cell experiments described below.

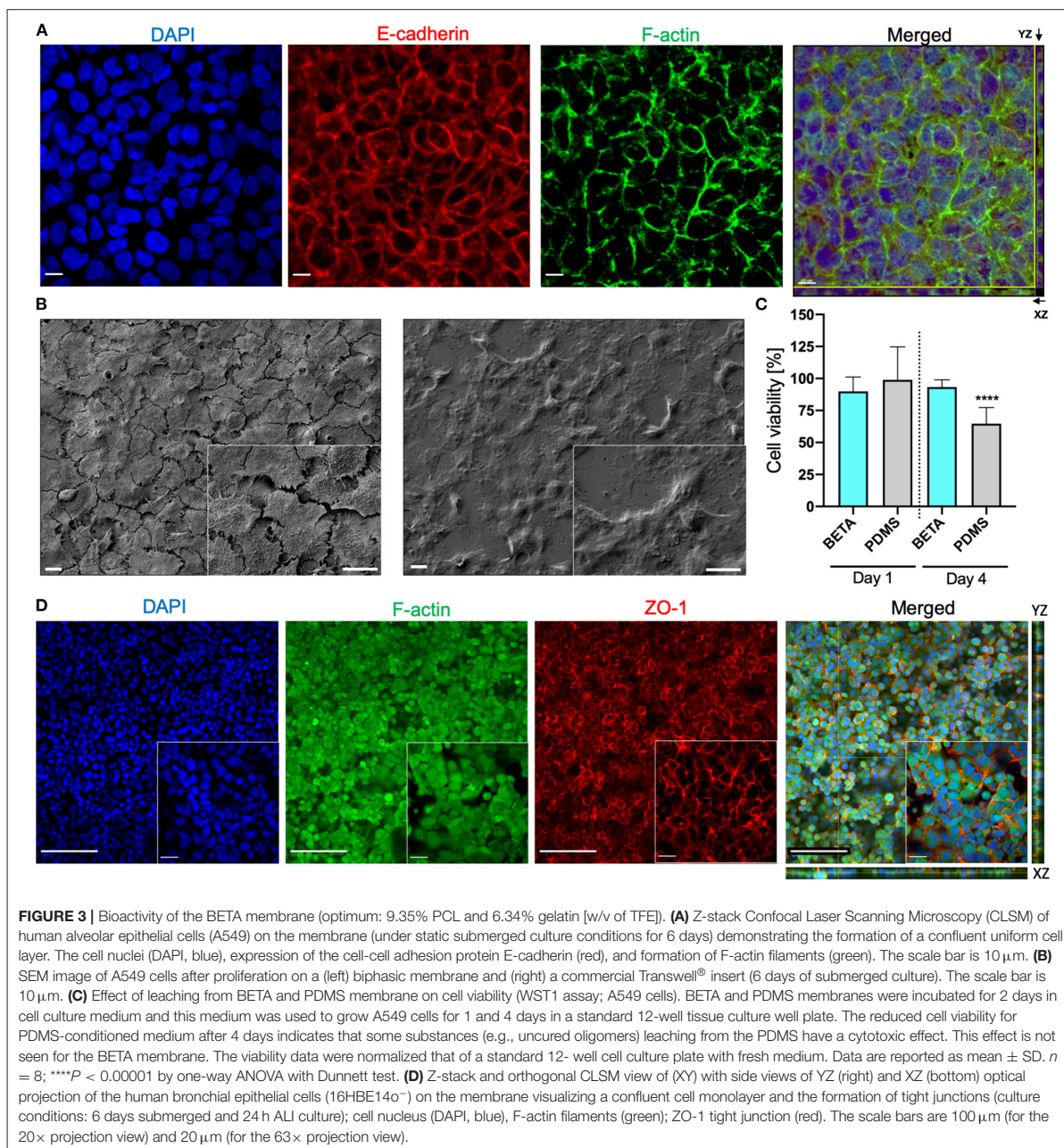
Bioactivity of the BETA Membrane

We also evaluated the bioactivity of the (optimum) BETA membrane using two lung epithelial cell lines namely human lung alveolar epithelial cells (A549) and human bronchial epithelial cells (16HBE14o⁻). CLSM (confocal laser scanning microscopy) analysis showed that A549 cells grew on the membrane into a confluent cell monolayer resulted in the formation of E-cadherin—a transmembrane adhesion protein—which plays a pivotal role in cell-cell contact and polarization of cells at the ALI. Moreover, F-actin rich regions representing a network of polymeric microfilaments of the cytoskeleton were formed, which is essential for important cellular functions, such as cell motility, cell division, vesicle and organelle movement, cell signaling as well as the establishment and maintenance of cell-cell junctions and cell morphology (Figure 3A; images reflect day 6). From the DAPI-stained images (Figure 3A) the number of cells (nuclei) per surface area was determined (4.3 \times 10⁵ cells cm⁻²). Since this value is 2.9-fold larger than the seeding density of the cells (1.5 \times 10⁵ cells cm⁻²), this indicates that substantial cell proliferation has occurred during the 6 days of cell growth under submerged culture conditions. For reference, we also compared the bioactivity of the BETA membrane with that of a commercially available standard Transwell® insert (PET) membrane. It is evident that while initial cell growth/metabolic activity (WST1 signal) on the BETA membrane was slower/lower, this difference



had disappeared on day 4–6 (**Figure 2H**). The ultrastructural analysis exhibited a flattened cell morphology when cells grew on the BETA membrane (**Figure 3B**). Furthermore,

cells showed superior interaction and integration with the BETA membrane as compared to the Transwell® insert (**Figure 3B**).



PDMS (Sylgard 184) membranes are commonly used in cell-stretch devices due to their mechano-elastic properties. However, it has been reported that uncured oligomers of PDMS are released into the culture medium during cell culture, which might be toxic for the cells (Regehr et al., 2009; Carter et al., 2020). Hence, we assessed the leaching of unwanted components of the PDMS membrane compared

to the (optimum) BETA membrane (Figure 3C). Medium incubated for 48 h with PDMS and BETA membranes was used to culture A549 cells under submerged conditions. After 1 day, no significant difference was detected in cell viability for the two materials. However, after 4 days of incubation, a 36% reduction in cell viability was detected for the cells incubated with PDMS-leached medium, while only 6% of

viability reduction was observed for the BETA membrane-leached medium as compared to cells cultured with pristine cell culture medium.

We also examined the bioactivity of the BETA membrane using the human bronchial epithelial cell line 16HBE14o⁻. Cells were grown on the (optimum) BETA membrane for 6 days under submerged and 1 day under ALI conditions. A confluent epithelial barrier with the formation of the F-actin was observed (Figure 3D). SEM analysis also confirmed the CLSM findings (Supplementary Figure 2). Excellent barrier integrity was also confirmed by a TEER value of $451 \pm 55 \Omega \text{ cm}^2$, which is consistent with data reported for 16HBE14o⁻ cells in the literature (Ehrhardt et al., 2002) and higher than the TEER value for A549 epithelial confluent cell monolayer on the BETA ($136 \pm 23 \Omega \text{ cm}^2$).

Nano- and Microparticle Kinetics Study

As an application of the *in vitro* cell-stretch lung model (CIVIC), we investigated the cellular uptake by and transepithelial transport of nano- and microparticles of A549 cells under physiologic cyclic mechanical stretch (10% linear, 0.33 Hz) applied for 2 h. The stability of the stretch parameters as well as the stiffness [Young's modulus: $0.78 \pm 0.24 \text{ MPa}$ (mean \pm SD, $n = 5$)] of the membrane was monitored continuously during the entire experiment with the differential pressure monitoring system of the CIVIC system. The metabolic activity of the cells did not show any evidence of reduced viability due to aerosol exposure and 2 h of cyclic stretch (Supplementary Figure 3).

This study shows that 2 h of cyclic stretch affects cellular uptake and intracellular distribution, but not trans-cellular transport in a size-dependent way. The former is qualitatively evident from CLSM images revealing that cellular uptake of 100 and 1,000 nm particles under unstretched (static) ALI conditions was very limited and cell-associated particles were mostly located close to the air-facing, apical cell surface (Figure 4B). In contrast, 100 nm NPs were internalized more efficiently under stretch conditions and co-localized with the F-actin cytoskeleton deeper within the cell (Figure 4B). On the other hand, stretch did not enhance cellular uptake of 1,000 nm microparticles and particles were still localized close to the apical cell surface, but positioned preferably between adjacent cells rather than randomly as without stretch (Figure 4B). Quantitative fluorescence analysis of the CLSM images revealed a 2.4-fold increase of cellular uptake of 100 nm NPs under stretch, while there was no statistically significant effect of stretch on cellular uptake for 1,000 nm microparticles (Figure 4C).

In addition, spectrophotometric analysis of the basal medium revealed the transepithelial transport (translocation) of particles after 2 h under static and stretch-activated conditions of A549 cells on the BETA membrane or on 3 μm pore (static) PET membranes of 6-well Transwell[®] inserts (Figure 4D). For Transwell[®] inserts, the particles were delivered with a VITROCELL[®] Cloud 6 system to A549 cells (Lenz et al., 2014) and then cultured under (static) ALI conditions.

After 2 h of incubation time under static conditions, the transport fractions across A549 cells on both Transwell[®] inserts and BETA membranes for 100 and 1,000 nm particles were

below the detection limit, except for the $1.8 \pm 0.4\%$ transport of 1,000 nm particles observed for Transwell[®] inserts (two-way ANOVA followed by *post-hoc* Tukey's multiple comparison test) (Figure 4D and Table 1).

For cell-stretch, the transepithelial transport of 100 and 1,000 nm particles across the A549 cell-covered BETA membrane was increased to 30.0 ± 1.7 and $21.0 \pm 11.3\%$, respectively, but no statistically significant dependence on size was observed (no stretch can be applied to Transwell[®] inserts). Hence, cell-stretch significantly increased the translocation of 100 and 1,000 nm particles across the alveolar epithelial barrier independent of particle diameter (see Table 1 and Figure 4D).

DISCUSSION

In the quest for overcoming limitations of traditional *in vitro* models of the lung, the field of bioengineering has witnessed significant efforts toward developing advanced *in vitro* models striving to mimic more closely the human pulmonary environment (de Souza Carvalho et al., 2014). This has led the way from mono-cellular submerged cell lines to primary co-culture cell models at the ALI (air-blood barrier), from static cell culture media and cell layers to medium perfusion (pulmonary blood flow) and cyclic stretch (breathing-induced mechanical tissue strain), and from millifluidic ($\sim\text{cm}^2$ cell area, mL of media) into microfluidic systems often referred to as lung/acinar-on-a-chip technologies (Huh et al., 2012, 2013; de Souza Carvalho et al., 2014; Benam et al., 2015; Tenenbaum-Katan et al., 2018; Ainslie et al., 2019; Artzy-Schnirman et al., 2019). While lung-on-a-chip technologies are starting to become commercially available (e.g., Alveolix, Switzerland and Emulate, USA), also millifluidic lung bioreactors are expected to continue to play a role due to their ease-of-handling, a larger amount of cell samples suitable for many standard assay kits, and lower maintenance efforts.

At the core of any cell-stretch lung bioreactor/chip is a porous and elastic membrane on which the cell culture model is cultured. For lung/acinar-on-a-chip systems mainly 3.5–10 μm thick PDMS membranes are used for cell seeding and growth of an alveolar or bronchial tissue barrier (Huh et al., 2010; Stucki et al., 2015). PDMS membranes are widely used for their high mechano-elasticity, with Young's modulus of $\approx 1\text{--}3 \text{ MPa}$ (Wang et al., 2014). While perforated PDMS membranes are suitable for small-sized lung-on-chip applications ($\sim\text{mm}^2$), they are too fragile for larger millifluidic ($\sim\text{cm}^2$) devices. Moreover, PDMS membranes have low wettability ($\text{WCA} \geq 115^\circ$) (Supplementary Figure 1) and therefore require pre-treatment and/or coating with ECM proteins to facilitate sufficient cell adhesion and proliferation (Wang et al., 2010). Another disadvantage is that uncured oligomers of PDMS can leach into the cell culture medium resulting in changes and cell physiology (Regehr et al., 2009; Carter et al., 2020). Our investigation of a PDMS film has confirmed reports from the literature that cells may experience reduced cell viability due to the leaching of toxins into the cultured in a medium (Regehr et al., 2009). Alternatively, commercial electrospun biocompatible

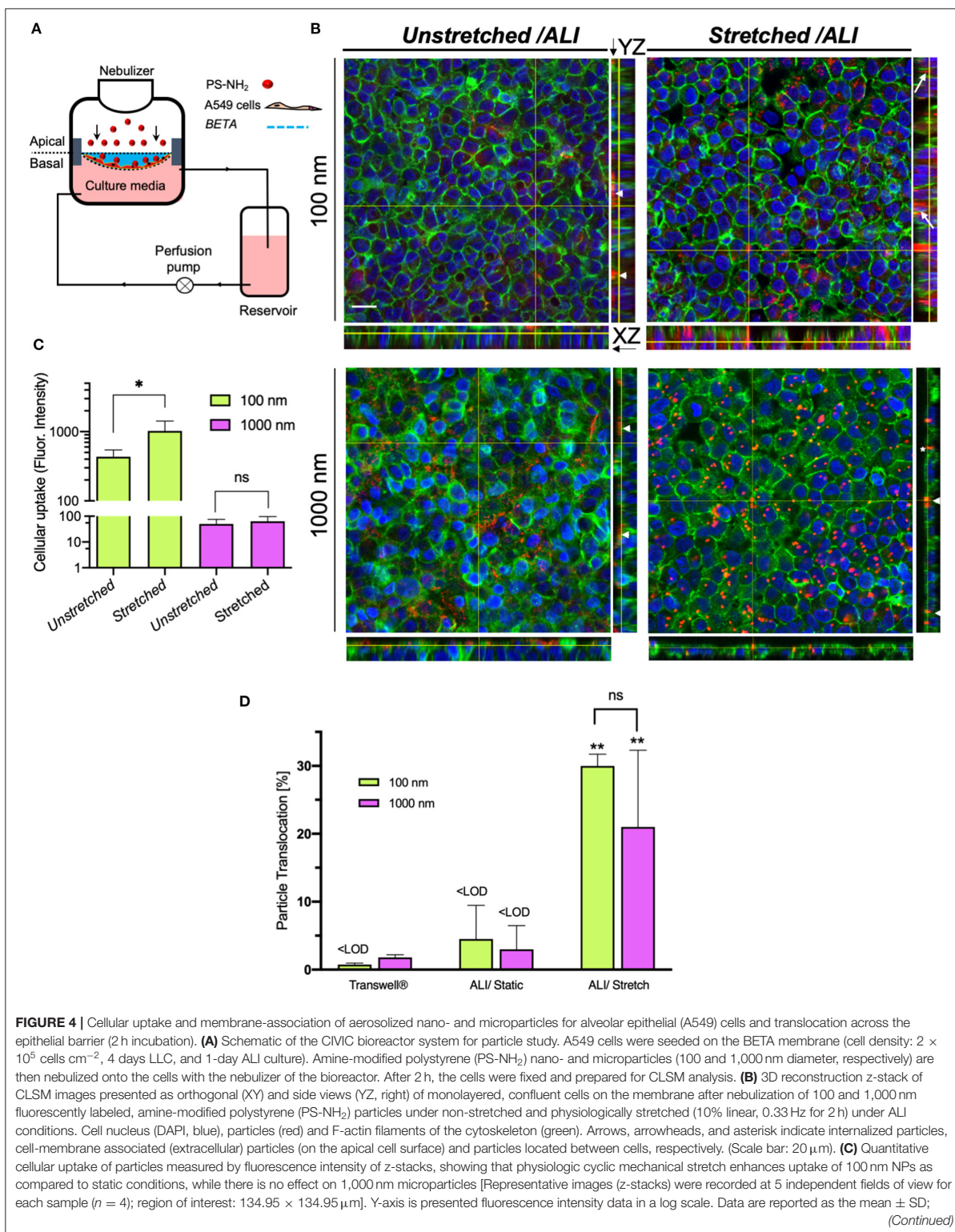


FIGURE 4 | * $P < 0.01$ by two-way ANOVA and data were corrected by Sidac for multiple comparison tests. **(D)** Translocation of 100 and 1,000 nm particles across the cell layer grown on unstretched PET Transwell® inserts and on the BETA membrane (under unstretched and stretched conditions) ($n = 3$). ** Show the comparison between stretched with the corresponding experiment under unstretched conditions. Data are reported as the mean \pm SD; ** $P < 0.001$ by two-way ANOVA and data were corrected by Tukey for multiple comparison tests.

TABLE 1 | Transport of 100 and 1,000 nm particles across A549 cell-layer grown on BETA or PET Transwell® insert membrane (3 μ m pores) at ALI within 2 h of particle exposure (mean \pm SD; $n = 3$).

Run	Translocation [%]	100 nm	1,000 nm
Transwell®/Unstretched		<LOD*	1.8 \pm 0.4
BETA/Unstretched		<LOD	<LOD
BETA/Stretched		30.0 \pm 1.7	21.0 \pm 11.3

* <LOD, below limit of detection.

poly(carbonate)urethane (PCU) membranes (Bionate® II 80A, The Electrospinning Company, UK) have been tested for cell growth in a millifluidic lung bioreactor. They proved inadequate due to their hydrophobic nature (in spite of pre-coating with ECM proteins) and associated poor cell proliferation, their relatively large thickness (ca. 75 μ m), and their inability to prevent the formation of multilayered epithelial tissue deep within the membrane rather than at its apical side (Cei et al., 2020).

The BETA membrane, which overcomes some of these limitations (Figure 5), has a thickness of ≤ 5 μ m, which is thinner than conventional PET or PC/PET membranes used in static Transwell® inserts (≈ 10 μ m) and similar to the lower range of advanced PDMS membranes (≈ 3.5 – 10 μ m) (Huh et al., 2010; Stucki et al., 2015). The two polymer components, i.e., gelatin and PCL were chosen for their wettability and mechanical properties, respectively. The presence of gelatin initial non-porous membrane (BETA in phase I) is conducive to cell adhesion/growth without requiring further surface modification and prevents apically seeded epithelial cells from unwanted migration through the membrane to the basal side, fostering the formation of a monolayer of epithelial cells on the apical side. The gradual dissolution of gelatin by cell culture medium induces sufficient porosity for culturing of cells at the ALI and even results in the secretion of innate ECM secreted by the cells. In contrast to PDMS, no adverse effect on cell viability due to leaching has been observed (Figure 3C).

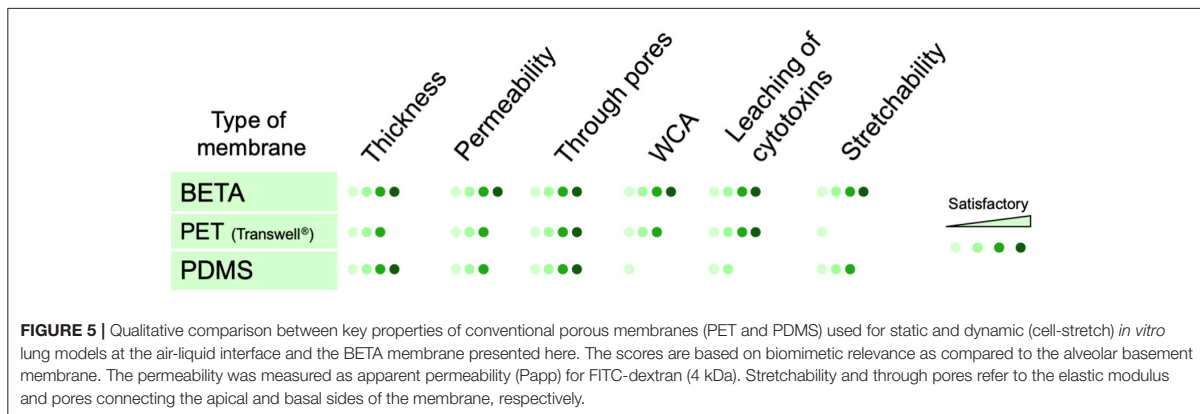
As mentioned above, one of the main advantages of the PDMS membranes is their high mechano-elasticity with Young's modulus of ≈ 1 – 3 MPa (Wang et al., 2014), which is still ca. 100-fold larger than that of alveolar tissue with 3–6 kPa (Polio et al., 2018; Bou Jawde et al., 2020). Since the previously derived optimized BETA membrane (PCL/gelatin = 9.35%/6.34% [w/v solvent] or P/G = 9.35/6.34) (Doryab et al., 2020) has an initial Young's modulus of 9.0 ± 1.9 MPa (prior dissolution of gelatin), the present study tested the hypothesis that an increased PCL concentration of 15% (rather than 6–10% as tested previously) will result in a more elastic membrane. It became evident, that

while a ca. 2-fold lower (uniaxial) Young's modulus (5.3 ± 1.2 MPa for P15G6) could be obtained (Figure 2F), the porosity would be prohibitively low (2% for P15G6) for sufficient trans-membrane nutrient transport during ALI culture conditions. Hence, the previously determined optimum BETA membrane (P/G = 9.35/6.34) was used for the cell-stretch cell experiments.

It is important to note that albeit the (optimum) BETA membrane has an initial (uniaxial) Young's modulus of 9.0 ± 1.9 MPa prior to the dissolution of gelatin (prior to phase I), the (uniaxial) Young's modulus reduces to 1.84 ± 0.66 MPa after dissolving sacrificial gelatin (day 6 under submerged conditions; end of phase II) (Doryab et al., 2020). When measured under more realistic, triaxial stretch conditions in the CIVIC (pressure monitoring method), the elastic modulus of the BETA membrane decreased from 1.33 ± 0.14 MPa (day 1; partial gelatin dissolution) to 0.78 ± 0.24 MPa (day 6) (Doryab et al., 2020), which is ca. 2-fold lower than the corresponding uniaxial value (1.84 ± 0.66 MPa). Considering that the latter was measured under dry conditions these two values can be considered equal within expected experimental uncertainties, which indicates that the BETA membrane is quite isotropic.

In the present study, we recognized the limited value of 2D porosity (pore-area fraction at the surface of the membrane), did not correlate well with the gelatin volume fraction of the membrane, for membrane optimization with respect to 3D porosity (through pores) as only an interconnected 3D pore structure allows for sufficient contact between apically located cells and basal medium during ALI cell culturing. The measurement method for 3D porosity described here was in excellent agreement with the theoretically predicted porosity from gelatin volume fraction, if the latter was larger than 41% (Figure 2G). This indicates that for gelatin volume fractions larger than 41% all of the available gelatin can eventually be reached and hence dissolved by culture medium, i.e., the gelatin-induced 3D pore structure is perfectly interconnected, which is optimum for ALI culture conditions. For gelatin fractions below ca. 35%, the 3D porosity falls below 10% implying that increasing "islands" of gelatin are formed, which are completely engulfed by non-soluble PCL (Figure 2B of Doryab et al., 2020). Thus, future efforts for improved membrane composition should focus on gelatin volume fractions near or above 40% to provide sufficient 3D porosity.

In summary, the optimum BETA membrane is relatively thin (≤ 5 μ m) with a suitable permeability (9.9×10^{-6} cm s^{-1} for FITC-dextran 4 kDa and 15.3% 3D porosity), which can provide sufficient contact between ALI cultured cells on the apical and medium on the basal side of the membrane (Weibel, 1970; Doryab et al., 2019). The BETA membrane is also stretchable up to 25% linear strain (during phase



II), which includes the range of physiologic strain (up to 12% linear) and non-physiologic over-stretch conditions as discussed below. While the BETA membrane is more biomimetic than most other membranes currently available due to the low WCA (68°) and 3D interconnectivity of the pores, the BETA membrane still has a ca. 100-fold higher elastic modulus and thickness of the alveolar tissue and basement membrane, respectively (Polio et al., 2018; Doryab et al., 2019; Bou Jawde et al., 2020). The former is expected to alter cell physiology as compared to lung conditions and the latter may result in bias transbarrier transport studies. Future research on membrane technology mimicking the alveolar basement membrane should focus not only on matching the physicochemical properties of the basement membrane but also on its microstructural (network of ECM fibers) and molecular structure.

Thus, further research is needed to close this physiologic gap. Several alternative synthetic scaffolds have presented promising results for lung, such as biofunctionalized or synthetic-peptide-based synthetic scaffold (Nishiguchi et al., 2017). Despite the natural-based scaffold (e.g., collagen type I), synthetic scaffolds can be tailored to have selective tunable properties, mimicking the microenvironment of cells to facilitate cell adherence, proliferation, and differentiation. However, artificial scaffolds, i.e., natural, synthetic, and natural/synthetic introduced until now are unable to concurrently mimic all the physical, mechanical, and biological properties of the natural ECM or basement membrane of the pulmonary cells. The biomimetic biphasic scaffold reported here has excellent structural, mechanical, and biophysical characteristics and can be a suitable alternative for growing epithelial cells not only in the monoculture but also in co-culture and triple co-culture models (Lehmann et al., 2011; Heydarian et al., 2019).

Ultimately, sufficiently biomimetic *in vitro* models of the alveolar tissue should not only focus on the basement membrane but also include more advanced primary alveolar cell models, such as the commercially available primary-derived hAELVi cells (Kuehn et al., 2016) or EpiAlveolar cell model (MatTek, Inc.) (Barosova et al., 2020). The combination of both aspects should

lead to even more biomimetic and hence clinically predictive models of the alveolar barrier.

The millifluidic CIVIC bioreactor utilizes positive pressure to mechanically stretch a cell-covered elastic membrane activate stretchable and thus allows for ALI cell culture conditions with medium perfusion, cyclic stretch, and monitoring of the pressures in the apical and basal compartment of the bioreactor is leveraged for real-time monitoring of amplitude and frequency of cyclic stretch and of tri-axial Young's modulus of the cell-covered membrane. This allows for precise selection of stretch conditions and quality control of key experimental conditions during the course of the cell-stretch experiment. Moreover, an aerosol-cell delivery unit using a clinically relevant nebulizer enhances its applicability to drug testing suitable for inhalation therapy.

It is instructive to relate the characteristic stretch and perfusion parameters of the CIVIC equipped with the BETA membrane to clinical conditions. The BETA membrane can sustain linear stretch amplitudes of up to 25% (Doryab et al., 2020). Population-based averages for breathing frequency and tidal volume during heavy exercise are 26 breaths per minute (33 bpm for women) and 1.92 L (1.36 L), respectively (ICRP, 1994). For typical lung inflation of 3.3 L (2.7 L) at functional residual capacity (FRC, at end of exhalation), this tidal volume corresponds to a 58% (50%) increase in lung volume yielding a 17% (15%) linear and 36% (31%) area change (assuming the alveolar sacs are spherical). Analogous, the stretch conditions were chosen here for the particokinetics study (10% linear at 0.33 Hz = 20 bpm) correspond to a tidal volume of 1.09 L (female 0.89 L), which is similar to "light exercise" conditions (male: 1.25 L, 20 bpm; female: 0.99 L, 21 bpm) (ICRP, 1994). Consequently, linear strain larger than 17% (or 35% ΔSA), which may occur for instance during positive pressure ventilation, is considered over-distension or non-physiologic strain, possibly provoking apoptosis and necrosis, increase permeability and release of inflammatory mediators (such as Interleukin-8) in alveolar epithelial cells (Edwards et al., 1999; Vlahakis et al., 1999; Hammerschmidt et al., 2004).

The maximum positive differential pressure applied to the apical side of the cells during a cyclic stretch in the CIVIC

(2.5 kPa) is higher than exerted onto the lung tissue during normal exhalation (0.1–0.5 kPa), but similar to conditions during mechanical ventilation at the intensive care unit of a hospital (normal: 1.5–2.0 kPa, 2.5 kPa acceptable peak value; 3.0 kPa should not be exceeded for an extended period of time) (Hall, 2016). Finally, the medium perfusion rate of $400 \mu\text{L min}^{-1}$ has to be put into context with the area of gas exchange (membrane area: 5 cm^2) for comparison with the lung. The ratio of area and perfusion rate of the CIVIC is with $1.25 \text{ m}^2/(\text{L min}^{-1})^{-1}$ considerably lower than that of the lung [$20 \text{ m}^2/(\text{L min}^{-1})^{-1} = 100 \text{ m}^2/(5 \text{ L min}^{-1})$], but the corresponding flow rate of 6.4 L min^{-1} in the CIVIC system technically not be difficult to establish since it would require tubing with much larger diameter enhancing the laboratory footprint unduly.

It is well known that the size of particles plays a key role in cellular uptake and internalization of the particles (Takenaka et al., 2012; Zhu et al., 2013). We found that both 100 and 1,000 nm amine-coated particles could not be internalized by alveolar epithelial cells (A549) under static/unstretched conditions (2 h after aerosolized particle delivery). Moreover, 1,000 nm microparticles were also not taken up by cells under stretched conditions, which can be explained by endocytic uptake (most relevant uptake mechanism for epithelial cells) being limited to ca. 500 nm particles (Winnik and Maysinger, 2013; Zhu et al., 2013; Annika Mareike Gramatke, 2014). In contrast, the relatively efficient cellular uptake of 100 nm NPs is consistent with previous observations that positively charged (amine-coated) NPs tend to interact with the negatively charged cell membrane, which enhances their uptake as compared to neutral or even negatively charged particles of the same size (Rothen-Rutishauser et al., 2006). The observed colocalization of NPs with the F-actin cytoskeleton in A549 cells is conducive for further intracellular trafficking and endocytosis of the NPs within cells (Foroozandeh and Aziz, 2018). For *in vitro* pharmacokinetic testing, ALI culture conditions have several advantages over submerged cell culture settings. In addition to more physiologic and tighter barrier function, burst-like pharmacokinetic profiles as typically seen in patients can only be observed for ALI conditions (Meindl et al., 2015; Schmid et al., 2017) since this resembles rapid depletion of the pulmonary drug reservoir due to drug transport into the blood. Moreover, the cell-delivered dose is often poorly known under submerged conditions due to variable particle-cell transport rates in cell culture medium (Teeguarden et al., 2007; Schmid and Cassee, 2017). In contrast, under ALI conditions, the aerosol dose is delivered immediately directly onto the epithelial barrier mimicking the conditions of inhaled particles in the lung. To date, *in vitro* particokinetic studies are mainly performed under submerged culture conditions, and to the best of our knowledge, no quantitative transbarrier particokinetic (translocation) studies under cell-stretch ALI conditions have been reported, yet.

For sub-100 nm NPs the translocated fraction of particles is inversely proportional to particle size in both static *in vitro* cell and *in vivo* animal models of the lung (Kreyling et al., 2014; Bachler et al., 2015). For A549 cells at ALI and rodent models after NP instillation, the first plateau of particle translocation is achieved within 2 h for 80 nm gold NPs, but it is considerably

larger for (static) A549 cells (ca. 2% of the delivered dose) as compared to particle instillation in rats (ca. 0.2%) (Kreyling et al., 2014; Bachler et al., 2015). For A549 cells, receiving doses larger than $0.1 \mu\text{g cm}^{-2}$ for gold NPs has resulted in a decrease in the transport rate (Bachler et al., 2015).

The 2 h translocation fraction of 100 nm amine-modified polystyrene particles observed in this study was below the detection limit [ca. 1.0% (Transwell) and ca. 3% BETA], which is in general agreement well with the results from Bachler and colleagues (Bachler et al., 2015), if we consider that the larger than $0.1 \mu\text{g cm}^{-2}$ (here $2.1 \mu\text{g cm}^{-2}$) cell-delivered dose may have lowered the transport fraction. On the other hand, the 1.8% of translocation fraction for 1,000 nm particles (Transwell inserts) appears relatively large considering that virtually no translocation of microparticles has been reported in *in vivo* biokinetics studies. The absence of 1,000 nm translocation for the BETA membrane (below detection limit of ca. 3%) is consistent with these *in vivo* results. While it may be expected that cyclic stretch affects the transepithelial mobility of particles by, e.g., additional convective particle transport, changes in paracellular barrier integrity, and effects on cellular uptake and transport mechanisms, the relatively large increase to 30 and 20% for 100 and 1,000 nm particles is unexpectedly high. Since these values even agree within experimental uncertainty it is unlikely that this is the result of an active cellular transport process especially since endo-/exocytosis as the most effective cellular uptake and transport mechanism for epithelial cells is limited to sizes below 500 nm. Moreover, substantially enhanced cellular uptake was only observed for 100 nm particles (Figure 4B). Therefore, we assume that this large increase in translocation fraction is due to a combination of passive mechanisms, such as rupture of the relatively weak tight junctions of A549 cells yielding intracellular gaps, which allows for enhanced convective transport of particles irrespective of particle size due to leakage of the medium in and out of the apical space where the particles are residing.

CONCLUSION

The “optimum” copolymeric BETA membrane ($P/G = 9.35/6.34$) applied here is biomimetic in the sense that it is thin ($\leq 5 \mu\text{m}$), surface wettable, permeable with proper pore size for cell growth and interconnected 3D pore structure, elastic and bioactive, and somewhat comparable to the ECM in the alveolar region. However, it still is ca. 100-fold too thick and stiff as compared to the basement membrane of the alveolar region. These limitations could not be alleviated by enhancing the poly(ϵ -caprolactone (PCL) concentration 15% (w/v). Using the “optimum” we showed that the CIVIC can be utilized for cellular uptake and transepithelial transport studies under physiologic stretch and ALI conditions including aerosolized substance delivery. While the results for static conditions are in general agreement with literature data, unexpectedly high translocation of both 100 and 1,000 nm particles under physiologic stretch (light exercise) was observed for an A549 alveolar lung barrier. This suggests that more appropriate cell (co-)culture models with more pronounced tight junctions and advanced primary cell

culture models should be employed for cell-stretch experiments. Studies in the field of respiratory diseases are expected to benefit greatly from the development of more biomimetic and reliable *in vitro* models of the lung as currently available. We believe our system presents a valuable step toward improvement of the predictive value of advanced lung cell models.

MATERIALS AND METHODS

Cell Culture

Human alveolar type-II like epithelial cells (A549) were cultured and maintained in Dulbecco's Modified Eagle Medium: Nutrient Mixture F-12 (DMEM/F12, 1:1 v/v, Gibco) supplemented with 10% FCS (Gibco), 1% (v/v) Pen/Strep (100 U mL⁻¹, Gibco), 1% L-glutamine (2 mM, Gibco), and 2-phospho-L-ascorbic acid (0.1 mM, Sigma). Human bronchial epithelial cells (16HBE14o⁻) were cultured in MEM/F12 medium (Gibco) supplemented with 10% FCS (Gibco), 1% (v/v) Pen/Strep (100 U mL⁻¹, Gibco) and 1% L-glutamine (2 mM, Gibco).

For longitudinal monitoring of cell viability (WST1), A549 cells were grown on the BETA membranes by seeding cells with a cell density of 1.5×10^5 cells cm⁻² on a UV sterilized BETA membrane (effective growth area: 1.3 cm², depending on application). A PTFE holder was used for keeping the BETA membranes and on Corning® Costar® Transwell® cell culture inserts (PET, 12-well, 1.1 cm²; 3 μm pore) (control). Cells were then cultured for 6 days under submerged conditions (basal and apical medium volumes were 1.5 and 0.5 mL, respectively) followed by 24 h under ALI conditions. Similarly, 16HBE14o⁻ cells were also grown on the BETA membrane (cell seeding density: 2×10^5 cells cm⁻²; effective growth area: 1.3 cm²) for 6 days under submerged and 24 h under ALI conditions.

Immediately prior to cell-stretch experiments the membrane was placed in the CIVIC and the media volume in the basal and reservoir chamber of the CIVIC were 4 and 12 mL (including 2 mL in the connecting tubing), respectively.

In vitro Cell-Stretch System (CIVIC)

We used the CIVIC system to apply cyclic stretch to cells grown on the BETA membrane under ALI culture conditions (Figure 1). The main chamber of the CIVIC bioreactor is separated by the BETA membrane into an apical (humidified air) and a basal (perfused cell culture medium) compartment mimicking the air-blood barrier of the lung including its breathing-related cyclic stretch induced by oscillation of the apical pressure (Figures 1A,B and Supplementary Video 1). The cell culture medium in the basal compartment is circulated using a peristaltic pump to mimic blood flow (400 μL min⁻¹). Cells grown on the membrane are subjected to a uniform cyclic triaxial strain by applying a cyclic (here: sinusoidal) positive pressure to the apical chamber by cyclic opening of a valve connected to pressurized cleaned house air and a valve connected to ambient air. The entire system is placed in an incubator (37°C) to maintain optimum cell culture conditions. The dry house air is entering the chamber for pressurization via a humidifier and the initially dry air in the apical compartment can be humidified by nebulization of small volume (2 μL) of saline using the nebulizer described

below (Figures 1A,B). Both amplitude and frequency of stretch can be set by an Arduino integrated development environment (or IDE) software (Arduino IDE 1.0.5 for Windows). For BETA membranes, the CIVIC bioreactor is able to apply physiologic linear strain: (0–17%) and non-physiologic (over-stretch; 17–25%) stretch conditions, as described below.

The CIVIC system is a modified version of the previously described MALI bioreactor system (Cei et al., 2020). The overall setup and geometry of the MALI system have not been changed. However, the following technical improvements were implemented. All of the components in contact with culture medium are now manufactured with PDMS-free material (namely polycarbonate, PC) to prevent potential artifacts due to leaching of toxicants from the PDMS into the cell culture medium. Moreover, an upgraded design of the PC holder more effectively prevents membrane slipping and leakage of culture medium during pressure oscillations required for inducing cyclic cell stretch as described below. The pressure sealing of the main chamber was improved and not only the pressure in the basal compartment (headspace of the medium reservoir, P₂), but also the pressure in the apical compartment was measured continuously (P₁) (Figure 1A) using two piezoresistive, monolithic silicon pressure transducers (MPX5050, Freescale Semiconductor, Munich, Germany).

A clinically used vibrating mesh nebulizer (Aeroneb Pro/Lab, Aerogen Inc., Galway, Ireland) is positioned at the top of the apical chamber for delivery of aerosolized substances to the cells on the BETA membrane. This type of nebulizer has liquid output rates and mass median droplet diameters ranging from 0.2 to 0.8 mL min⁻¹ and 2.5 to 6 μm, respectively, depending on the specific type of nebulizer (Ding et al., 2020). Nebulization of 10 μL of liquid and subsequent spatially uniform deposition onto the cells cultured on the BETA membrane (5 cm²) with a deposition efficiency of 52% occurs within 2 min due to cloud settling (Cei et al., 2020). These aerosol delivery parameters are, independent of nebulizer performance in terms of droplet diameter or liquid output rate (Lenz et al., 2014) since cloud settling depends on the fractional aerosol volume in the air only and hence on the nebulized aerosol volume (10 μL) and the volume of the apical compartment of the chamber. Vibrating mesh nebulizers contain a porous membrane for aerosol production, which may be affected by cyclic positive pressure. Since aerosolized substance delivery is short (2 min) relative to typical cell-stretch experiments (>2 h), aerosolized substance application is typically decoupled from cyclic cell stretch, i.e., cell-stretch is not applied during aerosolization. This patented aerosol-cell exposure unit has recently been made commercially available as VITROCELL® Cloud MAX (VITROCELL Systems, Waldkirch, Germany), albeit only for standard transwell inserts, which cannot be subjected to cyclic stretch. When positive pressure is applied apically to the membrane (P₁), the initially relaxed, flat, horizontally oriented membrane is stretched triaxially downwards expanding the volume of the apical compartment by a dome-shaped volume ΔV (Figures 1A, 4A). Due to the incompressible nature of water (culture medium), this change in apical volume reduces the air-filled headspace of the medium reservoir by ΔV and the

corresponding increase in pressure (P_2) can be directly related to the linear/area amplitude of membrane stretch (**Figure 1A**).

This special feature of the CIVIC bioreactor enables real-time monitoring of the experimental stretch parameters (amplitude, frequency) and Young's modulus of the cell-covered membrane with thickness t during triaxial stretch under wet conditions (contact with culture medium) by continuously monitoring the apical and basal pressures (P_1 and P_2 , respectively). While the stretch frequency can be directly derived from the time course of P_1 or P_2 , the linear (1D) and area (2D) amplitude as well as Young's modulus (elastic modulus; E , kPa) of the membrane can be determined from the maximal values of P_1 and P_2 according to the Equations (1)–(3) (Flory et al., 2007).

$$\Delta V = \Delta P \left(\frac{V_0}{P_0} \right), \text{ where } \Delta P = P_2 - P_0 \quad (1)$$

$$\Delta V = \pi \Delta h \left(\frac{a^2}{2} + \frac{\Delta h^2}{6} \right) \quad (2)$$

$$\Delta P' = (P_1 - P_2) = \frac{4E \left(\frac{\Delta h}{a} \right) t}{3a \left(\left(\frac{\Delta h}{a} \right)^2 + 1 \right)} \left(1 - \frac{1}{\left(1 + \left(\frac{\Delta h}{a} \right)^2 \right)^3} \right) \quad (3)$$

Initially, the membrane is non-stretched and the pressure in both the apical and basal compartment is at ambient pressure P_0 (on average 98.0 kPa in Munich, Germany) (see **Figure 1A**). Under these conditions, the radius (area) of the membrane a is 1.26 cm (5 cm^2) and the headspace volume in the medium reservoir V_0 is 30 mL (40 mL vessel filled with 10 mL medium). The deflection of the membrane perpendicular to the membrane (Δh) can be obtained from the corresponding change in apical/basal air volume ΔV , which is determined from Equations (1), (2) and the measured pressures P_1 and P_2 . Young's modulus (elastic modulus; E , kPa) of the membrane can then be obtained from Equation (3), where t is the thickness of the membrane (ca. $5 \mu\text{m}$; calculated by cross-sectional SEM analysis). For dome-shaped geometry (spherical cap), one can find the relative linear and area strain according to Equation (4).

$$\frac{\Delta L}{L} = \frac{\Delta h}{a} \quad \text{or} \quad \frac{\Delta S}{S} = \left(\frac{\Delta h}{a} \right)^2 \quad (4)$$

The amplitude of cell stretch can be calculated from Equation (4), where Δh is the membrane deflection ($0 \leq \Delta h \leq 0.11 \text{ cm}$) (Equations 1–3) and ΔS is membrane change in surface area during the stretch. P_1 and P_2 are 100.5 and 99.5 kPa for physiologic stretch (10% linear strain or 21% ΔS), respectively.

For optimum BETA membrane, the CIVIC bioreactor is able to apply a linear mechanical strain of up to 17% (or 3, which covers both physiologic and non-physiologic (overstretch) conditions. For those conditions, the optimum BETA membrane is resilient to 48 h cyclic stretch with no deformation, rupture, and creep.

Membrane Fabrication

We recently introduced a novel ultra-thin co-polymeric membrane (BETA) transitioning from an initially stiff,

hydrophilic, non-porous membrane to an elastic, porous substrate, providing optimum cell culture conditions during the two phases of typical *in vitro* alveolar cell-stretch experiments at the ALI (Doryab et al., 2020). Briefly, we employed a two-component (hybrid) polymeric material consisting of poly(ϵ -caprolactone) (PCL: Sigma-Aldrich, Mn 80,000) and gelatin (Type A from porcine skin, Sigma) chosen for their mechano-elastic and bioactivity properties, respectively. Different mass ratios of PCL and gelatin were dissolved in TFE [(2,2,2-trifluoroethanol) with >99.8% purity, Carl Roth GmbH, Karlsruhe, Germany] and stirred until the blend became homogenous. The PCL/gelatin mixture was then added to a custom-made spin-coater (2,000 rpm) to produce a thin film which was left to dry under vacuum (**Figure 2A**). The initially non-porous membrane (phase I: initial cell adhesion and growth) becomes gradually permeable (phase II: ALI culture) upon contact with the cell culture medium. The underlying concept of a biphasic membrane for cell-stretch experiments under ALI conditions mimicking the conditions in the alveolar tissue has been described in the introduction. The optimum concentrations of PCL and gelatin was determined previously as 9.35% PCL and 6.34% gelatin [w/v solvent]; solvent: $\geq 99\%$ TFE (2,2,2-trifluoroethanol) (Doryab et al., 2020). Here, three new membranes with 15% PCL and 6, 8, and 10% of gelatin were manufactured. The membranes were placed in a holder for placement in the CIVIC system during cell-stretch experiments as described below (**Figure 1C**). Membranes were sterilized before cell culture experiments with ethanol and ultraviolet (UV) light exposure. The membrane is optically transparent and hence suitable for modern cell microscopy technologies.

Membrane Characterization

The membranes were characterized in terms of thickness, ultrastructure, pore size, elemental and chemical composition, surface wettability, elastic modulus, 3D porosity, and cell proliferation (viability and cytotoxicity).

Physical, Elemental, and Chemical Characterization

Thickness, ultrastructure, and pore size of the membranes were analyzed by Scanning Electron Microscopy (SEM). The samples were fixed in 6% (v/v) glutaraldehyde (Sigma-Aldrich) and then dehydrated in gradient ethanol solutions followed by HDMS (hexamethyldisilazane, Sigma-Aldrich) for 15 min and subsequently mounted onto aluminum stubs, sputter-coated with platinum using Leica EM ACE600 vacuum coater, and imaged by SEM (Zeiss Crossbeam 340, Carl Zeiss AG, Oberkochen, Germany) with acceleration voltage of 2 kV. We also used Energy Dispersive X-ray Spectroscopy (EDS, X-max^N, Oxford instruments) with an acceleration voltage of 8 kV to study qualitative elemental and the local distributions of certain elements (Carbon and Nitrogen) in the sample. Focused Ion Beam (FIB)/SEM (Zeiss Crossbeam 340, Carl Zeiss AG, Oberkochen, Germany) and FIB/SEM/EDS were employed to investigate the cross-sectional structures of the membranes at high resolution (30 kV; 700 pA and 1.5 nA). Surface roughness was assessed by an Atomic Force Microscope (AFM, Nanosurf Flex-Axiom) at room temperature. A scanning area of $80 \mu\text{m}$ was

chosen. Scan rates of 0.5–0.15 Hz were used during mapping with 512 points per scan.

Surface Wettability (Water Contact Angle)

The surface wettability or Water Contact Angle (WCA) of the membranes was determined with the sessile drop method using an automated contact angle system OCA20 with an image processing system as described previously (Doryab et al., 2020).

Elastic Modulus (Young's Modulus)

Uniaxial (1D) tensile test (BOSE 5500 system, ElectroForce, Eden Prairie, MN, USA) with a load capacity of 22 N at a rate of 0.01 mm/s until rupture was used to calculate Young's modulus of the membrane (in phase I). Young's modulus of the membrane in wet (phase II) condition was measured using our novel pressure-based technique integrated into our CIVIC system described in more detail in Figure 1A.

Porosity

We used the liquid displacement method to measure the 3D porosity of the interconnected three-dimensional (3D) pore network of the membranes. Briefly, membranes were submerged in ethanol (EtOH, $\geq 99\%$ purity) for 24 h. Gravimetric analysis prior to and after soaking the membrane with EtOH revealed the volume of EtOH (V_{EtOH}) inside the pores ($V = m/\rho$; m_{EtOH} = difference of mass prior to and after soaking; $\rho_{\text{EtOH}} = 0.789 \text{ g cm}^{-3}$) and the volume of the dry membrane (V_m) [m_m = mass of membrane prior to soaking; ρ_m is the volume-weighted density of PCL (1.145 g cm^{-3}) and gelatin (1.3 g cm^{-3})]. The empirical 3D porosity can then be calculated according to Equation (5).

$$\text{Porosity} = \frac{V_{\text{EtOH}}}{V_{\text{EtOH}} + V_m} \quad (5)$$

To account for EtOH adsorption on and/or microporosity of PCL itself, the apparent porosity of the pure PCL membrane ($9.3 \pm 1.7\%$; according to Equation 5) was subtracted from the measured porosity of the PCL/gelatin membranes.

Moreover, one can estimate the upper limit of porosity from the chemical composition of the membrane. Assuming gelatin has been completely dissolved in the culture medium (PCL is insoluble), one finds a theoretical upper limit for porosity from the volume fraction of gelatin based on Equation (6), where V_g and V_{PCL} are the volume fraction of gelatin and PCL in the composite of PCL/gelatin, respectively, and ρ_g and ρ_{PCL} are the density of gelatin and PCL ($\rho_g = 1.30 \text{ g cm}^{-3}$ and $\rho_{\text{PCL}} = 1.45 \text{ g cm}^{-3}$), respectively.

$$\text{Theoretical Porosity} = \frac{\frac{V_g}{\rho_g}}{\frac{V_g}{\rho_g} + \frac{V_{\text{PCL}}}{\rho_{\text{PCL}}}} \quad (6)$$

Cell Proliferation, Morphology, and Cell Viability

Cell proliferation was assessed from the known number of cells seeded on the membrane (day 0) and the cells counted based on DAPI-stained (cell nucleus) CLSM images at the end of the submerged cell culture conditions (day 6). Moreover,

cell proliferation was monitored indirectly with higher time-resolution by measuring cell viability in terms of a non-destructive metabolic activity assay (WST1, Roche, Mannheim, Germany), provided the metabolic activity of the cells is similar during the 6 days of cell growth. This test was performed on cell covered BETA membranes (1.3 cm^3) and Corning® Costar® Transwell® cell culture inserts (PET, 12-well, $3 \mu\text{m}$ pore), which was used as a commercial membrane to compare cell viability, cell number and morphology with that of the BETA membrane. Each membrane was incubated with 1 mL diluted WST1 reagent (1:15) at 37°C . After 15 min, $150 \mu\text{L}$ supernatant was transferred to a 96-well plate (4 times for each membrane) and absorbance was measured in a plate reader (Magellan™ Tecan) at 450 nm . All the results were normalized to the mean value of blank.

Lactate Dehydrogenase (LDH) Release

The cytotoxicity effect of the manufactured membranes was assessed by the detection of the release of lactate dehydrogenase (LDH; Roche Applied Science, Mannheim, Germany) from the cells, which indicates perforation of the cell membrane. According to the manufacturer's protocol, the determination of LDH activity was determined in the basal (and apical) medium by absorbance measurement at a wavelength of 492 nm . The LDH release is presented as the ratio of LDH dose (LDH concentration times medium volume) in the cell culture medium and the high control (cells treated with 2% [w/v] Triton X-100). Transwell inserts were used as a positive control since BETA membranes are more limited in supply than standard Transwell inserts. The LDH release for each membrane was normalized by the maximum possible LDH level (LDH contained in all cells).

PDMS-Leached in Cell Culture Medium

We fabricated PDMS films for studying the leaching of PDMS oligomers into the culture medium. Briefly, the elastomers and crosslinker (1:10, Sylgard 184, Dow Corning) were mixed and degassed under vacuum. After casting, the film was cured in an oven at 60°C overnight. The PDMS film (thickness: $5 \mu\text{m}$) was then cut using a standard biopsy punch (size: 5.0 mm ; Kai medical, Solingen, Germany). The membranes were washed with PBS (three times) and disinfected using EtOH 80% and UV before immersing in the Dulbecco's Modified Eagle Medium: Nutrient Mixture F-12 (DMEM/F12, 1:1 v/v, Gibco) supplemented with 10% FCS (Gibco), 1% (v/v) Pen/Strep (100 U mL^{-1} , Gibco), 1% L-glutamine (2 mM , Gibco). The PDMS punches and BETA membranes of the same size were soaked in 2 mL of culture medium for 2 days (the ratio of the surface area and the bulk volume of the membrane to the culture medium were $0.1 \text{ cm}^2 \text{ mL}^{-1}$ and $4.9 \times 10^{-5} \text{ cm}^3 \text{ mL}^{-1}$).

The PDMS- and BETA-incubated media containing leached compounds were used to investigate their effect on cell viability with the WST1 assay. For this, A549 cells ($1.5 \times 10^5 \text{ cells cm}^{-2}$) were cultured under submerged conditions in 12-well multiwell plates using PDMS- and BETA membrane-leached media for up to 4 days and repeatedly analyzed for viability (WST1). As a control, A549 cells were seeded on the bottom of the well plate.

Immunofluorescence

Cells were fixed in 4% paraformaldehyde (Sigma-Aldrich), washed with PBS and, permeabilized by 0.3% Triton X-100 (Sigma-Aldrich) in PBS at room temperature. To prevent any unspecific antibody binding, a blocking buffer (5% BSA and 0.1% TritonX-100) was added for 10 min. The cells were then incubated overnight at 4°C with Anti-E-Cadherin (mouse, 1:1,000; Invitrogen) and anti-ZO-1 monoclonal (mouse, 1:100; Invitrogen), in a blocking buffer (5% BSA and 0.1% TritonX-100). Cells were then incubated with secondary antibody Alexa Fluor® 488 goat anti-mouse IgG (1:500; Invitrogen) and Alexa Fluor® 555 goat anti-mouse IgG (1:500; Invitrogen). The F-actin cytoskeleton and cell nuclei were stained with Phalloidin 594 (1:40) and DAPI (1:100), respectively. The cells were then embedded in Glycergel (DAKO Schweiz AG, Baar, Switzerland). All cell images were acquired using a confocal laser scanning microscope (CLSM; LSM710, Carl Zeiss; Oberkochen, Germany) coupled to the Zen2009 software. For intensity quantification of particles, the images were recorded at five independent fields of view (region of interest: 134.95 × 134.95 μm) for each sample. The rectangular tool (Fiji) was used to measure the mean fluorescence intensity of background-subtracted images.

TEER Measurement

Trans-epithelial electrical resistance (TEER) measurements of epithelial cells grown on the membrane were measured using the Millicell-ERS system (Millicell ERS-2, Millipore, USA). TEER is calculated by multiplying the cell-specific resistance (Ohm, Ω) and the effective surface area of the membrane (cm²). The TEER value of the blank BETA membrane was determined as 78 ± 10 (Ω cm²), which was then subtracted from the cell-covered membrane TEER values.

Particokinetic Studies

For particle studies, we chose fluorescent amine-modified polystyrene (PS-NH₂) spheres, fluorescent orange (Sigma-Aldrich, St. Louis, USA), with a mean diameter of 100 and 1,000 nm for particle study (Figure 4A) since amine-functionalized surfaces (positively charged particles) are associated with higher cellular uptake and internalization as compared to neutral or negatively charged ones (Rothen-Rutishauser et al., 2006; Zhu et al., 2013). A549 cells were grown on the optimized BETA membrane until confluence (submerged conditions for 6 days) and left for acclimatization at the ALI for 1 day. Particles were then nebulized directly onto the cells [deposited mass dose: 2.1 μg cm⁻²; surface area dose: 1.2 cm² cm⁻² (100 nm particles); 0.12 cm² cm⁻² (1,000 nm)] and incubate with the cells for 2 h under stretched or unstretched conditions.

For the unstretched experiments, the membranes were first put in special holders and placed in a 6-well plate which was then positioned in the aerosol-cell exposure chamber of a VITROCELL® Cloud 6 system (VITROCELL Systems, Waldkirch, Germany; aerosol exposed area: 146 cm², deposition factor: 0.97), followed by nebulization of 250 μL of particle suspensions (1.25 mg mL⁻¹ in 0.3% NaCl) with subsequent aerosol sedimentation onto the cells with 3 min

as described by Lenz and colleagues (Lenz et al., 2014). Corning® Costar® Transwell® cell culture inserts (6-well, PET membrane with 3 μm pores) were also used to compare transepithelial translocation of particles with cells cultured on the BETA membrane under unstretched and stretched conditions. For stretch experiments, particles are delivered to the cells using the nebulizer integrated in the CIVIC as described above (Figures 1A,B, 4A) with a known delivery efficiency of 52% (Doryab et al., 2020). Subsequently, a physiologic cyclic mechanical stretch (10% linear at 0.33 Hz) corresponding to respiratory conditions during light exercise was applied to the cells for 2 h.

The fractional particle transport across the epithelial barrier was determined by quantitative fluorescence spectroscopy of the culture media in the basal compartment of both unstretched and stretched treatment using a plate reader (Safire2™, Tecan; excitation: 520 nm, emission: 540 nm). For normalization to the cell-delivered dose a standard curve of the particle suspension in cell culture medium basal medium volume prepared and measured for fluorescence intensity. For the measurement of quantitative cellular uptake of particles with CLSM, the samples were washed with PBS to remove free or weakly adsorbed particles from the apical side of the cell layer. Subsequently, the cells on the membranes were fixed in 4% paraformaldehyde for CLSM analysis. The CLSM images (z-stacks) were then recorded at five randomly selected fields of view for each sample ($n = 4$; region of interest: 134.95 × 134.95 μm) and quantified for cumulative fluorescence intensity of z-stacks.

Statistical Analysis

All data were analyzed using GraphPad Prism 8.4 (GraphPad Software, La Jolla, CA, USA). The details of each statistical analysis were presented in the caption of the figures.

DATA AVAILABILITY STATEMENT

The original contributions presented in the study are included in the article/Supplementary Material, further inquiries can be directed to the corresponding author/s.

AUTHOR CONTRIBUTIONS

AD and OS designed the experiments, analyzed the data, and wrote the manuscript. AD manufactured and characterized the BETA membrane and performed all the cell experiments and particle and particokinetic studies. AD, OS, and AS modified the CIVIC bioreactor systems. AD and PS performed SEM, FIB-SEM, and EDS-SEM. SO assisted AD with particle study of the Transwell® insert under static conditions. JG, MT, TS, AH, CV, AA, and MR provided the input to data interpretation in their respective field of expertise and contributed to the writing of the manuscript. All authors contributed to the article and approved the submitted version.

FUNDING

This study was partially funded by the Helmholtz Association (Impuls- und Vernetzungsfond, PoC-0033) and the Helmholtz Zentrum München, Germany.

SUPPLEMENTARY MATERIAL

The Supplementary Material for this article can be found online at: <https://www.frontiersin.org/articles/10.3389/fbioe.2021.616830/full#supplementary-material>

Supplementary Figure 1 | The Water Contact Angle (WCA) of the PDMS and BETA membranes using an automated contact angle system OCA20 with an image processing system (mean \pm SD).

Supplementary Figure 2 | SEM micrograph of bronchial epithelial 16HBE140⁻ cells grown on the membrane (cultured 6 days submerged and 24 h ALI culture). (Left) Confluent cell layer scale bar of overview and the magnified insert is 25 and 2 μ m, respectively. (Right) Pseudocolored cells (using the GNU Image Manipulation Program (GIMP 2.10.8) (<http://www.gimp.org/>), showing cracks between cells, which were induced due to dehydration of the samples for SEM. The scale bar is 10 μ m.

Supplementary Figure 3 | No significant effect of 2 h physiologic stretch and particle exposure (diameter: 100 and 1,000 nm) on cell viability (WST1 assay; A549 cells) was observed. The viability data were normalized by the corresponding value of the Transwell inserts (no stretch) (Data are reported as mean \pm SD. $n = 3$; Two-way ANOVA with Sidak test).

Supplementary Video 1 | BETA membrane motion in the CIVIC bioreactor system when a cyclic mechanical stretch (linear strain: 10%; breathing/stretch frequency: 0.33 Hz) is applied to the membrane.

REFERENCES

- Ainslie, G. R., Davis, M., Ewart, L., Lieberman, L. A., Rowlands, D. J., Thorley, A. J., et al. (2019). Microphysiological lung models to evaluate the safety of new pharmaceutical modalities: a biopharmaceutical perspective. *Lab Chip* 19, 3152–3161. doi: 10.1039/C9LC00492K
- Annika Mareike Gramatke, I. L. H. (2014). Size and cell type dependent uptake of silica nanoparticles. *J. Nanomed. Nanotechnol.* 5:6. doi: 10.4172/2157-7439.1000248
- Artzy-Schnirman, A., Lehr, C. M., and Sznitman, J. (2020). Advancing human *in vitro* pulmonary disease models in preclinical research: opportunities for lung-on-chips. *Expert Opin. Drug Deliv.* 17, 621–625. doi: 10.1080/17425247.2020.1738380
- Artzy-Schnirman, A., Zidan, H., Elias-Kirma, S., Ben-Porat, L., Tenenbaum-Katan, J., Carius, P., et al. (2019). Capturing the onset of bacterial pulmonary infection in acini-on-chips. *Adv. Biosyst.* 3:1900026. doi: 10.1002/adbi.201900026
- Bachler, G., Losert, S., Umehara, Y., von Goetz, N., Rodriguez-Lorenzo, L., Petri-Fink, A., et al. (2015). Translocation of gold nanoparticles across the lung epithelial tissue barrier: combining *in vitro* and *in silico* methods to substitute *in vivo* experiments. *Part. Fibre Toxicol.* 12:18. doi: 10.1186/s12989-015-0090-8
- Barosova, H., Maione, A. G., Septiadi, D., Sharma, M., Haeni, L., Balog, S., et al. (2020). Use of EpiAlveolar lung model to predict fibrotic potential of multiwalled carbon nanotubes. *ACS Nano* 14, 3941–3956. doi: 10.1021/acsnano.9b06860
- Benam, K. H., Dauth, S., Hassell, B., Herland, A., Jain, A., Jang, K.-J., et al. (2015). Engineered *in vitro* disease models. *Annu. Rev. Pathol. Mech. Dis.* 10, 195–262. doi: 10.1146/annurev-pathol-012414-040418
- Bou Jawde, S., Takahashi, A., Bates, J. H. T., and Suki, B. (2020). An analytical model for estimating alveolar wall elastic moduli from lung tissue uniaxial stress-strain curves. *Front. Physiol.* 11:121. doi: 10.3389/fphys.2020.00121
- Carter, S. D., Atif, A., Kaddekar, S., Lanekoff, I., Engqvist, H., Varghese, O. P., et al. (2020). PDMS leaching and its implications for on-chip studies focusing on bone regeneration applications. *Organs Chip* 2:100004. doi: 10.1016/j.ooc.2020.100004
- Cei, D., Doryab, A., Lenz, A., Schröppel, A., Mayer, P., Burgstaller, G., et al. (2020). Development of a dynamic *in vitro* stretch model of the alveolar interface with aerosol delivery. *Biotechnol. Bioeng.* 1–13. doi: 10.1002/bit.27600
- de Souza Carvalho, C., Daum, N., and Lehr, C.-M. (2014). Carrier interactions with the biological barriers of the lung: advanced *in vitro* models and challenges for pulmonary drug delivery. *Adv. Drug Deliv. Rev.* 75, 129–140. doi: 10.1016/j.addr.2014.05.014
- Ding, Y., Weindl, P., Lenz, A. G., Mayer, P., Krebs, T., and Schmid, O. (2020). Quartz crystal microbalances (QCM) are suitable for real-time dosimetry in nanotoxicological studies using VITROCELL® Cloud cell exposure systems. *Part. Fibre Toxicol.* 17, 1–20. doi: 10.1186/s12989-020-00376-w
- Doryab, A., Amoabediny, G., and Salehi-Najafabadi, A. (2016). Advances in pulmonary therapy and drug development: lung tissue engineering to lung-on-a-chip. *Biotechnol. Adv.* 34, 588–596. doi: 10.1016/j.biotechadv.2016.02.006
- Doryab, A., Tas, S., Taskin, M. B., Yang, L., Hilgendorff, A., Groll, J., et al. (2019). Evolution of bioengineered lung models: recent advances and challenges in tissue mimicry for studying the role of mechanical forces in cell biology. *Adv. Funct. Mater.* 29:1903114. doi: 10.1002/adfm.201903114
- Doryab, A., Taskin, M. B., Stahllhut, P., Schröppel, A., Wagner, D. E., Groll, J., et al. (2020). Stretch experiments with pulmonary epithelial cells at the air-liquid interface. *Adv. Funct. Mater.* 2004707. doi: 10.1002/adfm.202004707
- Edwards, Y. S., Sutherland, L. M., Power, J. H., Nicholas, T. E., and Murray, A. W. (1999). Cyclic stretch induces both apoptosis and secretion in rat alveolar type II cells. *FEBS Lett.* 448, 127–130. doi: 10.1016/S0014-5793(99)00357-9
- Ehrhardt, C., Kneuer, C., Fiegel, J., Hanes, J., Schaefer, U., Kim, K.-J., et al. (2002). Influence of apical fluid volume on the development of functional intercellular junctions in the human epithelial cell line 16HBE140⁻: implications for the use of this cell line as an *in vitro* model for bronchial drug absorption studies. *Cell Tissue Res.* 308, 391–400. doi: 10.1007/s00441-002-0548-5
- Ehrmann, S., Schmid, O., Darquenne, C., Rothen-Rutishauser, B., Sznitman, J., Yang, L., et al. (2020). Innovative preclinical models for pulmonary drug delivery research. *Expert Opin. Drug Deliv.* 17, 463–478. doi: 10.1080/17425247.2020.1730807
- Flory, A. L., Brass, D. A., and Shull, K. R. (2007). Deformation and adhesive contact of elastomeric membranes. *J. Polym. Sci. B Polym. Phys.* 45, 3361–3374. doi: 10.1002/polb.21322
- Foroozandeh, P., and Aziz, A. A. (2018). Insight into cellular uptake and intracellular trafficking of nanoparticles. *Nanoscale Res. Lett.* 13:339. doi: 10.1186/s11671-018-2728-6
- Guenat, O. T., and Berthiaume, F. (2018). Incorporating mechanical strain in organs-on-a-chip: lung and skin. *Biomicrofluidics* 12:042207. doi: 10.1063/1.5024895
- Hall, J. E. (2016). *Guyton and Hall Textbook of Medical Physiology, 13th Edn.* London: Elsevier.
- Hammerschmidt, S., Kuhn, H., Grasnick, T., Gessner, C., and Wirtz, H. (2004). Apoptosis and necrosis induced by cyclic mechanical stretching in alveolar type II cells. *Am. J. Respir. Cell Mol. Biol.* 30, 396–402. doi: 10.1165/rcmb.2003-0136OC
- Hänninen, O., Bröske-Hohfeld, I., Loh, M., Stoeger, T., Kreyling, W., Schmid, O., et al. (2010). Occupational and consumer risk estimates for nanoparticles emitted by laser printers. *J. Nanoparticle Res.* 12, 91–99. doi: 10.1007/s11051-009-9693-z
- Heydarian, M., Yang, T., Schweinlin, M., Steinke, M., Walles, H., Rudel, T., et al. (2019). Biomimetic human tissue model for long-term study of neisseria gonorrhoeae infection. *Front. Microbiol.* 10:1740. doi: 10.3389/fmicb.2019.01740
- Higueta-Castro, N., Nelson, M. T., Shukla, V., Agudelo-Garcia, P. A., Zhang, W., Duarte-Sanmiguel, S. M., et al. (2017). Using a novel microfabricated model of the alveolar-capillary barrier to investigate the effect of matrix structure on atelectrauma. *Sci. Rep.* 7:11623. doi: 10.1038/s41598-017-12044-9
- Huh, D., Kim, H. J., Fraser, J. P., Shea, D. E., Khan, M., Bahinski, A., et al. (2013). Microfabrication of human

- organs-on-chips. *Nat. Protoc.* 8, 2135–2157. doi: 10.1038/nprot.2013.137
- Huh, D., Matthews, B. D., Mammoto, A., Montoya-Zavala, M., Hsin, H. Y., and Ingber, D. E. (2010). Reconstituting organ-level lung functions on a chip. *Science* 328, 1662–1668. doi: 10.1126/science.1188302
- Huh, D., Torisawa, Y., Hamilton, G. a., Kim, H. J., and Ingber, D. E. (2012). Microengineered physiological biomimicry: organs-on-chips. *Lab Chip* 12:2156. doi: 10.1039/c2lc40089h
- ICRP (1994). Human respiratory tract model for radiological protection. A report of a Task Group of the International Commission on Radiological Protection. *Ann. ICRP* 24, 1–482.
- Kreyling, W. G., Hirn, S., Möller, W., Schleh, C., Wenk, A., Celik, G., et al. (2014). Air–blood barrier translocation of tracheally instilled gold nanoparticles inversely depends on particle size. *ACS Nano* 8, 222–233. doi: 10.1021/nn403256v
- Kreyling, W. G., Semmler-Behnke, M., Takenaka, S., and Möller, W. (2013). Differences in the biokinetics of inhaled nano- versus micrometer-sized particles. *Acc. Chem. Res.* 46, 714–722. doi: 10.1021/ar300043r
- Kuehn, A., Kletting, S., de Souza Carvalho-Wodarz, C., Repnik, U., Griffiths, G., Fischer, U., et al. (2016). Human alveolar epithelial cells expressing tight junctions to model the air–blood barrier. *ALTEX* 33, 1–20. doi: 10.14573/altex.1511131
- Lehmann, A. D., Daum, N., Bur, M., Lehr, C. M., Gehr, P., and Rothen-Rutishauser, B. M. (2011). An *in vitro* triple cell co-culture model with primary cells mimicking the human alveolar epithelial barrier. *Eur. J. Pharm. Biopharm.* 77, 398–406. doi: 10.1016/j.ejpb.2010.10.014
- Lenz, A. G., Stoeger, T., Cei, D., Schmidmeir, M., Semren, N., Burgstaller, G., et al. (2014). Efficient bioactive delivery of aerosolized drugs to human pulmonary epithelial cells cultured in air–liquid interface conditions. *Am. J. Respir. Cell Mol. Biol.* 51, 526–535. doi: 10.1165/rcmb.2013-0479OC
- Meindl, C., Stranzinger, S., Dzidic, N., Salar-Behzadi, S., Mohr, S., Zimmer, A., et al. (2015). Permeation of therapeutic drugs in different formulations across the airway epithelium *in vitro*. *PLoS ONE* 10:e0135690. doi: 10.1371/journal.pone.0135690
- Nishiguchi, A., Singh, S., Wessling, M., Kirkpatrick, C. J., and Möller, M. (2017). Basement membrane mimics of biofunctionalized nanofibers for a bipolar-cultured human primary alveolar-capillary barrier model. *Biomacromolecules* 18, 719–727. doi: 10.1021/acs.biomac.6b01509
- Paur, H.-R., Cassee, F. R., Teeguarden, J., Fissan, H., Diabate, S., Aufderheide, M., et al. (2011). *In-vitro* cell exposure studies for the assessment of nanoparticle toxicity in the lung—a dialog between aerosol science and biology. *J. Aerosol Sci.* 42, 668–692. doi: 10.1016/j.jaerosci.2011.06.005
- Peters, A., Wichmann, H. E., Tuch, T., Heinrich, J., and Heyder, J. (1997). Respiratory effects are associated with the number of ultrafine particles. *Am. J. Respir. Crit. Care Med.* 155, 1376–1383. doi: 10.1164/ajrccm.155.4.9105082
- Polio, S. R., Kundu, A. N., Dougan, C. E., Birch, N. P., Aurian-Blajeni, D. E., Schiffman, J. D., et al. (2018). Cross-platform mechanical characterization of lung tissue. *PLoS ONE* 13:e0204765. doi: 10.1371/journal.pone.0204765
- Pope, C. A., Ezzati, M., and Dockery, D. W. (2009). Fine-particulate air pollution and life expectancy in the United States. *N. Engl. J. Med.* 360, 376–386. doi: 10.1056/NEJMsa0805646
- Regehr, K. J., Domenech, M., Koepsel, J. T., Carver, K. C., Ellison-Zelski, S. J., Murphy, W. L., et al. (2009). Biological implications of polydimethylsiloxane-based microfluidic cell culture. *Lab Chip* 9:2132. doi: 10.1039/b903043c
- Rothen-Rutishauser, B. M., Schürch, S., Haenni, B., Kapp, N., and Gehr, P. (2006). Interaction of fine particles and nanoparticles with red blood cells visualized with advanced microscopic techniques. *Environ. Sci. Technol.* 40, 4353–4359. doi: 10.1021/es0522635
- Schaumann, F., Frömke, C., Dijkstra, D., Alessandrini, F., Windt, H., Karg, E., et al. (2014). Effects of ultrafine particles on the allergic inflammation in the lung of asthmatics: results of a double-blinded randomized crossover clinical pilot study. *Part. Fibre Toxicol.* 11:39. doi: 10.1186/s12989-014-0039-3
- Schmid, O., and Cassee, F. R. (2017). On the pivotal role of dose for particle toxicology and risk assessment: exposure is a poor surrogate for delivered dose. *Part. Fibre Toxicol.* 14:52. doi: 10.1186/s12989-017-0233-1
- Schmid, O., Jud, C., Umehara, Y., Mueller, D., Bucholski, A., Gruber, F., et al. (2017). Biokinetics of aerosolized liposomal cyclosporin a in human lung cells *in vitro* using an air–liquid cell interface exposure system. *J. Aerosol Med. Pulm. Drug Deliv.* 30, 411–424. doi: 10.1089/jamp.2016.1361
- Schmid, O., and Stoeger, T. (2016). Surface area is the biologically most effective dose metric for acute nanoparticle toxicity in the lung. *J. Aerosol Sci.* 99, 133–143. doi: 10.1016/j.jaerosci.2015.12.006
- Stucki, A. O., Stucki, J. D., Hall, S. R. R., Felder, M., Mermoud, Y., Schmid, R. A., et al. (2015). A lung-on-a-chip array with an integrated bio-inspired respiration mechanism. *Lab Chip* 15, 1302–1310. doi: 10.1039/C4LC01252F
- Takenaka, S., Möller, W., Semmler-Behnke, M., Karg, E., Wenk, A., Schmid, O., et al. (2012). Efficient internalization and intracellular translocation of inhaled gold nanoparticles in rat alveolar macrophages. *Nanomedicine* 7, 855–865. doi: 10.2217/nnm.11.152
- Teeguarden, J. G., Hinderliter, P. M., Orr, G., Thrall, B. D., and Pounds, J. G. (2007). Particokinetics *in vitro*: dosimetry considerations for *in vitro* nanoparticle toxicity assessments. *Toxicol. Sci.* 95, 300–312. doi: 10.1093/toxsci/kfl165
- Tenenbaum-Katan, J., Artzy-Schnirman, A., Fishler, R., Korin, N., and Sznitman, J. (2018). Biomimetics of the pulmonary environment *in vitro*: a microfluidics perspective. *Biomicrofluidics* 12:042209. doi: 10.1063/1.5023034
- Vlahakis, N. E., Schroeder, M. A., Limper, A. H., and Hubmayr, R. D. (1999). Stretch induces cytokine release by alveolar epithelial cells *in vitro*. *Am. J. Physiol. Cell. Mol. Physiol.* 277, L167–L173. doi: 10.1152/ajplung.1999.277.1.L167
- Wang, L., Sun, B., Ziemer, K. S., Barabino, G. A., and Carrier, R. L. (2010). Chemical and physical modifications to poly(dimethylsiloxane) surfaces affect adhesion of Caco-2 cells. *J. Biomed. Mater. Res. A* 93, 1260–1271. doi: 10.1002/jbm.a.32621
- Wang, Z., Volinsky, A. A., and Gallant, N. D. (2014). Crosslinking effect on polydimethylsiloxane elastic modulus measured by custom-built compression instrument. *J. Appl. Polym. Sci.* 131:41050. doi: 10.1002/app.41050
- Weibel, E. R. (1970). Morphometric estimation of pulmonary diffusion capacity. *Respir. Physiol.* 11, 54–75. doi: 10.1016/0034-5687(70)90102-7
- Weibel, E. R. (2009). What makes a good lung? *Swiss Med. Wkly.* 139, 375–86. doi: 10.4414/smw.2009.12270
- Winnik, F. M., and Maysinger, D. (2013). Quantum dot cytotoxicity and ways to reduce it. *Acc. Chem. Res.* 46, 672–680. doi: 10.1021/ar3000585
- Young, B. M., Shankar, K., Allen, B. P., Pouliot, R. A., Schneck, M. B., Mikhalei, N. S., et al. (2017). Electrospun decellularized lung matrix scaffold for airway smooth muscle culture. *ACS Biomater. Sci. Eng.* 3, 3480–3492. doi: 10.1021/acsbomaterials.7b00384
- Zhu, M., Nie, G., Meng, H., Xia, T., Nel, A., and Zhao, Y. (2013). Physicochemical properties determine nanomaterial cellular uptake, transport, and fate. *Acc. Chem. Res.* 46, 622–631. doi: 10.1021/ar300031y

Conflict of Interest: OS declares that the aerosol-cell delivery methods described here are patent-protected and made commercially available by VITROCELL Systems under a license agreement with the Helmholtz Zentrum München.

The remaining authors declare that the research was conducted in the absence of any commercial or financial relationships that could be construed as a potential conflict of interest.

Copyright © 2021 Doryab, Taskin, Stahlhut, Schröppel, Orak, Voss, Ahluwalia, Rehberg, Hilgendorff, Stöger, Groll and Schmid. This is an open-access article distributed under the terms of the Creative Commons Attribution License (CC BY). The use, distribution or reproduction in other forums is permitted, provided the original author(s) and the copyright owner(s) are credited and that the original publication in this journal is cited, in accordance with accepted academic practice. No use, distribution or reproduction is permitted which does not comply with these terms.

Supporting Information

Figure S1. The Water Contact Angle (WCA) of the PDMS and BETA membranes using an automated contact angle system OCA20 with an image processing system (mean \pm SD).

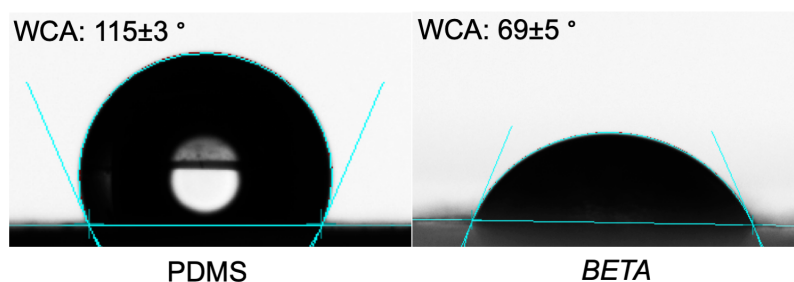


Figure S2. SEM micrograph of bronchial epithelial 16HBE14o- cells grown on the membrane (cultured 6 days submerged and 24 h ALI culture). Left: Confluent cell layer scale bar of overview and the magnified insert is 25 μ m and 2 μ m, respectively. Right: Pseudocolored cells (using the GNU Image Manipulation Program (GIMP 2.10.8) (<http://www.gimp.org/>), showing cracks between cells, which were induced due to dehydration of the samples for SEM. The scale bar is 10 μ m.

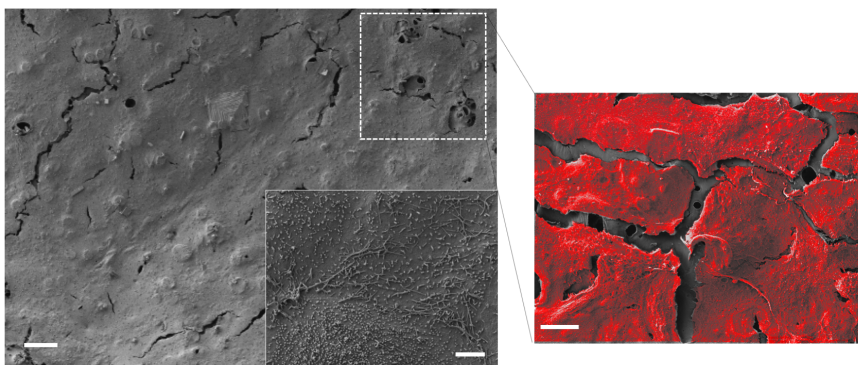
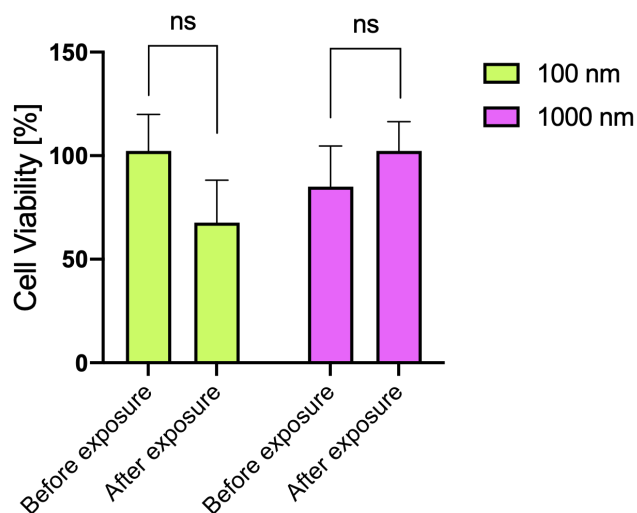


Figure S3. No significant effect of 2 h physiologic stretch and particle exposure (diameter: 100 nm and 1000 nm) on cell viability (WST1 assay; A549 cells) was observed. The viability data were normalized by the corresponding value of the Transwell inserts (no stretch). (Data are reported as mean \pm SD. $n=3$; Two-way ANOVA with Sidak test).



Supplementary Movie 1. BETA membrane motion in the CIVIC bioreactor system when a cyclic mechanical stretch (linear strain: 10%; breathing/stretch frequency: 0.33 Hz) is applied to the membrane.

5. Paper III




Received: 29 June 2020 | Revised: 1 October 2020 | Accepted: 9 October 2020

DOI: 10.1002/bit.27600

ARTICLE

BIOTECHNOLOGY
BIOENGINEERING WILEY

Development of a dynamic in vitro stretch model of the alveolar interface with aerosol delivery

Daniele Cei^{1,2,3} | Ali Doryab^{3,4}  | Anke-Gabriele Lenz^{3,4} | Andreas Schröppel^{3,4} | Paula Mayer^{3,4} | Gerald Burgstaller^{3,4} | Roberta Nossa^{1,2} | Arti Ahluwalia^{1,2}  | Otmar Schmid^{3,4} 

¹Research Center "E. Piaggio", University of Pisa, Pisa, Italy

²Department of Information Engineering, University of Pisa, Pisa, Italy

³Comprehensive Pneumology Center, Member of the German Center for Lung Research (DZL), Munich, Germany

⁴Institute of Lung Biology and Disease, Helmholtz Zentrum Muenchen, Neuherberg, Germany

Correspondence

Arti Ahluwalia, Research Center "E. Piaggio," University of Pisa, Largo Lucio Lazzarino 2, 56126 Pisa, Italy.

Email: arti.ahluwalia@ing.unipi.it

Otmar Schmid, Helmholtz Zentrum Muenchen, Institute of Lung Biology and Disease, Ingolstaedter Landstrasse 1, D-85764 Neuherberg, Germany.

Email: otmar.schmid@helmholtz-muenchen.de

Abstract

We describe the engineering design, computational modeling, and empirical performance of a moving air–liquid interface (MALI) bioreactor for the study of aerosol deposition on cells cultured on an elastic, porous membrane which mimics both air–liquid interface exposure conditions and mechanoelastic motion of lung tissue during breathing. The device consists of two chambers separated by a cell layer cultured on a porous, flexible membrane. The lower (basolateral) chamber is perfused with cell culture medium simulating blood circulation. The upper (apical) chamber representing the air compartment of the lung is interfaced to an aerosol generator and a pressure actuation system. By cycling the pressure in the apical chamber between 0 and 7 kPa, the membrane can mimic the periodic mechanical strain of the alveolar wall. Focusing on the engineering aspects of the system, we show that membrane strain can be monitored by measuring changes in pressure resulting from the movement of media in the basolateral chamber. Moreover, liquid aerosol deposition at a high dose delivery rate ($>1 \mu\text{l cm}^{-2} \text{min}^{-1}$) is highly efficient (ca. 51.5%) and can be accurately modeled using finite element methods. Finally, we show that lung epithelial cells can be mechanically stimulated under air–liquid interface and stretch-conditions without loss of viability. The MALI bioreactor could be used to study the effects of aerosol on alveolar cells cultured at the air–liquid interface in a biodynamic environment or for toxicological or therapeutic applications.

KEYWORDS

aerosol exposure, air–liquid interface, bioreactor, flexing membrane

1 | INTRODUCTION

During the past decade, the development of bioreactors and microfluidic systems (organ-on-chip) for organotypic in vitro models has been a dynamic field of research with the vision of reducing or even replacing in vivo animal studies in drug development and risk

assessment. One of the keys to success is the establishment of biomimetic culture and exposure conditions, which is expected to enhance the capacity of in vitro models to predict outcomes for human health.

The lung is one of the most challenging organs for in vitro modeling since it is not only perfused by blood, but also in direct

Daniele Cei and Ali Doryab share first authorship; Arti Ahluwalia and Otmar Schmid share senior authorship.

contact with ambient air. Inhalation of gaseous toxins, viruses, and dispersed particles (aerosols) may cause inflammation and stress, contributing to the development or exacerbation of diseases such as asthma or chronic obstructive pulmonary disease (Hänninen et al., 2010; Peters et al., 1997). The smallest, ultrafine, or nano-sized particles (less than 100–300 nm in diameter) are especially under intense scrutiny due to their enhanced surface area (per unit mass), which has been associated with the prevalence of acute and chronic lung disease (Peters et al., 1997; Schmid & Stoeger, 2017), and their enhanced probability of translocation from the lung to blood circulation and from there to almost all secondary organs such as liver, brain, and even placenta (Kreyling et al., 2013). On the other hand, inhalation of medical aerosol has a long-standing history in the treatment of lung diseases (Stein & Thiel, 2017).

Upon deposition of the aerosol onto the lung epithelium, the soluble fraction of the aerosol is quickly diluted by bodily fluids, while the nonsoluble particles remain on the epithelium. The subsequent interaction of (nonsoluble) particles with the pulmonary epithelium is a complex process, mediated by the breathing-induced rhythmical contraction of the diaphragm, which generates a periodic change in alveolar volume accompanied by stretching and relaxation of the alveolar walls. How this movement contributes to biokinetics and cellular uptake of particles within and beyond the alveolar tissue, or to downstream inflammatory processes is not clearly understood, partly because of the lack of appropriate models which can recapitulate the dynamic alveolar microenvironment (Min et al., 2013; Roan & Waters, 2011).

In vivo studies on the effects of inhaled aerosols are traditionally performed on animal models (Nahar et al., 2013; Sakagami, 2006). While animal models capture the general effects on a peripheral tissue, the whole lung, and the entire organism, biomimetic in vitro testing with human cells accounts for human-specific responses to stimuli and in-depth analysis of cell/tissue-specific response pathways.

However, the predictive power of in vitro test systems for clinical conditions in humans is expected to depend on their biomimetic qualities, that is, their ability to adequately model the most biologically relevant features of the in vivo conditions (Darquenne et al., 2016). To this end, several alternative methods for mimicking the lung epithelial barrier have been developed. Perhaps the best known is the air–liquid interface (ALI) barrier model, based on a static culture of lung-derived cells grown on a permeable membrane with the apical side of the cells in contact with air and the basolateral side is wetted by the medium. ALI pulmonary epithelial cells polarize, that is, the air-side is structured differently than the medium side resembling the in vivo conditions in various aspects including cilia-formation, the formation of tight cell–cell contacts as well as secretion of lung lining fluid (Paur et al., 2011). Nevertheless, growing pulmonary cells on a static membrane at the ALI does not mimic the periodic mechanical strain experienced by alveolar cells under in vivo conditions due to breathing, which may affect the cellular response to toxins or therapeutics (Cavanaugh et al., 2006; Min et al., 2013; Savla et al., 1997; Schmekel et al., 1992).

ALI cultures also allow for direct deposition of aerosols onto epithelial cells mimicking the humid pulmonary environment in vivo. The currently available technologies for aerosol-cell deposition can be classified according to their employed deposition mechanisms (Paur et al., 2011), namely diffusion and/or sedimentation (Bitterle et al., 2006), impaction (Schreier et al., 1998), electrostatic precipitation (Savi et al., 2008), thermophoretic deposition (Broßell et al., 2013), gravitational settling (Hein et al., 2010), and cloud motion (Lenz et al., 2014). Although many of these devices (except for thermophoretic deposition), are commercially available, to the best of our knowledge no aerosol delivery system has yet been reported for studies on cell systems encountering cyclic stretch (Doryab et al., 2019), which has been shown to substantially alter cell physiology in terms of secretion of alveolar surfactant, metabolic activity, and cytotoxicity for human alveolar epithelial cells (Huh et al., 2010). To address the issue of cyclic stretch, more advanced in vitro cell models have been developed and have been systematically reviewed by Doryab et al. (2019). Most devices apply pneumatic or motor-driven cyclic stretch in liquid–liquid conditions (Campillo et al., 2016). The FlexCell Culture System® (Flexcell International Corp.) is one such commercial device with a mechanically active substrate: Epithelial cells are cultured on a silicone membrane and stretched by applying negative differential pressure on the other side of the membrane. However, due to the mechanism of actuation, the membrane cannot be porous and thus cannot provide ALI conditions. A number of ALI systems have been developed such as the well-based system with moving walls reported by Choe et al. (2006) and Tomei et al. (2008), but they do not allow for fluid flow or aerosol deposition. One of the most cited cell-stretch models is the micro-scaled lung-on-a-chip developed by the WYSS Institute combines ALI conditions, and a stretchable silicone membrane and medium flow (Huh et al., 2010). The two-channel system also employs negative pressure actuation, but in a different configuration than the FlexCell device: the rectangular membrane is attached to a flexible frame on the two shorter sides. Upon mechanical activation of the frame by the application of a vacuum, the membrane stretches. Stucki et al. (2015) reported a lung on a chip system with a two-chamber configuration separated by a flexible membrane; the basal chamber also has a flexible bottom which is actuated by the application of pressure. Both of these chip devices allow for perforation of the membrane and hence for ALI cell culture conditions but neither are amenable to effective and reproducible aerosol-cell delivery which are necessary for quantitative aerosol dose-cell response studies. Moreover, the handling of the peripheral microfluidic technology for maintenance of adequate cell culture conditions can be a challenge which is acknowledged by researchers developing lung-on-a-chip devices (Artzy-Schnirman et al., 2019; Doryab et al., 2016; Ehrmann et al., 2020). Here we report the engineering of a moving air–liquid interface (MALI), bioreactor as an enabling tool for studies on pulmonary cells and tissues in physiological and pathological conditions. The bioreactor consists of an apical and basolateral compartment separated by a pressure-actuated flexible membrane. Designed on the scale of a standard six-well Transwell, the bioreactor's basolateral compartment contains

cell culture medium, which flows through the bioreactor mimicking blood circulation while the apical side is interfaced with a nebulizer for efficient, dose-controlled aerosol delivery to cells. MALI's performance was investigated in terms of cyclic membrane stretch and aerosol delivery characteristics. An evaluation of the cytocompatibility of the system components was performed assessing the effect of physiologic cyclic stretch on A549 lung epithelial cells.

2 | DESIGN OF THE MALI SYSTEM

2.1 | The overall design and working principle

At the heart of the MALI system is the modular MALI bioreactor, similar to that described in Mazzei et al. (2010) and Giusti et al. (2013). The bioreactor with its two chambers and their respective hydraulic and pneumatic circuits is depicted in Figure 1a. Between the two chambers is a flexible porous membrane for cell culture which mimics the alveolar air–tissue interface. A peristaltic pump drives medium through the basolateral chamber modeling the blood side and providing a continuous nutrient supply to the cell layer as well as the removal of metabolites and signaling molecules which may also be delivered to other bioreactors with cells or tissues from other organs (e.g., liver). The apical chamber simulates the air-facing side of the alveolar barrier and includes a pair of electropneumatic regulators and a clinically relevant aerosol generator. The latter provides dose-controlled aerosolized substance delivery to the cells simulating drug delivery during inhalation therapy or exposure to airborne particles.

The membrane is actuated by cyclic switching of two pressure regulators, which allow oscillation of air pressure in the apical chamber between ambient and a few kPa above ambient pressure. This in turn leads to a periodic downward deflection and relaxation of the membrane simulating the inhalation and exhalation phase during respiration. Figure 1b shows the complete MALI system which is described in detail herein. The system was designed to recapitulate the cyclic stretch of the alveoli during breathing, covering both physiological and pathological levels of strain (physiological: 4%–12% linear strain[†], pathological up to 20% linear strain) at a typical breathing frequency of 0.2 Hz (Huh et al., 2010; Patel, 2011; Ren et al., 2009; Roan & Waters, 2011; Vlahakis et al., 1999; Waters et al., 2012).

2.2 | Finite element method modeling of the MALI bioreactor

The MALI bioreactor's design and performance were simulated using finite element methods (FEMs). A first model of the basolateral chamber was used to optimize its dimensions by evaluating the displacement field of the membrane at different bioreactor heights and

different pressures applied apically to the elastic membrane (described in Section 3). A second FEM model was used to estimate the deposition of aerosol on the membrane in the apical chamber both in terms of total dose and spatial distribution.

2.3 | FEM model of the basolateral chamber including membrane activation

The basolateral chamber model was generated using the fluid-structure interaction (FSI) module of the Comsol Multiphysics 4.3a software (COMSOL AB). The domain consists of a cylindrical chamber with variable height and an inlet and outlet for cell culture media (Figure S1), while the membrane is modeled as a deformable disk (with the same elastic modulus as the membrane used for cell culture, see Section 3) placed on top of the basolateral chamber of the bioreactor and subject to a variable positive pressure from the top simulating air pressure in the apical chamber. A sequence of quasi-static conditions is used to simulate the stretching motion of the membrane. In particular, the steady-state condition for constant apical pressure is modeled for a range of pressures covering that applied during dynamic activation of the membrane. Viscous drag and fluid pressure on the membrane resulting from the flow of medium is also accounted for. The fluid dynamics were solved in the laminar flow regime for an inflow of 0.4 ml min^{-1} as suggested by Mazzei et al. (2010). No-slip conditions were assumed at all interfaces including the virtual wall representing the membrane, which was also coupled with the FSI module to account for its displacement.

The model was solved for different bioreactor heights ($H = 10\text{--}20 \text{ mm}$, 1-mm increments) and various apical differential pressures across the membrane (1–10 kPa, 1-kPa increments). The optimum height is the best compromise between a small chamber volume (i.e., low height, yet sufficient to allow obstruction-free membrane stretching) and low applied pressure to achieve a given membrane deformation. In fact, the larger the chamber, the lower the flow resistance when the medium is squeezed out of the chamber by membrane motion. To simulate pathological strains (20%), the maximum vertical displacement of the center of the membrane in the z-direction required during the operation was estimated as $\approx 7 \text{ mm}$. A total chamber height of 14 mm was considered the best compromise to allow unencumbered displacement of the membrane with low-pressure values (maximum 7 kPa in the model) while maintaining a chamber with a volume reasonably close to that of a typical cell culture well. An example of membrane displacement is shown in Figure 2a, while videos of the model can be downloaded from the Supporting Information.

2.4 | FEM modeling of the apical chamber including aerosol deposition

To guarantee dose-controlled aerosol delivery, we based the dimensions of the apical chamber on that of the ALICE Cloud device reported in Lenz et al. (2009). The patented technology takes

[†]The term "linear strain", when applied to alveolar distension, refers to a change in alveolar radius as described in the Supporting Information, Section H.

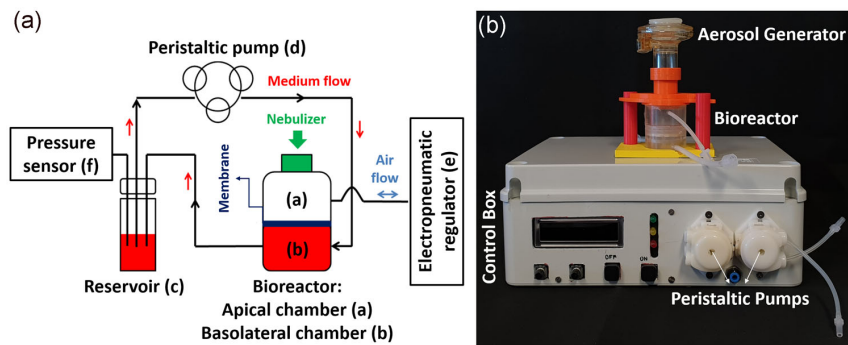


FIGURE 1 Setup and components of the moving air-liquid interface (MALI) system: (a) Schematic of the MALI system (without electronics) consisting of the bioreactor (here referred to as MALI bioreactor) with a basolateral (a) and an apical (b) chamber separated by a flexing porous membrane. The fluidic circuit for the cell culture medium comprises a chamber (a), a media reservoir (c), and a pump (d). Compressed air (e) for pressure actuation of the stretchable membrane is driven through the upper circuit. A pressure sensor (f) is used to evaluate membrane deflection in real-time. The top of the bioreactor is fitted with an aerosol inlet tube for the positioning of a nebulizer above the membrane. (b) Photo of the entire MALI system [Color figure can be viewed at wileyonlinelibrary.com]

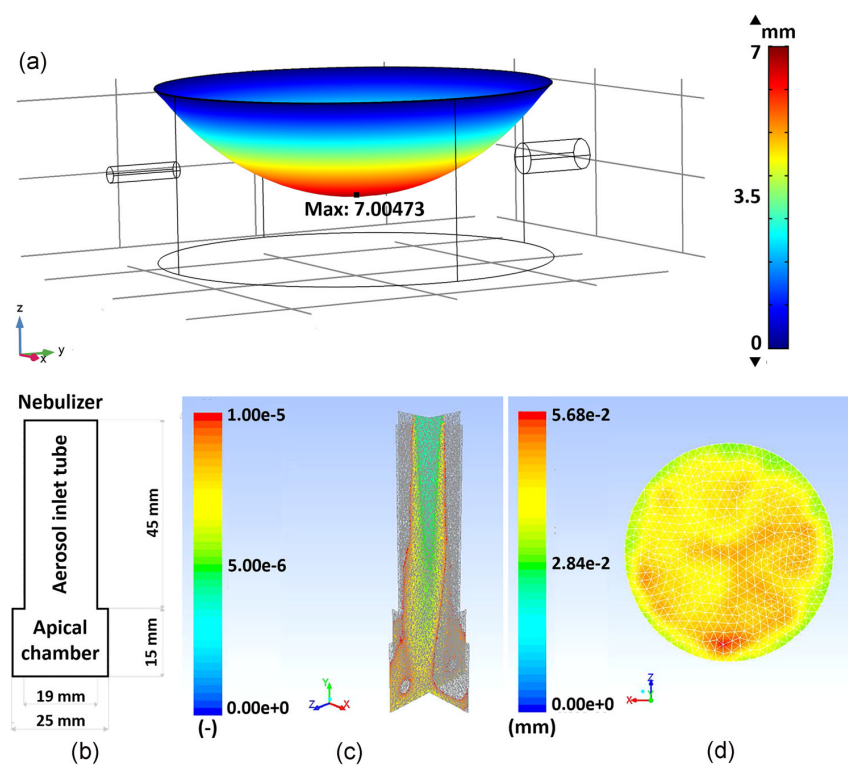


FIGURE 2 Finite element method models: (a) Model of the stretchable Bionate® membrane showing three-dimension membrane displacement surface plot for a basolateral chamber of height 14 mm with an applied apical pressure of 7 kPa. Example of CFD analysis of cloud settling: (b) Lateral view of the apical compartment of the bioreactor and the nebulizer tube representing the relevant domain for aerosol delivery to the membrane, which is located at the bottom of the domain. (c) Volume fraction of water in aerosol cloud at 0.4 s after activation of the nebulizer; (d) Thickness in mm and spatial distribution of deposited aerosol (liquid film) on the membrane 5 min after the start of the nebulization [Color figure can be viewed at wileyonlinelibrary.com]

advantage of the generation of a cloud which is more efficient for aerosol deposition onto cells in ALI conditions with respect to single droplet dynamics. The main technical refinement of the aerosol unit of the MALI bioreactor relates to the use of a cylindrical aerosol exposure chamber with a cross-sectional area just large enough to expose the ca. 5-cm² membrane in the bioreactor as compared to the relatively large cubical exposure chamber of the ALICE Cloud system (ca. 125 cm²), which was designed for simultaneous exposure of up to six 6-well Transwell inserts (Lenz et al., 2014). The FEM model of the apical chamber was developed to evaluate aerosol-cloud deposition on the membrane. As the geometry is axially symmetric (Figure 2b) it was solved with a two-dimension (2D) model.

Typically, the nebulizer is filled with 10 µl of an aqueous solution. It emits a dense cloud of aerosol with a speed of about 2.5 m/s directly into the aerosol inlet tube which leads into the apical chamber (Figure 2b). Using the computational fluid dynamics software Fluent 14.0 (Ansys Inc.), cloud motion in the air-filled chamber was modeled with the Eulerian Multiphase module (here two phases: air and cloud), where the dense cloud (i.e., droplet suspension) is treated as a secondary fluid interacting with the primary fluid (air). Each fluid phase was solved with the Eulerian discretization method and their interaction was taken into account assuming no slip at the boundaries of the domain. Input parameters for the model are reported in the Supporting Information.

As the Eulerian-Eulerian method is not able to evaluate particle deposition onto surfaces due to the two-phase approach taken, an Eulerian Wall Film module was added to the model. Here, the interaction between the fluid phase and wall surface is considered to evaluate film formation due to particle settling. Continuity and momentum equations were modified to evaluate deposition effects due to liquid-wall collision under the influence of inertial impaction and gravitational settling. A user-defined function (UDF) was compiled to simulate the accumulation of liquid on the bottom of the apical chamber where the membrane is located. The UDF generates a negative source term (sink) extracting the part of the fluid that collides with the membrane and considers it as “collected” from the liquid phase.

As seen from Figure 2c and the Supporting Information Videos, the modeled cloud velocity profile at the beginning of the aerosol exposure (0.4 s after activation of the nebulizer) propagates through the center of the tube and deposits at the base and sides of the apical chamber. Figure 2d depicts the spatial uniformity of the aerosol deposited on the membrane at the end of the exposure. The result indicates uniform aerosol deposition over the entire cell-covered area except for a narrow region at the rim. An analysis of the deposition efficiency reveals that 85% (asymptotic value) of the liquid settles on the membrane within 5 min.

3 | MATERIALS AND EXPERIMENTAL METHODS

The design, construction, and testing of the main components of the MALI system are described here, with further technical details reported in the Supporting Information.

3.1 | Membrane fabrication and characterization

Electrospun Bionate® II 80A (The Electrospinning Company) was used as a flexing membrane and porous support for epithelial cells. Bionate is a biocompatible poly(carbonate)urethane copolymer used in chronically implanted devices (i.e., pacemaker leads, ventricular assist devices, catheters, hip/knee joints, etc.; Bélanger et al., 2000; Khan et al., 2005; Zdrahala & Zdrahala, 1999). According to the manufacturer's specifications, the membranes are 75.4 ± 6.6 -µm thick (Lehmann et al., 2011), with a fibre diameter of 3.06 ± 0.36 µm. These parameters are consistent with our measurements from confocal microscopy.

The mechanical properties of the Bionate membranes were evaluated for assessing their suitability as a stretchable support for alveolar cell culture systems. First, the elastic modulus was evaluated using a twin column testing machine (Z005; Zwick-Roell) equipped with a high precision load cell (loading 10 N, resolution 20 mN) under dry conditions, with a uniaxial strain rate of $0.1\% s^{-1}$. Rectangular samples were stretched up to 30% of their initial length in order to determine the extent of the elastic region. The Bionate membrane was also soaked for 0, 1, 2, 4, and 7 days in culture media (Dulbecco's modified Eagle's medium [DMEM], see Section 3 and Supporting Information E) at 37°C and the mechanical tests were repeated for evaluation of fatigue effects while submerged in DMEM at 37°C. In addition, cyclic deformation was applied for 3 h at a strain corresponding to normal breathing conditions (5% strain, 0.2 Hz, 37°C in DMEM). The elastic modulus was evaluated at different time points (1, 2, 4, and 24 h) through the least-squares linear fitting of the uniaxial stress-strain curve.

3.2 | Fabrication of MALI bioreactor

Both chambers of the MALI bioreactor are fabricated from polydimethylsiloxane (PDMS; Sylgard 184 Kit; Mascherpa), using millimolding as described in Vozzi et al. (2011). The Bionate membrane is clamped between two 3D-printed polylactide acid (PLA) rings designed with a press-and-click male-female coupling as shown in Figure S3c. Once assembled in the ring, the membrane can be easily handled without touching or damaging. The PLA ring with the membrane is lodged in a PDMS hoop and inserted between the apical and basolateral chambers (see Figure S3b).

3.3 | Fluidic system and membrane displacement

The basolateral chamber is perfused with media through a peristaltic pump and a fluid reservoir. When positive pressure is applied in the apical chamber, the actuation of the membrane results in the displacement of some of the basolateral medium into the media reservoir (Figure 1a). As the reservoir is airtight, any change in medium volume will result in a change of air pressure in the vessel, which is directly related to the displaced medium volume according

to the general gas law or by performing a simple pressure–volume calibration. Assuming that no liquid passes through the membrane (which is the case here) and that the membrane actuation results in a hemispherical deformation of the membrane, the displaced medium volume can be related to the linear strain exerted on the deformed membrane through classical equations of thin shell mechanics (see Supporting Information). Hence, by monitoring the differential air pressure in the medium reservoir during the application of cyclic overpressure in the apical chamber, the membrane strain can be monitored in real-time. Further details on the components of the fluidic and control system are reported in the Supporting Information.

3.4 | Aerosol delivery system and aerosol dosimetry

The apical compartment consists of three parts (Figures 1 and 2a): the cylindrical apical chamber, a vibrating mesh nebulizer (Aeroneb Pro/Lab; Aerogen Inc.) positioned axially above the stretchable membrane and a cylindrical aerosol tube connecting both elements (Barapatre et al., 2015; Lenz et al., 2014). Membrane actuation is interrupted during the operation of the nebulizer and subsequent aerosol settling, which typically takes less than a couple of minutes (for 10 μ l of nebulized liquid).

Measurements of aerosol dose and distribution on the membrane were performed with quantitative spectrophotometry and a fluorescence imaging system, respectively (Barapatre et al., 2015; Lenz et al., 2014). For dosimetry analysis, the nebulizer was loaded with 10 μ l of a 15 μ g/ml fluorescein sodium salt solution in phosphate-buffered saline (Sigma-Aldrich Chemie GmbH) and attached to MALI bioreactor, replacing the membrane with a glass slide to facilitate retrieval of the deposited fluorescein. After the experiment, the glass slide was carefully rinsed with 500 μ l water and the fluorescein concentration in the retrieved solution was measured using a microplate fluorescence reader (Safire II; Tecan Inc.; excitation/emission = 483/525 nm). The aerosol delivery efficiency was determined by normalizing the measured dose to the amount of liquid nebulized. Using this technique, the retrieval efficiency was determined to be 100% (within experimental uncertainties; data not shown).

For assessment of spatial uniformity of aerosol deposition on the cells, 10 μ l of an aqueous suspension (0.05% wt/vol) of fluorescent polystyrene nanoparticles (SkyBlue; Kisker Biotech GmbH & CoKG; particle diameter: 450 nm, excitation/emission = 680/720 nm) was nebulized in MALI. Again, nanoparticles were deposited on a glass slide located at the position of the membrane and the resulting fluorescence pattern on the glass slides was measured with a fluorescence imaging system (IVIS Lumina II; PerkinElmer).

Both sets of experiments (deposition efficiency and spatial uniformity of deposition) were performed at five different nebulizer duty cycles (100, 50, 25, 12.5%, and 6%), corresponding to a range between 500 (100%) and 30 ms (6%) of nebulizer on-time per 500 ms time period. We note that SkyBlue nanoparticles cannot be used for

the determination of aerosol delivery efficiency since their retrieval efficiency from the glass slide is less than 100%. On the other hand, fluorescein cannot be used for measuring spatial uniformity of aerosol delivery onto the membrane (glass slide) due to the rapid drying of the aerosol droplets after deposition which results in quenching of the fluorescence signal. Hence, two different fluorescent tracers had to be employed for the determination of both efficiency (dose) and spatial uniformity of aerosols delivered to the cells.

3.5 | Cell culture

An alveolar epithelial type II-like cell line derived from a human adenocarcinoma (A549) was used to assess the impact of handling and set up of the MALI bioreactor on cells, in terms of cyto-compatibility, viability, and confluency of the cell layer. These cells are widely employed as a model of the alveolar epithelial barrier (Lehmann et al., 2011; Lenz et al., 2013, 2009; Oostingh et al., 2008; Ren et al., 2009; Schmid, Jud et al., 2017). We used a standard DMEM based medium, with the source and components reported in the Supporting Information.

Bronchial epithelial 16HBE14o- cells (cell seeding density: 2×10^5 cells cm^{-2}) were also used to study cell adherence to the electrospun Bionate membrane. Cells were cultured in minimum essential medium (Gibco) supplemented with 10% fetal calf serum (Gibco), 1% (vol/vol) Pen/Strep (100 U ml^{-1} ; Gibco) for 6 days under submerged culture conditions and 2 days under ALI culture.

3.6 | Preparation Bionate membranes and cell culture

The Bionate membranes were hydrophobic (water contact angle > 90°) and not cell adhesive in their pristine state. Thus, as detailed in the Supporting Information, they were treated with ethanol and Matrigel, which contains components present in the alveolar basal lamina. The Matrigel-coated membranes were mounted in the hoops and placed in 50-mm diameter Petri dishes; 1×10^6 cells were seeded on the apical (top) side of the membrane (0.2×10^6 cells/ cm^2). A number of different conditions were examined to assess the impact of the various preparation and handling steps.

- I. "Membrane control" (negative control)—cells were grown on the Bionate membrane (mounted in the PLA ring) under optimum growth conditions, that is, cells in submerged culture conditions applying 2 ml of cell culture medium on the apical side and 8 ml in the Petri dish (basolateral side) and in an incubator (5% CO_2 , 37°C, 100% humidity) for the entire experimental time (7 days).
- II. "Bioreactor control"—same as membrane control, but after Day 6 the mounted membranes were transferred into the bioreactor pre-filled with the medium in the lower (basolateral) chamber and left for a further day in the incubator with no medium on the apical side.

III. "MALI non-stretched" and "MALI stretched"—same as "Bioreactor control," but, after 21 h of ALI, cells were exposed to a flow (0.4 ml min^{-1}) and flow and stretch (5% strain, 0.2 Hz with a perfusion rate of 0.4 ml min^{-1}) conditions, respectively for 3 h.

The assessment was based on cell viability (protein content), cytotoxicity, and confluency of the epithelial cell layer.

3.7 | Cell assays and imaging

Cytotoxicity was assessed by the detection of the enzyme lactate dehydrogenase (LDH) in the supernatant of the cell culture (LDH; Roche Applied Science). The leakage of LDH from the cytoplasm into the supernatant is characteristic of membrane damage.

The total protein content of cells is an indirect measure of the number of cells populating the membrane and hence of their growth and viability. It was determined from the protein concentration of the cells using the Bio-Rad Protein assay (Cat. No 500-0006; Bio-Rad) according to the manufacturer's protocol.

Confocal microscopy analysis allows for visualization of the cell layer on the membrane, providing information on the degree of confluency of the cell layer, their morphology, and their viability status. To this end, a series of z-stack images were acquired and processed using a Carl Zeiss LSM710 system and associated software. Scanning electron microscopy (Zeiss Crossbeam 340; Carl Zeiss AG; operating voltage of 2 kV) was used to evaluate cell attachment of bronchial epithelial 16HBE14o- cells on the Bionate membrane. Additional technical details on cell assays are given in the Supporting Information.

3.8 | Data analysis

Unless stated otherwise, all data are reported as mean \pm SD for at least three independent measurements ($n \geq 3$). The one-way analysis of variance test was used to evaluate the statistical significance of effects. The significance level was set at $p < .05$ for each test.

4 | RESULTS

4.1 | Membrane elasticity and real-time monitoring of cyclic strain

The (uniaxial) stress-strain behavior of the Bionate membrane is depicted in Figure 3a. An approximately linear elastic behavior was observed up to about 15% uniaxial strain, with an elastic modulus of $2.14 \pm 0.18 \text{ MPa}$ as derived from a linear least-square fit of the stress-strain curve. The elastic modulus obtained for the Bionate membrane was not affected by incubation in DMEM at 37°C , even after 7 days of complete submersion. Moreover, cyclic stretching for uniaxial strains between 1% and 15% for up to 3 h under wet conditions did not alter its elastic modulus, suggesting its suitability for operation in dynamic conditions in a cell culture environment.

By measuring the change in pressure and hence volume in the mixing chamber during the application of cyclic overpressure in the apical chamber, we were able to estimate the linear strain of the membrane. As seen from Figure 3b, in the range 0–6 kPa overpressure, the response is approximately linear. Moreover, the MALI bioreactor was found to be leak-tight for medium flow rates up to 1 ml min^{-1} and apical differential air pressures up to 20 kPa.

It is noteworthy, that membrane activation at a physiologic linear strain of 5% requires application of about 2–3 kPa on the apical side (Figure 3b), slightly larger than differential pressure occurring during physiological breathing (for rest and heavy exercise conditions about 0.3 and 0.9 kPa, respectively; Ravikrishnan, 2006). However, since cells consist mainly of water and water is incompressible, they can easily cope with these small increases in pressure conditions as evidenced by our cell culture data presented in Section 4.3.

4.2 | Aerosol delivery

As seen from Figure 4a, we found that the delivery efficiency is $51.5 \pm 1.0\%$ of the $10 \mu\text{l}$ of a liquid filled into the nebulizer independent of the duty cycle. The aerosol was nebulized within a few

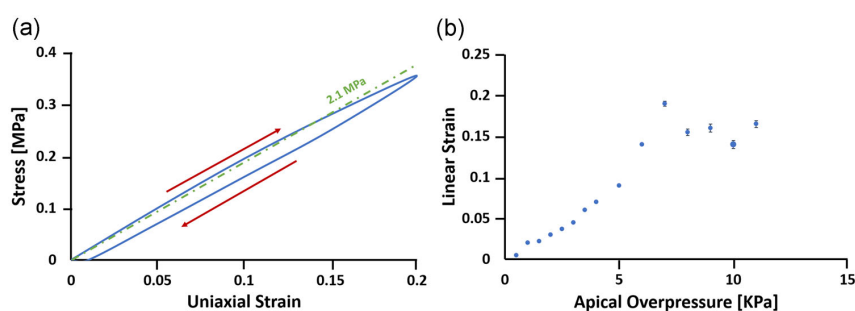


FIGURE 3 (a) Typical uniaxial stress-strain curve of the Bionate membrane. Red arrows indicate the direction of the test and the green dashed line is the least-squares linear fit for 0%–15% strain, giving a slope of $2.14 \pm 0.18 \text{ MPa}$. (b) Calibration of the membrane's linear strain by the application of cyclic overpressure in the apical chamber, using the equations reported in the Supporting Information [Color figure can be viewed at wileyonlinelibrary.com]

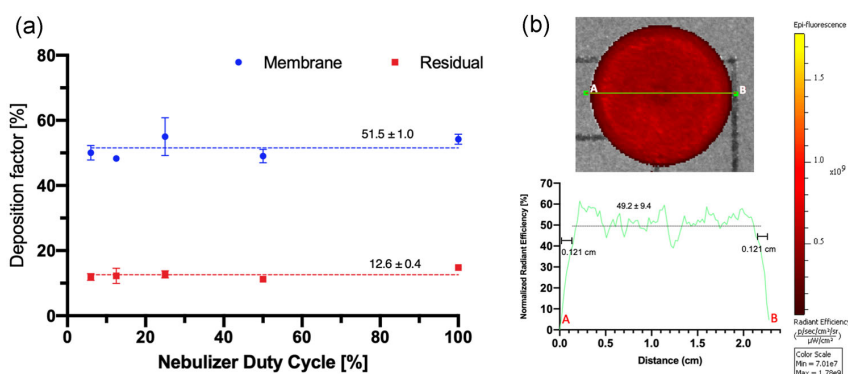


FIGURE 4 Aerosol delivery to the cells in the moving air–liquid interface system for different nebulizer duty cycles (fractional on-time of the nebulizer) is effective, reproducible, and spatially uniform. (a) Aerosol deposition (delivery) efficiency of a fluorescein salt solution was $51.5 \pm 1.0\%$ (mean \pm SD; for five duty cycle settings) and reproducibility of better than 11% (of mean delivery). Moreover, $12.6 \pm 0.4\%$ of the administered liquid (red symbols) cannot be nebulized and remains in the nebulizer independent of the duty cycle. (b) Fluorescence intensity image of SkyBlue nanoparticles nebulized on a glass slide shows uniform delivery over the entire cell-covered area on a cellular resolution level ($49.5 \pm 9.4\%$; pixel: $5 \times 5 \mu\text{m}$) except near the rim (0.121 cm), where the intensity drops sharply to zero due to the presence of the bioreactor wall [Color figure can be viewed at wileyonlinelibrary.com]

seconds and subsequent cloud settling onto the cells took 1–2 min. We estimated the dose delivery rate to be higher than $1 \mu\text{l cm}^{-2} \text{ min}^{-1}$. After nebulization $12.6 \pm 0.4\%$ of the invested liquid remained in the nebulizer reservoir, again without any statistically significant dependence on the duty cycle. The rest of ca. 35% must have been deposited on the lateral and top walls of the bioreactor.

Moreover, the aerosol is deposited uniformly as seen from Figure 4b, which depicts the measured fluorescence intensity on the apical surface after the nebulization of fluorescent aerosol. The pixel-by-pixel fluorescence (dose) variability resolved on a cellular scale (pixel: $5 \times 5 \mu\text{m}$) across the centreline of the membrane is 19% ($9.4\%/49.2\%$). This indicates that aerosol deposition on the cells is somewhat less uniform than predicted by the computational model

(ca. 10%; see Figure 2c), which may be due to the larger grid size in the FEM model ($200 \times 200 \mu\text{m}$). Within 0.12 cm of the wall, there is a steep decrease in dose due to edge effects, as predicted by the model.

4.3 | Cell viability, cytotoxicity, and stretch experiments

Figure 5 indicates that the handling of the cells in the MALI system does not have any detrimental effect on cell viability and cytotoxicity levels (necrosis). For all investigated cases, the protein content of the cells is constant at about $450 \mu\text{g}$ and the cytotoxicity of 4%–6% is

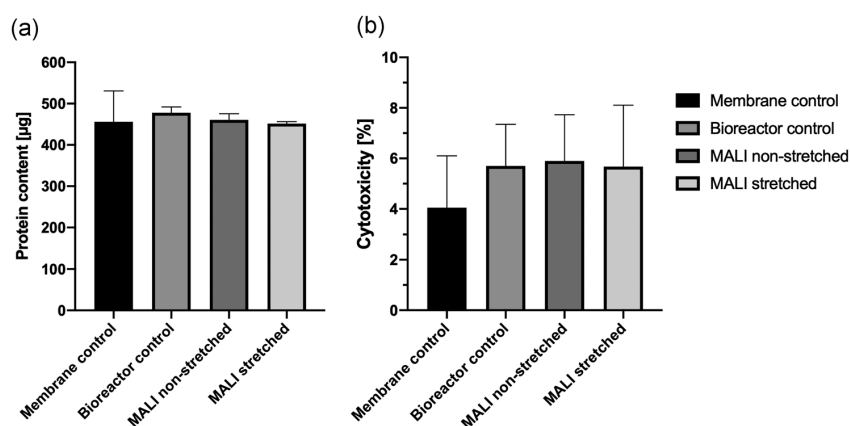


FIGURE 5 There are no statistically significant adverse effects on cells during handling and operation of the moving air–liquid interface (MALI) system: (a) Cell growth/viability (protein content). (b) Cytotoxicity (lactate dehydrogenase release) relative to membrane control (<10% is typically considered noncytotoxic). $n = 2\text{--}4$; mean \pm SEM

well below 10%, which is typically considered as nontoxic regime. Moreover, none of the investigated conditions differs significantly from the “Membrane control.”

Confluency of the cell layer was investigated with confocal microscopy after staining for cell nuclei and actin filaments of the cytoskeleton. Figure 6 shows that cells reach confluency by the end of Day 7. While there is reasonably good cell coverage over most of the membrane (Figure 7a), cells were not confluent near the rim (Figure 7b). In fact, the morphology of A549 cells changes from a rounded shape in confluent regions to an elongated morphology of a migrating cell in these regions. An elongated shape indicates less healthy cells, which may be due to insufficient Matrigel coating on the fibers at the edges. We did not observe significant differences in cell morphology between the negative control and any of the MALI conditions in Figure 5, including dynamic stretch conditions. Bronchial epithelial 16HBE14o- cells also adhered to the surface of the membrane, again some regions of the membrane were not covered by the cells likely due to nonuniform coating of Matrigel (Figure S9).

5 | DISCUSSION

Despite significant efforts, lung-on-a-chip devices which include perfusion and cyclic cell-stretch such as that reported in the groundbreaking work of Hu et al. (2010) are not widely used, partially due to technical challenges associated with microfluidic systems such as clogging of fluidic channels and aerosol delivery via micro-scale air channels (Ehrmann et al., 2020). Therefore, a milli-scale lung bioreactor “MALI,” where cells are cultured under ALI conditions with perfusion of media, cyclic cell-stretch, and dose-controlled aerosolized drug delivery was developed as an alternative, to facilitate a more wide-spread use of advanced biomimetic lung models. In this study, the key engineered elements of the MALI system were tested and evaluated. Firstly, a key element of the MALI system is dose-controlled delivery, based on a vibrating mesh nebulizer, which is

widely used in clinical settings (Aeroneb Pro). Typically, the fraction of invested substance deposited on the cell layer can vary significantly between 0.1% to ca. 20% depending on the experimental setup and chosen deposition mechanism (Desantes et al., 2006; Paur et al., 2011). For testing of experimental drugs deposition efficiencies of less than 10% are often prohibitive due to high substance cost. The setup presented here is a dose-optimized version of the previously described ALICE Cloud technology (commercially available as VITROCELL@Cloud; VITROCELL Systems), which leverages cloud dynamics for uniform deposition of aerosols onto cells (Lenz et al., 2014; Röhm et al., 2017). The change in design reported here increases the deposition efficiency from 2.8% per six-well Transwell insert in the ALICE Cloud to 51.5% of the invested drug onto the cells in a spatially uniform and highly reproducible way, which is a significant improvement over the traditional Cloud technology. The MALI aerosol unit described here has recently become commercially available as VITROCELL Cloud MAX technology (VITROCELL Systems), for use with standard Transwell inserts in static cell culture systems. Aerosol deposition in the MALI occurs within ca. 1 min and is performed under static conditions, that is, it is decoupled from the cyclic stretch. This mimics aerosol therapy under clinical conditions where patients inhale therapeutic aerosols with a single breath followed by a ca. 1 min breath-hold period for enhanced aerosol deposition. For applications requiring long-term aerosol delivery, the nebulizer could be activated periodically during the cyclic stretch experiment, but this mode of operation was not investigated here.

Modeling the complex dynamic motion of the highly-dense cloud of aerosol in the apical chamber of the MALI bioreactor is not a simple task, since the cloud density is high enough to induce multiphase coupling. Nonetheless, the Eulerian Multiphase FEM model predicted the experimentally determined cell-delivered aerosol dose reasonably well. Empirical data show that the aerosol is relatively uniformly deposited on the cells with a dose variability of about 20% about the mean dose (for cellular resolution; Figure 4b) and a narrow annular region near the walls for the bioreactor with steeply

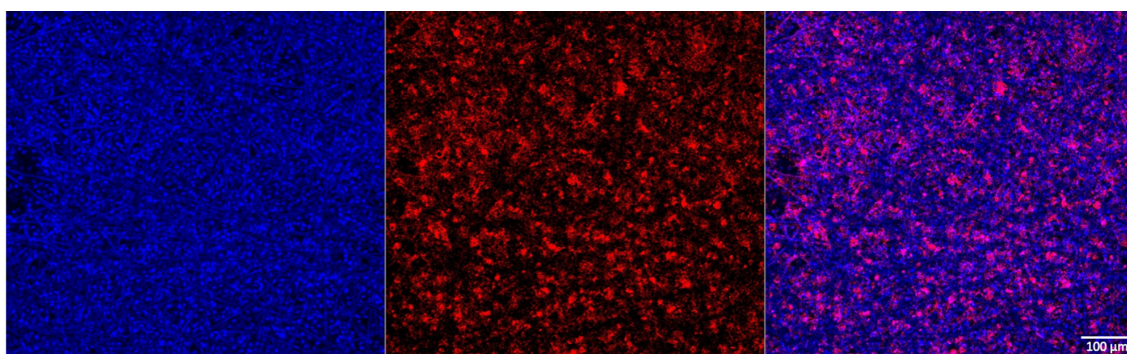


FIGURE 6 Confocal microscopy images showing confluent cell regions of A549 cells on Bionate® membrane (typical for all conditions). The right panel represents the cell nuclei (4',6-diamidino-2-phenylindole staining, blue); the middle panel shows the actin cytoskeleton (phalloidin staining, red); the right panel presents the merged images from the left and middle panel (Scale bar = 100 μm) [Color figure can be viewed at wileyonlinelibrary.com]

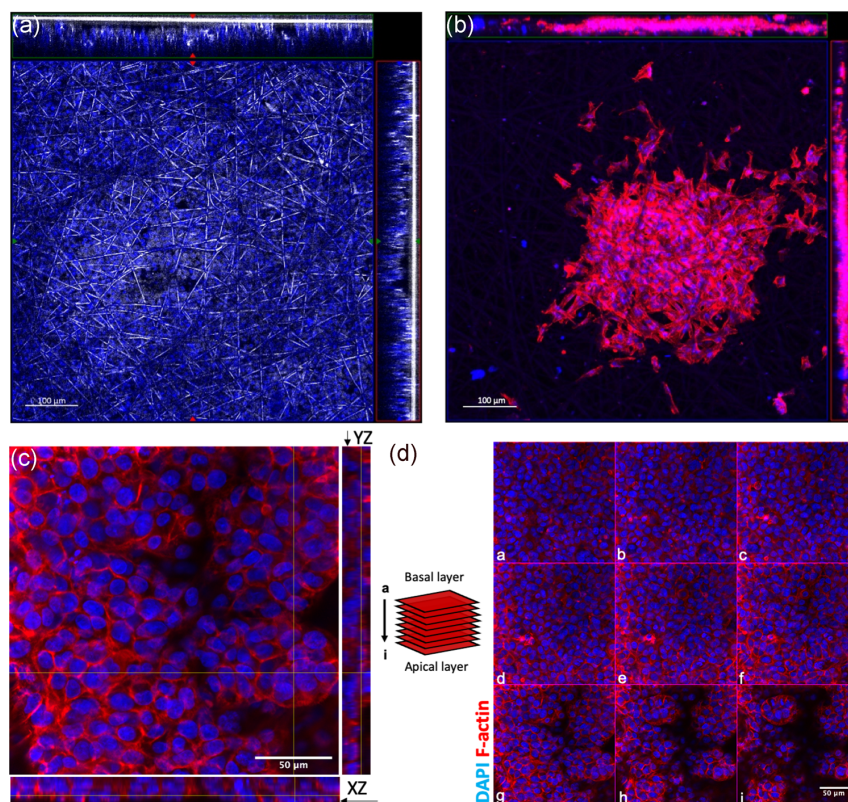


FIGURE 7 Confocal microscopy images showing confluent and nonconfluent regions of A549 cells and their penetration into the Bionate® membrane after 3 h of stretching. (a) Large confluent cell region (cell nuclei are depicted in blue) embedded in the fibrous structure of the Bionate® membrane (white lines indicate fibers of the membrane). From the xz- and yz-cross sections through the membrane (top and right section of the image, respectively), it is evident that the position of the cell layer within the membrane varies. It is often found near the apical side (thick white line of xz-/yz-images represent the glass coverslip on the apical side), but it can also reside within the membrane as also shown in Figure S8. (Scale bar = 100 μm). (b) Nonconfluent cell regions (cell nuclei in blue; cytoskeleton in red) are most prevalent near the rim of the membrane (wall of the bioreactor). (Scale bar = 100 μm). (c) Higher-resolution orthogonal view of confocal microscopy images (XY) with side views of YZ (right) and XZ (bottom) (Scale bar = 50 μm). (d) Confocal z-stack of A549 cells on Bionate membrane (covering a total depth of 16 μm), showing confluent cell regions of A549 cells. Both Panel c and d demonstrate that the alveolar epithelial cell layer is at least partially multi-layered rather than the mono-layered structure found in the lung. (Scale bar = 50 μm). The cell nucleus (4',6'-diamidino-2-phenylindole, blue), F-actin cytoskeleton (phalloidin, red) [Color figure can be viewed at wileyonlinelibrary.com]

decreasing dose. Both of these aspects are captured by the FEM model (Figure 2c). Moreover, the FEM model predicted an aerosol deposition efficiency of 85%, which was corrected to 74.3% to account for the fact that only 12.6% of the invested liquid remained in the nebulizer. Considering the degree of uncertainty in the initial conditions, namely spatial distribution, speed, and angular direction of the cloud droplets emitted from the vibrating mesh which were assumed to be uniform, constant (2.5 m s^{-1}) and perpendicular to the plane of the vibrating mesh, respectively (all values are approximations), the FEM model is in reasonably good agreement with the empirically determined cell-delivered dose of 51.5%. Thus, the model can be used to guide further optimization of the aerosol delivery efficiency.

The MALI bioreactor was purposely designed to be modular, housing both purposely designed and commercial membranes.

Indeed, one of the most crucial elements of any stretching in vitro model of the lung is the membrane for cell seeding and growth, which should be elastic, stretchable, resilient to long-term cyclic strain under aqueous conditions, and porous/permeable to allow for ALI culture conditions. Mechanical tests showed that the electrospun Bionate is a suitable material with respect to its mechanical properties revealing no degradation or hysteresis in the uniaxial stress-strain curve for up to 24 h cyclic stretch (up to 15% uniaxial strain, 0.2 Hz). It also has a porous structure and a high surface area to volume ratio, mimicking the natural extracellular matrix in native tissues. As an important feature of quality control during experiments, the MALI system allows for real-time monitoring of the stretch level and frequency by monitoring the pressure change in the medium reservoir and relating it to a corresponding linear strain.

The membrane also has to be conducive to cell growth which implies wettability, biocompatibility, and good cell adhesion. Here, the alveolar lung epithelium cell line A549 and bronchial epithelial cell line 16HBE14o were used for basic biologic validation experiments of the MALI bioreactor system. Advanced cell culture models such as cocultures or (immortalized) primary lung epithelial cells (hAELVi; Kuehn, 2016), are planned for future investigations.

Cell growth and cytotoxicity assays showed that alveolar lung epithelial cells (A549) form a viable cell layer within 7 days and 3 h of physiologic cyclic stretch (5% linear strain, 0.2 Hz) did not impair cell viability or morphology. These results are consistent with previous stretch studies with A549 cells and other lung epithelial cells (DiPaolo et al., 2010; McAdams et al., 2006; Tschumperlin & Margulies, 1998; Vlahakis et al., 1999). However, the hydrophobic membrane has to be pretreated with ethanol and water to render it wettable and then coated with Matrigel to allow for sufficient growth of A549 alveolar epithelial cells. It is also noteworthy that the cells penetrate into the porous structure, which is much thicker than the basal lamina (typically less than 1 μm). Thus, the cells assemble along with the multiple layers within the structure instead of forming a single epithelial monolayer on top of the membrane. The thickness of the membrane may also interfere with transbarrier transport processes. Besides improving the uniformity of the coating, other biocompatible materials such as natural/artificial hybrid composites with similar elastic properties but more conducive to cell growth and more effective at ensuring the formation of a contiguous cell monolayer or 3D full-thickness epithelial tissue could be developed (Doryab et al., 2019). In this direction, we have recently fabricated a biohybrid membrane with mechanical properties suitable for use in stretching experiments in MALI under both physiologic and pathological conditions (Doryab et al., 2020).

6 | CONCLUSION

The MALI bioreactor system represents a novel dynamic in vitro stretch model of the alveolar air–blood interface with aerosol delivery. It combines physiologic ALI culture conditions with medium perfusion and cyclic cell-stretch mimicking blood circulation and breathing activity of the lung, respectively. The MALI system provides uniform aerosol distribution on the cells and extremely high dose efficiency (51.5%) making it suitable for testing of even costly substances such as experimental drug candidates. Finally, in consistency with previous cell stretch studies, lung epithelial cell morphology, growth, and cytotoxicity were not affected by physiological strains.

ACKNOWLEDGMENTS

The authors would like to thank Sezer Orak for performing the nebulization and imaging of the aerosol deposition profile in the bioreactor using the IVIS. The study was partly funded by LAV (Italian Antivivisection League) through a fellowship to Roberta Nossa. The funders had no role in study design, data collection and analysis, decision to publish, or preparation of the manuscript.

AUTHOR CONTRIBUTIONS

Daniele Cei: *design, fabrication, modeling, experiments*; Ali Doryab: *dosimetry, cell culture and imaging acquisition and processing, revisions*; Anke-Gabriele Lenz, Andreas Schröppel, and Paula Mayer: *cell culture experiments*; Gerald Burgstaller: *imaging*; Roberta Nossa: *manuscript preparation, revisions*. Arti Ahluwalia and Otmar Schmid: *conception, manuscript preparation, and procurement of funding*.

DATA AVAILABILITY STATEMENT

Data is available in the Supporting Information and upon reasonable request to authors.

ORCID

Ali Doryab  <https://orcid.org/0000-0002-5976-5361>

Arti Ahluwalia  <https://orcid.org/0000-0001-5370-6750>

Otmar Schmid  <https://orcid.org/0000-0002-8012-7786>

REFERENCES

- Artzy-Schnirman, A., Hobi, N., Schneider-Daum, N., Guenat, O. T., Lehr, C.-M., & Sznitman, J. (2019). Advanced in vitro lung-on-chip platforms for inhalation assays: From prospect to pipeline. *European Journal of Pharmaceutics and Biopharmaceutics*, 144, 11–17. <https://doi.org/10.1016/j.ejpb.2019.09.006>
- Barapatre, N., Symvoulidis, P., Möller, W., Prade, F., Deliolanis, N. C., Hertel, S., Winter, G., Yildirim, A. Ö., Stoeger, T., Eickelberg, O., Ntziachristos, V., & Schmid, O. (2015). Quantitative detection of drug dose and spatial distribution in the lung revealed by Cryoslicing Imaging. *Journal of Pharmaceutical and Biomedical Analysis*, 102, 129–136.
- Bélanger, M. C., Marois, Y., Roy, R., Mehri, Y., Wagner, E., Zhang, Z., King, M. W., Yang, M., Hahn, C., & Guidoin, R. (2000). Selection of a polyurethane membrane for the manufacture of ventricles for a totally implantable artificial heart: Blood compatibility and biocompatibility studies. *Artificial Organs*, 24, 879–888.
- Bitterle, E., Karg, E., Schroepel, A., Kreyling, W. G., Tippe, A., Ferron, G. A., Schmid, O., Heyder, J., Maier, K. L., & Hofer, T. (2006). Dose-controlled exposure of A549 epithelial cells at the air-liquid interface to airborne ultrafine carbonaceous particles. *Chemosphere*, 65, 1784–1790.
- Broßell, D., Tröller, S., Dziurawitz, N., Plitzko, S., Linsel, G., Asbach, C., Azong-Wara, N., Fissan, H., & Schmidt-Ott, A. (2013). A thermal precipitator for the deposition of airborne nanoparticles onto living cells-Rationale and development. *Journal of Aerosol Science*, 63, 75–86. <https://doi.org/10.1016/j.jaerosci.2013.04.012>
- Campillo, N., Jorba, I., Schaedel, L., Casals, B., Gozal, D., Farré, R., Almendros, I., & Navajas, D. (2016). A novel chip for cyclic stretch and intermittent hypoxia cell exposures mimicking obstructive sleep apnea. *Frontiers in Physiology*, 7, 1–12.
- Cavanaugh, K. J., Cohen, T. S., & Margulies, S. S. (2006). Stretch increases alveolar epithelial permeability to uncharged micromolecules. *American Journal of Physiology. Cell Physiology*, 290, C1179–C1188.
- Choe, M. M., Sporn, P. H. S., & Swartz, M. A. (2006). Extracellular matrix remodeling by dynamic strain in a three-dimensional tissue-engineered human airway wall model. *American Journal of Respiratory Cell and Molecular Biology*, 35, 306–313. <https://doi.org/10.1165/rcmb.2005-0443OC>
- Darquenne, C., Fleming, J. S., Katz, I., Martin, A. R., Schroeter, J., Usmani, O. S., Venegas, J., & Schmid, O. (2016). Bridging the gap between science and clinical efficacy: Physiology, imaging, and modeling of aerosols in the lung. *Journal of Aerosol Medicine and Pulmonary Drug Delivery*, 29, 107–126.

- Desantes, J. M., Margot, X., Gil, A., & Fuentes, E. (2006). Computational study on the deposition of ultrafine particles from Diesel exhaust aerosol. *Journal of Aerosol Science*, 37, 1750–1769.
- DiPaolo, B. C., Lenormand, G., Fredberg, J. J., & Margulies, S. S. (2010). Stretch magnitude and frequency-dependent actin cytoskeleton remodeling in alveolar epithelia. *American Journal of Physiology. Cell Physiology*, 299, C345–C353. <https://doi.org/10.1152/ajpcell.00379.2009>
- Doryab, A., Amoabediny, G., & Salehi-Najafabadi, A. (2016). Advances in pulmonary therapy and drug development: Lung tissue engineering to lung-on-a-chip. *Biotechnology Advances*, 34, 588–596.
- Doryab, A., Tas, S., Taskin, M. B., Yang, L., Hilgendorff, A., Groll, J., Wagner, D. E., & Schmid, O. (2019). Evolution of bioengineered lung models: Recent advances and challenges in tissue mimicry for studying the role of mechanical forces in cell biology. *Advanced functional materials*, 29. <https://doi.org/10.1002/adfm.201903114>
- Doryab, A., Taskin, M. B., Stahlhut, P., Schroepfel, A., Wagner, D. E., Groll, J., & Schmid, O. (2020). A biomimetic, copolymeric membrane for cell-stretch experiments with pulmonary epithelial cells at the air-liquid interface. *Advanced functional materials*. <https://doi.org/10.1002/adfm.202004707>
- Ehrmann, S., Schmid, O., Darquenne, C., Rothen-Rutishauser, B., Sznitman, J., Yang, L., Barosova, H., Vecellio, L., Mitchell, J., & Heuze-Vourc'h, N. (2020). Innovative preclinical models for pulmonary drug delivery research. *Expert Opinion on Drug Delivery*, 17, 1–16. <https://doi.org/10.1080/17425247.2020.1730807>
- Giusti, S., Pagliari, F., Vozzi, F., Tirella, A., Mazzei, D., Cabiati, M., Del Ry, S., & Ahluwalia, A. (2013). SQPR 3.0: A sensorized bioreactor for modulating cardiac phenotype. *Procedia Engineering* 59, 219–225.
- Hein, S., Bur, M., Kolb, T., Muellinger, B., Schaefer, U. F., & Lehr, C. M. (2010). The Pharmaceutical Aerosol Deposition Device On Cell Cultures (PADD OCC) in vitro system: Design and experimental protocol. *Alternatives to Laboratory Animals: ATLA* 38, 285–295.
- Huh, D., Matthews, B. D., Mammoto, A., Montoya-Zavala, M., Hsin, H. Y., & Ingber, D. E. (2010). Reconstituting organ-level lung functions on a chip. *Science*, 328, 1662–1668. <https://doi.org/10.1126/science.1188302>
- Hänninen, O., Bröske-Hohlfeld, I., Loh, M., Stoeger, T., Kreyling, W., Schmid, O., & Peters, A. (2010). Occupational and consumer risk estimates for nanoparticles emitted by laser printers. *Journal of Nanoparticle Research*, 12, 91–99.
- Khan, I., Smith, N., Jones, E., Finch, D. S., & Cameron, R. E. (2005). Analysis and evaluation of a biomedical polycarbonate urethane tested in an in vitro study and an ovine arthroplasty model. Part I: Materials selection and evaluation. *Biomaterials*, 26, 621–631.
- Kreyling, W. G., Semmler-Behnke, M., Takenaka, S., & Möller, W. (2013). Differences in the biokinetics of inhaled nano- versus micrometer-sized particles. *Accounts of Chemical Research*, 46, 714–722. <https://doi.org/10.1021/ar300043r>
- Kuehn, A. (2016). Human alveolar epithelial cells expressing tight junctions to model the air-blood barrier. *ALTEX: Alternativen zu Tierexperimenten*.
- Lehmann, A. D., Daum, N., Bur, M., Lehr, C.-M., Gehr, P., & Rothen-Rutishauser, B. M. (2011). An in vitro triple cell co-culture model with primary cells mimicking the human alveolar epithelial barrier. *European Journal of Pharmaceutics and Biopharmaceutics*, 77, 398–406.
- Lenz, A.-G., Karg, E., Brendel, E., Hinze-Heyn, H., Maier, K. L., Eickelberg, O., Stoeger, T., & Schmid, O. (2013). Inflammatory and oxidative stress responses of an alveolar epithelial cell line to airborne zinc oxide nanoparticles at the air-liquid interface: A comparison with conventional, submerged cell-culture conditions. *BioMed Research International*, 2013, 1–12.
- Lenz, A., Karg, E., Lentner, B., Dittrich, V., Brandenberger, C., Rothen-Rutishauser, B., Schulz, H., Ferron, G. A., & Schmid, O. (2009). A dose-controlled system for air-liquid interface cell exposure and application to zinc oxide nanoparticles. *Particle and Fibre Toxicology*, 6, 32. <https://doi.org/10.1186/1743-8977-6-32>
- Lenz, A.-G., Stoeger, T., Cei, D., Schmidmeir, M., Semren, N., Burgstaller, G., Lentner, B., Eickelberg, O., Meiners, S., & Schmid, O. (2014). Efficient bioactive delivery of aerosolized drugs to human pulmonary epithelial cells cultured in air-liquid interface conditions. *American Journal of Respiratory Cell and Molecular Biology*, 51, 526–535. <https://doi.org/10.1165/rcmb.2013-0479OC>
- Mazzei, D., Guzzardi, M. A., Giusti, S., & Ahluwalia, A. (2010). A low shear stress modular bioreactor for connected cell culture under high flow rates. *Biotechnology and Bioengineering*, 106, 127–137.
- McAdams, R. M., Mustafa, S. B., Shenberger, J. S., Dixon, P. S., Henson, B. M., & DiGeronimo, R. J. (2006). Cyclic stretch attenuates effects of hyperoxia on cell proliferation and viability in human alveolar epithelial cells. *American Journal of Physiology. Lung Cellular and Molecular Physiology*, 291, L166–L174. <https://doi.org/10.1152/ajplung.00160.2005>
- Min, K. A., Talattof, A., Tsume, Y., Stringer, K. A., Yu, J. Y., Lim, D. H., & Rosania, G. R. (2013). The extracellular microenvironment explains variations in passive drug transport across different airway epithelial cell types. *Pharmaceutical Research*, 30, 2118–2132.
- Nahar, K., Gupta, N., Gauvin, R., Absar, S., Patel, B., Gupta, V., Khademhosseini, A., & Ahsan, F. (2013). In vitro, in vivo and ex vivo models for studying particle deposition and drug absorption of inhaled pharmaceuticals. *European Journal of Pharmaceutical Science*, 49, 805–818.
- Oostingh, G. J., Schmittner, M., Ehart, A. K., Tischler, U., & Duschl, A. (2008). A high-throughput screening method based on stably transformed human cells was used to determine the immunotoxic effects of fluoranthene and other PAHs. *Toxicology In vitro*, 22, 1301–1310.
- Patel, H. J. (2011). *Characterization and application of dynamic in vitro models of human airway* (All Graduate Theses and Dissertations). Utah State University Library. (936). Retrieved from <https://digitalcommons.usu.edu/etd/926>
- Paur, H.-R., Cassee, F. R., Teeguarden, J., Fissan, H., Diabate, S., Aufderheide, M., Kreyling, W. G., Hänninen, O., Kasper, G., Riediker, M., Rothen-Rutishauser, B., & Schmid, O. (2011). In-vitro cell exposure studies for the assessment of nanoparticle toxicity in the lung—A dialog between aerosol science and biology. *Journal of Aerosol Science*, 42, 668–692.
- Peters, A., Wichmann, H. E., Tuch, T., Heinrich, J., & Heyder, J. (1997). Respiratory effects are associated with the number of ultrafine particles. *American Journal of Respiratory and Critical Care Medicine*, 155, 1376–1383. <https://doi.org/10.1164/ajrccm.155.4.9105082>
- Ravikrishnan, K. P. (2006). Physiologic basis of respiratory disease. *Shock*, 26, 222.
- Ren, Y., Zhan, Q., Hu, Q., Sun, B., Yang, C., & Wang, C. (2009). Static stretch induces active morphological remodeling and functional impairment of alveolar epithelial cells. *Respiration*, 78, 301–311.
- Roan, E., & Waters, C. M. (2011). What do we know about mechanical strain in lung alveoli? *American Journal of Physiology*, 301, L625–L635. <https://doi.org/10.1152/ajplung.00105.2011>
- Röhm, M., Carle, S., Maigler, F., Flamm, J., Kramer, V., Mavoungou, C., Schmid, O., & Schindowski, K. (2017). A comprehensive screening platform for aerosolizable protein formulations for intranasal and pulmonary drug delivery. *International Journal of Pharmaceutics*, 532, 537–546. <https://doi.org/10.1016/j.ijpharm.2017.09.027>
- Sakagami, M. (2006). In vivo, in vitro and ex vivo models to assess pulmonary absorption and disposition of inhaled therapeutics for systemic delivery. *Advanced Drug Delivery Reviews*, 58, 1030–1060.
- Savi, M., Kalberer, M., Lang, D., Ryser, M., Fierz, M., Gaschen, A., Ricka, J., & Geiser, M. (2008). A novel exposure system for the efficient and controlled deposition of aerosol particles onto cell cultures. *Environmental Science and Technology*, 42, 5667–5674.

- Savla, U., Sporn, P. H. S., & Waters, C. M. (1997). Cyclic stretch of airway epithelium inhibits prostanoid synthesis. *American Journal of Physiology*, 273, L1013–L1019. <https://doi.org/10.1152/ajplung.1997.273.5.L1013>
- Schmekel, B., Borgstrom, L., & Wollmer, P. (1992). Exercise increases the rate of pulmonary absorption of inhaled terbutaline. *Chest*, 101, 742–745.
- Schmid, O., Jud, C., Umehara, Y., Mueller, D., Bucholski, A., Gruber, F., Denk, O., Egle, R., Petri-Fink, A., & Rothen-Rutishauser, B. (2017). Biokinetics of aerosolized liposomal ciclosporin in human lung cells in vitro using an air-liquid cell interface exposure system. *Journal of Aerosol Medicine and Pulmonary Drug Delivery*, 30, 411–424. <https://doi.org/10.1089/jamp.2016.1361>
- Schmid, O., & Stoeger, T. (2017). Corrigendum to “Surface area is the biologically most effective dose metric for acute nanoparticle toxicity in the lung” [Journal of Aerosol Science 99 (2016) 133–143] (S0021850215301166). *Journal of Aerosol Science*, 113, 276. <https://doi.org/10.1016/j.jaerosci.2015.12.006>
- Schreier, H., Gagné, L., Conary, J. T., & Laurian, G. (1998). Simulated lung transfection by nebulization of liposome cDNA complexes using a cascade impactor seeded with 2-CFSMEO-cells. *Journal of Aerosol Medicine*, 11, 1–13.
- Stein, S. W., & Thiel, C. G. (2017). The history of therapeutic aerosols: A chronological review. *Journal of Aerosol Medicine and Pulmonary Drug Delivery*, 30, 20–41.
- Stucki, A. O., Stucki, J. D., Hall, S. R. R., Felder, M., Mermoud, Y., Schmid, R. A., Geiser, T., & Guenat, O. T. (2015). A lung-on-a-chip array with an integrated bio-inspired respiration mechanism. *Lab on a Chip*, 15, 1302–1310. <http://xlink.rsc.org/?DOI=C4LC01252F>
- Tomei, A. A., Choe, M. M., & Swartz, M. A. (2008). Effects of dynamic compression on lentiviral transduction in an in vitro airway wall model. *American Journal of Physiology. Lung Cellular and Molecular Physiology*, 294, L79–L86. <https://doi.org/10.1152/ajplung.00062.2007>
- Tschumperlin, D. J., & Margulies, S. S. (1998). Equibiaxial deformation-induced injury of alveolar epithelial cells in vitro. *American Journal of Physiology. Lung Cellular and Molecular Physiology*, 275, L1173–L1183.
- Vlahakis, N. E., Schroeder, M. a, Limper, aH., & Hubmayr, R. D. (1999). Stretch induces cytokine release by alveolar epithelial cells in vitro. *American Journal of Physiology*, 277, L167–L173.
- Vozzi, F., Mazzei, D., Vinci, B., Vozzi, G., Sbrana, T., Ricotti, L., Forgione, N., & Ahluwalia, A. (2011). A flexible bioreactor system for constructing in vitro tissue and organ models. *Biotechnology and Bioengineering*, 108, 2129–2140.
- Waters, C. M., Roan, E., & Navajas, D. (2012). Mechanobiology in lung epithelial cells: Measurements, perturbations, and responses. *Comprehensive Physiology* (Vol. 33, pp. 48–56). John Wiley & Sons, Inc.
- Zdrachala, R. J., Zdrachala, I. J. (1999). Biomedical applications of polyurethanes: A review of past promises, present realities, and a vibrant future *Journal of Biomaterials Application* 14, 67–90.

SUPPORTING INFORMATION

Additional supporting information may be found online in the Supporting Information section.

How to cite this article: Cei D, Doryab A, Lenz A, et al. Development of a dynamic in vitro stretch model of the alveolar interface with aerosol delivery. *Biotechnology and Bioengineering*. 2020;1–13. <https://doi.org/10.1002/bit.27600>

SUPPLEMENTARY INFORMATION

Development of a dynamic *in vitro* stretch model of the alveolar interface with aerosol delivery

Daniele Cei, Ali Doryab, Anke-Gabriele Lenz, Andreas Schröppe, Paula Mayer, Gerald Burgstaller, Roberta Nossa, Arti Ahluwalia, Otmar Schmid

A. Videos of the FEM models

Videos can be downloaded from this link:

<https://drive.google.com/drive/folders/1wYa3CEJ0wxSAEZ8wve5JfYpGgBgLXK2-?usp=sharing>

B. Basal chamber domain in FEM model

The basolateral chamber (see Figure S1) was scaled to allow the membrane to expand freely during breathing.

Figure S1 shows the dimensions of the basal chamber as implemented in the FEM model. The model was solved parametrically for different heights H , which led to the identification of 14 mm as the optimum.

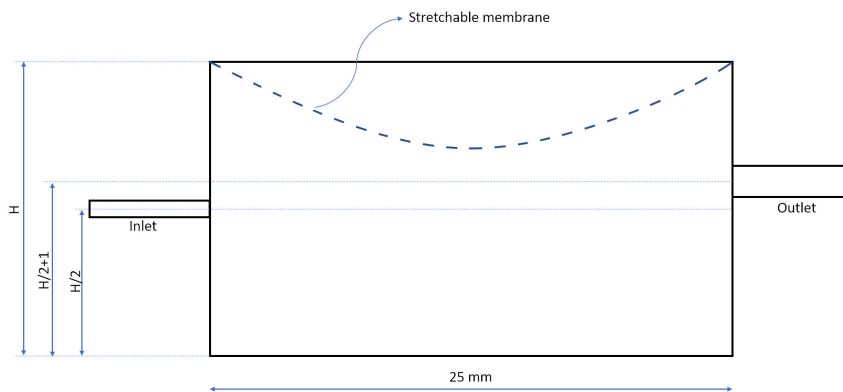


Fig. S1: Basolateral chamber domain as described by the FEM model. The inlet and outlet diameters are 1 and 2 mm respectively. The height H was varied between 10 and 20 mm in the parametric model.

C. Input parameters for the FEM model representing the apical chamber

The following constants were used for the two-phase model:

AIR phase: air density = 1.225 kg/m^3 and viscosity = $1.7894 \cdot 10^{-5} \text{ Pa}\cdot\text{s}$, pressure = 101.3 kPa, temperature = 37 °C.

For the CLOUD phase (secondary fluid): considering a total aqueous volume of 10 μL in an apical chamber of 18.8 mL over a period of 2 s, a mean water volume fraction of 2×10^{-4} was assumed (water: viscosity = 10^{-3} Pa·s and density = 1000 kg/m^3).

For a water volume fraction of 2×10^{-4} the cloud density is 16% higher than that of air, thus we can consider a two phase air-droplet system in which cloud motion is present (Hinds, 1999).

The nebulizer was modelled as an inlet surface for water on the top of the aerosol inlet tube. The initial speed of both water droplets and air at the inlet was set to 2.5 m/s (as determined by a setup having the cloud pass through two consecutive light gates placed at a known distance from each other). Considering that nebulizer is typically on for 2 s, the liquid volume output rate was set at 5 $\mu\text{L/s}$ with an active period of 2 s by implementing a User Defined Function (UDF) in the FEM model.

D. MALI design and prototype

MALI bioreactor components were fabricated using the "milli-molding" method: a polydimethylsiloxane solution was casted into molds made of stainless steel (Figure S2). SolidWorks 2017 software (Dassault System, Vlizy-Villacoublay, France) was used to design both the bioreactor and the molds. Polydimethylsiloxane (PDMS, Sylgard 184 1.1 kg Kit, Mascherpa, Milan, Italy) was prepared according to the manufacturer's instructions (1:10 PDMS monomer-catalyser mix). The bubbles formed during the PDMS preparation and casting were removed putting the molds in vacuum for at least 30 minutes.

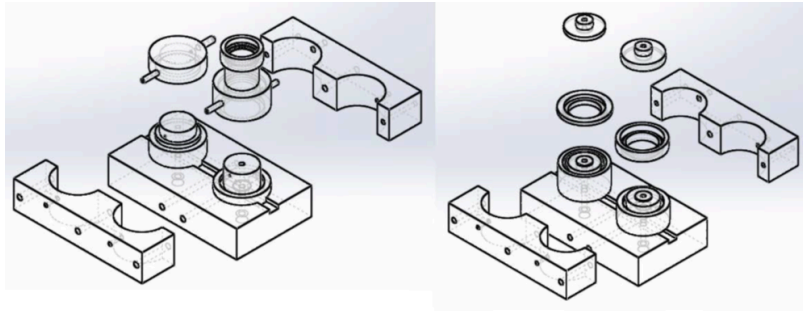


Fig. S2: 3D sketch of MALI molds and bioreactor designed using SolidWorks.

The bioreactor is divided into four parts: the two chambers (basolateral and apical chamber, Figure S3A) and a membrane holder (Figure S3 B and C). Any type of membrane or even a gravimetric sensor can be housed in the holder.

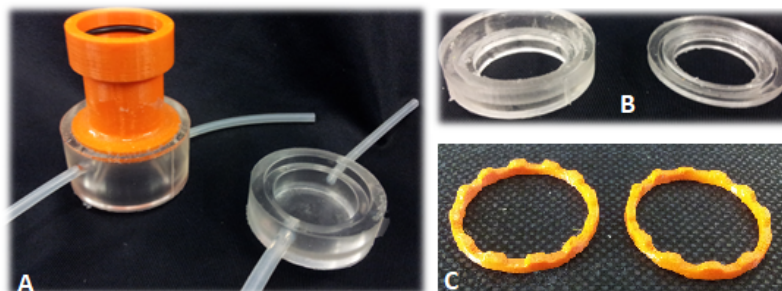


Fig. S3: MALI prototype parts: A) basolateral chamber (on the right) and apical chamber (on the left) with tubing, B) PDMS hoops, C) PLA retaining ring (Dint= 25 mm, Dext = 29 mm).

The holder is composed of two 3D printed rings that hold the membrane (Figure S3C), embedded in two PDMS hoops coupled by a male-female joint (Figure S3B). An Ultimaker 3D printer (3D Printing, Geldermalsen, Netherlands) was used to realize the polylactide acid (PLA) holding rings. In addition to ensuring no slippage of the membrane, the PLA rings enable easy handling of the membrane without touching or damaging it – particularly important during cell culture (see Section 3B&E, main text). The PLA ring assembly with the membrane is lodged in a PDMS hoop and held in between the apical and basolateral chambers. As all three parts (basolateral chamber, membrane hoop and apical chamber) are made of PDMS, the self-adhesive properties of PDMS allow O-ring-free sealing by applying a small squeezing pressure. In the final configuration, the membrane has a total area of 4.9 cm², while the useful area for cell seeding is 4.2 cm².

The chambers and the holder are held together by a 3D fabricated ABS (acrylonitrile butadiene styrene) clamping system (yellow parts, Figure S4). It is composed of a base, where the bioreactor is housed, and a lid, which seals the bioreactor when the external parts are included into the base column's buttonholes.

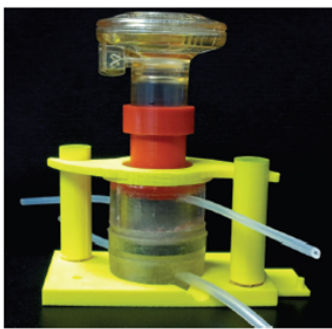


Fig. S4: MALI bioreactor enclosed and sealed in the clamping system.

The waterproofness of the bioreactor is guaranteed by the clamping system and the use of PDMS, which is self-adhesive and deformable. The whole device (bioreactor and clamping system) can be sterilized by ethanol solution, gas plasma, or ultraviolet light. All wetted parts of the MALI system were sterilized with 80% ethanol (EtOH) and ultraviolet light before the cell culture experiments.

As shown in Figure 1A (main text), the basolateral chamber is perfused with media through a closed loop circuit consisting of a peristaltic pump (Ismatec IPC 4, IDEX Health & Science, Germany - component d in Figure 1A, main text) and a medium reservoir (a 40 mL polystyrene bottle, Falcon- component c in Figure 1A, main text) all connected by 1 mm id silicone tubing. The flow rate is typically set to 0.4 mL/min (Mazzei et al., 2010) and the whole basolateral circuit contains 10 mL of medium. For mechanical activation of the membrane, two electro-pneumatic regulators (ITV0010-2BL-Q, SMC, Italy - component e in Figure , main text) controlled by a microcontroller (Arduino Uno board with additional PCB board, Arduino, Turin, Italy) were connected to a compressed air supply (house air between 0.001 and 0.1 MPa) and to ambient air allowing for cyclic pressure variations. The residual air volume is compressible, which allows for direct measurement of the degree of stretching of the membrane during pressure activation using a differential

pressure sensor (component f in Figure 1A, main text - MPX5050, Freescale Semiconductor, Munich, Germany).

E. Control System

A control box was designed for containing all the components that regulate the membrane distension and the fluid flow, i.e. for the hardware for the control of both hydraulic and pneumatic circuits. Currently, the system can monitor and control 2 bioreactors (2 membranes) at the same time, but it can be expanded to allow for multiplexed membrane exposure. The main limitation to adding more bioreactors is the requirement for additional pumps or multiple pump heads.

A dedicated microprocessor manages the cyclic inflow and outflow of compressed air in the apical chamber, while a user-friendly interface allows the control of stretching entity. The control system can be divided into four different parts (Figure S5):

- *a controlled pressure air circuit*: for controlled air injection to stretch the membrane, with a controller board and a dedicated microcontroller;
- *a peristaltic pump*: for fluid flow in the basolateral chamber;
- *a liquid reservoir*: used as a liquid reserve and oxygen exchange point, for evaluating membrane displacement through the measurement of air pressure;
- *a user interface*: a user-friendly analogue interface to control test parameters and performance.

Each part was designed and validated before connecting to the whole system.

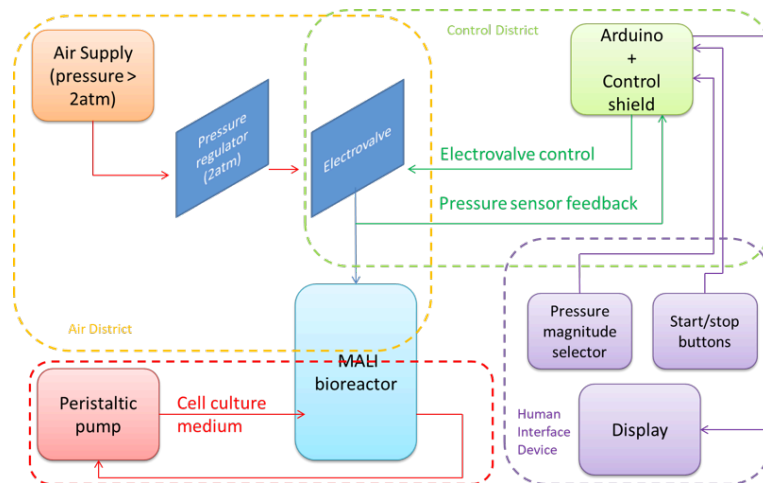


Fig. S5: Schematic of the control box layout.

F. Membrane preparation and cell culture

The membranes used in this work were hydrophobic and not cell adhesive in their pristine state. Thus, prior to coating with an adhesive layer and seeding with cells, the Bionate® membranes mounted in the rings were rendered hydrophilic by dipping in 40% EtOH and then sterilized in 80% EtOH for 15 min followed by 15 min exposure to UV light on both sides, as instructed by the manufacturer. To promote cell adhesion and spreading, the membranes were then coated with 1.72 mg/mL MatriGel (Corning, cat. # 356234, Kaiserslautern, Germany) which contains components present in the alveolar basal lamina. Specifically, MatriGel was thawed in the refrigerator (4°C) overnight and diluted to a protein concentration of 1.72 mg/mL with medium (DMEM, serum-free, Invitrogen, Germany) to ensure a uniform coating on all

fibers of the Bionate® membrane. Each membrane was placed in a well of a 6-well plate filled with 1 mL MatriGel and incubated for 1 h at room temperature followed by 30 min at 37°C. Subsequently, the excess MatriGel was aspirated and the membranes in their rings were mounted between the two PDMS hoops for integration in the bioreactor. The cell culture medium for the A549 cells consisted of DMEM/F12/L-Glut/15 mM HEPES buffered medium (Invitrogen, Germany) containing 100 Unit/mL penicillin, 100 µg/mL streptomycin, 0.5 mg/mL gentamycin sulfate (G418, Invitrogen, Germany), 25 µg/mL of Amphotericin B (Antimycotic) and 10 % fetal calf serum (FCS).

G. Cell assays and imaging: technical details

The LDH assay was performed using the Cytotoxicity Detection Kit from Roche (Roche Diagnostics, Cat. No. 11644793001, Mannheim, Germany) according to the manufacturer's protocol. The LDH concentration in 500 µL of the cell culture supernatant was determined by absorbance measurements at a wavelength of 492 nm. As 100% control of the available LDH, cells cultured on a Bionate® membrane under submerged conditions in the petri dish in the incubator were treated with 2 % (w/v) Triton X-100 (100% level). The relative LDH release of a given sample (LDH concentration normalized to the 100% control level) is defined as cytotoxicity value. Less than 10% LDH release was regarded as non-toxic. The effect of different media volumes was accounted for by converting the LDH concentration of each sample into the LDH dose (= LDH concentration times the volume of media).

For imaging, cells on the Bionate® membrane were fixed for 15 min at room temperature in 3% paraformaldehyde (in PBS) and stored in 0.1M glycine (in PBS). Cell membranes were permeabilized for 15 min at room temperature using 0.2% Triton X-100 (in PBS). Cytoskeletal actin was visualized by incubation with Phalloidin (BodipyFL, Invitrogen) diluted 1:40 in 1% BSA (in PBS) for 1 h at room temperature. Nuclear staining was achieved with ProLong® Gold Antifade Reagent containing DAPI (Invitrogen).

Confocal imaging was performed at various locations of the Bionate® membrane (Z-stacks, 512 x 512 pixels, 8 bit) using a LSM710 system (Carl Zeiss) and a Plan-Apochromat 63x/1.40 Oil Ph3 objective lens (Carl Zeiss). The confocal data sets were analyzed and processed either with Imaris 7.4.0 (Bitplane) or with AxioVision 4.8 (Zeiss) software.

For Figure 6, cells were fixed in 4% paraformaldehyde (Sigma-Aldrich), washed with PBS and, permeabilized by 0.3% Triton X-100 (Sigma-Aldrich) in PBS at room temperature. To prevent any unspecific antibody binding, a blocking buffer (5% BSA and 0.1% TritonX-100) was added for 10 min. The F-actin cytoskeleton and cell nuclei were stained with Phalloidin 594 (1:40) and DAPI (1:100), respectively. The cells were then embedded in Glycergel (DAKO Schweiz AG, Baar, Switzerland). All cell images were acquired using a confocal laser scanning microscope (LSM710, Carl Zeiss; Oberkochen, Germany) coupled to the Zen2009 software. For the scanning electron microscopy (Figure S9), the samples were fixed in 6% (v/v) glutaraldehyde (Sigma-Aldrich) and then dehydrated in gradient ethanol solutions followed by HDMS (hexamethyldisilazane, Sigma-Aldrich).

H. Thin shell theory for relating membrane linear strain to overpressure in the medium reservoir

When referring to alveolar distension, the term "linear strain" refers to a change in alveolar radius. To determine the linear strain in the MALI bioreactor, we represent the deformed membrane as a spherical cap with height h as shown in Figure S6.

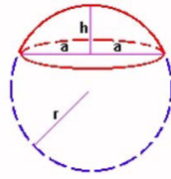


Fig. S6: The membrane is approximated as a spherical cap with variable height h .

Assuming an isotropic elastic membrane with negligible thickness subject to uniform pressure load, the linear strain (i.e. the change in membrane radius as it undergoes deformation) is related to the axial displacement h as in E1 (Mazzei et al., 2010; Polyanin and Alexander V. Manzhurov, 2006; Rausch et al., 2011; Roan and Waters, 2011; Timoshenko and Woinowsky-Krieger, 1959; Wade, 1954) :

$$h = a \sqrt{2 \frac{\delta r}{r} + \left(\frac{\delta r}{r}\right)^2} \quad \text{E1}$$

Assuming that the deformations are small ($h \ll r$), the expression simplifies to (Wade, 1954):

$$h = a \sqrt{2 \frac{\delta r}{r}} \quad \text{E2}$$

Thus, the maximal membrane displacement in the axial direction can be correlated with the linear strain of its surface. Moreover, the volume of water displaced by the membrane (ΔV)- and the resulting overpressure in the reservoir- as it stretches and relaxes during the application of cyclic pressure in the apical chamber is also correlated with the axial displacement according to (Polyanin and Alexander V. Manzhurov, 2006):

$$\Delta V = \pi h \left(\frac{a^2}{2} + \frac{h^2}{6} \right) \quad \text{E3}$$

The change in air volume in the reservoir is directly proportional to the change in overpressure and the proportionality constant can easily be determined from the ratio of ambient air pressure (absolute) and the air volume in the medium reservoir without membrane stretch, i.e. $h=0$). Thus, h can be derived from the overpressure signal. Subsequently, E2 can be used to derive the corresponding linear strain ($\delta r/r$).

Figure S7 shows an example of the overpressure measured in the reservoir during an exposure experiment.

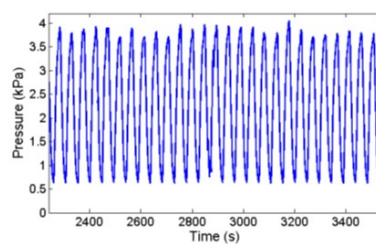


Figure S7: An example of cyclic oscillation of the pressure in the reservoir chamber during the breathing cycle.

I. Cell penetration into the scaffold

Figure S8 shows how cells penetrate around 35 μm into the scaffold forming 6 to 7 multiple layers. The inter-stack distance is 4 μm .

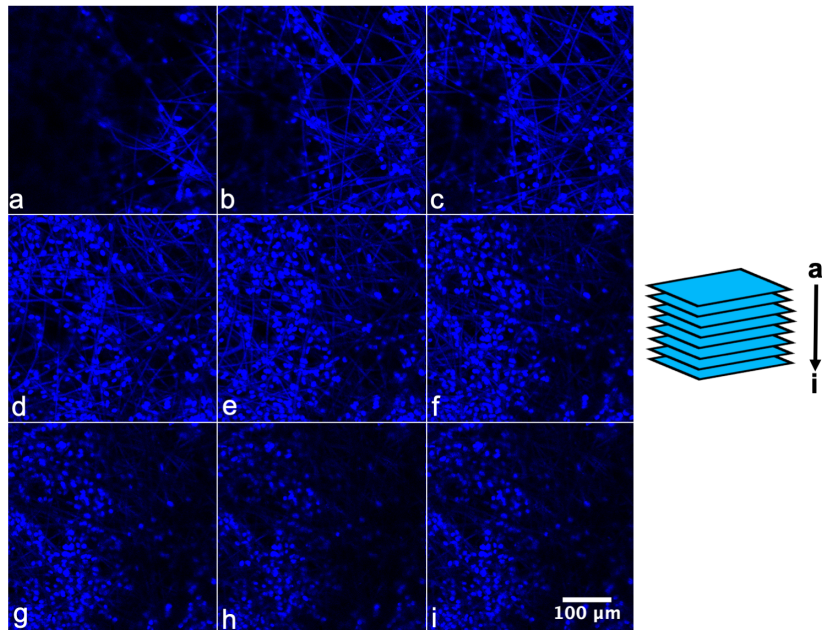


Figure S8. Confocal microscopy of A549 cells on the Bionate® membrane after 3h of stretching. Confocal stack of DAPI stained cells (Blue) with the Bionate membrane (apical surface=a; basal surface=i), showing ca. 35 μm of cell infiltration into the scaffold. Inter stack-distance is 4 μm . The scale bar is 100 μm .

J. Adherence and proliferation of bronchial epithelial 16HBE14o- cells to the scaffold

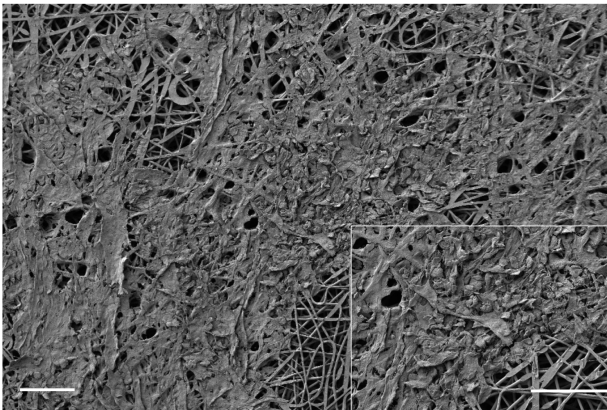


Figure S9. Scanning electron microscopy (SEM) micrograph shows bronchial epithelial 16HBE14o- cells forming a confluent layer on the electrospun Bionate membrane (cell density: 2×10^5 cells cm^{-2} , 6 days under submerged conditions and 2 days under ALI culture), except for a few regions, possibly due to localized, non-sufficient Matrigel coating. The scale bar is 100 μm .

BIBLIOGRAPHY

- Hinds WC. 1999. *Aerosol technology: properties, behavior, and measurement of airborne particles*. John Wiley & Sons.
- Mazzei D, Guzzardi MA, Giusti S, Ahluwalia A. 2010. A low shear stress modular bioreactor for connected cell culture under high flow rates. *Biotechnol. Bioeng.* **106**:n/a-n/a. <http://doi.wiley.com/10.1002/bit.22671>.
- Polyanin AD, Alexander V, Manzhirov. 2006. *Handbook of Mathematics for Engineers and Scientists*. <http://onlinelibrary.wiley.com/doi/10.1002/cbdv.200490137/abstract>.
- Rausch SMK, Haberthür D, Stampanoni M, Schittny JC, Wall WA. 2011. Local Strain Distribution in Real Three-Dimensional Alveolar Geometries. *Ann. Biomed. Eng.* **39**:2835–2843. <http://link.springer.com/10.1007/s10439-011-0328-z>.
- Roan E, Waters CM. 2011. What do we know about mechanical strain in lung alveoli? *Am. J. Physiol. Cell. Mol. Physiol.* **301**:L625–L635. <https://www.physiology.org/doi/10.1152/ajplung.00105.2011>.
- Timoshenko SP, Woinowsky-Krieger S. 1959. *Theory of plates and shells*, Engineering Societies Monographs 2nd ed. New York: McGraw-Hill 580 p.
- Wade OL. 1954. Movements of the thoracic cage and diaphragm in respiration. *J. Physiol.* **124**:193–212. <http://doi.wiley.com/10.1113/jphysiol.1954.sp005099>.

References

- Akhtar, A. (2015). The flaws and human harms of animal experimentation. *Camb. Q. Healthc. Ethics* 24, 407–19. doi:10.1017/S0963180115000079.
- Arold, S. P., Bartolák-Suki, E., and Suki, B. (2009). Variable stretch pattern enhances surfactant secretion in alveolar type II cells in culture. *Am. J. Physiol. Cell. Mol. Physiol.* 296, L574–L581. doi:10.1152/ajplung.90454.2008.
- Beasley, R., Semprini, A., and Mitchell, E. A. (2015). Risk factors for asthma: is prevention possible? *Lancet* 386, 1075–1085. doi:10.1016/S0140-6736(15)00156-7.
- Birkness, K. A., Deslauriers, M., Bartlett, J. H., White, E. H., King, C. H., and Quinn, F. D. (1999). An in vitro tissue culture bilayer model to examine early events in Mycobacterium tuberculosis infection. *Infect. Immun.* 67, 653–8. Available at: <http://www.ncbi.nlm.nih.gov/pubmed/9916072>.
- Bölükbas, D. A., Datz, S., Meyer-Schwickerath, C., Morrone, C., Doryab, A., Gößl, D., et al. (2020). Organ-Restricted Vascular Delivery: Organ-Restricted Vascular Delivery of Nanoparticles for Lung Cancer Therapy (Adv. Therap. 7/2020). *Adv. Ther.* 3, 2070016. doi:10.1002/adtp.202070016.
- Bölükbas, D. A., De Santis, M. M., Alsafadi, H. N., Doryab, A., and Wagner, D. E. (2019). “The Preparation of Decellularized Mouse Lung Matrix Scaffolds for Analysis of Lung Regenerative Cell Potential,” in *Methods Mol. Biol.*, 275–295. doi:10.1007/978-1-4939-9086-3_20.
- Bou Jawde, S., Takahashi, A., Bates, J. H. T., and Suki, B. (2020). An Analytical Model for Estimating Alveolar Wall Elastic Moduli From Lung Tissue Uniaxial Stress-Strain Curves. *Front. Physiol.* 11, 1–11. doi:10.3389/fphys.2020.00121.
- Carter, S. D., Atif, A., Kadekar, S., Lanekoff, I., Engqvist, H., Varghese, O. P., et al. (2020). PDMS leaching and its implications for on-chip studies focusing on bone regeneration applications. *Organs-on-a-Chip*, 100004. doi:10.1016/j.ooc.2020.100004.
- Castranova, V., Rabovsky, J., Tucker, J. H., and Miles, P. R. (1988). The alveolar type II epithelial cell: a multifunctional pneumocyte. *Toxicol. Appl. Pharmacol.* 93, 472–83. Available at: <http://www.ncbi.nlm.nih.gov/pubmed/3285521>.
- Cavanaugh, K. J., Cohen, T. S., and Margulies, S. S. (2006). Stretch increases alveolar epithelial permeability to uncharged micromolecules. *Am. J. Physiol. Physiol.* 290, C1179–C1188. doi:10.1152/ajpcell.00355.2004.
- Cei, D. (2015). Development of a dynamic model of the alveolar interface for the study of aerosol deposition (Ph.D. Thesis). Available at: <https://etd.adm.unipi.it/t/etd-05062015-181832/>.
- Cei, D., Doryab, A., Lenz, A.-G., Schröppel, A., Mayer, P., Burgstaller, G., et al. (2021). Development of a dynamic in vitro stretch model of the alveolar interface with aerosol delivery. *Biotechnol. Bioeng.* 118, 690–702. doi:10.1002/bit.27600.
- Chang, J., Xia, Y., Wasserloos, K., Deng, M., Blose, K. J., Vorp, D. A., et al. (2017). Cyclic stretch induced IL-33 production through HMGB1/TLR-4 signaling pathway in murine respiratory epithelial cells. *PLoS One* 12, e0184770. doi:10.1371/journal.pone.0184770.
- Chaturvedi, L. S., Marsh, H. M., and Basson, M. D. (2007). Src and focal adhesion kinase mediate mechanical strain-induced proliferation and ERK1/2 phosphorylation in human H441 pulmonary epithelial cells. *Am. J. Physiol. Physiol.* 292, C1701–C1713. doi:10.1152/ajpcell.00529.2006.
- Chess, P. R., Toia, L., and Finkelstein, J. N. (2000). Mechanical strain-induced proliferation and signaling in pulmonary epithelial H441 cells. *Am. J. Physiol. Cell. Mol. Physiol.* 279, L43–L51. doi:10.1152/ajplung.2000.279.1.L43.
- Chuah, Y. J., Koh, Y. T., Lim, K., Menon, N. V., Wu, Y., and Kang, Y. (2016). Simple surface engineering of polydimethylsiloxane with polydopamine for stabilized mesenchymal stem cell adhesion and multipotency. *Sci. Rep.* 5, 18162. doi:10.1038/srep18162.
- Copland, I. B., and Post, M. (2007). Stretch-activated signaling pathways responsible for early response gene expression in fetal lung epithelial cells. *J. Cell. Physiol.* 210, 133–143. doi:10.1002/jcp.20840.

- Crapo, J. D., Barry, B. E., Gehr, P., Bachofen, M., and Weibel, E. R. (1982). Cell number and cell characteristics of the normal human lung. *Am. Rev. Respir. Dis.* 125, 740–745. doi:10.1164/arrd.1982.126.2.332.
- Doryab, A., Amoabediny, G., and Salehi-Najafabadi, A. (2016). Advances in pulmonary therapy and drug development: Lung tissue engineering to lung-on-a-chip. *Biotechnol. Adv.* 34, 588–596. doi:10.1016/j.biotechadv.2016.02.006.
- Doryab, A., Tas, S., Taskin, M. B., Yang, L., Hilgendorff, A., Groll, J., et al. (2019). Evolution of Bioengineered Lung Models: Recent Advances and Challenges in Tissue Mimicry for Studying the Role of Mechanical Forces in Cell Biology. *Adv. Funct. Mater.* 29, 1903114. doi:10.1002/adfm.201903114.
- Doryab, A., Taskin, M. B., Stahlhut, P., Schröppel, A., Orak, S., Voss, C., et al. (2021a). A Bioinspired in vitro Lung Model to Study Particokinetics of Nano-/Microparticles Under Cyclic Stretch and Air-Liquid Interface Conditions. *Front. Bioeng. Biotechnol.* 9, 42. doi:10.3389/fbioe.2021.616830.
- Doryab, A., Taskin, M. B., Stahlhut, P., Schröppel, A., Wagner, D. E., Groll, J., et al. (2021b). A Biomimetic, Copolymeric Membrane for Cell-Stretch Experiments with Pulmonary Epithelial Cells at the Air-Liquid Interface. *Adv. Funct. Mater.* 31, 2004707. doi:10.1002/adfm.202004707.
- Edwards, Y. S., Sutherland, L. M., Power, J. H., Nicholas, T. E., and Murray, A. W. (1999). Cyclic stretch induces both apoptosis and secretion in rat alveolar type II cells. *FEBS Lett.* 448, 127–130. doi:10.1016/S0014-5793(99)00357-9.
- Felder, M., Trueeb, B., Stucki, A. O., Borcard, S., Stucki, J. D., Schnyder, B., et al. (2019). Impaired Wound Healing of Alveolar Lung Epithelial Cells in a Breathing Lung-On-A-Chip. *Front. Bioeng. Biotechnol.* 7, 1–5. doi:10.3389/fbioe.2019.00003.
- Forrest, J. B. (1970). The effect of changes in lung volume on the size and shape of alveoli. *J. Physiol.* 210, 533–547. doi:10.1113/jphysiol.1970.sp009225.
- Fredberg, J. J., and Kamm, R. D. (2006). Stress Transmission in the Lung: Pathways from Organ to Molecule. *Annu. Rev. Physiol.* 68, 507–541. doi:10.1146/annurev.physiol.68.072304.114110.
- Freese, C., Schreiner, D., Anspach, L., Bantz, C., Maskos, M., Unger, R. E., et al. (2014). In vitro investigation of silica nanoparticle uptake into human endothelial cells under physiological cyclic stretch. *Part. Fibre Toxicol.* 11, 68. doi:10.1186/s12989-014-0068-y.
- Gard, A. L., Maloney, R., Cain, B. P., Miller, C. R., Luu, R. J., Coppeta, J. R., et al. (2020). High-Throughput Human Primary Cell-Based Airway Model for Evaluating Influenza, Coronavirus, or other Respiratory Viruses &emdash;in vitro&emdash;. *bioRxiv*, 2020.05.23.112797. doi:10.1101/2020.05.23.112797.
- Gil, J., Bachofen, H., Gehr, P., and Weibel, E. R. (1979). Alveolar volume-surface area relation in air- and saline-filled lungs fixed by vascular perfusion. *J Appl Physiol* 47, 990–1001. doi:10.1143/JPSJ.58.4643.
- Gueven, N., Glatthaar, B., Manke, H.-G., and Haemmerle, H. (1996). Co-cultivation of rat pneumocytes and bovine endothelial cells on a liquid-air interface. *Eur. Respir. J.* 9, 968–975. doi:10.1183/09031936.96.09050968.
- Hall, J. E. (2016). *Guyton and Hall Textbook of Medical Physiology*. 13th ed. Elsevier.
- Hammerschmidt, S., Kuhn, H., Grasenack, T., Gessner, C., and Wirtz, H. (2004). Apoptosis and Necrosis Induced by Cyclic Mechanical Stretching in Alveolar Type II Cells. *Am. J. Respir. Cell Mol. Biol.* 30, 396–402. doi:10.1165/rcmb.2003-0136OC.
- Heise, R. L., Stober, V., Cheluvharaju, C., Hollingsworth, J. W., and Garantziotis, S. (2011). Mechanical Stretch Induces Epithelial-Mesenchymal Transition in Alveolar Epithelia via Hyaluronan Activation of Innate Immunity. *J. Biol. Chem.* 286, 17435–17444. doi:10.1074/jbc.M110.137273.
- Herland, A., Maoz, B. M., Das, D., Somayaji, M. R., Prantil-Baun, R., Novak, R., et al. (2020). Quantitative prediction of human pharmacokinetic responses to drugs via fluidically coupled vascularized organ chips. *Nat. Biomed. Eng.* 4, 421–436. doi:10.1038/s41551-019-0498-9.
- Higueta-Castro, N., Nelson, M. T., Shukla, V., Agudelo-Garcia, P. A., Zhang, W., Duarte-

- Sanmiguel, S. M., et al. (2017). Using a Novel Microfabricated Model of the Alveolar-Capillary Barrier to Investigate the Effect of Matrix Structure on Atelectrauma. *Sci. Rep.* 7, 11623. doi:10.1038/s41598-017-12044-9.
- Huh, D., Matthews, B. D., Mammoto, A., Montoya-Zavala, M., Hsin, H. Y., and Ingber, D. E. (2010). Reconstituting Organ-Level Lung Functions on a Chip. *Science* (80-.). 328, 1662–1668. doi:10.1126/science.1188302.
- ICRP (1994). Human respiratory tract model for radiological protection. A report of a Task Group of the International Commission on Radiological Protection. *Ann. ICRP* 24, 1–482. Available at: <http://www.ncbi.nlm.nih.gov/pubmed/7726471>.
- Ingber, D. E. (2020). Is it Time for Reviewer 3 to Request Human Organ Chip Experiments Instead of Animal Validation Studies? *Adv. Sci.* 2002030, 2002030. doi:10.1002/adv.202002030.
- Jafari, B., Ouyang, B., Li, L.-F., Hales, C. A., and Quinn, D. A. (2004). Intracellular glutathione in stretch-induced cytokine release from alveolar type-2 like cells. *Respirology* 9, 43–53. doi:10.1111/j.1440-1843.2003.00527.x.
- Jain, A., Barrile, R., van der Meer, A., Mammoto, A., Mammoto, T., De Ceunynck, K., et al. (2018). Primary Human Lung Alveolus-on-a-chip Model of Intravascular Thrombosis for Assessment of Therapeutics. *Clin. Pharmacol. Ther.* 103, 332–340. doi:10.1002/cpt.742.
- Kreyling, W. G., Semmler-Behnke, M., Takenaka, S., and Möller, W. (2013). Differences in the Biokinetics of Inhaled Nano- versus Micrometer-Sized Particles. *Acc. Chem. Res.* 46, 714–722. doi:10.1021/ar300043r.
- Kuhn, H., Nieuwenhuijsen, H., Karthe, B., and Wirtz, H. (2017). Stretch-induced apoptosis in rat alveolar epithelial cells is mediated by the intrinsic mitochondrial pathway. *Exp. Lung Res.* 43, 49–56. doi:10.1080/01902148.2017.1287228.
- Li, J., Wen, A. M., Potla, R., Benschir, E., Seebarran, A., Benz, M. A., et al. (2019). AAV-mediated gene therapy targeting TRPV4 mechanotransduction for inhibition of pulmonary vascular leakage. *APL Bioeng.* 3, 046103. doi:10.1063/1.5122967.
- Liu, M., Xu, J., Souza, P., Tanswell, B., Tanswell, A. K., and Post, M. (1995). The effect of mechanical strain on fetal rat lung cell proliferation: Comparison of two- and three-dimensional culture systems. *Vitr. Cell. Dev. Biol. - Anim.* 31, 858–866. doi:10.1007/BF02634570.
- Matthews, R. A. J. (2008). Medical progress depends on animal models - doesn't it? *J. R. Soc. Med.* 101, 95–98. doi:10.1258/jrsm.2007.070164.
- May, S. M., and Li, J. T. C. (2015). Burden of chronic obstructive pulmonary disease: Healthcare costs and beyond. *Allergy Asthma Proc.* 36, 4–10. doi:10.2500/aap.2015.36.3812.
- McAdams, R. M., Mustafa, S. B., Shenberger, J. S., Dixon, P. S., Henson, B. M., and DiGeronimo, R. J. (2006). Cyclic stretch attenuates effects of hyperoxia on cell proliferation and viability in human alveolar epithelial cells. *Am. J. Physiol. Cell. Mol. Physiol.* 291, L166–L174. doi:10.1152/ajplung.00160.2005.
- Nakamura, T., Liu, M., Mourgeon, E., Slutsky, A., and Post, M. (2000). Mechanical strain and dexamethasone selectively increase surfactant protein C and tropoelastin gene expression. *Am. J. Physiol. Cell. Mol. Physiol.* 278, L974–L980. doi:10.1152/ajplung.2000.278.5.L974.
- Ning, Q. M., and Wang, X. R. (2007). Response of alveolar type II epithelial cells to mechanical stretch and lipopolysaccharide. *Respiration* 74, 579–585. doi:10.1159/000101724.
- Nishiguchi, A., Singh, S., Wessling, M., Kirkpatrick, C. J., and Möller, M. (2017). Basement Membrane Mimics of Biofunctionalized Nanofibers for a Bipolar-Cultured Human Primary Alveolar-Capillary Barrier Model. *Biomacromolecules* 18, 719–727. doi:10.1021/acs.biomac.6b01509.
- Polio, S. R., Kundu, A. N., Dougan, C. E., Birch, N. P., Aurian-Blajeni, D. E., Schiffman, J. D., et al. (2018). Cross-platform mechanical characterization of lung tissue. *PLoS One* 13, e0204765. doi:10.1371/journal.pone.0204765.
- Pontes, J. F., and Grenha, A. (2020). Multifunctional Nanocarriers for Lung Drug Delivery. *Nanomaterials* 10, 183. doi:10.3390/nano10020183.

- Pound, P., and Ritskes-Hoitinga, M. (2018). Is it possible to overcome issues of external validity in preclinical animal research? Why most animal models are bound to fail. *J. Transl. Med.* 16, 304. doi:10.1186/s12967-018-1678-1.
- Regehr, K. J., Domenech, M., Koepsel, J. T., Carver, K. C., Ellison-Zelski, S. J., Murphy, W. L., et al. (2009). Biological implications of polydimethylsiloxane-based microfluidic cell culture. *Lab Chip* 9, 2132. doi:10.1039/b903043c.
- Rentzsch, I., Santos, C. L., Huhle, R., Ferreira, J. M. C., Koch, T., Schnabel, C., et al. (2017). Variable stretch reduces the pro-inflammatory response of alveolar epithelial cells. *PLoS One* 12, e0182369. doi:10.1371/journal.pone.0182369.
- Roan, E., and Waters, C. M. (2011). What do we know about mechanical strain in lung alveoli? *Am. J. Physiol. - Lung Cell. Mol. Physiol.* 301, L625–L635. doi:10.1152/ajplung.00105.2011.
- Sanchez-Esteban, J., Tsai, S.-W., Sang, J., Qin, J., Torday, J. S., and Rubin, L. P. (1998). Effects of Mechanical Forces on Lung-Specific Gene Expression. *Am. J. Med. Sci.* 316, 200–204. doi:10.1016/S0002-9629(15)40402-1.
- Savla, U., and Waters, C. M. (1998). Mechanical strain inhibits repair of airway epithelium in vitro. *Am. J. Physiol.* 274, L883-92. Available at: <http://www.ncbi.nlm.nih.gov/pubmed/9609726>.
- Schmitz, C., Welck, J., Tavernaro, I., Grinberg, M., Rahnenführer, J., Kiemer, A. K., et al. (2019). Mechanical strain mimicking breathing amplifies alterations in gene expression induced by SiO₂ NPs in lung epithelial cells. *Nanotoxicology* 13, 1227–1243. doi:10.1080/17435390.2019.1650971.
- Scott, J. E., Yang, S.-Y., Stanik, E., and Anderson, J. E. (1993). Influence of Strain on [3 H]thymidine Incorporation, Surfactant-related Phospholipid Synthesis, and cAMP Levels in Fetal Type II Alveolar Cells. *Am. J. Respir. Cell Mol. Biol.* 8, 258–265. doi:10.1165/ajrcmb/8.3.258.
- Si, L., Bai, H., Rodas, M., Cao, W., Oh, C. Y., Jiang, A., et al. (2020). Human organs-on-chips as tools for repurposing approved drugs as potential influenza and COVID19 therapeutics in viral pandemics. doi:10.1101/2020.04.13.039917.
- Stucki, A. O., Stucki, J. D., Hall, S. R. R., Felder, M., Mermoud, Y., Schmid, R. A., et al. (2015). A lung-on-a-chip array with an integrated bio-inspired respiration mechanism. *Lab Chip* 15, 1302–1310. doi:10.1039/C4LC01252F.
- Stucki, J. D., Hobi, N., Galimov, A., Stucki, A. O., Schneider-Daum, N., Lehr, C.-M., et al. (2018). Medium throughput breathing human primary cell alveolus-on-chip model. *Sci. Rep.* 8, 14359. doi:10.1038/s41598-018-32523-x.
- Trepap, X. (2006). Effect of stretch on structural integrity and micromechanics of human alveolar epithelial cell monolayers exposed to thrombin. *AJP Lung Cell. Mol. Physiol.* 290, L1104–L1110. doi:10.1152/ajplung.00436.2005.
- Trepap, X., Grabulosa, M., Puig, F., Maksym, G. N., Navajas, D., and Farré, R. (2004). Viscoelasticity of human alveolar epithelial cells subjected to stretch. *Am. J. Physiol. Cell. Mol. Physiol.* 287, L1025–L1034. doi:10.1152/ajplung.00077.2004.
- Tschumperlin, D. J., and Margulies, S. S. (1998). Equibiaxial deformation-induced injury of alveolar epithelial cells in vitro. *Am. J. Physiol. Cell. Mol. Physiol.* 275, L1173–L1183. doi:10.1152/ajplung.1998.275.6.L1173.
- Valentine, M. S., Link, P. A., Herbert, J. A., Kamga Gninzeko, F. J., Schneck, M. B., Shankar, K., et al. (2018). Inflammation and Monocyte Recruitment Due to Aging and Mechanical Stretch in Alveolar Epithelium are Inhibited by the Molecular Chaperone 4-Phenylbutyrate. *Cell. Mol. Bioeng.* 11, 495–508. doi:10.1007/s12195-018-0537-8.
- Vlahakis, N. E., Schroeder, M. A., Limper, A. H., and Hubmayr, R. D. (1999). Stretch induces cytokine release by alveolar epithelial cells in vitro. *Am. J. Physiol. Cell. Mol. Physiol.* 277, L167–L173. doi:10.1152/ajplung.1999.277.1.L167.
- Wacker, M. E., Jörres, R. A., Schulz, H., Heinrich, J., Karrasch, S., Karch, A., et al. (2016). Direct and indirect costs of COPD and its comorbidities: Results from the German COSYCONET study. *Respir. Med.* 111, 39–46. doi:10.1016/j.rmed.2015.12.001.
- Wang, Y., Maciejewski, B. S., Lee, N., Silbert, O., McKnight, N. L., Frangos, J. A., et al. (2006). Strain-induced fetal type II epithelial cell differentiation is mediated via cAMP-PKA-

- dependent signaling pathway. *Am. J. Physiol. Cell. Mol. Physiol.* 291, L820–L827. doi:10.1152/ajplung.00068.2006.
- Wang, Z., Volinsky, A. A., and Gallant, N. D. (2014). Crosslinking effect on polydimethylsiloxane elastic modulus measured by custom-built compression instrument. *J. Appl. Polym. Sci.* 131, 41050. doi:10.1002/app.41050.
- Waters, C. M., Roan, E., and Navajas, D. (2012). “Mechanobiology in Lung Epithelial Cells: Measurements, Perturbations, and Responses,” in *Comprehensive Physiology* (Hoboken, NJ, USA: John Wiley & Sons, Inc.), 48–56. doi:10.1002/cphy.c100090.
- Weibel, E. R. (1963). *Morphometry of the Human Lung*. Berlin, Heidelberg: Springer Berlin Heidelberg doi:10.1007/978-3-642-87553-3.
- Weibel, E. R. (1970). Morphometric estimation of pulmonary diffusion capacity. *Respir. Physiol.* 11, 54–75. doi:10.1016/0034-5687(70)90102-7.
- Weibel, E. R. (2009). What makes a good lung? *Swiss Med. Wkly.* 139, 375–86. doi:smw-12270.
- Wirtz, H. R., and Dobbs, L. G. (1990). Calcium mobilization and exocytosis after one mechanical stretch of lung epithelial cells. *Science* 250, 1266–9. doi:2173861.
- Yehya, N., Song, M. J., Lawrence, G. G., and Margulies, S. S. (2019). HER2 signaling implicated in regulating alveolar epithelial permeability with cyclic stretch. *Int. J. Mol. Sci.* 20. doi:10.3390/ijms20040948.
- Young, B. M., Shankar, K., Allen, B. P., Pouliot, R. A., Schneck, M. B., Mikhael, N. S., et al. (2017). Electrospun Decellularized Lung Matrix Scaffold for Airway Smooth Muscle Culture. *ACS Biomater. Sci. Eng.* 3, 3480–3492. doi:10.1021/acsbmaterials.7b00384.

Appendix A: Paper IV

This publication was reprinted with permission from the corresponding publishers. Copyright © 2019 The Authors. *Advanced Functional Materials* published by Wiley-VCH GmbH.

REVIEW

Bioengineered Lung Models

ADVANCED
FUNCTIONAL
MATERIALS

www.afm-journal.de

Evolution of Bioengineered Lung Models: Recent Advances and Challenges in Tissue Mimicry for Studying the Role of Mechanical Forces in Cell Biology

Ali Doryab, Sinem Tas, Mehmet Berat Taskin, Lin Yang, Anne Hilgendorff, Jürgen Groll, Darcy E. Wagner, and Otmar Schmid*

Mechanical stretch under both physiological (breathing) and pathophysiological (ventilator-induced) conditions is known to significantly impact all cellular compartments in the lung, thereby playing a pivotal role in lung growth, regeneration and disease development. In order to evaluate the impact of mechanical forces on the cellular level, *in vitro* models using lung cells on stretchable membranes have been developed. Only recently have some of these cell-stretching devices become suitable for air–liquid interface cell cultures, which is required to adequately model physiological conditions for the alveolar epithelium. To reach this goal, a multi-functional membrane for cell growth balancing biophysical and mechanical properties is critical to mimic (patho)physiological conditions. In this review, i) the relevance of cyclic mechanical forces in lung biology is elucidated, ii) the physiological range for the key parameters of tissue stretch in the lung is described, and iii) the currently available *in vitro* cell-stretching devices are discussed. After assessing various polymers, it is concluded that natural-synthetic copolymers are promising candidates for suitable stretchable membranes used in cell-stretching models. This work provides guidance on future developments in biomimetic *in vitro* models of the lung with the potential to function as a template for other organ models (e.g., skin, vessels).

1. Introduction

Respiratory diseases such as chronic obstructive pulmonary disease (COPD) and asthma are among the leading causes of death worldwide and will be the third leading cause of death by 2020. In the US alone it is estimated that the direct and indirect healthcare expenditure of COPD will be \$50 billion.^[1] In spite of the expected increase in prevalence of chronic lung disease, there are currently no cures—only symptomatic therapies and lung transplantation for end-stage disease patients.^[2,3]

The lung gains its most critical and sophisticated functionality through the defined arrangement of an extracellular matrix (ECM), which is maintained and populated by a variety of ≈60 different cell types. All of the different cellular compartments in the lung face a continuous but dynamic environment due to mechanical forces occurring with each breath. The

A. Doryab, L. Yang, Dr. O. Schmid
Comprehensive Pneumology Center Munich (CPC-M)
Member of the German Center for Lung Research (DZL)
81377 Munich, Germany
E-mail: otmar.schmid@helmholtz-muenchen.de
A. Doryab, L. Yang, Dr. O. Schmid
Institute of Lung Biology and Disease (iLBD)
Helmholtz Zentrum München—German Research Center for
Environmental Health
85764 Neuherberg, Germany
A. Doryab
Munich Medical Research School (MMRS)
Faculty of Medicine
Ludwig-Maximilians-University of Munich (LMU)
80336 Munich, Germany
Dr. S. Tas, Dr. D. E. Wagner
Department of Experimental Medical Sciences
Lung Bioengineering and Regeneration
Lund University
22100 Lund, Sweden

Dr. S. Tas, Dr. D. E. Wagner
Stem Cell Centre
Lund University
22184 Lund, Sweden
Dr. S. Tas, Dr. D. E. Wagner
Wallenberg Center for Molecular Medicine
Lund University
22100 Lund, Sweden
Dr. M. B. Taskin, Prof. J. Groll
Department of Functional Materials in Medicine and Dentistry
and Bavarian Polymer Institute (BPI)
University of Würzburg
97070 Würzburg, Germany
Dr. A. Hilgendorff
Center for Comprehensive Developmental Care
Dr. von Haunersches Children's Hospital University
Hospital Ludwig-Maximilians University
81377 Munich, Germany
Dr. A. Hilgendorff
Institute for Lung Biology and Disease
Helmholtz Zentrum Muenchen
Member of the Comprehensive Pneumology Center Munich (CPC-M)
German Center for Lung Research (DZL)
81377 Munich, Germany

 The ORCID identification number(s) for the author(s) of this article can be found under <https://doi.org/10.1002/adfm.201903114>.

DOI: 10.1002/adfm.201903114

main pulmonary function of gas exchange at the epithelial-endothelial interface goes hand in hand with the surveillance of complex environment-host interactions. Although these critical functions are enabled by the presence and interaction of various cell types, direct exposure to gases, and airborne particles, including cigarette smoking, combustion/industrial/occupational emissions or inadvertently released (nano-)particles from consumer products is known to put the lungs at risk for environmentally induced diseases outlined above.^[4]

In light of the urgent need for further research into the mechanisms of lung disease and novel therapeutic concepts, experimental approaches have largely utilized animal models or isolated primary cells.^[5,6] Despite sophisticated effort in this research field, translation of promising drug candidates from animal, mostly rodent, models into the clinical setting often fails. In order to meet this need, an increasing number of biomimetic *in vitro* and *ex vivo* lung tissue models have been developed to i) study specific cellular effects and ii) translate observations into the clinic.

Efforts toward more biomimetic *in vitro* cell models include multicell co-culture models consisting of up to five different cell types and the shift from cell lines to potentially more physiologic primary cell cultures, which includes the most recent lung-on-a-chip technology.^[7] In recent years, these efforts also started to recognize the role of mechanical stimuli, that not only play a role in lung development and regeneration, but when pathologic, have also been shown to have a role in disease onset, mitigation, and chronicity.^[8,9] Mechanical stretch has been shown to modify cell proliferation, differentiation, secretion, and migration through regulation of specific signaling pathways leading to changes in gene expression and protein synthesis.^[10,11] **Figure 1** depicts an overview over the most relevant mechanisms induced or impacted by a cellular stretch.

Despite acknowledging of the importance of mechanical forces to mimic (patho)physiologic conditions (and thus reliably study relevant treatment and injury mechanisms), only a very limited number of *in vitro* models allow mechanical stretching of pulmonary epithelial cells. Moreover, nearly all of these models were designed for nonphysiologic submerged conditions with cell culture medium completely covering the cells, rather than physiologic air-liquid interface (ALI) culture conditions (**Figure 2a**), where epithelial cells are exposed to air resulting in cell polarization and secretion of a protective liquid layer such as mucus and/or alveolar lining fluid.^[10,12-16] This was mainly owed to establishing feasibility, i.e., the technological simplicity of submerged cell culture systems. Only a few of these cell-stretching devices are commercially available (e.g., Bioflex culture plate, Flexcell International Corp., USA) and thus there has been a challenge of bringing these setups to biologists with expertise in pulmonary biology (**Figure 2e**).

On the other hand, the advantages of cell and tissue-based bioreactor systems includes the creation of biomimetic culture conditions that significantly improve the physiological relevance of cell and tissue cultures by controlling microenvironment parameters and facilitating mass transfer of nutrients.^[17-20] Nonetheless, one of the main limitations of the currently available stretchable systems is the lack of suitable membranes, which are both suitable for ALI cell culture conditions and closely mimicking the physiologic conditions in the lung.



Ali Doryab received his B.Sc. (2011) in materials engineering at the Tehran Polytechnic and continued to pursue his M.S. (2013) in biomedical engineering at the University of Tehran. He is currently a Ph.D. student at the Helmholtz Zentrum München and Faculty of Medicine, Ludwig-Maximilians-University (LMU)

of Munich under the supervision of Dr. Otmar Schmid. His current research focuses on the next generation of biomimetic bioreactor for the lung with cyclic mechanical stretch. His research interests include synthesis of polymeric biomembranes for the lung and studying the physiology of mechanically stretched pulmonary cells.



Darcy E. Wagner is an assistant professor in the Faculty of Medicine at the Lund University and she is the head of the Lung Bioengineering and Regeneration Group. She is a principal investigator in the Lund Wallenberg Molecular Medicine Center as well as the Lund Stem Cell Center. Her lab focuses on generation of lung tissue *ex vivo* for eventual transplantation and building new humanized models of lung tissue to study chronic diseases and evaluate potential therapies. Her group takes a multidisciplinary approach using advances in materials science, manufacturing, and lung stem cell biology to construct these new models.



Otmar Schmid is head of the Pulmonary Aerosol Delivery Group at the Helmholtz Zentrum München and the Comprehensive Pneumology Center in Munich, Germany. He is also adjunct assistant professor at the Missouri University of Science and Technology (USA). He is a physicist with more than 20 years of experience in

aerosol science, inhalation toxicology, and pulmonary drug delivery. He has developed advanced methods for aerosol delivery to preclinical *in vitro* and *in vivo* models of the lung including the patented ALICE-CLOUD technology. He has also worked on lung imaging, *in vitro* cell models, and bioreactors of the lung.

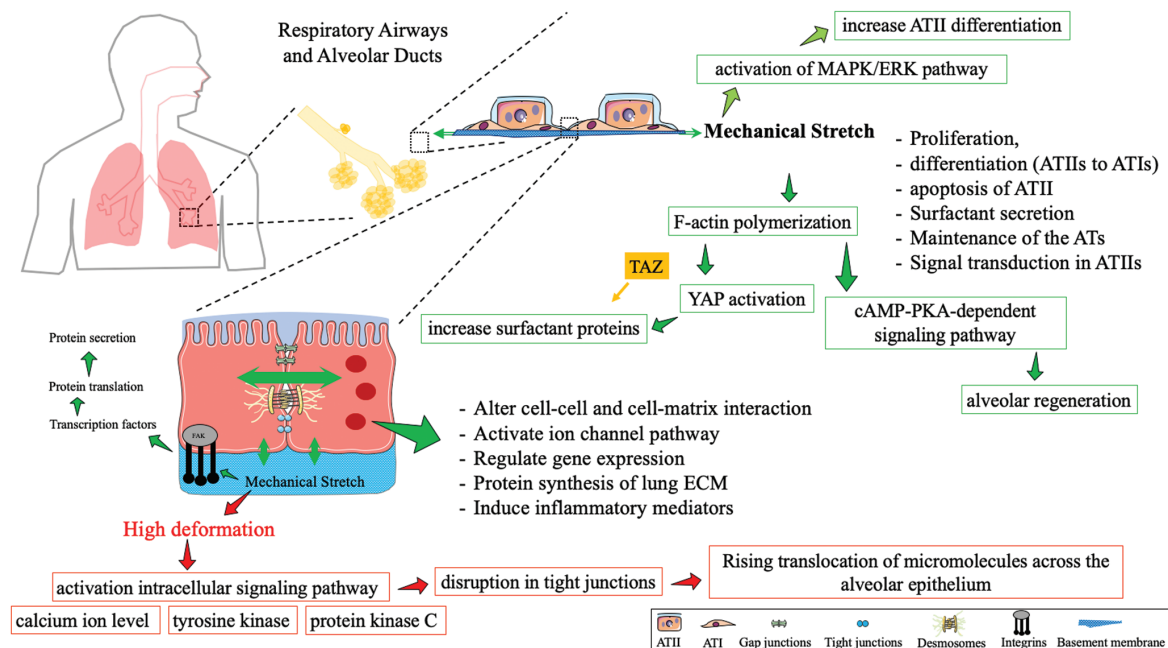


Figure 1. Role of (cyclic) mechanical forces in lung epithelium. Proliferation, differentiation, adhesion, migration, and apoptosis of lung epithelial cells are regulated by cyclic stretch. These effects can be initiated by several distinct cellular pathways such as the MAPK/ERK pathway, which results in the differentiation of fetal epithelial cells,^[45] the cAMP-PKA-dependent signaling pathway mediating differentiation of fetal ATIIIs,^[46] and activation of YAP/TAZ and the signaling cascade of Cdc42/F-actin/MAPK mediating alveolar regeneration.^[47,48,200] Cyclic strain induced by ventilation regulates pulmonary epithelial morphology by a pathway involving Src, focal adhesion kinase (FAK), and then MAPK/ERK signaling.^[49] High deformation opens the tight junctions, disrupts barrier integrity, and increases translocation of micromolecules across the alveolar epithelium by activation of intracellular signaling pathways.^[13,201]

In order to address these questions, the present review focuses on *in vitro* devices for cyclic stretch as well as ALI culture conditions of pulmonary epithelial cells, which have been developed in the past decade (Figure 2b). The technical aspects of these systems are presented and the physiologic implications of stretch on cellular function and biological response as well as membrane design, candidate materials, and manufacturing processes are reviewed. Furthermore, the potential of alternative membrane materials for improved biomimetic characteristics are discussed.

2. Stretch-Related Lung Biology

Lung has a complex architecture partitioned into 23 generations of airways enabling oxygen transport and carbon dioxide transport in and out of the blood, respectively, via the large air-liquid interface presented by the surface area of the alveolar tissue (gas exchange region of the lung).^[21] Figure 3a depicts the whole murine lung from trachea, bronchus, bronchioles (I and II) down to the typical three-dimensional (3D) honeycomb architecture of the alveoli (III–V). The surface of the lung is covered with epithelial cells, which represent the interface between air and liquid (tissue) typically referred to as ALI. Strictly speaking, the entire epithelium is not directly exposed to air, since epithelial cells secrete a protective liquid layer

consisting of mucus and/or alveolar lining fluid in the bronchial and alveolar region, respectively. These conditions can be mimicked *in vitro* by air-lifting epithelial cells and exposing them to air (ALI culture). The alveolar region is an elastic and mechanically dynamic part of the lung experiencing nearly constant cyclic stretch motion with significant impact on many aspects of lung metabolism, function, and growth.^[22,23] The mechanical forces are mainly a result from inspiratory inflation and expiratory deflation of the lung and to a lesser degree due to pulsatile blood flow.

2.1. Physiologic Stretch and Biological Membrane Conditions

During normal tidal breathing at rest (≈ 500 mL tidal volume), a healthy lung normally inflates at a frequency of ≈ 0.20 Hz (12–15 inhalation-exhalation cycles per minute for rest conditions) causing the alveoli to increase in size and surface area (Table 1). Under these respiratory conditions, the basement membrane, which represents the structural core of the air-blood barrier, is stretched to a linear strain of 4%.^[24–26] During heavy exercise the respiratory frequency and tidal volume can increase up to about 0.55 Hz (26–33 breaths per minute) and 1900 mL, respectively,^[27] resulting in an increase in linear strain of $\approx 12\%$ in the alveoli^[28] reaching even 20% in pathological scenarios such as acute respiratory distress syndrome (ARDS).^[29]

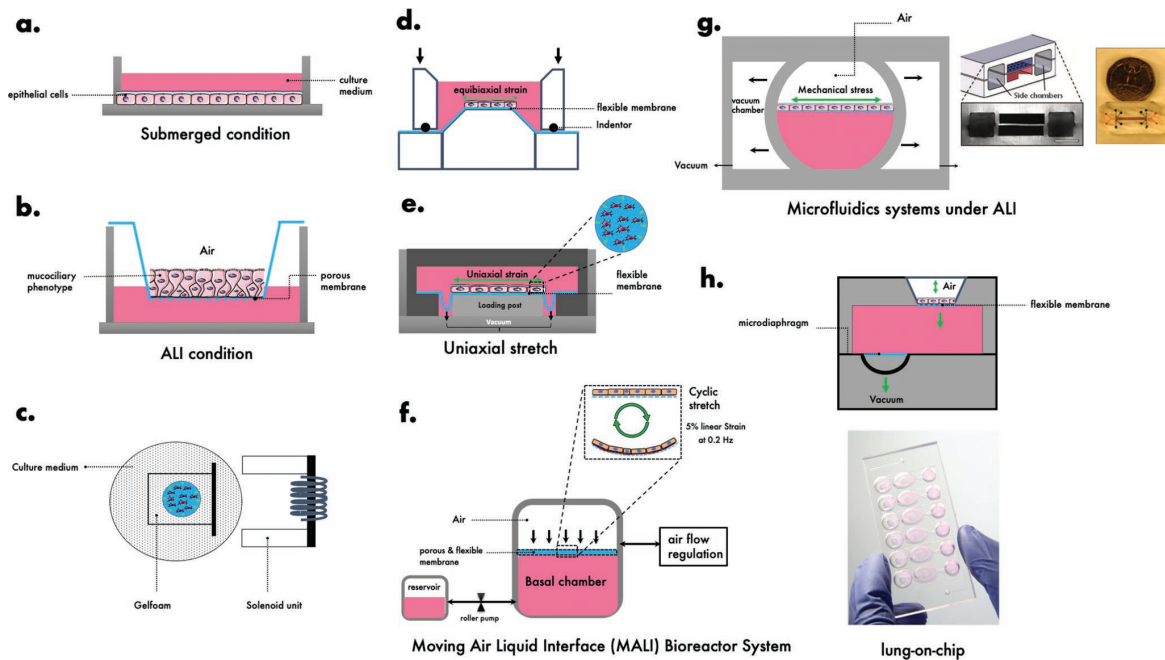


Figure 2. Schematic depictions and photos of in vitro epithelial cell culture systems and stretching devices. a) In vitro cell culture model under submerged conditions. b) In vitro static cell culture model under ALI conditions using Transwell insert. c) A stretching system using a solenoid unit: Fetal rat lung cell on a Gelfoam sponge fixed to the dish at one end, and another end is stretched using an electromagnetic field.^[74] d) A cell-stretching device to apply a uniform, equibiaxial strain to the cells: The membrane deformed by moving the indenter to provide an equibiaxial strain.^[75] e) Commercial Flexcell strain unit (Flexcell International Corporation): This device applies uniaxial radial strain by regulating vacuum pressure underneath a flexible silicone membrane. f) The MALI bioreactor system: The system is composed of a basal and an apical chamber separated by a stretchable, porous membrane and two fluidic systems for cell culture medium. Epithelial cells cultured on a membrane under ALI conditions. A pressure regulator in the apical chamber to actuate the flexible membrane in a controlled manner.^[91] g) (left) A microfluidic system for co-culture of epithelial and endothelial cells under ALI and mechanical stretch: This microsystem applies a uniaxial strain on a stretchable, porous PDMS membrane by regulating the pressure in the side chambers (right) Image of a side and top view of an actual microfluidic. Reproduced with permission.^[94] Copyright 2010, American Association for the Advancement of Science h) (top) A lung-on-a-chip array: The membrane is stretched in a triaxial direction using pneumatic microchannels located at the bottom of the basolateral chamber.^[60] (down) Photograph of a modified lung-on-chip with 6 independent chamber, reproduced under the terms and conditions of the Creative Commons Attribution 4.0 International License.^[99] Copyright 2018, The Authors, published by Springer Nature.

A thin basement membrane (thickness ≈ 50 nm) lies underneath both the epithelial and endothelial cell layers and consists of small fibrils of collagen and elastin and rare fibroblasts (Figure 3a–c). In the alveolar-capillary barrier these two basal laminae are fused so that no interstitial tissue can form between them.^[30] These basement membranes are a permeable barrier with diminutive tiny pores. Although there is no general opinion about the size of these pores, some reports on animal lungs^[31,32] suggest two types of pores one being <2.5 nm in diameter and a small fraction of larger pores (<400 nm).^[33] The mean thickness of the alveolar-capillary barrier (region of fused epithelial-endothelial basement membrane) is $1.1 \mu\text{m}$.^[30,34] The average thickness of the air–blood barrier (alveolar-capillary barrier at the site of gas exchange) is smaller ($0.62 \mu\text{m}$),^[30,35] since the gas exchanges occurs preferentially at the sites of closest proximity between air and blood. The stiffness of healthy whole human alveolar tissue (measured as Young's elastic modulus) is estimated to range $1\text{--}2$ kPa.^[36,37] Under pathological conditions such as idio-

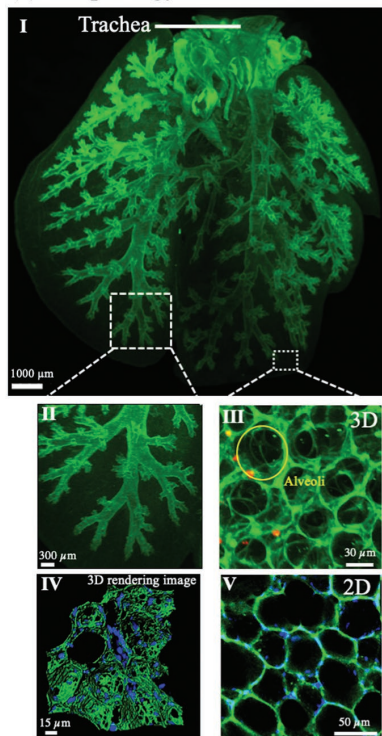
pathic pulmonary fibrosis (IPF), the stiffness of the basement membrane can increase to ≈ 16.5 kPa^[37] due to enhanced secretion and deposition of ECM proteins by both epithelial cells and fibroblasts.

2.2. Role of Mechanical Stretch in Lung Biology

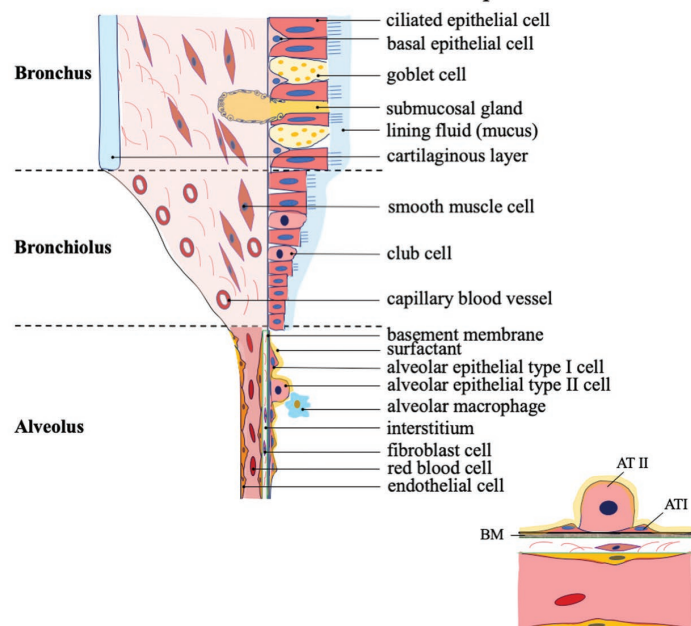
Mechanoreceptors on the cell surface can detect mechanical stretch and subsequently convert this stimulation into biochemical signals activating downstream signaling pathways.^[38] The consequences of mechanical forces on lung biology has been determined from numerous in vivo and in vitro experiments and is summarized in Figure 1. **Table 2** presents an overview of the results from in vitro studies covering a wide range of stretch conditions and cell types.

Cyclic mechanical stretch has been shown to alter proliferation, differentiation, and migration of pulmonary epithelial cells.^[10,11,39–44] These effects can be mediated by activation

(a) Morphology of whole murine lung tissue



(b) Human airway wall cellular composition



(d) State-of-the-art of the basement membrane

(c) EM of alveolar-capillary region

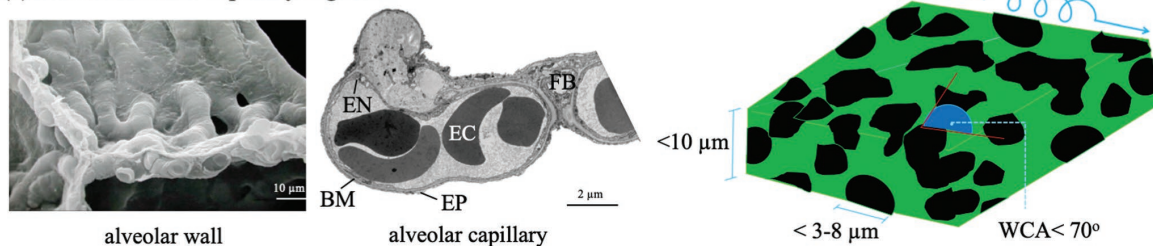


Figure 3. Lung morphology and cellular structure as guidance for bioinspired lung models. a) A 3D reconstruction of the entire murine lung tissue obtained with light sheet fluorescence microscopy (LSFM) depicting trachea, bronchi, small (terminal) bronchioles (I), distal bronchial tree (II) and 3D honeycomb structure of the alveolar region as observed with confocal microscopy on precision cut lung slices (III) as well as surface rendering, (IV) and 2D images thereof (V). Panels I-III reproduced with permission.^[202] Copyright 2019, American Chemical Society. Green: tissue structure, blue: nuclei. b) Schematic of cellular composition of the human airway tree from upper bronchus to alveolus. c) (left) SEM image of the human alveolar wall showing the very thin tissue barrier separating capillary blood and air (right) TEM image of alveolar-capillary region depicting the alveolar epithelium (EP), capillary endothelium (EN), basement membranes (BM) as part of the air–blood barrier, fibroblast (FB), and erythrocyte (EC) (Electron microscopy images Reproduced with permission^[35] Copyright 1978, Elsevier. Reproduced with permission.^[203] Copyright 2011, Wiley-VCH). d) Schematic depiction of characteristics of a state-of-the-art membrane mimicking the alveolar-capillary basement membrane.

of several distinct cellular pathways such as the mitogen-activated protein kinase/extracellular-regulated protein kinase (MAPK/ERK) pathway via binding of the epidermal growth factor (EGF) to the epidermal growth factor receptor (EGFR), which results in the differentiation of fetal epithelial cells.^[45] Fetal alveolar epithelial type II cells (ATII) can be induced via activation of the transcription factor-dependent protein kinase (cyclic adenosine 3',5'-monophosphate (cAMP)-protein kinase

A (PKA)-dependent) signaling pathway during cyclic equibiaxial elongation.^[46] It has also been shown that YAP (Yes-associated protein) is a key mediator in regulating cyclic mechanical stretch and together with the signaling cascade (the Cdc42/F-actin/MAPK), they can promote alveolar regeneration.^[47] YAP and TAZ (transcriptional co-activator with PDZ-binding motif), the Hippo signal-regulated transcriptional co-activators, can also be stimulated by the mechanical signals that are sensed

Table 1. The stretch- and permeability-related physiologic parameters of the native basement membrane of the human alveolar-capillary tissue.

Parameter	Value	Ref.
Level of mechanical linear (1D) strain	4% ^{a)} –12% ^{b)} (20%) ^{c)}	[24–28]
Corresponding 2D strain	8% ^{a)} –25% ^{b)} (44%) ^{c)}	
Stiffness of human alveolar tissue	1–2 kPa	[36,37]
Pore diameter of alveolar-capillary barrier	0.5–2.5 nm ^{d)}	[33]
Thickness of basement membrane	≈50 nm	[30]
Thickness of air–blood tissue barrier	0.62 μm ± 0.04 ^{e)}	[30,35]
Total alveolar-capillary barrier thickness	1.1 μm ± 0.1 ^{e)}	[30,34]

^{a)}normal breathing; ^{b)}deep inspiration and heavy exercise; ^{c)}pathological conditions; ^{d)}with a small portion of larger pores (<400 nm); ^{e)}harmonic mean.

by cells and trigger cell survival signaling.^[48] In addition, cyclic stretch can alter cell morphology of alveolar epithelial cells (ATs) and activate Src protein tyrosine kinase^[49] including actin cytoskeleton remodeling and cell alignment (and orientation) in fetal ATIs and can be regulated via RhoA and Rac1 signaling proteins, members of the Rho small GTPase family of hydrolyzing enzymes, when cells experience mechanical stretch.^[50]

Studying the effects of mechanical distension on the expression of specific markers for the alveolar epithelial type I (ATI) and type II (ATII) cell phenotypes showed that mechanical distension (21%, surface area) influences alveolar epithelial phenotypic expression in vitro at the transcriptional level and it appears that both transcriptional and posttranscriptional mechanisms are involved.^[51]

Mechanical stretch can influence the expression of ECM components,^[52] proliferation rate^[10] and may also impact the expression of surfactant protein C and B (SP-C and SP-B),^[53–56] synthesis of surfactant-related phospholipids,^[57] calcium mobilization,^[55,58] and induce tropoelastin^[59] in ATIs. Furthermore, applying cyclic mechanical strain (21%, surface area) on primary human pulmonary ATs increases epithelial barrier permeability for small hydrophilic molecules and enhances metabolic activity.^[60] The role of amplitude, frequency, or uniformity of stretch on these aspects has not been systematically investigated, yet.

Excessive mechanical stretch can also induce apoptosis, phosphatidylcholine secretion, necrosis in ATIs^[61,62] and more severe release of cytokines, especially inflammatory mediators such as interleukin-8 (IL-8). Vlahakis et al. have reported that excessive cyclic cell stretch (30%, surface area) for up to 48 h upregulated the production and release of IL-8 by immortalized human alveolar epithelium (A549 cells).^[63]

Moreover, it has been shown that mechanical strain can affect wound healing and wound closure of both airway and alveolar epithelium. Closure was inhibited by excessive mechanical strain such as distention, elongation, and compression.^[39–41] In addition to cyclic strain, the combined effects of fluid and interface flows (surface tension) and high transmural pressures during mechanical ventilation can play a role in the development of ventilator-induced lung injury (VILI) especially in patients who are suffering from ARDS. These aspects can exacerbate lung injury through overdistension of

alveolar sacs (volutrauma), cyclic alveolar collapse, and expansion (atelectrauma), as well as activation of the inflammatory cascades.^[64]

In summary, it is evident that cyclic mechanical forces are governing factors in numerous critical regulatory functions of the lung particularly during lung development.^[65,66]

3. Stretch Devices for In Vitro Cell Models of the Lung

The currently available stretch devices for in vitro cell models of the lung can be stratified by their applicability in cell culture conditions, i.e., submerged or ALI and by their degree of miniaturization (macro-/microfluidic; **Table 3**). The fundamental concepts of the traditional submerged and the more physiologic ALI cell culture conditions are schematically depicted in Figure 2a,b. While in submerged conditions cells are typically attached to plastic wells and culture medium covering the cells, under ALI conditions, epithelial cells are grown on a perforated membrane (typically polyethylene terephthalate, PET) with air on the apical side and cell culture medium on the basal side. ALI cell cultures are a more physiologic model of the lung epithelium as they

- mimic the interfacial function of the epithelial barrier of the lung separating air from interstitial or blood fluid.
- allow for polarization of the epithelial cells, which results in a more tightly regulated cell barrier and apical secretion of natural protective liquid layers such as mucus or alveolar lining fluid.^[67]
- allow for more complex and hence more physiologic multicell co-cultures consisting of, e.g., epithelial cells with macrophages on the apical side and dendritic or endothelial cells on the basal side of the porous membrane serving as cell support.^[68–70]
- allow for delivery of airborne gases or aerosols (drugs or toxins) directly to the epithelial cells, which is both conducive for direct measurement of the cell delivered dose via, e.g., quartz crystal microbalances^[69] and more predictive for clinical outcome than pipetting of these substances into the cell culture medium as done under submerged culture conditions.^[7,67]

In the following section, we present an overview of the currently available stretch devices for in vitro models of the lung epithelium under submerged and ALI cell culture conditions and the more recently introduced microfluidic devices typically referred to as lung-on-a-chip models.

3.1. Devices for Submerged Cell/Tissue Culture Models

The vast majority of cell-stretching devices described in the literature refer to submerged cell culture models of the lung (**Table 3**). One of the earliest cellular stretch devices was introduced by Skinner et al.^[71–74] They cultured fetal rat lung cells on a Gelfoam sponge with one side of it fixed to the culture dish and the other end elongated using an electromagnetic field generated by a solenoid unit (**Figure 2c**). However, the extent of cellular deformation applied by this system was nonuniform and difficult to quantify.^[11,75]

Another early type of stretch device was used by Wirtz and Dobbs.^[51,55] Their device consisted of a flexible poly(dimethylsiloxane) (PDMS, Sylgard 184) membrane, on

Table 2. In vitro effects of (cyclic) mechanical forces on epithelial cell physiology of the lung and associated cell stretch-conditions.

Type	Mechanical stretch		Cell stretching device	Cell type	Key results	Ref.
	Level	Frequency [cycles per minute]				
Single	16–17% (surface area)	27	Hydrostatic force unit	rATII ⁽⁹⁾	Mechanical stretch of ATIIs caused an increase in cytosolic Ca ²⁺ followed by stimulation of surfactant secretion.	[55]
Intermittent	12–18% (linear)	30	Solenoid stretch unit	fetal rat lung organotypic	Both frequency and amplitude of cyclic stretch affects production of prostacyclin by lung cells.	[74]
Cyclic	10% (surface area)	3 or 50	Flexcell strain unit	fetal rabbit ATII	Mechanical stretch alters ATII proliferation rate and may also affect synthesis of surfactant-related phospholipids.	[57]
Cyclic	27–30% (surface area)	15	Flexcell strain unit	ASMs	Cyclic stretch resulted in proliferation of ASMs and it may contribute to increased ASMs hyperplasia and airway resistance.	[42]
Cyclic	12.5% (max.), Ave. <5.7% (linear)	60	Solenoid stretch unit/Flexcell Strain Unit	Organotypic epithelial/fibroblasts	Stretch enhanced DNA synthesis of mixed cells, epithelial cells, and fibroblasts in 3D culture conditions.	[10]
Cyclic	12%, 24%, 37%, and 50% (surface area)	15	Stretch Hydrostatic force unit	rATII ⁽⁹⁾	Deformation-induced injury is an important factor in the development of lung injury during mechanical ventilation.	[75]
Cyclic	Max. 20–22% (surface area)	10–30	Flexcell strain unit	Calu-3, Cat tracheal epithelial, 1HAEO- ⁽³⁾	Wound healing affected by cyclic mechanical strain and wound closure was inhibited by both strain and compression (decreased ability to repair).	[41]
Static distention	21% (surface area)	–	Hydrostatic force unit	rATII ⁽⁹⁾	Mechanical stretch influenced alveolar epithelial phenotypic expression in vitro, at least in part, at the transcriptional level (increase in the marker for the type I phenotype (rT140) and decrease in mRNA content of SFTPB, SFTPC, and no effect on mRNA content of SFTPA or GAPDH ⁽⁹⁾).	[51]
Cyclic	5–15% (radial)	50	Flexcell strain unit	NCI-H441 ⁽⁴⁾	Cyclic mechanical stretching of H441 cells for 24 h increased SFTPB and SFTPA expression.	[56]
Cyclic	20–30% (surface)	20 and 40	Flexcell strain unit	A549	High deformation (more than 20%) can activate inflammatory response IL8.	[63]
Cyclic	5% (linear)	60	Solenoid stretch unit	Organotypic epithelial and fibroblasts	Cyclic mechanical strain differentially regulates gene and protein expression of ECM molecules in fetal lung cells.	[52]
Cyclic	Max. 22% (surface area)	3	Flexcell strain unit	rATII ⁽⁹⁾	Mechanical stretch can induce both apoptosis and phosphatidylcholine secretion in ATII.	[61]
Cyclic	25%, 37%, and 50% (surface area)	15 and 60	Over-distension injury model	rATII ⁽⁹⁾	The frequency of sustained cyclic deformations (not the deformation rate during a single stretch) increased deformation-induced injury.	[78]
Cyclic	5% (linear)	60	Solenoid stretch unit	Organotypic epithelial and fibroblasts	Mechanical strain significantly increased SFTPC and tropoelastin mRNA expression.	[59]
Cyclic	20% (surface area)	60	Flexcell strain unit	NCI-H441 ⁽⁴⁾	Mechanical stretch induces proliferation of pulmonary epithelial cells. Tyrosine kinase activity is necessary to signal the proliferative response to mechanical strain. Activation of FAK via tyrosine phosphorylation does not appear to have a role in the strain response.	[43]
Cyclic	5% (linear)	50	Flexcell strain unit	fetal ATII	Cyclic mechanical stretch enhances differentiation of fetal ATIIs in mesenchymal-epithelial interactions.	[54]
Cyclic biaxial	Max. 10% (linear)	30	Biaxial stretching device	1HAEO-and 16HBE14o- ⁽³⁾	Uniform biaxial elongation inhibits epithelial wound closure.	[39]
Cyclic	5% and 30% (surface area)	30	Flexcell strain unit	rATII ⁽⁹⁾	Cyclic stretch induces a rapid ERK1/2 activation, which is transduced via G proteins and EGFR tyrosine kinase. Stretch-induced MAPK/ERK pathway activation is independent of Na ⁺ and Ca ²⁺ influxes and the Grb2-SOS, Ras, Raf-1 pathway.	[200]
Cyclic	10% (surface area)	60	Flexcell strain unit	A549	Cyclic stretch altered the intracellular transport of plasmids to increase gene expression.	[62]
Cyclic	20% (surface area)	30	Flexcell strain unit	A549	Mechanical stretch changed cell morphology of ATII-like A549 and activated Src protein tyrosine kinase.	[49]

Table 2. Continued.

Type	Mechanical stretch		Cell stretching device	Cell type	Key results	Ref.
	Level	Frequency [cycles per minute]				
Cyclic	5% (linear)	60	Flexcell strain unit	fetal rATII ^{a)}	Mechanical stretch, at least in part, induces differentiation of fetal ATII via EGFR activation of the MAPK/ERK pathway.	[45]
Cyclic	13% and 30% (surface area)	40 and 60	Flexcell strain unit	rATII ^{a)}	Increased mechanical stretch contributes to lung injury by induction of apoptosis and necrosis in ATIIs.	[62]
Cyclic	5% (linear)	60	Flexcell strain unit	E19 fetal ATII	Various integrins contribute to mechanical control of ATII cell differentiation on laminin substrates. Strain-induced differentiation of fetal ATIIs is mediated by specific ECM-integrin interactions.	[204]
Cyclic	5% (linear)	60	Flexcell strain unit	E19 fetal ATII	The transcription factor-dependent protein kinase (cAMP-PKA-dependent) signaling pathway is activated by force in fetal ATIIs and participates in strain-induced fetal ATII cell differentiation.	[46]
Cyclic	Average 10% (max. 20%) (surface area)	20	Flexcell strain unit	NCI-H441 ^{a)} , A549	Cyclic mechanical stretch induced by ventilation supports pulmonary epithelial proliferation by a pathway involving Src, FAK, and then MAPK/ERK signaling.	[44]
Cyclic continuous	5%, 10%, or 17% (radial elongations)	30	Flexcell strain unit	Fetal rATII ^{a)}	Mechanical stretch of fetal ATIIs evokes a complex network of signaling molecules, which diverge downstream to regulate the temporal expression of a unique set of early response genes.	[58]
Cyclic	25%, 50%, 75%, and 100% (surface area)	12	Over-distension injury model	MLE-12 ^{a)}	The basement ECM plays a key role in both cell death and signal transduction in response to strain.	[205]
Cyclic	5%, 10%, and 15% (linear)	10–30	Flexcell strain unit	Primary rATII ^{a)}	Different types of mechanical strain inhibited wound closure of ATIIs compared with static controls. Mechanical stretch decreases migration of AT cells through mechanisms involving Tiam1, a Rac1-specific guanine nucleotide exchange factor.	[40]
Cyclic	12.5%, 25%, or 50% (surface area)	3	Over-distension injury model	rATII ^{a)}	Variable mechanical stretch may enhance surfactant secretion (reducing the risk of ventilator-induced lung injury).	[53]
Cyclic	38% in the latitudinal and up to 44% in the longitudinal direction (linear)	15	Strain-applying bioreactor	PCLS	Stretching of PCLS on PDMS-membranes represents a useful model to investigate lung stretch in intact lung tissue in vitro for several hours.	[83]
Cyclic	5–15% (linear)	12	Human alveolar-capillary interface model	A549	Studying the effects of the mechanical strain on inflammatory response by mimicking the lung alveolar-capillary barrier.	[94]
Cyclic	15% (surface area)	52	Flexcell strain unit	Primary murine ATII	Cyclic stretch induces epithelial-mesenchymal transition (EMT) in ATIIs through production of the matrix component hyaluronan, which activates the Wnt/beta-catenin pathway downstream of MyD88 signaling.	[14]
Cyclic	15–50% (surface area)	12–18	Microfluidic alveolar model	Murine ATII, A549	Studying the combined effects of surface-tension stresses and cyclic stretch on AT cells	[206]
Cyclic	5% (linear)	40	Flexcell strain unit	Fetal mATII ^{a)}	EGFR and ErbB4 regulate stretch-induced ATIIs differentiation via MAPK/ERK pathway.	[207]
Cyclic	5% (linear)	40	Flexcell strain unit	E19 fetal ATII	Mechanical strain enhances binding of alpha6beta1 integrin to TACE ^{a)} to promote fetal ATIIs differentiation.	[208]
Cyclic	21% (surface area)	12	Alveolar-on-a-chip	16HBE14o, pHPAEC ^{a)}	Investigation of the effect of cyclic stretch on the metabolic activity and the cytokine secretion of pHPAEC using an alveolus-on-a-chip array.	[60]
Cyclic	6% (linear)	60	A chip to partially mimic OSA	rMSCs ^{a)}	HIF-1 α expression in rMSCs increases in response to intermittent hypoxia and mechanical stretch.	[96]

^{a)}1HAEo- and 16HBE14o: airway epithelial cells, GAPDH: glyceraldehyde 3-phosphate dehydrogenase, mATII: mouse alveolar epithelial type II cells, MLE-12: mouse lung epithelial cells, NCI-H441: human pulmonary epithelial cell line, pHPAEC: primary human pulmonary alveolar epithelial cells, rATII: rat alveolar epithelial type II cells, rMSCs: rat mesenchymal stem cells, TACE: tumor necrosis factor-alphaconverting enzyme.

Table 3. Overview of cell stretch devices employed in vitro studies on the effect of mechanical stretch on cell and tissue models of the lung.

Type of device (depicted in Figure 2 panel c–h)	Cell culture conditions	Type of stretch		Membrane material				Ref.
		Direction	Max. strain applicable	Material	Pore size	Cell growth area [mm ²]	Thickness [μm]	
Solenoid stretch unit (C)	Submerged	1D, uniaxial	18% (linear)	Gelfoam sponge	NP ^{a)}	14 × 10	2000	[71,72]
Stretch unit by applying hydrostatic pressure	Submerged	2D, biaxial	50% (surface area)	Silicoelastic	NP	415	230	[55]
Cell stretching device to model over-distension injury (D)	Submerged	2D, equibiaxial	50% (surface area)	Silicone	NP	–	200	[75]
Flexcell strain unit (Flexcell International Corp., NC) (E)	Submerged	2D, equibiaxial	15% (radial)	Bioflex silicone	NP	420	–	[57,209,210]
Strain-applying bioreactor	Ex vivo model	1D, uniaxial	≈30% (longitudinally and latitudinally)	PCLS-PDMS	–	–	436 ^{b)}	[83]
Stretch apparatus (ST-150; Strex, Osaka, Japan)	Submerged	1D, uniaxial	30% (surface area)	Silicone chamber	NP	10 × 10	–	[79,80]
Human alveolar-capillary interface model (G)	ALI	1D, uniaxial	15% (linear)	PDMS	10 μm ^{c)}	0.028 ^{d)}	10	[94]
Alveolar-on-a-chip (H)	ALI	3D, triaxial	21% (surface area)	PDMS	3 or 8 μm	2 × 7.1	3	[60]
A chip to mimic OSA	Submerged	1D, uniaxial	6% (linear)	PDMS	–	12.5 ^{e)}	10	[96]
MALI bioreactor system (F)	ALI	3D, triaxial	17% (linear)	Bionate II 80A (PCU)	–	420	75.4	[91]

^{a)}Nonporous; ^{b)}PCLS: 400 μm, PDMS: 33–36 μm; ^{c)}wide pentagonal; ^{d)}cross sectional: 400 μm (width) in 70 μm (height); ^{e)}only diameter of main chamber reported.

which primary ATIIs were cultured on the apical side and mechanical stretch was applied by changing the hydrostatic pressure below the membrane. However, this device also applied a nonuniform strain to the cells, which caused changes in cell behavior due to heterogeneous deformation. In addition, the amount of mechanical stress in this system was adjusted by altering the hydrostatic pressure manually and as a result, this model was not suitable for applying stable cyclic mechanical stretch for an extended period of time.

One of the earliest studies on equibiaxial deformation-induced injury was carried out by Tschumperlin and Margulies who designed a cell-stretching device that applied a uniform, equibiaxial strain to AT cells cultured on a fibronectin-coated nonporous Silastic membranes.^[73] An annular indenter was designed to contact the bottom of the silicone membrane (near the rim) and the membrane stretched by moving the indenter. Deformation rate and cycles are regulated by the motor speed (Figure 2d). The strain field (2D, equibiaxial, maximum applied strain 50% surface area) is unchanged during 1 h of continuous cycling (Table 3). This method allowed application of a predictable uniform strain to ATs resulting in more quantifiable investigations of the response of the alveolar epithelium to cyclic mechanical stretch.

This device and other commercially available instruments such as the Flexcell strain unit (Flexcell International Corporation) and stretching apparatus (STREX Inc.) (Table 3) have been utilized by numerous researchers to study the effect of mechanical stretch on ATII,^[14,61,63,76–78] human pulmonary microvascular endothelial,^[79] and airway smooth muscle (ASM)^[80] cells (Table 2). The general mechanism of the majority of the commercially available cell-stretching devices is based on controlling vacuum pressure underneath the culture plates to apply uniaxial or uniform radial strain to the cell monolayer, which

is cultured on a flexible silicone membrane (Figure 2e). However, the membranes used in these systems are nonporous due to the application of vacuum on the basal side for stretching the membrane and thus cells cannot be cultured under ALI conditions. Therefore, the in vitro devices in these studies do not allow the study of the lung epithelium at ALI, which limits their ability to recapitulate the in vivo scenario.

In addition to in vitro cell culture models, ex vivo lung slices have been used to investigate the effects of contraction on ASMs.^[81] Ex vivo precision-cut lung slices (PCLS) can be derived from human or animal lungs. Lung tissue explants can be processed into lung slices of defined thickness (200–500 μm; a few alveolar sacs), which are viable up to 5 days.^[82] In contrast to in vitro models, PCLS preserve cellular and structural organization of the lung tissue and maintain complex physiologic features not only for healthy, but also diseased lungs.^[82] The lung slices can also be stretched to investigate the pulmonary responses to mechanical stretch.^[83,84] For instance, the lung slices (PCLS/PDMS: a PDMS membrane used as a supportive layer) were stretched by applying pressure to the basal chamber (biaxial, 0.2 Hz, 4 h).^[83] The average stretch was 24.9 ± 4.1% in alveolar perimeter (1D) at 3.5 kPa and 35 ± 8.5% at 5.2 kPa (Table 3).

3.2. Devices for Air–Liquid Interface Cell Culture Models

In recent years, recognition of the previously described advantages of ALI as compared to submerged cell have led to an increase in ALI cell cultures studies with static Transwell Inserts,^[69] where epithelial cells are cultured on a static porous membrane (typically PET) with air on the apical side and cell culture medium on the basal side (Figure 2b).^[85,86] Only very

recently, devices for stretching of ALI cell culture systems have become available (Table 3). Pulmonary cells are normally cultured on rigid substrates (mainly plastic dishes with a stiffness ranging from 2 to 4 GPa), which does not recapitulate the much less stiff basement membranes *in vivo*.^[87] For cell stretch under ALI conditions, cells should be grown on membranes which are not only elastic, but also porous for nutrient exchange between apical cells and basal cell culture medium.

To provide better culture conditions during cell seeding and increase the efficiency of cell culturing, bioreactor systems are essential. These systems, allow for tight control of temperature, pressure, and biomechanical stimuli as well as mass transfer of nutrients and oxygen by providing *in vitro* biomechanical and biochemical conditions mimicking *in vivo* conditions.^[88,89] Some of these systems are now even capable of studying the responses of ALI cell cultures to mechanical and biochemical cues.^[90]

Recently, the moving air–liquid interface (MALI) bioreactor system has been developed to study the role of mechanical stretching on the permeability of epithelial cells to soluble and airborne nanoparticles *in vitro* (Figure 2f). An elastic electrospun membrane made of polycarbonate polyurethane (Bionate80), where ATIIs are grown under ALI culture conditions, is stretched using air regulation in the apical chamber to mimic natural breathing.^[91] However, cell culture was challenging with the Bionate membrane, even if a highly proliferative lung epithelial cell line (A549) was used.

In the last decade, microfluidic cell-culture platforms (Figure 2g) have been introduced, which mimic the main *in vivo* physiological functions and mechanical microenvironment of the alveolar epithelial barrier (Table 3). Microfluidic systems are able to create and regulate small amounts of fluid flows (10^{-9} to 10^{-18} L), and transfer nutrients and other biochemical cues to cells in a controlled manner.^[92] In 2009, a continuously-perfused microfluidic system designed to culture human ATs at ALI under dynamic conditions was developed.^[93] It has been reported that cells cultured using this platform showed a better degree of monolayer integrity, had higher rates of surfactant production, and lower surface tension of the lining fluid in comparison to the traditional Transwell culture model. In 2010, Huh et al. designed a miniaturized co-culture cell model with microfluidic perfusion.^[94] This microsystem is modeled to study functions of the lung by integrating a co-culture of epithelial and endothelial cells on a stretchable, porous PDMS membrane separating the air-filled apical from the liquid-/medium-filled basal compartment of the PDMS bioreactor. Physiologic breathing movements and blood flow have been mimicked by applying cyclic mechanical strain and constant intermittent medium flow on the apical and basal side of the *in vitro* alveolar barrier, respectively.^[94] Although this multifunctional microdevice may provide superior culturing conditions for human lung cells rather as compared to conventional culture systems, it does not fulfill all of the characteristics of the alveolar-capillary barrier *in vivo*, such as barrier thickness (PDMS membrane is 10 μm ; alveolar tissue barrier <1 μm thick). Moreover, it does not include all of the major cell types native to the lung and can therefore hardly be considered as a lung-on-a-chip, but a miniaturized version of the widely used 2D

co-culture models of the lung. Recently, a new version of this device updated to regenerate a 3D cross-section of a human lung alveolus (co-culturing of primary human ATs (mixture of type I and II) with human umbilical vascular endothelial cells (HUVECs)); but, not subjected to cyclic mechanical stretch.^[95]

Another simplified microfluidic device was designed to mimic obstructive sleep apnea (OSA) for studying cellular responses to cyclical hypoxia and stretch.^[96] They showed that hypoxia-inducible factor 1 α (HIF-1 α) is upregulated in mesenchymal stem cells under both intermittent hypoxia and cyclic stretch. The circular PDMS membrane of this device is stretched over a rigid post resulting in two regions with uniform but different strain profile. While in the center region (on post), there is uniform radial strain with an added circumferential strain field, the circumferential strain is small in the off-post region (rim).^[97] In fact, this is a common limitation with other commercial stretchable devices such as Bioflex culture plates (Flexcell International Corporation, Burlington, NC).^[97] Hence, for cell experiments under identical uniform strain conditions only the on-post region of the membrane should be populated with cells.

In 2015, another microplatform was designed which sought to recreate the pulmonary parenchymal environment to investigate the effects of breathing movements on human primary cells derived from patients.^[60] In this perhaps most physiological lung-on-a-chip microdevice to date, the membrane is actuated indirectly (3D, triaxial) using a bioinspired microdiaphragm located at the bottom of the basolateral chamber (Figure 2h). Cells are seeded on a surface modified (oxygen plasma) and fibronectin-coated porous PDMS membrane (thickness is 10 μm ; pore size 3 or 8 μm). After that, a cyclic mechanical stretch is applied to the PDMS membrane (21%, 2D, at frequency of 0.2 Hz) by exerting a negative pressure. The modified version of this model enables online monitoring of transepithelial electrical resistance (TEER) in real-time using a microimpedance tomography system (at a distance of 1 mm from the electrodes).^[98] In addition, the microfluidic device used in this study can be equipped with a passive medium exchange unit to provide long-term culture conditions under ALI.^[99,100]

In summary, there has been substantial progress toward establishing an *in vitro* cell culture model of the lung, which mimics an increasing number of the core features of the lung including mechanical stretch and ALI conditions. A silicone-based membrane is commonly used in commercially available devices and microfluidic studies. Even after coating with ECM proteins (such as collagen, fibronectin, and mixtures of ECM proteins such as Matrigel), epithelial cells do not always grow to a complete confluent cell layer on these hydrophobic membranes and if they do then one often finds multilayered regions, which are a poor model of the monolayered lung epithelium. In addition, other biophysical parameters of the membrane such as porosity and thickness are very essential for cell proliferation and *in vivo*-like permeability of the *in vitro* air–blood (alveolar-capillary) barrier. Therefore, there is a need to design more biomimetic membranes, which more closely mimic the physiological aspects of the native basement membrane.

4. Alveolar-Capillary Basement Membrane for ALI Cell Cultures

For submerged cell culture conditions, stretchable cell support membranes are mainly selected based on elasticity, wettability, durability, biocompatibility, and availability (cost). However, alveolar epithelium represents the ALI with air on the apical side and tissue/liquid on the other basal side. ALI conditions can be mimicked under in vitro conditions by seeding cells on a permeable membrane allowing for contact with air from the apical side and nutrient supply with cell culture medium from the basal side via the permeable membrane. Therefore, to manufacture an appropriate membrane for ALI conditions, additional biophysical parameters such as porosity, permeability, and multicellular compatibility should be considered. In addition, compatibility with optical imaging techniques (e.g., confocal microscopy) is a desirable, albeit not absolutely necessary feature of the membrane.

Various membrane materials and manufacturing techniques have been assessed for lung tissue as summarized in Table 4. Currently, silicone-based materials such as PDMS are by far the most favored material type due to its high compliance with a Young's modulus of $\approx 1\text{--}3$ MPa (however, also values below 1 MPa are possible depending on base to cross-linker ratio^[101]), as well as good gas permeability, optical transparency, low cost, and ease of use.^[102,103] However, silicone is known to be highly adsorptive toward many small and large molecules relevant for drug testing or nourishment of the cells, which renders it problematic for drug transport studies and cytokine release monitoring in the basal compartment.^[103,104] Alternative approaches such as electrospun membranes made of various materials (e.g., polycarbonate polyurethane (PCU),^[91] polycaprolactone (PCL),^[105] polydioxanone (PDS),^[106] and poly(lactic-co-glycolic acid) (PLGA)^[107]) yielded acceptable results in terms of stretch conditions, but often suffer from limitations regarding cell growth and proliferation due to the hydrophobic nature of these materials, which cannot be completely eliminated even after coating with ECM proteins (such as collagen and fibronectin^[108]). As a consequence, the selection of a suitable membrane has been one of the most challenging aspects in the development of stretch-actuated, ALI lung bioreactors.

4.1. Membrane Properties

Ideally, the biophysical properties of membranes used for stretch-activated bioreactors of the lung should closely mimic the native basement membrane of the alveolar-capillary barrier, which have been summarized in Table 1. Careful consideration and close matching of these physiologic parameters is essential for membrane design yielding biomimetic culture conditions for pulmonary cells. Collating physiologic properties with technical limitations of current membrane technologies results in a list of membrane characteristics guiding the selection of membrane material and fabrication as summarized in Figure 3d.

As mentioned above elasticity or stiffness is among the most important membrane characteristic. However, compliance of

the membrane should also be considered, i.e., the membrane should be elastic enough to endure prolonged cyclic mechanical stretch (for at least days) with an amplitude of up to 12% (1D) or even 20% (pathological conditions) without experiencing plastic deformation, creep or rupture^[109] under realistic cell culture conditions (contact with cell culture medium). Moreover, a sufficiently high degree of wettability with contact angles below 70° is desirable for the growth of confluent epithelial and endothelial cell monolayers as encountered at the air–blood interface. Wettability (hydrophilicity/hydrophobicity) is governed by surface characteristics of the membrane including charge, chemistry, and roughness of the membrane.^[110–112] Membrane permeability governed by porosity and pore interconnectivity is also an important aspect of membrane design as it is essential for various processes facilitating cell growth such as nutrient absorption, and metabolic waste removal,^[113,114] but also for cell–cell signaling processes.

Cells secrete signaling molecules (e.g., interleukins) and extracellular vesicles (EVs) (e.g., exosomes) across the basement membrane under both homeostatic and pathological conditions, but also in response to environmental challenges including pathogens, gaseous irritants, cigarette smoke, and environmental particles.^[115,116] Monitoring of these cell signaling processes is vital for understanding the role of cell signaling in disease development and requires the use of porous membrane.

Transport rates are a function of membrane porosity and thickness.^[117] As stated above the air–blood barrier can be considered as a permeable membrane with submicron thickness ($0.62\ \mu\text{m}$) perforated with nanosized pores (<2.5 nm in diameter^[33]) (Table 1 and Figure 3c). For in vitro cell cultures, size and topography of the pores in the membrane need to be large enough to achieve desirable gas and nutrient exchange between apical and basal compartment (at least 10 nm diameter for large biomolecules to pass through), but small enough to prevent inadvertent cell migration across the membrane ($<3\text{--}8\ \mu\text{m}$ depending on cell type). Hence, the most widely used pore size of $\approx 3\ \mu\text{m}$ facilitates the formation of epithelial-endothelial cell bilayers mimicking the alveolar-capillary barrier, while allowing transport of nutrients, growth factors and cell signaling molecules (e.g., cytokines, chemokines, and extracellular vesicles) at physiologic rates.^[118–121] Another major factor in mimicking the properties of the air–blood barrier of the lung is its thickness $\approx 0.6\ \mu\text{m}$ in the gas exchange region.^[35] On the other hand, the human basement membrane in the alveolar-capillary region is only $\approx 0.6\ \mu\text{m}$ thick (Table 1). Since submicron membranes, are difficult to handle, the majority of artificial membranes reported in the literature are in the 10 micron range. The increased membrane thickness results in additional resistance to respiratory gas and macromolecular exchange and hence remains a major limiting factor in the design of biomimetic membranes for in vitro approaches to the alveolar-capillary barrier.

4.2. Membrane Fabrication

Membrane fabrication is one of the key determinants of membrane properties. The conventional techniques for

Table 4. Synthetic and natural- based polymers as candidate materials for stretchable and porous membranes.

Type	Material	Manufacturing method	Physical properties				Mechanical properties				Cell type	Ref.	
			Water contact angle [°]	Thickness [μm]	Porosity [%]	Pore size/area	Tensile stress [MPa]	Elastic modulus [MPa]	Elongation at break [%]	Max. elastic Strain [%]/ Compliance			
Synthetic-based	PCL ^{a)}	ES	90	30	85	0.2–0.4 μm	1.74	3.55	30.08	NA	HLEC ^{c)}	[185]	
	PCL ^{b)}	ES	NA	NA	52.5	NA	0.032	0.036	129.29	NA	L6 rat myoblasts	[186]	
	P(LLA-CL)	Melt spinning	NA	33 and 118 ^{c)}	<85	1–16 μm ²	26.1	23.5	578.2	0.0149 mL mm Hg ^{-1d)}	C: 3T3 fibroblasts	[109]	
	PET	ES	NA	120	83.6	NA	NA	NA	NA	NA	CALU-3 and MRC5	[147]	
	PET	ES	NA	60	NA	NA	NA	NA	NA	NA	CALU-3, MRC5, and DCs ^{c)}	[148]	
	Silicone/PTFE ^{f)}	iCVD ^{f)}	NA	0.5–3 ^{g)} , 20 ^{f)}	Non	0.1 μm ^{g)}	NA	6.24–9.72	NA	NA	Not studied	[211]	
	Bionate II 80A (PCU)	ES	121.5	75.4	NA	NA	54.2	2.2	501	NA	A549	[91]	
	Silk	Casting	NA	10–15	NA	0.5–5 μm	NA	NA	NA	NA	HLEC ^{c)}	[212]	
	Collagen	ES	NA	187	NA	NA	1.5 ^{h)} , 0.7 ⁱ⁾	52.3 ^{h)} , 26.1 ⁱ⁾	NA	NA	Aortic SMCs ^{f)}	[213]	
	Fibrinogen	ES	NA	700	NA	NA	2	80	NA	NA	Not studied	[214]	
Natural-based	PCL/NCO-sP(EO-stat-PO)	ES	NA	10	71	1.5 μm	3.8 ^{j)}	5.2	430 ^{j)}	15 ^{j)}	NCI H441 ^{f)} , HUVECs /HPMEC ^{c)} , HPAEC	[215]	
	PEGdma/PLA ⁱ⁾	PLA	ES	131.8	NA	NA	1836 μm ²	2	64.1	275	NA	VECs and VICs ^{f)}	[216]
	Blend	ES	38.7	<50 ^{j)}	NA	8.27 μm ²	2.1	141	4	NA	NA	NA	[216]
	PLLA/Lung dECM	ES	129.2	139 ± 53	86.75	NA	NA	16.35	NA	NA	HBSMCs ^{f)}	[171]	
	PGS ^{j)} /PLLA	Freeze-drying	NA	830	92	109–141 μm	0.007	0.030	NA	26.17	ADSCs ^{f)}	[217]	
	Fibronectin grafted P(LLA-CL)	ES	NA	3000	60.4	1–3 μm	5.2	50 ^{k)}	80	80	PEECs ^{f)}	[190]	
	PCL/rhTE ^{f)}	ES	NA	<100–200	NA	NA	0.510	<0.3	NA	<0.007 kPa ⁻¹	HUVECs	[188]	
	PCL/Gelatin ^{l)}	PCL	ES	NA	<20	NA	NA	NA	7.20	NA	NA	A549/ HSAEC ^{c)} , and HUVECs	[159]
	PCL/Gelatin ^{m)}	PCL	ES	NA	<20	NA	NA	NA	2.10	NA	NA	NA	[159]
	PCL/Gelatin ⁿ⁾	PCL	ES	130.52	NA	NA	37.6 μm	1.18	4.41	614.90	NA	HUVECs	[187]
Blend	Blend	ES	58.18–70.85 ⁿ⁾	NA	NA	8–12.4 μm ⁿ⁾	0.55–0.76 ⁿ⁾	3.02–5.85 ⁿ⁾	551–742 ⁿ⁾	NA	NA	NA	[187]
	PDS/Gelatin/Elastin	PDS	ES	NA	500	80–82	NA	5.61	17.11	216.7	NA	Not studied	[151]
	Blend	ES	NA	500	80–82	NA	1.77	5.74	75.08	NA	NA	NA	[151]
	PCL/PDS	PCL	ES	131.28	NA	NA	≈23 μm ^{l)}	<4 ^{l)}	<1 ^{l)}	<260 ^{l)}	NA	In vivo vascular graft	[106]
	PDS	ES	11.54	NA	NA	≈18 μm ^{l)}	<9.5 ^{l)}	<4.2 ^{l)}	<70 ^{l)}	NA	NA	NA	[106]
	Blend	ES	78.06	NA	NA	20.06 μm	<7.1 ^{l)}	<2.5 ^{l)}	121.3	NA	NA	NA	[106]
	PLGA/Gelatin/ Elastin	ES	NA	20–1000	NA	0.6–4.74 μm ²	0.130	0.770	NA	NA	Human EA.hy926& BSMCs ^{f)}	[107]	
	PCL/PGA ^{o)}	PCL	ES	118	NA	81.3	1.05 nm	<1.8 ^{l)}	<1.5 ^{l)}	<10 ^{l)}	NA	Not studied	[218]
	PGA	ES	0	NA	90	2.3 nm	<8 ^{l)}	<19 ^{l)}	<105 ^{l)}	NA	NA	NA	[218]
	Blend	ES	54–103	NA	84–87.8	1.3–1.9 nm	<2.5–5.5 ^{l)}	<2–15 ^{l)}	<25–95 ^{l)}	NA	NA	NA	[218]

Table 4. Continued.

Type	Material	Manufacturing method	Physical properties				Mechanical properties				Cell type	Ref.
			Water contact angle [°]	Thickness [μm]	Porosity [%]	Pore size/area	Tensile stress [MPa]	Elastic modulus [MPa]	Elongation at break [%]	Max. elastic strain [%]/Compliance		
PCL/HA	PCL	ES	123	200	NA	NA	4.1	0.68	213	NA	FEK4 ^{d)}	[219]
	PCL/HA, 5:1	ES	78	200	NA	NA	10 ^{h)}	0.275 ^{h)}	90 ^{h)}	NA		
	PCL/HA, 5:2	ES	54	200	NA	NA	11 ^{h)}	0.420 ^{h)}	50 ^{h)}	NA		
	Collagen/ P(LLA-CL)	ES	46.6	20	NA	NA	4.0	1.77	4.912 mmHg ^{o)}	NA	HUSMCs ^{c)}	[160]
	Gelatin/Elastin/sodium hyaluronate	3D printing	NA	150	NA	400–500 μm ^{p)}	1.15	1.95 ^{q)}	60	NA	NOF and NOK ^{r)}	[220]

^{a)}Solvent: trifluoroethanol (TFE); ^{b)}solvent: acetic acid and dimethylsulfoxide (DMSO); ^{c)}two different solvents (acetone and 1,1,1,3,3,3-Fluoro-2-propanol (HFIP)); ^{d)}resembles actual arteries; ^{e)}iCVD skin layer; ^{f)}PTFE supporting membrane; ^{g)}pore size of the PTFE membrane; ^{h)}longitudinal; ⁱ⁾across the fiber; ^{j)}taken from graphical depictions; ^{k)}no creep up to 15% strain at 0.25 Hz; ^{l)}PCL (MW 14000), solvent: hexafluoro-2-propanol (HFP); ^{m)}PCL (MW 80000), solvent: HFIP; ⁿ⁾preparation in two different flow rates; ^{o)}burst pressure; ^{p)}pore size of another side of the membrane is 50–150 μm; ^{q)}dynamic tensile storage modulus is 314 kPa; ^{r)}ADSCs: human adipose-derived stem cells, BASMCs: bovine aortic smooth muscle cell, DCs: dendritic cells, FEK4: human skin primary fibroblast cells, HBSMCs: human bronchial smooth muscle cells, HLEC: Human limbal epithelial cell, HPMEC: primary human pulmonary microvascular endothelial cell, HSAEC: primary human small airway epithelial cells, HUSMCs: human umbilical arterial smooth muscle cells, iCVD: initiated chemical vapor deposition, NCI H44: human lung carcinoma epithelial cell line, NOF: normal oral fibroblasts, NOK: normal oral keratinocytes, PEECs: porcine esophageal epithelial cells, PEGdma: poly(ethylene glycol) dimethacrylate, PGA: Polyglutamic acid, PGS: poly(glycerol sebacate), PLA: polylactic acid, PTFE: poly(tetrafluoroethylene), rhTE: recombinant human tropoelastin, SMCs: smooth muscle cells, VEC: valvular endothelial cells, VIC: valvular interstitial cells.

porous membrane fabrication are phase separation,^[122] self-assembly,^[123] freeze-drying,^[124] solvent casting,^[125] and electrospinning (ES).^[126]

Thermally induced phase separation is a convenient technique for casting a wide range of polymers such as poly-L-lactic acid (PLLA) and PLGA into an interconnected porous film.^[127] This method is easy to use, reproducible and obtained membranes have high porosity and narrow pore size distribution. However, control of pore size and shape is difficult due to the lack of control over fiber arrangement.^[127,128]

Solvent casting is a simple and inexpensive way to manufacture a porous scaffold, albeit further modifications are required to overcome innate abnormal pore shape and interconnectivity.^[129] Organizing and arranging materials by molecule or self-assembly is another way to fabricate a porous membrane. With this method, the physical and structural properties of nanofibers can be controlled by oligopeptide composition and chemistry. However, limited choice of proper molecules and lack of control over pore size and shape are the main disadvantages of this “bottom-up” approach.^[130,131]

Electrospinning stands out as a powerful method in creating porous membranes that resemble the fibrous architecture of natural ECM.^[132] Electrospinning is a versatile technique, which can be applied to virtually any polymer as well as many macromolecules, reshaping a rich library of materials into fibers with a diameter ranging from a few nanometers to micrometers. The nano/micro scale fibrous morphology of the scaffolds provides a unique high surface area to volume ratio,^[133] which is one of the main parameters that affects the surface area and overall porosity of the membranes, together with packing density. Intricate interplay between process and solvent parameters such as feeding rate, voltage, concentration and choice of solvents, enables control over the fiber size.^[132] In addition, membrane porosity can be further increased via salt

leaching^[134] and sacrificial polymers,^[135] whereas the packing density of fibrous membranes can be tailored via electrostatic repulsion^[136] and wet electrospinning.^[137] It should be noted that the choice of the material, e.g., hydrophobic/hydrophilic, is to be considered in the context of fiber morphology and permeability analysis, which will be addressed in more detail below.^[138] Manipulation of the shape of the electrospun fibers can be utilized to match the mechanical features, required by the lung-tissue models, such as stiffness and elasticity. Previously, lower packing density in electrospun fibers was reported to decrease the bulk stiffness of the membranes.^[139] Moreover, fabrication of coiled fibers allowed increased stretchability/extensibility compared to straight fibers and further contributed to the contraction of cardiomyocytes.^[140] Such mechanical actuation capacity may prove useful for the cyclic stress mimicry in vitro lung tissue models.

Furthermore, bioprinting technology engaging cells, growth factors, and biomaterials (synthetic and natural ECM) is another promising strategy to maximally mimic the alveolar-capillary tissue.

In the study that is first of its kind, Horvath et al. engineered an air–blood barrier via layer by layer bioprinting of endothelial and epithelial cells that are separated with a thin layer of Matrigel, which mimics the basement membrane in the native lung tissue.^[141] Both types of printed cells exhibited high viability and formed into thin confluent monolayers, which facilitated necessary cell–cell interactions. The authors suggested that the reproducible biofabrication of such air–blood barrier could serve as a high-throughput screening platform for safety assessment and drug efficacy testing. Recently, an even more applied study reported bioprinting of A549 cells into 3D cell-laden constructs.^[142] Once the printability, structural stability, and cell friendliness of the bioinks were established, the infection patterns were analyzed for a seasonal influenza A

strain.^[142] The authors concluded that the virus was distributed throughout the 3D printed structure and caused a clustered infection pattern that is comparable to the natural infection in the lung tissue, which cannot be replicated with traditional 2D cell culture models.

Bioprinting is a rapid production technique, which provides powerful control over the fabrication process and patterning. However, it is in an early technological phase of development and high-resolution cell patterning and distribution are among its main technical challenges. In addition, selecting a tunable biocompatible material is another concern for bioprinting to achieve an appropriate resolution in a scale of the air–blood barrier.^[143,144]

4.3. Material Selection

The type of material is another controlling factor of membrane features. Polymers are as the most widely used type of biomaterials because of their diversity in chemical groups, which allows fine-tuning of unique physical properties such as high surface-to-volume ratio, high porosity, and mechanical property.^[145,146] A wide variety of synthetic and natural-based materials and composite materials (natural–synthetic hybrids) has been employed to obtain a thin scaffold, which is appropriate for soft tissue applications (Table 4).

One of the most widely used synthetic-based materials is PCL which is a biodegradable, biocompatible, and bioresorbable polymer. PCL scaffold can be manufactured by various fabrication methods due to its breadths in rheological and viscoelastic properties.^[105] In addition to PCL, other synthetic-based polymers such as polyethylene terephthalate (PET) and^[147,148] PCU^[91] have been used to culture epithelial cells. Besides, PDS has been broadly used^[149–151] in tissue engineering applications as a biodegradable polymer with a relatively fast degradation rate. PDS shows enhancing cell infiltration and tissue regeneration when grafted with low-degradation rate polymers such as PCL in which large pore spaces created by degradation of PDS.^[106] Synthetic-based polymers have many advantages including suitable mechanical properties, tunable biodegradability, easy sourcing, great flexibility in synthesis and modification, and—last but not the least—low cost.

However, synthetic polymers lack cell affinity because of their low hydrophilicity and lack of surface cell recognition sites.^[152,153] To overcome this drawback, synthetic-based materials are often functionalized prior to biological use. Hydrophilicity can be enhanced via several ways including plasma and polyvinyl alcohol (PVA) treatment, chemical coupling of hydrophilic polymers either via copolymerization or surface grafting, surface patterning, and preparing hydrophobic/hydrophilic polymer blends.^[108,154] Membranes with appropriate hydrophilicity promote adsorption of ECM proteins, secreted from the seeded cells, without interfering with their functional/physiological conformation and thus render the scaffold bioactive.^[155,156] Direct inclusion of (natural) bioactive molecules offers the possibilities to overcome the lack of surface cell recognition sites in synthetic-based polymers. The most common bioactive molecules are ECM proteins, such as collagen (or gelatin as surrogate), laminin, fibronectin, and elastin or other protein-based

materials such as silk.^[108] Such natural polymers can provide better cell–matrix interactions and biocompatibility as compared to synthetic-based polymers. However, natural polymers tend to display poor processing ability, batch to batch variance and poor mechanical properties such as elasticity, stiffness, and durability.^[157] Although mechanical features of natural-based polymers can be improved with an additional crosslinking process,^[158] using membranes solely composed of natural-based polymers is likely not suitable for long-term culturing of cells under mechanically challenging conditions like cyclic stress.

Instead, natural/synthetic composite materials can be formulated to exploit bioactive features of biologic materials combined with tunable/stable mechanical features of synthetic-based polymers. In a recent study, an electrospun PCL/gelatin polymer blend was fabricated to mimic ECM and study the effect of ECM mechanics and topography on alveolar-capillary barrier permeability and cell injury during airway reopening.^[159] In this study, a nonbiological polymer (PCL) not only provided elasticity and mechanical durability, but also allowed for better control of membrane production (various PCL/gelatin mixtures yielded elastic modulus: 0.36–7.20 MPa) (Table 4). The manufactured membranes were used to study surface tension forces during airway reopening. Other natural–synthetic hybrid polymers such as PDS/gelatin/elastin,^[151] PLGA/gelatin/elastin,^[107] and collagen/poly(L-lactide-*co*-caprolactone) (P(LLA-CL))^[160] have shown good biocompatibility, mechanical properties, and other physical characteristics desirable for *in vitro* models of the alveolar-capillary membrane.

Alternatively, cell adhesion peptides derived from ECM proteins, such as RGD (arginylglycylaspartic acid) and IKVAV (isoleucine-lysine-valine-alanine-valine), can be immobilized on synthetic polymers to create selectively bioactivated synthetic membranes. Employing short peptide sequences rather than whole proteins offers tailor-made synthesis options and efficient/precise conjugation possibilities, which increase the overall impact of the functional epitopes.^[161,162] Although bioactive peptides can be directly blended with the polymers, chemical conjugation assures more reproducible and stable bioactivation. Among various conjugation methods, carbodiimide chemistry, Michael-addition, and photoinitiation based reactions are widely reported.^[163–165] It has also been demonstrated that covalent chemical coupling of peptides can be achieved *in situ* through the application of a reactive hydrophilic additive to hydrophobic polyesters in the spinning solution.^[166] Grafahrend et al.^[166] conjugated the cell adhesion peptide GRGDS to a reactive hydrophilic pre-polymer, NCO-sP(EO-stat-PO) (star-shaped poly(ethylene oxide-stat-propylene oxide) with isocyanate end groups) already in the solution that was used for electrospinning. Subsequent co-spinning of bioconjugated NCO-sP(EO-stat-PO) with PLGA rendered electrospun fibers hydrophilic, reduced the unspecific protein adsorption and cultivated strong cell–substrate adhesion. In a similar way, Rossi et al. fabricated electrospun membranes, which mimicked the bipolar structure of the basement membrane by conjugating ECM proteins (collagen IV, fibronectin, and laminin) to NCO-sP(EO-stat-PO). A bipolar membrane is then fabricated through subsequent spin-coating with solutions, bioconjugated with different ECM derived peptide sequences.^[167]

Bioactivated fibrous membranes supported the bipolar co-culture of keratinocytes and fibroblast, mimicking the basal and reticular side of the basement membrane. A similar approach can be utilized for capturing the bipolar structure of the pulmonary epithelial barrier. Most recently, this approach has been extended to combine ECM-peptide bioconjugation with the covalent immobilization of biochemically active molecules such as antibodies to combine selective cell adhesion with, in this case, immunomodulatory effects.^[168]

Furthermore, it has been shown that decellularized extracellular matrix (dECM) containing essential proteins for cell attachment and proliferation, could be a good candidate to improve the biocompatibility of copolymers.^[169,170] In a recent study, hybrid electrospun scaffold of poly-L-lactic acid and dECM (derived from pig lung) for in vitro ASM model showed that dECM improved physical characteristics (e.g., wettability).^[171]

PDMS is the most widely used membrane material for in vitro cell-stretching devices of the alveolar-capillary barrier (section 3). However, inadvertent adsorption of small molecules onto the surface of PDMS can affect cellular responses or prohibit drug transport studies. Copolymers (natural and synthetic-based) have been suggested to overcome the limitations of PDMS-based membranes. However, relatively few studies are available demonstrating successful cell culturing on these membranes both at the ALI and under cyclic mechanical stretch as encountered at the alveolar-capillary barrier.

In summary, it is evident that there is a need for development of alternative materials suitable for manufacturing a biocompatible, porous, thin, and stretchable membrane mimicking the physiologic parameters of the native basement membrane of the alveolar-capillary barrier. Moreover, the optimum choice of manufacturing method will also play a crucial role for obtaining the most biomimetic properties. The optimum material and processing techniques should ideally result in a final product that is not only bioactive enough to facilitate a fully confluent cell monolayer on the membrane, but also meet the high requirements on mechanical properties and chemical integrity for long-term studies with lung tissue models.

5. Future Directions: Biomimetic Models of the Lung

Currently, the vast majority of in vitro efficacy, toxicity, and pharmacokinetics studies of the lung are performed using static pulmonary cell models culturing a single cell type under submerged conditions.^[172,173] While this approach is well established, it often lacks predictive power for in vivo/clinical outcome due to nonphysiologic and simplistic cell model conditions and an unknown dose of the test substance delivered to the cells.^[7,67] Recent advances in biomimetic lung models include ALI culture conditions (polarization of epithelial cells at the ALI), apical coverage of epithelial cells with lung lining fluid (surfactant and alveolar lining fluid), and multiple-cell co-culture models providing more biomimetic barrier function (epithelial and endothelial cells), immune competence (dendritic cells), and clearance capability (macrophage and mucus).^[14,67] With the availability of commercial aerosol-cell delivery systems (e.g., VITROCELL CLOUD, Precise Inhale,

and CULTEX technology), an increasing number of studies employs aerosolized drug/substance delivery for more realistic pharmacokinetics and dose-response measurements.^[174] Any of these aspects enhances the biomimetic characteristics of in vitro cell models but depending on the endpoint of interest either all or only a subset of them may have to be included for adequate prediction of in vivo outcome. Unraveling the link between in vitro prediction of certain in vivo endpoints and the most suitable lung models will remain a field of intense research.

Moreover, there is also a trend toward microfluidic platforms of in vitro lung models offering the perspective of optimized process control, more efficient substance use, real-time monitoring systems via computer-control and automation ultimately leading to high-throughput capabilities.^[18] Analogous to standard cell culture systems and bioreactors, these micro-platforms are also able to mimic certain aspects of the pulmonary parenchymal environment such as epithelial-endothelial barrier, ALI, and mechanical stimulation induced by breathing and blood perfusion. However, these so-called lung-on-a-chip devices are often not easy to handle, provide a relatively small number of cells limiting the available amount of sample for biological (multiomics) analysis. This may at least partially explain why there are very few lab-on-a-chip devices commercially available, yet.

Notwithstanding even more advanced technologies are already pursued such as more complex 3D organ-specific cell structures representing functional organ units (organoids) and the integration of organ-specific chips/organoids into in vitro organism systems. Although these methods are still in an early stage, they hold the promise to overcome remaining shortcomings of current advanced in vitro models of the lung such as failure of fully mimicking the complexity of the 3D alveolar structure, the multicell interplay in the lung (~60 different cell types) and inter-organ connectedness via blood circulation.^[175,176]

In addition to these so-called bottom-up approaches, where biomimetic organ-specific models are built up from single-cell structures, also top-down approaches are available, where the lung (or a single lobe) is cut into smaller tissue slices.^[7] These ex vivo PCLS models, which can also be used under dynamic stretch conditions, represent a thin slice of the multicell 3D architecture of the lung which has been shown to maintain physiologic functions such as ciliary beating, macrophage migration, and response to, e.g., pro-inflammatory stimuli.^[177,178] Among other applications, PCLS have been used to study pathological and therapeutic measures of COPD/emphysema in lung tissue,^[82] and more recently to visualize the location and migration of different cell types in the lung tissue such as dendritic cells.^[179] Lung slices with a supportive layer such as PDMS have been exerted to cyclic mechanical stretch without causing cell injury.^[83] However, even this complex 3D multicell model of the lung can only partly reflect the properties of native lung tissue. For instance, it does not represent an intact epithelial-endothelial tissue barrier, ALI conditions as encountered in the lung and an intact immune system causing nonphysiological responses.^[180] Moreover, these top-down approaches still require the use of animals or donor organs, while bottom-up approaches bear the potential of animal free drug/toxicity testing.

All of these developments toward more biomimetic, miniaturized, and complex models of the lung will benefit from the implementation of cyclic mechanical stretch as one of the fundamental stimuli in the lung. Until now, commercially available cell-stretching devices have only been available for submerged, but not for more physiologic ALI cell culture conditions. The suggested technologies for cell-stretching under ALI conditions mainly rely on silicone-based membranes such as PDMS,^[181,182] which have plenty of advantages such as good compliance and permeability. However, due to the hydrophobic nature of PDMS, surface modifications or ECM protein coatings are required to enhance cell adhesion and biocompatibility.^[183,184] However, the hydrophobic nature of PDMS requires surface modifications such as coating with ECM proteins for adequate cell growth. But even then, multilayered or nonconfluent monolayered cell regions can often not be avoided.^[11] In spite of these efforts, PDMS membranes may adversely affect cellular response even for short-term studies (1 h)^[102] and silicone-based materials are known for their adsorptive nature and hence their potential bias when considering transmembrane transport of drugs and biomolecules.^[103,104] The latter is not the case for PET membranes implemented in the standard Transwell insert technology used for static ALI cell cultures. However, PET is not elastic and hence not suitable for mimicking cyclic stretch. Hence, neither PET nor silicone-based materials meet all of the requirements of a biomimetic basement membrane. In principle, the next generation of ALI cell culture membranes for even more physiologic *in vitro* models of the lung should also mimic the curvature of the alveolar epithelium (alveolar diameter: $\approx 250 \mu\text{m}$) and the interaction between cells and ECM.

As discussed above the essential characteristics of suitable basement membranes include porous architecture, dimension, biocompatibility, stiffness, and permeability. The physiologic parameter range of these parameters is summarized in Table 1. A thin (ideally $< 1 \mu\text{m}$) and porous membrane is required to mimic the structural and mechanical properties of the alveolar wall supporting growth and maintenance of an intact epithelial monolayer under ALI culture conditions. Thus, designed membranes should have sufficient elasticity, durability for long-term stretch in cell culture systems and act as cell substrate as well as allow for nutrient exchange between basal and apical compartment.

At this time, there is no widely accepted material meeting all of the physiologic requirements for the native basement membrane of the alveolar-capillary barrier (Table 1). However, there is evidence that rather than using a single material the application of hybrid copolymers may prove advantageous for representing all of the desired mechanical and biophysical properties. Among them, scaffolds obtained by PCL^[185,186] and P(LLA-CL)^[109] blended with natural-based polymers such as gelatin,^[159,187] collagen,^[160] and elastin^[188] showed a suitable porosity and surface hydrophilicity. Blends of PCL/natural polymers met the mechanical properties such as elasticity, reversible elongation and energy absorbed up to the elastic point reported for the basement membrane in the alveolar region. Other synthetic polymers such as P(LLA-CL) also showed appropriate mechanical properties for soft tissue applications.^[160,189,190] For instance, electrospun hybrid scaffolds of collagen/P(LLA-CL) has been used for application of cardiovascular tissue engineering.^[160] The hydrophilicity, biocompatibility, and

mechanical properties (Young's modulus: $1.77 \pm 0.09 \text{ MPa}$) of these hybrid materials make them promising membrane materials for lung models, although they have not been widely applied in lung research, yet. dECM-derived native lung tissue, a biomimetic mixture of natural ECM proteins, is another promising natural material because of its excellent biocompatibility features, although it does not have sufficiently biomimetic mechanical properties.^[170] As this deficiency can be compensated by hybridization with a synthetic polymer, several synthetic/dECM copolymers have been recently manufactured for tissue engineering application.^[191–193]

In addition to selecting a proper (composite) material, which fulfills the physiologic properties of the alveolar basement membrane, fabrication methods should also be considered. Electrospinning is a simple and cost-effective technique which enables control over the shape, thickness, architecture, and biophysical characteristics of the scaffold. A tunable porous structure with a high surface area to volume ratio, mimicking natural ECM in native tissues, can be manufactured within this method. However, poor cellular infiltration is still the main limitation of electrospun scaffolds, which can be improved somewhat when combined with other techniques such as phase separation and solvent casting.^[194,195]

Moreover, biofabrication is a young and vibrant field of research, which offers great potential for the generation of skin and lung tissue. This technique aims at the generation of biological functional tissue analogs either through an automated assembly of cell-containing building blocks, or by bioprinting of cells, biomaterials, and biologically active factors into 3D constructs.^[208] Bioprinting inherently requires a bioink, a cell-containing formulation that can be processed by a suitable technology.^[196,197] The design and application of bioinks have expanded greatly in the last decade, with numerous materials—primarily natural and synthetic hydrogels—being applied or developed to meet the stringent demands of bioprinting.^[198,199]

Recently, an endothelium-epithelium along with basement membrane has been fabricated using a layer-by-layer method in order to mimic the pulmonary air–blood tissue barrier.^[141] A 3D bioprinted tissue model employing cell-laden bioinks has been also used as a model for studying influenza infection in the lung.^[142] These examples clearly show the potential of biofabrication for the engineering of functional lung tissue. However, many challenges still need to be overcome, such as the development of materials and techniques that specifically suit lung cells forming the bipolar architecture of an air–blood barrier and providing mechanically tuned constructs that mimic the dynamic nature in native lung tissue.

6. Conclusions

Mechanical forces play a key role in proliferation, differentiation, function, and metabolism of lung cells. The main stretch-related regulatory pathways include the MAPK/ERK- and cAMP-PKA-dependent signaling pathways triggering differentiation of ATIIs as well as activation of YAP/TAZ and the signaling cascade of Cdc42/F-actin/MAPK controlling alveolar regeneration. The main stretch- and permeability-related physiologic parameters of the native basement membrane of the alveolar-capillary tissue

are the level of mechanical linear (1D) strain (4–12%; up to 20% under pathological conditions), elasticity (1–2 kPa), thickness (≈ 50 nm), and porosity (pore size < 2.5 nm) and total air-blood barrier thickness (≈ 0.6 μm). In addition to matching these biophysical conditions, suitable in vitro membranes for pulmonary cell-stretching also require biocompatibility, which includes wetability (WCA $< 70^\circ$) and conduciveness to cell growth.

Meeting all of these biophysical parameters in current in vitro systems is a challenge, which has not yet been fully accomplished. The currently available body of in vitro data on the effects of cyclic mechanical stretch on lung biology was almost exclusively obtained for nonphysiologic submerged cell culture conditions using nonporous silicon-based membranes (e.g., PDMS). Even the few currently proposed systems for pulmonary cell-stretching under more physiologic ALI culture conditions mainly rely on super-micron thick silicone membranes (even the microfluidic systems) with micron-sized pores. Moreover, silicone has well known material-specific deficiencies such as limited biocompatibility (requires surface treatment) and capturing of relevant biomolecules and potentially applied drug molecules, which poses serious limitations for drug efficacy and pharmacokinetics studies.

Our review of natural and synthetic-based polymers revealed that natural/artificial hybrid materials combine high biocompatibility (natural-based polymers) with favorable mechanical properties (artificial polymers) for soft tissue membrane applications such as alveolar tissue models. For the lung, PCL and P(LLA-CL) have been identified as appropriate synthetic-based polymer candidates, while collagen, dECM and gelatin may qualify as suitable natural-based polymer components. Further research into the exact ratio of natural–artificial copolymers is required to obtain the most suitable membrane for next generation, ALI, cell-stretching bioreactors of the lung.

Acknowledgements

The authors are grateful to Prof. Ewald Weibel for the electron microscopy images. S.T. is supported by a RESPIRE3 Postdoctoral Fellowship supported by the European Respiratory Society and the European Union's H2020 research and innovation programme under the Marie Skłodowska-Curie grant agreement (Grant No. 713406). The Knut and Alice Wallenberg foundation is acknowledged for generous support (DEW). This project has received funding from a European Research Council (ERC) Starting Grant (grant agreement No 805361) under the European Union's Horizon 2020 research and innovation programme (Grant No. 805361) (DEW). L.Y. was (partially) supported by China Scholarship Council (CSC, Grant No. 201506820008).

Conflict of Interest

The authors declare no conflict of interest.

Keywords

air–liquid interface cell culture, alveolar-capillary barrier, in vitro cell-stretching model, porous ultra-thin scaffolds, tunable polymeric membranes

Received: April 18, 2019

Revised: June 8, 2019

Published online:

- [1] U. Hatipoğlu, *Ann. Thorac. Med.* **2018**, *13*, 1.
- [2] R. Beasley, A. Semprini, E. A. Mitchell, *Lancet* **2015**, *386*, 1075.
- [3] S. M. May, J. T. C. Li, *Allergy Asthma Proc.* **2015**, *36*, 4.
- [4] C. A. Pope, M. Ezzati, D. W. Dockery, *N. Engl. J. Med.* **2009**, *360*, 376.
- [5] J. G. Muscedere, J. B. Mullen, K. Gan, A. S. Slutsky, *Am J. Respir. Crit. Care Med.* **1994**, *149*, 1327.
- [6] K. Zscheppang, J. Berg, S. Hedtrich, L. Verheyen, D. E. Wagner, N. Suttrop, S. Hippenstiel, A. C. Hocke, *Biotechnol. J.* **2018**, *13*, 1700341.
- [7] C. Darquenne, J. S. Fleming, I. Katz, A. R. Martin, J. Schroeter, O. S. Usmani, J. Venegas, O. Schmid, *J. Aerosol Med. Pulm. Drug Delivery* **2016**, *29*, 107.
- [8] D. J. Riley, D. E. Rannels, R. B. Low, L. Jensen, T. P. Jacobs, *Am. Rev. Respir. Dis.* **1990**, *142*, 910.
- [9] M. E. Chicurel, C. S. Chen, D. E. Ingber, *Curr. Opin. Cell Biol.* **1998**, *10*, 232.
- [10] M. Liu, J. Xu, P. Souza, B. Tanswell, A. K. Tanswell, M. Post, *In Vitro Cell. Dev. Biol.: Anim.* **1995**, *31*, 858.
- [11] H. R. Wirtz, L. G. Dobbs, *Respir. Physiol.* **2000**, *119*, 1.
- [12] X. Trepap, *Am. J. Physiol.: Lung Cell. Mol. Physiol.* **2006**, *290*, L1104.
- [13] X. Trepap, M. Grabulosa, F. Puig, G. N. Maksym, D. Navajas, R. Farré, *Am. J. Physiol.: Lung Cell. Mol. Physiol.* **2004**, *287*, L1025.
- [14] R. L. Heise, V. Stober, C. Chelvaraju, J. W. Hollingsworth, S. Garantzios, *J. Biol. Chem.* **2011**, *286*, 17435.
- [15] N. Gueven, B. Glatthaar, H.-G. Manke, H. Haemmerle, *Eur. Respir. J.* **1996**, *9*, 968.
- [16] K. A. Birkness, M. Deslauriers, J. H. Bartlett, E. H. White, C. H. King, F. D. Quinn, *Infect. Immun.* **1999**, *67*, 653.
- [17] T. H. Petersen, E. A. Calle, L. Zhao, E. J. Lee, L. Gui, M. B. Raredon, K. Gavrilov, T. Yi, Z. W. Zhuang, C. Breuer, E. Herzog, L. E. Niklason, *Science* **2010**, *329*, 538.
- [18] A. Doryab, G. Amoabediny, A. Salehi-Najafabadi, *Biotechnol. Adv.* **2016**, *34*, 588.
- [19] A. Doryab, M. Heydarian, G. Amoabediny, E. Sadroddiny, S. Mahfouzi, *J. Med. Biol. Eng.* **2017**, *37*, 53.
- [20] D. E. Gorman, T. Wu, S. E. Gilpin, H. C. Ott, *Tissue Eng., Part C* **2018**, *24*, 671.
- [21] A. Patwa, A. Shah, *Indian J. Anaesth.* **2015**, *59*, 533.
- [22] V. D. Varner, C. M. Nelson, *Development* **2014**, *141*, 2750.
- [23] B. Suki, S. Ito, D. Stamenović, K. R. Lutchen, E. P. Ingenito, *J. Appl. Physiol.* **2005**, *98*, 1892.
- [24] E. Roan, C. M. Waters, *Am. J. Physiol.: Lung Cell. Mol. Physiol.* **2011**, *301*, L625.
- [25] J. B. Forrest, *J. Physiol.* **1970**, *210*, 533.
- [26] J. J. Fredberg, R. D. Kamm, *Annu. Rev. Physiol.* **2006**, *68*, 507.
- [27] *Ann. ICRP* **1994**, *24*, 1.
- [28] C. M. Waters, E. Roan, D. Navajas, in *Comprehensive Physiology*, Vol. 33, John Wiley & Sons, Inc., Hoboken, NJ, USA **2012**, pp. 48–56.
- [29] O. T. Guenat, F. Berthiaume, *Biomicrofluidics* **2018**, *12*, 042207.
- [30] E. R. Weibel, *Respir. Physiol.* **1970**, *11*, 54.
- [31] A. Taylor, K. A. Gaar, *Am. J. Physiol.* **1970**, *218*, 1133.
- [32] P. N. Lanken, J. H. Hansen-Flaschen, P. M. Sampson, G. G. Pietra, F. R. Haselton, A. P. Fishman, *J. Appl. Physiol.* **1985**, *59*, 580.
- [33] C. Hermans, A. Bernard, *Eur. Respir. J.* **1998**, *11*, 801.
- [34] E. R. Weibel, *Swiss Med. Wkly.* **2009**, *139*, 375.
- [35] P. Gehr, M. Bachofen, E. R. Weibel, *Respir. Physiol.* **1978**, *32*, 121.
- [36] B. C. Goss, K. P. McGee, E. C. Ehman, A. Manduca, R. L. Ehman, *Magn. Reson. Med.* **2006**, *56*, 1060.
- [37] A. J. Booth, R. Hadley, A. M. Cornett, A. A. Dreffs, S. A. Matthes, J. L. Tsui, K. Weiss, J. C. Horowitz, V. F. Fiore, T. H. Barker, B. B. Moore, F. J. Martinez, L. E. Niklason, E. S. White, *Am J. Respir. Crit. Care Med.* **2012**, *186*, 866.

- [38] N. F. Jufri, A. Mohamedali, A. Avolio, M. S. Baker, *Vasc. Cell* **2015**, 7, 8.
- [39] C. M. Waters, M. R. Glucksberg, E. P. Lautenschlager, C.-W. Lee, R. M. Van Matre, R. J. Warp, U. Savla, K. E. Healy, B. Moran, D. G. Castner, J. P. Bearinger, *J. Appl. Physiol.* **2001**, 91, 1600.
- [40] L. P. Desai, K. E. Chapman, C. M. Waters, *Am. J. Physiol.: Lung Cell. Mol. Physiol.* **2008**, 295, L958.
- [41] U. Savla, C. M. Waters, *Am. J. Physiol.: Cell Physiol.* **1998**, 274, C883.
- [42] P. G. Smith, K. E. Janiga, M. C. Bruce, *Am. J. Respir. Cell Mol. Biol.* **1994**, 10, 85.
- [43] P. R. Chess, L. Toia, J. N. Finkelstein, *Am. J. Physiol.: Lung Cell. Mol. Physiol.* **2000**, 279, L43.
- [44] L. S. Chaturvedi, H. M. Marsh, M. D. Basson, *Am. J. Physiol.: Cell Physiol.* **2007**, 292, C1701.
- [45] J. Sanchez-Esteban, Y. Wang, P. A. Gruppuso, L. P. Rubin, *Am. J. Respir. Cell Mol. Biol.* **2004**, 30, 76.
- [46] Y. Wang, B. S. Maciejewski, N. Lee, O. Silbert, N. L. McKnight, J. A. Frangos, J. Sanchez-Esteban, *Am. J. Physiol.: Lung Cell. Mol. Physiol.* **2006**, 291, L820.
- [47] Z. Liu, H. Wu, K. Jiang, Y. Wang, W. Zhang, Q. Chu, J. Li, H. Huang, T. Cai, H. Ji, C. Yang, N. Tang, *Cell Rep.* **2016**, 16, 1810.
- [48] S. Piccolo, S. Dupont, M. Cordenonsi, *Physiol. Rev.* **2014**, 94, 1287.
- [49] C. C. dos Santos, B. Han, C. F. Andrade, X. Bai, S. Uhlig, R. Hubmayr, M. Tsang, M. Lodyga, S. Keshavjee, A. S. Slutsky, M. Liu, *Physiol. Genomics* **2004**, 19, 331.
- [50] O. Silbert, Y. Wang, B. S. Maciejewski, H. Lee, S. K. Shaw, J. Sanchez-Esteban, *Exp. Lung Res.* **2008**, 34, 663.
- [51] J. A. Gutierrez, R. F. Gonzalez, L. G. Dobbs, *Am. J. Physiol.* **1998**, 274, L196.
- [52] J. Xu, M. Liu, M. Post, *Am. J. Physiol.* **1999**, 276, L728.
- [53] S. P. Arold, E. Bartolák-Suki, B. Suki, *Am. J. Physiol.: Lung Cell. Mol. Physiol.* **2009**, 296, L574.
- [54] J. Sanchez-Esteban, L. a. Cicchiello, Y. Wang, S.-W. Tsai, L. K. Williams, J. S. Torday, L. P. Rubin, *J. Appl. Physiol.* **2001**, 91, 589.
- [55] H. R. Wirtz, L. G. Dobbs, *Science* **1990**, 250, 1266.
- [56] J. Sanchez-Esteban, S.-W. Tsai, J. Sang, J. Qin, J. S. Torday, L. P. Rubin, *Am. J. Med. Sci.* **1998**, 316, 200.
- [57] J. E. Scott, S.-Y. Yang, E. Stanik, J. E. Anderson, *Am. J. Respir. Cell Mol. Biol.* **1993**, 8, 258.
- [58] I. B. Copland, M. Post, *J. Cell. Physiol.* **2007**, 210, 133.
- [59] T. Nakamura, M. Liu, E. Mourgeon, A. Slutsky, M. Post, *Am. J. Physiol.: Lung Cell. Mol. Physiol.* **2000**, 278, L974.
- [60] A. O. Stucki, J. D. Stucki, S. R. R. Hall, M. Felder, Y. Mermoud, R. A. Schmid, T. Geiser, O. T. Guenat, *Lab Chip* **2015**, 15, 1302.
- [61] Y. S. Edwards, L. M. Sutherland, J. H. Power, T. E. Nicholas, A. W. Murray, *FEBS Lett.* **1999**, 448, 127.
- [62] S. Hammerschmidt, H. Kuhn, T. Grasenack, C. Gessner, H. Wirtz, *Am. J. Respir. Cell Mol. Biol.* **2004**, 30, 396.
- [63] N. E. Vlahakis, M. A. Schroeder, A. H. Limper, R. D. Hubmayr, *Am. J. Physiol.: Lung Cell. Mol. Physiol.* **1999**, 277, L167.
- [64] S. Ghadiali, Y. Huang, *Crit. Rev. Bioeng.* **2011**, 39, 297.
- [65] B. Suki, D. Stamenovic, in *Comprehensive Physiology*, Vol. 1, John Wiley & Sons, Inc., Hoboken, NJ, USA **2011**, pp. 1317–1351.
- [66] M. Liu, A. K. Tanswell, M. Post, *Am. J. Physiol.: Lung Cell. Mol. Physiol.* **1999**, 277, L667.
- [67] H.-R. Paur, F. R. Cassee, J. Teeguarden, H. Fissan, S. Diabate, M. Aufderheide, W. G. Kreyling, O. Hänninen, G. Kasper, M. Riediker, B. Rothen-Rutishauser, O. Schmid, *J. Aerosol Sci.* **2011**, 42, 668.
- [68] O. Schmid, F. R. Cassee, *Part. Fibre Toxicol.* **2017**, 14, 52.
- [69] A. Lenz, E. Karg, B. Lentner, V. Dittrich, C. Brandenberger, B. Rothen-Rutishauser, H. Schulz, G. A. Ferron, O. Schmid, *Part. Fibre Toxicol.* **2009**, 6, 32.
- [70] B. M. Rothen-Rutishauser, S. G. Kiama, P. Gehr, *Am. J. Respir. Cell Mol. Biol.* **2005**, 32, 281.
- [71] S. J. M. Skinner, *Adv. Fetal Physiol.* **1989**, 8, 133.
- [72] M. Liu, S. J. Skinner, J. Xu, R. N. Han, A. K. Tanswell, M. Post, *Am. J. Physiol.: Lung Cell. Mol. Physiol.* **1992**, 263, L376.
- [73] M. Liu, S. Montazeri, T. Jedlovsky, R. van Wert, J. Zhang, R.-K. Li, J. Yan, *In Vitro Cell. Dev. Biol.: Anim.* **1999**, 35, 87.
- [74] S. J. M. Skinner, C. E. Somervell, D. M. Olson, *Prostaglandins* **1992**, 43, 413.
- [75] D. J. Tschumperlin, S. S. Margulies, *Am. J. Physiol.: Lung Cell. Mol. Physiol.* **1998**, 275, L1173.
- [76] C. M. Waters, K. M. Ridge, G. Sunio, K. Venetsanou, J. I. Sznajder, *J. Appl. Physiol.* **1999**, 87, 715.
- [77] F. Rose, K. Zwick, H. A. Ghofrani, U. Sibelius, W. Seeger, D. Walmrath, M. Grimminger, *Am. J. Respir. Crit. Care Med.* **1999**, 160, 846.
- [78] D. J. Tschumperlin, J. Oswari, A. S. S. Margulies, *Am. J. Respir. Crit. Care Med.* **2000**, 162, 357.
- [79] S. Ito, B. Suki, H. Kume, Y. Numaguchi, M. Ishii, M. Iwaki, M. Kondo, K. Naruse, Y. Hasegawa, M. Sokabe, *Am. J. Respir. Cell Mol. Biol.* **2010**, 43, 26.
- [80] S. Ito, H. Kume, K. Naruse, M. Kondo, N. Takeda, S. Iwata, Y. Hasegawa, M. Sokabe, *Am. J. Respir. Cell Mol. Biol.* **2008**, 38, 407.
- [81] A. Bergner, M. J. Sanderson, *Am. J. Physiol.: Lung Cell. Mol. Physiol.* **2002**, 283, L1271.
- [82] F. E. Uhl, S. Vierkotten, D. E. Wagner, G. Burgstaller, R. Costa, I. Koch, M. Lindner, S. Meiners, O. Eickelberg, M. Königshoff, *Eur. Respir. J.* **2015**, 46, 1150.
- [83] C. Dassow, L. Wiechert, C. Martin, S. Schumann, G. Müller-Newen, O. Pack, J. Guttman, W. A. Wall, S. Uhlig, *J. Appl. Physiol.* **2010**, 108, 713.
- [84] A. R. Froese, C. Shimbori, P. S. Bellaye, M. Inman, S. Obex, S. Fatima, G. Jenkins, J. Gaudie, K. Ask, M. Kolb, *Am. J. Respir. Crit. Care Med.* **2016**, 194, 84.
- [85] A.-G. Lenz, E. Karg, E. Brendel, H. Hinze-Heyn, K. L. Maier, O. Eickelberg, T. Stoeger, O. Schmid, *Biomed Res. Int.* **2013**, 2013, 652632.
- [86] A.-G. Lenz, T. Stoeger, D. Cei, M. Schmidmeir, N. Semren, G. Burgstaller, B. Lentner, O. Eickelberg, S. Meiners, O. Schmid, *Am. J. Respir. Cell Mol. Biol.* **2014**, 51, 526.
- [87] D. T. Butcher, T. Alliston, V. M. Weaver, *Nat. Rev. Cancer* **2009**, 9, 108.
- [88] R. Pörtner, S. Nagel-Heyer, C. Goepfert, P. Adamietz, N. M. Meenen, *J. Biosci. Bioeng.* **2005**, 100, 235.
- [89] B. J. Lawrence, M. Devarapalli, S. V. Madhally, *Biotechnol. Bioeng.* **2009**, 102, 935.
- [90] H.-C. Chen, Y.-C. Hu, *Biotechnol. Lett.* **2006**, 28, 1415.
- [91] D. Cei, *Ph.D. Thesis*, University of Pisa, **2015**.
- [92] D. Huh, G. A. Hamilton, D. E. Ingber, *Trends Cell Biol.* **2011**, 21, 745.
- [93] D. D. Nalayanda, C. Puleo, W. B. Fulton, L. M. Sharpe, T.-H. Wang, F. Abdullah, *Biomed. Microdevices* **2009**, 11, 1081.
- [94] D. Huh, B. D. Matthews, A. Mammoto, M. Montoya-Zavala, H. Y. Hsin, D. E. Ingber, *Science* **2010**, 328, 1662.
- [95] A. Jain, R. Barrile, A. van der Meer, A. Mammoto, T. Mammoto, K. De Ceunynck, O. Aisiku, M. Otieno, C. Louden, G. Hamilton, R. Flaumenhaft, D. Ingber, *Clin. Pharmacol. Ther.* **2018**, 103, 332.
- [96] N. Campillo, I. Jorba, L. Schaedel, B. Casals, D. Gozal, R. Farré, I. Almendros, D. Navajas, *Front. Physiol.* **2016**, 7, 1.
- [97] J. P. Vande Geest, E. S. Di Martino, D. A. Vorp, *J. Biomech.* **2004**, 37, 1923.
- [98] Y. Mermoud, M. Felder, J. D. Stucki, A. O. Stucki, O. T. Guenat, *Sens. Actuators, B* **2018**, 255, 3647.
- [99] J. D. Stucki, N. Hobi, A. Galimov, A. O. Stucki, N. Schneider-Daum, C.-M. Lehr, H. Huwer, M. Frick, M. Funke-Chambour, T. Geiser, O. T. Guenat, *Sci. Rep.* **2018**, 8, 14359.

- [100] M. Felder, B. Trueeb, A. O. Stucki, S. Borcard, J. D. Stucki, B. Schnyder, T. Geiser, O. T. Guenat, *Front. Bioeng. Biotechnol.* **2019**, *7*, 1.
- [101] Z. Wang, A. A. Volinsky, N. D. Gallant, *J. Appl. Polym. Sci.* **2014**, *131*, 41050.
- [102] E. Berthier, E. W. K. Young, D. Beebe, *Lab Chip* **2012**, *12*, 1224.
- [103] K. J. Regehr, M. Domenech, J. T. Koepsel, K. C. Carver, S. J. Ellison-Zelski, W. L. Murphy, L. A. Schuler, E. T. Alarid, D. J. Beebe, *Lab Chip* **2009**, *9*, 2132.
- [104] M. W. Toepke, D. J. Beebe, *Lab Chip* **2006**, *6*, 1484.
- [105] A. Cipitria, A. Skelton, T. R. Dargaville, P. D. Dalton, D. W. Huttmacher, *J. Mater. Chem.* **2011**, *21*, 9419.
- [106] Y. Pan, X. Zhou, Y. Wei, Q. Zhang, T. Wang, M. Zhu, W. Li, R. Huang, R. Liu, J. Chen, G. Fan, K. Wang, D. Kong, Q. Zhao, *Sci. Rep.* **2017**, *7*, 3615.
- [107] J. Han, P. Lazarovici, C. Pomerantz, X. Chen, Y. Wei, P. I. Lelkes, *Biomacromolecules* **2011**, *12*, 399.
- [108] H. S. Yoo, T. G. Kim, T. G. Park, *Adv. Drug Delivery Rev.* **2009**, *61*, 1033.
- [109] S. Chung, N. P. Ingle, G. A. Montero, S. H. Kim, M. W. King, *Acta Biomater.* **2010**, *6*, 1958.
- [110] U. Hersel, C. Dahmen, H. Kessler, *Biomaterials* **2003**, *24*, 4385.
- [111] S. Sano, K. Kato, Y. Ikada, *Biomaterials* **1993**, *14*, 817.
- [112] R. Vasita, G. Mani, C. M. Agrawal, D. S. Katti, *Polymer* **2010**, *51*, 3706.
- [113] A. Khademhosseini, R. Langer, *Biomaterials* **2007**, *28*, 5087.
- [114] M. Mader, V. Jérôme, R. Freitag, S. Agarwal, A. Greiner, *Biomacromolecules* **2018**, *19*, 1663.
- [115] C. J. E. Wahlund, A. Eklund, J. Grunewald, S. Gabrielsson, *Front. Cell Dev. Biol.* **2017**, *5*, 39.
- [116] Y. Lee, S. EL Andaloussi, M. J. A. Wood, *Hum. Mol. Genet.* **2012**, *21*, R125.
- [117] M. Mulder, *Basic Principles of Membrane Technology*, Springer Netherlands, Dordrecht **1996**.
- [118] J.-M. Anaya, Y. Shoenfeld, A. Rojas-Villarraga, R. A. Levy, R. Cervera, *Autoimmunity: From Bench to Bedside*, El Rosario University Press, Bogota, Colombia **2013**.
- [119] M. P. Tibbe, A. D. van der Meer, A. van den Berg, D. Stamatialis, L. I. Segerink, in *Biomedical Membranes and (Bio)Artificial Organs*, World Scientific, USA **2018**, pp. 295–321.
- [120] Y. Shao, J. Fu, *Adv. Mater.* **2014**, *26*, 1494.
- [121] T. Pasman, D. W. Grijpma, D. F. Stamatialis, A. A. Poot, *Polym. Adv. Technol.* **2017**, *28*, 1258.
- [122] P. Sofokleous, M. H. W. Chin, R. Day, in *Functional 3D Tissue Engineering Scaffolds*, Woodhead Publishing, Sawston, Cambridge **2018**, pp. 101–126.
- [123] G. Toskas, S. Heinemann, C. Heinemann, C. Cherif, R.-D. Hund, V. Roussis, T. Hanke, *Carbohydr. Polym.* **2012**, *89*, 997.
- [124] W. Sun, G. Chen, F. Wang, Y. Qin, Z. Wang, J. Nie, G. Ma, *Carbohydr. Polym.* **2018**, *181*, 183.
- [125] K. M. Z. Hossain, R. M. Felfel, P. S. Ogbilikana, D. Thakker, D. M. Grant, C. A. Scotchford, I. Ahmed, *Macromol. Mater. Eng.* **2018**, *303*, 1700628.
- [126] H. Li, Y. Xu, H. Xu, J. Chang, *J. Mater. Chem. B* **2014**, *2*, 5492.
- [127] V. Beachley, X. Wen, *Prog. Polym. Sci.* **2010**, *35*, 868.
- [128] U. G. T. M. Sampath, Y. C. Ching, C. H. Chuah, J. J. Sabariah, P. C. Lin, *Materials* **2016**, *9*, 991.
- [129] V. Raeisdasteh Hokmabad, S. Davaran, A. Ramazani, R. Salehi, *J. Biomater. Sci., Polym. Ed.* **2017**, *28*, 1797.
- [130] S. Zhang, *Nat. Biotechnol.* **2003**, *21*, 1171.
- [131] D. Puppi, X. Zhang, L. Yang, F. Chiellini, X. Sun, E. Chiellini, *J. Biomed. Mater. Res., Part B* **2014**, *102*, 1562.
- [132] S. Agarwal, J. H. Wendorff, A. Greiner, *Adv. Mater.* **2009**, *21*, 3343.
- [133] N. Bhardwaj, S. C. Kundu, *Biotechnol. Adv.* **2010**, *28*, 325.
- [134] J. Nam, Y. Huang, S. Agarwal, J. Lannutti, *Tissue Eng.* **2007**, *13*, 2249.
- [135] B. M. Baker, R. P. Shah, A. M. Silverstein, J. L. Esterhai, J. A. Burdick, R. L. Mauck, *Proc. Natl. Acad. Sci. USA* **2012**, *109*, 14176.
- [136] B. Sun, Y.-Z. Long, F. Yu, M.-M. Li, H.-D. Zhang, W.-J. Li, T.-X. Xu, *Nanoscale* **2012**, *4*, 2134.
- [137] M. S. Kim, G. H. Kim, *Mater. Lett.* **2014**, *120*, 246.
- [138] A. Schneider, X. Y. Wang, D. L. Kaplan, J. A. Garlick, C. Egles, *Acta Biomater.* **2009**, *5*, 2570.
- [139] M. B. Taskin, R. Xu, H. Gregersen, J. V. Nygaard, F. Besenbacher, M. Chen, *ACS Appl. Mater. Interfaces* **2016**, *8*, 15864.
- [140] S. Fleischer, R. Feiner, A. Shapira, J. Ji, X. Sui, H. Daniel Wagner, T. Dvir, *Biomaterials* **2013**, *34*, 8599.
- [141] L. Horvath, Y. Umehara, C. Jud, F. Blank, A. Petri-Fink, B. Rothen-Rutishauser, L. Horváth, Y. Umehara, C. Jud, F. Blank, A. Petri-Fink, B. Rothen-Rutishauser, *Sci. Rep.* **2015**, *5*, 7974.
- [142] J. Berg, T. Hiller, M. S. Kissner, T. H. Qazi, G. N. Duda, A. C. Hocke, S. Hippenstiel, L. Elomaa, M. Weinhart, C. Fahrenson, J. Kurreck, *Sci. Rep.* **2018**, *8*, 1.
- [143] C. Mandrycky, Z. Wang, K. Kim, D. Kim, *Biotechnol. Adv.* **2016**, *34*, 422.
- [144] S. Derakhshanfar, R. Mbeleck, K. Xu, X. Zhang, W. Zhong, M. Xing, *Bioact. Mater.* **2018**, *3*, 144.
- [145] V. K. Vendra, L. Wu, S. Krishnan, in *Nanotechnologies for the Life Sciences*, Vol. 5, Wiley-VCH Verlag GmbH & Co. KGaA: Weinheim, Germany **2011**.
- [146] B. Dhandayuthapani, Y. Yoshida, T. Maekawa, D. S. Kumar, *Int. J. Polym. Sci.* **2011**, *2011*, 1.
- [147] G. E. Morris, J. C. Bridge, L. A. Brace, A. J. Knox, J. W. Aylott, C. E. Brightling, A. M. Ghaemmaghami, F. R. A. J. A. J. Rose, *Biofabrication* **2014**, *6*, 035014.
- [148] H. Harrington, P. Cato, F. Salazar, M. Wilkinson, A. Knox, J. W. Haycock, F. Rose, J. W. Aylott, A. M. Ghaemmaghami, *Mol. Pharmaceutics* **2014**, *11*, 2082.
- [149] J. A. Ray, N. Doddi, D. Regula, J. A. Williams, A. Melveger, *Surg., Gynecol. Obstet.* **1981**, *153*, 497.
- [150] S. A. Sell, M. J. McClure, C. P. Barnes, D. C. Knapp, B. H. Walpoth, D. G. Simpson, G. L. Bowlin, *Biomed. Mater.* **2006**, *1*, 72.
- [151] V. Thomas, X. Zhang, Y. K. Vohra, *Biotechnol. Bioeng.* **2009**, *104*, 1025.
- [152] R. Shi, J. Xue, H. Wang, R. Wang, M. Gong, D. Chen, L. Zhang, W. Tian, *J. Mater. Chem. B* **2015**, *3*, 4063.
- [153] I. J. Hall Barrientos, E. Paladino, P. Szabó, S. Brozio, P. J. Hall, C. I. Oseghale, M. K. Passarelli, S. J. Moug, R. A. Black, C. G. Wilson, R. Zelkó, D. A. Lamprou, *Int. J. Pharm.* **2017**, *531*, 67.
- [154] S. K. Nemani, R. K. Annavarapu, B. Mohammadian, A. Raiyan, J. Heil, M. A. Haque, A. Abdelaal, H. Sojoudi, *Adv. Mater. Interfaces* **2018**, *5*, 1801247.
- [155] A. J. García, M. D. Vega, D. Boettiger, *Mol. Biol. Cell* **1999**, *10*, 785.
- [156] M. Rabe, D. Verdes, S. Seeger, *Adv. Colloid Interface Sci.* **2011**, *162*, 87.
- [157] X. Wang, B. Ding, B. Li, *Mater. Today* **2013**, *16*, 229.
- [158] N. Reddy, R. Reddy, Q. Jiang, *Trends Biotechnol.* **2015**, *33*, 362.
- [159] N. Higuera-Castro, M. T. Nelson, V. Shukla, P. A. Agudelo-Garcia, W. Zhang, S. M. Duarte-Sanmiguel, J. A. Englert, J. J. Lannutti, D. J. Hansford, S. N. Ghadiali, *Sci. Rep.* **2017**, *7*, 11623.
- [160] W. Fu, Z. Liu, B. Feng, R. Hu, X. He, H. Wang, M. Yin, H. Huang, H. Zhang, W. Wang, *Int. J. Nanomed.* **2014**, *9*, 2335.
- [161] M. P. Lutolf, J. A. Hubbell, *Nat. Biotechnol.* **2005**, *23*, 47.
- [162] A. Shekaran, A. J. Garcia, *Biochim. Biophys. Acta, Gen. Subj.* **2011**, *1810*, 350.
- [163] X. Ren, Y. Feng, J. Guo, H. Wang, Q. Li, J. Yang, X. Hao, J. Lv, N. Ma, W. Li, *Chem. Soc. Rev.* **2015**, *44*, 5680.
- [164] J. R. J. Paletta, S. Bockelmann, A. Walz, C. Theisen, J. H. Wendorff, A. Greiner, S. Fuchs-Winkelmann, M. D. Schofer, *J. Mater. Sci.: Mater. Med.* **2010**, *21*, 1363.

- [165] J. Li, M. Ding, Q. Fu, H. Tan, X. Xie, Y. Zhong, *J. Mater. Sci.: Mater. Med.* **2008**, *19*, 2595.
- [166] D. Grafahrend, K.-H. Heffels, M. V. Beer, P. Gasteier, M. Möller, G. Boehm, P. D. Dalton, J. Groll, *Nat. Mater.* **2011**, *10*, 67.
- [167] A. Rossi, L. Wistlich, K.-H. Heffels, H. Walles, J. Groll, *Adv. Healthcare Mater.* **2016**, *5*, 1939.
- [168] L. Wistlich, J. Kums, A. Rossi, K.-H. Heffels, H. Wajant, J. Groll, *Adv. Funct. Mater.* **2017**, *27*, 1702903.
- [169] D. E. Wagner, N. R. Bonenfant, D. Sokocevic, M. J. DeSarno, Z. D. Borg, C. S. Parsons, E. M. Brooks, J. J. Platz, Z. I. Khalpey, D. M. Hoganson, B. Deng, Y. W. Lam, R. A. Oldinski, T. Ashikaga, D. J. Weiss, *Biomaterials* **2014**, *35*, 2664.
- [170] M. M. De Santis, D. A. Bölükbas, S. Lindstedt, D. E. Wagner, *Eur. Respir. J.* **2018**, *52*, 1601355.
- [171] B. M. Young, K. Shankar, B. P. Allen, R. A. Pouliot, M. B. Schneck, N. S. Mikhael, R. L. Heise, *ACS Biomater. Sci. Eng.* **2017**, *3*, 3480.
- [172] C. Monteiller, L. Tran, W. MacNee, S. Faux, A. Jones, B. Miller, K. Donaldson, *Occup. Environ. Med.* **2007**, *64*, 609.
- [173] A. Martin, A. Sarkar, *Nanotoxicology* **2017**, *11*, 1.
- [174] O. Schmid, C. Jud, Y. Umehara, D. Mueller, A. Bucholski, F. Gruber, O. Denk, R. Egle, A. Petri-Fink, B. Rothen-Rutishauser, *J. Aerosol Med. Pulm. Drug Delivery* **2017**, *30*, 411.
- [175] J.-P. Ng-Blichfeldt, A. Schrik, R. K. Kortekaas, J. A. Noordhoek, I. H. Heijink, P. S. Hiemstra, J. Stolk, M. Königshoff, R. Gosens, *EBioMedicine* **2018**, *36*, 461.
- [176] B. R. Dye, D. R. Hill, M. A. H. Ferguson, Y. Tsai, M. S. Nagy, R. Dyal, J. M. Wells, C. N. Mayhew, R. Nattiv, O. D. Klein, E. S. White, G. H. Deutsch, J. R. Spence, *eLife* **2015**, *4*, e05098.
- [177] M. Henjakovic, K. Sewald, S. Switalla, D. Kaiser, M. Müller, T. Z. Veres, C. Martin, S. Uhlig, N. Krug, A. Braun, *Toxicol. Appl. Pharmacol.* **2008**, *231*, 68.
- [178] P. Delmotte, M. J. Sanderson, *Am. J. Respir. Cell Mol. Biol.* **2006**, *35*, 110.
- [179] M. R. Lyons-Cohen, S. Y. Thomas, D. N. Cook, H. Nakano, *J. Vis. Exp.* **2017**, *122*, e55465.
- [180] H. N. Alsafadi, C. A. Staab-Weijnitz, M. Lehmann, M. Lindner, B. Peschel, M. Königshoff, D. E. Wagner, *Am. J. Physiol.: Lung Cell. Mol. Physiol.* **2017**, *312*, L896.
- [181] B. Zhang, M. Radisic, *Lab Chip* **2017**, *17*, 2395.
- [182] H. Kamble, M. J. Barton, M. Jun, S. Park, N. T. Nguyen, *Lab Chip* **2016**, *16*, 3193.
- [183] P. Hamerli, *Biomaterials* **2003**, *24*, 3989.
- [184] K. L. Sellgren, E. J. Butala, B. P. Gilmour, S. H. Randell, S. Grego, *Lab Chip* **2014**, *14*, 3349.
- [185] S. Sharma, S. Mohanty, D. Gupta, M. Jassal, A. K. Agrawal, R. Tandon, *Mol. Vision* **2011**, *17*, 2898.
- [186] A. Elamparithi, A. M. Punnoose, S. Kuruvilla, M. Ravi, S. Rao, S. F. D. Paul, *Artif. Cells, Nanomed., Biotechnol.* **2016**, *44*, 878.
- [187] K. Wang, X. Chen, Y. Pan, Y. Cui, X. Zhou, D. Kong, Q. Zhao, *Biomed Res. Int.* **2015**, *2015*, 1.
- [188] S. G. Wise, M. J. Byrom, A. Waterhouse, P. G. Bannon, M. K. C. Ng, A. S. Weiss, *Acta Biomater.* **2011**, *7*, 295.
- [189] C. P. Laurent, C. Vaquette, X. Liu, J.-F. Schmitt, R. Rahouadj, *J. Biomater. Appl.* **2018**, *32*, 1276.
- [190] Y. Zhu, M. Leong, W. Ong, M. Chanpark, K. Chian, *Biomaterials* **2007**, *28*, 861.
- [191] F. Pati, T.-H. Song, G. Rijal, J. Jang, S. W. Kim, D.-W. Cho, *Biomaterials* **2015**, *37*, 230.
- [192] J. Liao, X. Guo, K. J. Grande-Allen, F. K. Kasper, A. G. Mikos, *Biomaterials* **2010**, *31*, 8911.
- [193] E. Lih, K. W. Park, S. Y. Chun, H. Kim, T. G. Kwon, Y. K. Joung, D. K. Han, *ACS Appl. Mater. Interfaces* **2016**, *8*, 21145.
- [194] A. Burgess, K. Shah, O. Hough, K. Hynynen, *Expert Rev. Neurother.* **2015**, *15*, 477.
- [195] K. Wang, M. Zhu, T. Li, W. Zheng, L. Li, M. Xu, Q. Zhao, D. Kong, L. Wang, *J. Biomed. Nanotechnol.* **2014**, *10*, 1588.
- [196] J. Groll, J. A. Burdick, D. Cho, B. Derby, M. Gelinsky, S. C. Heilshorn, T. Jüngst, J. Malda, V. A. Mironov, K. Nakayama, A. Ovsianikov, W. Sun, S. Takeuchi, J. J. Yoo, T. B. F. Woodfield, *Biofabrication* **2018**, *11*, 013001.
- [197] L. Moroni, T. Boland, J. A. Burdick, C. De Maria, B. Derby, G. Forgacs, J. Groll, Q. Li, J. Malda, V. A. Mironov, C. Mota, M. Nakamura, W. Shu, S. Takeuchi, T. B. F. Woodfield, T. Xu, J. J. Yoo, G. Vozzi, *Trends Biotechnol.* **2018**, *36*, 384.
- [198] J. Malda, J. Visser, F. P. Melchels, T. Jüngst, W. E. Hennink, W. J. A. Dhert, J. Groll, D. W. Huttmacher, *Adv. Mater.* **2013**, *25*, 5011.
- [199] T. Jungst, W. Smolan, K. Schacht, T. Scheibel, J. Groll, *Chem. Rev.* **2016**, *116*, 1496.
- [200] E. Correa-Meyer, L. Pesce, C. Guerrero, J. I. Sznajder, *Am. J. Physiol.: Lung Cell. Mol. Physiol.* **2002**, *282*, L883.
- [201] K. J. Cavanaugh, T. S. Cohen, S. S. Margulies, *Am. J. Physiol.: Cell Physiol.* **2006**, *290*, C1179.
- [202] L. Yang, A. Feuchtinger, W. Möller, Y. Ding, D. Kutsche, G. Möller, J. C. Schittny, G. Burgstaller, W. Hofmann, T. Stoeger, Daniel Razansky, A. Walch, O. Schmid, *ACS Nano* **2019**, *13*, 1029.
- [203] E. R. Weibel, in *Comprehensive Physiology*, John Wiley & Sons, Inc., Hoboken, NJ, USA **2011**.
- [204] J. Sanchez-esteban, Y. Wang, E. J. Filardo, L. P. Rubin, D. E. Ingber, Y. Wang, E. J. Filardo, L. P. Rubin, D. E. I. Integrins, *Am. J. Physiol. Lung Cell. Mol. Physiol.* **2006**, *290*, L343.
- [205] S. P. Arold, J. Y. Wong, B. Suki, *Ann. Biomed. Eng.* **2007**, *35*, 1156.
- [206] N. J. Douville, P. Zamankhan, Y.-C. Tung, R. Li, B. L. Vaughan, C.-F. Tai, J. White, P. J. Christensen, J. B. Grotberg, S. Takayama, *Lab Chip* **2011**, *11*, 609.
- [207] Z. Huang, Y. Wang, P. S. Nayak, C. E. Dammann, J. Sanchez-Esteban, *J. Biol. Chem.* **2012**, *287*, 18091.
- [208] Y. Wang, Z. Huang, P. S. Nayak, B. D. Matthews, D. Warburton, W. Shi, J. Sanchez-Esteban, *J. Biol. Chem.* **2013**, *288*, 25646.
- [209] J. A. Gilbert, P. S. Weinhold, A. J. Banes, G. W. Link, G. L. Jones, *J. Biomech.* **1994**, *27*, 1169.
- [210] J. E. Anderson, E. Yen, R. S. Carvalho, J. E. Scott, *In Vitro Cell. Dev. Biol. – Anim.* **1993**, *29*, 183.
- [211] R. Sreenivasan, E. K. Bassett, D. M. Hoganson, J. P. Vacanti, K. K. Gleason, *Biomaterials* **2011**, *32*, 3883.
- [212] T. V. Chirila, Z. Barnard, Zainuddin, D. G. Harkin, I. R. Schwab, L. W. Hirst, *Tissue Eng., Part A* **2008**, *14*, 1203.
- [213] J. A. Matthews, G. E. Wnek, D. G. Simpson, G. L. Bowlin, *Biomacromolecules* **2002**, *3*, 232.
- [214] G. E. Wnek, M. E. Carr, D. G. Simpson, G. L. Bowlin, *Nano Lett.* **2003**, *3*, 213.
- [215] A. Nishiguchi, S. Singh, M. Wessling, C. J. Kirkpatrick, M. Möller, *Biomacromolecules* **2017**, *18*, 719.
- [216] S. Hinderer, J. Seifert, M. Votteler, N. Shen, J. Rheinlaender, T. E. Schäffer, K. Schenke-Layland, *Biomaterials* **2014**, *35*, 2130.
- [217] M. Frydrych, S. Román, S. MacNeil, B. Chen, *Acta Biomater.* **2015**, *18*, 40.
- [218] R. M. Aghdam, S. Najarian, S. Shakhshi, S. Khanlari, K. Shaabani, S. Sharifi, *J. Appl. Polym. Sci.* **2012**, *124*, 123.
- [219] Y. Qian, L. Li, C. Jiang, W. Xu, Y. Lv, L. Zhong, K. Cai, L. Yang, *Int. J. Biol. Macromol.* **2015**, *79*, 133.
- [220] L. Tayebi, M. Rasoulianboroujeni, K. Moharamzadeh, T. K. D. Almela, Z. Cui, H. Ye, *Mater. Sci. Eng., C* **2018**, *84*, 148.

Acknowledgements

As Persian poet *Rumi* said, “*everyone who is left far from his source wishes back the time when he was united with it*”. I started my academic carrier with material science and engineering and after learning more about biomedical engineering, I conducted my Ph.D. project in the field of biomaterials engineering. It was a long journey and I would share my deepest gratitude to my mentors and supervisors during the last almost 13 years of my education and research.

First of all, I wish to express my sincere appreciation to my mentor and supervisor, Dr. Otmar Schmid, who supported and helped me not only in science and research but also in my personal life. I experienced with him the joy of science and life. His persistent support as well as mentorship assisted me to find always the best way in my research. I value the insights and guidance he provided. Otmar, you were a fundamental part of me being able to get it done.

I am also grateful to my Ph.D. committee, PD Dr. med. Anne Hilgendorff and Prof. Dr. Markus Rehberg. I couldn't be more thankful to have you on my PhD committee. Every time that we had a TAC meeting, your inputs were valuable for moving my project forward in the right direction.

I would like to say my greatest thanks to our external collaborators at the University of Würzburg, Prof. Dr. Jürgen Groll, Dr. Berat Taskin, and Philipp Stahlhut. Without your support, I wouldn't have made it.

I wish to express my deepest gratitude to Dr. Rüdiger Neun, Dr. Tilo Foerster, and Borys Hagemann for the invaluable comments and assistance that you all provided during the patent application.

I would say thanks to Prof. Dr. Nader Parvin for his kindest supports during my bachelor's study. He taught me how to think as a researcher, how to design experiments as an engineer, and how to do research as a scientist.

I would like to thank the CPC Research School "Lung Biology & Disease" and HELENA Graduate Student for the advanced training and education platform during my Ph.D. project.

I would like to pay my special regards to my beloved wife, *Motaharehsadat*. You're the elite. I wouldn't have done this without your non-stop support, assistance, and love.

I wish to acknowledge the great love of my mother (maman), and my father (baba), who kept me going on –this work would not have been possible without the emotional supports you gave me. Baba, you always say this to me that motivated me –I love it “*whoever saved a soul, it should be regarded as he had saved all mankind*”.

During this project, we designed and manufactured numerous “*hand-made*” and “*customized*” devices. Special thanks to Andreas Schröppel for his great support and Thomas Gerlach and Josef Promoli from central workshop of Helmholtz Zentrum München for their kind assistance.

I truly appreciate everyone's assistance during my project. I would like to extend my sincere thanks to Sezer Orak, Paula Mayer, Prof. Dr. Arti Ahluwalia, Dr. Sinem Taş, Dr. Deniz A. Bölükbaş, Dr. Darcy Wagner, Dr. Carola Voss, Dr. Tobias Stöger, Manuela Roesner, Dr. Lin Yang, and Dr. Yaobo Ding for their technical assistance and insights during my project.

Last but not least, I wish to thank Helmholtz Zentrum München for supporting me during my research. I am also indebted to Germany, the country which offered me a decent life-work balance conditions to pursue my academic carrier and follow my ambitious, and at the same time live with my family –vielen Dank tausendmal und Servus!